New scaffolding materials for the regeneration of infarcted myocardium

MARÍA PILAR ARNAL PASTOR

EDITORIAL
UNIVERSITAT POLITÈCNICA DE VALÈNCIA

New scaffolding materials for the regeneration of infarcted myocardium

María Pilar Arnal Pastor

Dr. Eng. Sci. Thesis

Valencia, 4th November 2014

UNIVERSITAT POLITÈCNICA DE VALÈNCIA

Thesis supervisors:

Dr. Manuel Monleón Pradas

Dr. Ana Vallés Lluch

NEW SCAFFOLDING MATERIALS FOR THE REGENERATION OF INFARCTED MYOCARDIUM

Thesis submitted by

María Pilar Arnal Pastor

to obtain the degree of Dr. Eng. Sci.

at the Universitat Politècnica de València

Valencia (Spain), 2014

Thesis supervisors:

Dr. Manuel Monleón Pradas

Dr. Ana Vallés Lluch

Collection Doctoral Thesis

© María Pilar Arnal Pastor

© 2015, of the present edition: Editorial Universitat Politècnica de València
Telf.: 963 877 012 / www.lalibreria.upv.es

ISBN: 978-84-9048-325-1 (printed version)

Any unauthorized copying, distribution, marketing, editing, and in general any other exploitation, for whatever reason, of this piece of work or any part thereof, is strictly prohibited without the authors' expressed and written permission.

The research described in this Thesis was carried out at the Center for Biomaterials and Tissue Engineering of the Universitat Politècnica de València, Valencia, Spain. The work was funded by the project FP7 NMP3-SL-2009-229239 "Regeneration of cardiac tissue assisted by bioactive implants" (RECATABI) and by the Spanish Ministry of Education through the FPU2009-1870 grant.

A mi familia,

a quienes tantas horas robé

pero nunca el afecto

"...en fin, que lo que da verdadero sentido al encuentro es la búsqueda, y que es preciso andar mucho para alcanzar lo que está cerca"

José Saramago

Acknowledgements

At this point I look back, and I would like to show my gratitude to all the people that somehow have contributed to this work in one way or another.

I would like to especially thank my thesis supervisors, Dr. Ana Vallés and Dr. Manuel Monleón for their time and dedication. I have been very lucky to have them by my side during my PhD. Their different and complementary ways to face the problems was really enriching and helpful.

I would also like to thank Dr. Nicole zur Nieden for welcoming me in her laboratory during my international stay at the UCR, and teaching me the nuances of the cell biology work.

I would like to thank the Microscopy Service of the Universitat Politècnica de València for their guidance and help; and the Cytomics Core Facility at Príncipe Felipe Research Center (Valencia, Spain) for the support and advice in flow cytometry experiments.

I am also very thankful to all the CBIT people, without hesitation the best part of doing this PhD. Thanks to all the CBIT crew for the laughs, coffee breaks, jokes and lunches we have shared these years. Thanks a lot for the patience, support and advices.

In particular I want to thank Manuel Pérez. Doing this Thesis side by side actually made it possible. I will always keep a very special place in my heart for our long talks, sharing hopes and disappointments.

Thanks to the “La 13-14” office members: Cristina Martínez and Myriam Lebourg, it was a pleasure having the chance to learn from you; but more importantly your friendship and support really touched me. Thank you girls!

I would also like to thank Matthias Keicher, Line Vikingsson, Guillermo Vilariño, Sara Comín and Débora González, I guided you at your beginnings in the lab, and you taught me and rewarded me with much more. I am lucky to have met you and counted with your help.

I want to thank Laura Teruel for doing such a wonderful work keeping the labs working, and especially for always doing it with a smile in her face.

I also want to thank my friends: your support and healing conversations helped me out in the toughest moments of this PhD. I would also want to give my deepest thank to Verònica Puig for simply being wonderful.

Finally I would like to thank my family for their unconditional support through these years. Your love and continuous encouraging, especially in the darkest times, led me to this moment.

At last I would like to thank Fede for being by my side whenever I needed him.

Thank you all!

Table of contents

Abstract

There is growing interest in the development of biomimetic matrices that are simultaneously cell-friendly, allow rapid vascularization, exhibit enough mechanical integrity to be comfortably handled and resist mechanical stresses when implanted in the site of interest. Meeting all these requirements with a single component material has proved to be very challenging.

The hypothesis underlying this work was that hybrid materials obtained by combining scaffolds with bioactive hydrogels would result in a synergy of their best properties: a construct with good mechanical properties, easily handled and stable thanks to the scaffold; but also, because of the gel, cell-friendly and with enhanced oxygen and nutrients diffusion, and promoter of cell colonization. Moreover, such a composite material would also be useful as a controlled release system because of the gel's incorporation.

Poly (ethyl acrylate) (PEA) scaffolds prepared with two different morphologies were envisaged to provide the mechanical integrity to the system. Both types of scaffolds were physico-chemically characterized and the effect of the scaffolds production process on the PEA properties was examined. The scaffolds preparation methods affected the PEA properties; nevertheless, the modifications induced were not detrimental for the PEA biological performance.

Two different bioactive gels were studied as fillers of the scaffolds' pores: hyaluronan (HA), which is a natural polysaccharide, and a synthetic self-assembling peptide, RAD16-I. HA is ubiquitously present in the body and its degradation products have been reported to be angiogenic. RAD16-I is a synthetic polypeptide that mimics the

extracellular matrix providing a favourable substrate for cell growth and proliferation.

Given the hydrophobic nature of poly(ethyl acrylate), the combination of PEA scaffolds with aqueous gels raised a number of problems regarding the methods to combine such different elements, the ways to gel them inside the pores, and the procedures to seed cells in the new composite materials. Different alternatives to solve these questions were thoroughly studied and yielded protocols to reliably obtain these complex structures and their biohybrids.

An extensive physico-chemical characterization of the components' interaction and the combined systems was undertaken. As these materials were intended for cardiac tissue engineering applications, the mechanical properties and the effect of the fatigue on them were studied. The different composite systems here developed were homogeneously filled or coated with the hydrogels, were easy to manipulate, and displayed appropriate mechanical properties. Interestingly, these materials exhibited a very good performance under fatigue.

The use of the composite systems as a controlled release device was based on the possibility of incorporating active soluble molecules in the hydrogel within the pores. A release study of bovine serum albumin (BSA), intended as a model protein, was performed, which served as a proof of concept.

The biological performance of the hybrid scaffolds was first evaluated with fibroblasts to discard the materials cytotoxicity and to optimize the cell seeding procedure. Subsequently, human umbilical vein endothelial cells (HUVECs) cultures were performed for their interest in angiogenic and vascularization processes. Finally, co-cultures of HUVECs with adipose-tissue derived mesenchymal cells (MSCs) were

carried out. These last cells are believed to play an important role for clinical regenerative medicine, and their cross-talk with the endothelial cells enhances the viability and phenotypic development of HUVECs. Through the different experiments undertaken, hybrid scaffolds exceeded the outcome achieved by bare PEA scaffolds.

Resumen

Existe un interés creciente en el desarrollo de matrices biomiméticas que por un lado constituyan un entorno favorable para albergar células y sean fácilmente vascularizables, y que por otro lado posean suficiente integridad para ser cómodamente manejadas y resistan los esfuerzos mecánicos que sufrirán una vez implantadas. Lograr que un material unicomponente cumpla todas estas especificaciones resultaría muy complicado.

La hipótesis subyacente en este trabajo es que la combinación de andamiajes poliméricos porosos (*scaffolds*) con hidrogeles bioactivos en un material híbrido, generaría sinergias que mejorarían las características de ambos componentes. Gracias al *scaffold,* el material resultante presentaría buenas propiedades mecánicas, sería fácilmente manipulable a la vez que estable. Al mismo tiempo, gracias al gel, presentaría un mejor comportamiento con las células, el gel mejoraría la difusión de oxígeno y nutrientes mientras que favorecería la colonización celular. A su vez, la incorporación del gel permitiría la utilización de este material compuesto como sistema de liberación controlada.

Los *scaffolds* empleados para contribuir a la integridad física y mecánica del sistema se prepararon con poli(etil acrilato) (PEA) con dos morfologías distintas. Se caracterizó físico-químicamente ambos tipos de *scaffolds*, así como el efecto de su proceso de producción sobre las propiedades del PEA. En esta caracterización se observó que algunos pasos involucrados en la elaboración de los *scaffolds* alteraban de algún modo la matriz polimérica. Sin embargo, estas modificaciones no resultaron perjudiciales para el comportamiento biológico de los materiales.

Se seleccionó dos geles distintos como elementos de relleno para los poros de los *scaffolds*: el ácido hialurónico (HA), que es un polisacárido natural, y el péptido sintético autoensamblable RAD16-I. El HA está presente en la matriz extracelular de numerosos tejidos y sus productos de degradación son angiogénicos. A su vez, el RAD16-I es un polipéptido que proporciona una estructura de nanofibras que mimetiza la matriz extracelular, lo que constituye un entorno muy favorable para el crecimiento y la proliferación celular.

La obtención de *scaffolds* híbridos de PEA con geles acuosos conllevó una serie de problemas dada la naturaleza hidrofóbica del PEA. Fue necesario establecer protocolos para: combinar dos elementos tan distintos, gelificar los hidrogeles dentro de los poros y sembrar tales hidrogeles eficientemente con células una vez incorporados en el *scaffold*. Se consideró y estudió distintas alternativas para resolver estas cuestiones, dando lugar al establecimiento de procedimientos para obtener estas estructuras complejas y sus biohíbridos.

La interacción de los componentes empleados, así como el sistema combinado de ambos, fueron objeto de una intensa caracterización físico-química. Puesto que se pretende utilizar estos materiales en ingeniería tisular cardíaca, se estudió tanto sus propiedades mecánicas como el efecto que la fatiga tiene sobre ellos. Los sistemas compuestos obtenidos, bien sea con los poros rellenos o con recubrimientos homogéneos de ambos hidrogeles, se manipulaban con facilidad y presentaban propiedades mecánicas adecuadas. Es de destacar, que además presentaban un buen comportamiento a fatiga.

El potencial de los *scaffolds* combinados para ser utilizados como sistemas de liberación controlada (por la incorporación de moléculas solubles activas en el

hidrogel), fue verificado al llevar a cabo una prueba de concepto con albúmina de suero bovino (BSA) como proteína modelo.

El comportamiento biológico de los *scaffolds* híbridos se evaluó en primer lugar con fibroblastos para descartar su citotoxicidad y optimizar el protocolo de siembra. A continuación, se llevó a cabo cultivos con células endoteliales de cordón umbilical (HUVECs), por su interés en procesos angiogénicos y de vascularización. Finalmente, se realizó co-cultivos de HUVECs y células mesenquimales derivadas del tejido adiposo (MSCs). Estas últimas fueron seleccionadas por ser candidatas a desempeñar un papel clave en la traslación clínica de la terapia regenerativa. Además, las MSCs mejoran la viabilidad y el desarrollo fenotípico de las células endoteliales. A lo largo de los experimentos llevados a cabo, los *scaffolds* híbridos superaron, en lo que se refiere a su desempeño biológico, los resultados alcanzados con los *scaffolds* de PEA que no incorporaban ningún hidrogel en sus poros.

Resum

Existeix un interès creixent en el desenvolupament de matrius biomimètiques que d'una banda proporcionen un entorn favorable per a albergar cèl·lules i siguen fàcilment vascularizables, i que d'un altra banda posseeixen suficient integritat per a ser còmodament manipulades a més de ser capaces de resistir els esforços mecànics que patiran una vegada implantades. Aconseguir un material unicomponent que compleixi totes aquestes especificacions resultaria molt complicat.

La hipòtesi subjacent en aquest treball és que la combinació de bastides polimèriques poroses (*scaffolds*) amb hidrogels bioactius en un material híbrid, generaria sinergies que millorarien les característiques de cadascun dels components. El material resultant, gràcies al *scaffold*, presentaria bones propietats mecàniques i seria fàcilment manipulable alhora que estable. Al mateix temps, gràcies al gel, presentaria un millor comportament amb les cèl·lules, el gel milloraria la difusió d'oxigen i nutrients mentre que afavoriria la colonització cel·lular. Al seu torn, la incorporació del gel permetria la utilització d'aquest material compost com a sistema d'alliberament controlat.

Els *scaffolds* emprats per a contribuir a la integritat física i mecànica del sistema es prepararen amb poli(etil acrilat) (PEA) en dos morfologies distintes. Es va caracteritzar ambdós tipus de *scaffolds,* així com l'efecte del seu procés de producció sobre les propietats del PEA. Al llarg d'aquesta caracterització es va observar que alguns dels passos involucrats en la elaboració dels *scaffolds* alteraven d'alguna manera la matriu polimérica. Tot i això, estes modificacions no resultaren perjudicials per al comportament biològic dels materials.

Es va seleccionar dos gels diferents com a elements de farcit per als porus dels *scaffolds*: l'àcid hialurònic (HA), que és un polisacàrid, i el pèptid sintètic autoensamblable RAD16-I. L'HA està present en nombrosos teixits i els seus productes de degradació son angiogènics. Al seu torn, el RAD16-I és un polipèptid que proporciona una estructura de nanofibres que mimetitzen la matriu extracel·lular, pel què constitueix un entorn molt favorable per al creixement i la proliferació cel·lular.

L'obtenció de *scaffolds* híbrids de PEA amb gels aquosos va comportar una sèrie de problemes per la naturalesa hidrofòbica del PEA. Fou necessari establir protocols per a: combinar dos elements tan diferents, trobar formes de gelificar els hidrogels dins dels porus, i de sembrar-los eficientment amb cèl·lules una vegada incorporats a l'estructura del *scaffold*. Distintes alternatives per a resoldre aquestes qüestions foren considerades i estudiades, donant lloc a l'establiment de procediments per a obtindre aquestes estructures complexes i els seus biohíbrids.

La interacció dels components emprats, així com el sistema combinat foren objecte d'una intensa caracterització física-química. Donat que es pretén utilitzar aquests materials per a enginyeria tissular cardíaca, es va estudiar tant les propietats mecàniques com l'efecte que la fatiga té en ells. Els sistemes compostos obtinguts, bé siga amb els porus farcits o amb recobriments homogenis d'ambdós hidrogels, es manipulaven amb facilitat i presentaven bones propietats mecàniques. Cal destacar que a més a més presentaven un bon comportament a fatiga.

El potencial dels *scaffolds* combinats per a ser utilitzats com a sistemes d'alliberament controlat (per la incorporació de molècules solubles actives en l'hidrogel), va ser corroborat al dur a terme una prova de concepte amb albúmina de sèrum boví (BSA) com a proteïna model.

El comportament biològic dels *scaffolds* híbrids es va avaluar en primer lloc amb fibroblasts per a descartar la seua citotoxicitat i optimitzar el protocol de sembra. A continuació es van realitzar cultius amb cèl·lules endotelials de cordó umbilical (HUVECs), pel seu interès en processos angiogènics i de vascularització. Finalment es dugueren a terme co-cultius de HUVECs amb cèl·lules mesenquimals derivades del teixit adipós (MSCs). Les darreres es seleccionaren perquè son candidates a exercir un rol clau en la translació clínica de la teràpia regenerativa, a més a més de que al interactuar amb les endotelials, aquestes milloren la seua viabilitat i desenvolupament fenotípic. Al llarg dels experiments empresos, els *scaffolds* híbrids superaren, en termes de desenvolupament biològic, els resultats assolits amb els *scaffolds* de PEA que no incorporaven cap hidrogel en els seus porus.

Chapter 1:

Introduction

1.- Introduction

1.1.- The cardiac tissue and its peculiarities (extracted from [1])

1.1.1.- The heart

The heart is a complex organ that pumps 7000 litres of blood to all the tissues in the body per day [2]. This pumping function precisely determines its anatomy. Heart tissue basically is formed by cardiac myocytes (contractile elements) [3], smooth muscle cells, fibroblasts, blood vessels, nerves and the extracellular matrix components (cardiac interstitium and collagen) [4] organized in a very particular way. Myocytes form muscular fibres with changing orientation across the ventricular wall up to 180^{o} [5]. At the same time, muscular fibres are organized into myocardial laminas 4-6 myocytes thick separated from neighbouring laminas by extracellular collagen [6]. The particular arrangement of ventricular myocytes influences the mechanical and electrical function of the heart and small changes in it can lead to severe alterations in these functions [7].

The extracellular matrix (ECM) connects the cells into a 3D-architecture and bridles the forces produced by the myocytes [8]. The anatomical model proposed by Torrent-Guasp [6], which considers the heart as one muscle band plied in a double helical loop, explains how the ventricles contract and get an efficient pumping in every heartbeat, achieving an ejection fraction of 60% when sarcomeres individually contract 15% only [9].

Myocytes are intimately connected, forming a functional syncytium [6]. Each myocardial cell is coupled in average to 9.1 $\pm$ 2.2 [10] myocytes, by 99 [11] gap junctions where the transfer of ionic currents takes place. Gap junctions are a specialized form of cell connection; they are formed by a cluster of ionic channels essential to the rapid propagation of the action potential. The action potential is the

electrical impulse responsible for cells contraction [12]. A proper electrical coupling of the cells is critical to avoid arrhythmias and re-entries and essential for the contraction to spread as a wave front.

1.1.2.- Cardiovascular diseases and the myocardial infarction

Cardiovascular diseases (CVD) are a leading death cause in developed countries (*i.e.* 1 of every 3 deaths in the United States in 2008) [13]. Changes in diet and habits are causing CVD to become major mortality pathologies in developing countries too [14]. As a consequence, they are already responsible for 30% of the world deaths. This group of diseases constitutes a great burden for the national health systems, consuming great percentages of the health systems budgets. In the particular case of the coronary heart diseases (CHD), 3.8 million men and 3.4 million women die a year worldwide because of them [15]. In the United States 1 of every 6 deaths in 2008 was caused by CHD [13].

Acute myocardial infarction (AMI) occurs when a coronary artery is clogged, in 80% of the cases by coronary atherosclerosis with superimposed luminal thrombus [16]. This occlusion leaves the downstream zone of the heart without blood supply, what means lack of oxygen, nutrients and metabolites wash for the affected zone. As a consequence, the aerobic metabolism changes to anaerobic glycolysis [16], leading to a decrease in the pH and reduction in the contractile function. Within 20 to 40 minutes without blood supply cells start to die and as times passes more myocardial tissue is compromised. There is also a zone of the heart affected by the infarction, where myocytes remain viable but lower their activity to reduce the metabolism and oxygen consumption to survive under hypoxic conditions; they can recover their contractibility after revascularization [17].

In the infarcted area there is a great number of dead myocytes, and the host response to the injury consists in activating the inflammatory response and producing

cytokines [18]. Thereupon neutrophils, monocytes and macrophages will migrate into this area to remove the necrotic tissue [19]. Then, matrix metalloproteases (MMPs) will be activated, which will have a deleterious effect on the collagen matrix of the heart and in the surrounding coronary vasculature by degrading them [20]. The weakening of collagen will lead to wall thinning and ventricular dilation, as well as mural realignment of myocytes bundles [21]. After the inflammatory phase and the resorption of the necrotic tissue, there is an increase in the deposition of crosslinked collagen in the infarcted area that will lead to scar tissue formation. During the remodelling process a change in the collagen composition occurs, the type I collagen fraction is reduced from 80% to 40% and the collagen III is increased [22].

Against what was thought, this scar is a living tissue with a fibroblast-like cell population nourished by a neovasculature; these cells regulate the collagen turnover of the scar tissue [19]. The scar tissue has a reduced or absent contractility as compared with the original healthy myocardium [23], what leads to a reduction in the overall cardiac function [24].

The remodelling process initially is a compensatory mechanism to overcome the loss of contractile tissue. But with time this adaptative process of overload will become maladaptative [17]. To compensate the additional effort, the remaining beating tissue will hypertrophy trying to overcome the reduction in the cardiac function. This overload will lead to myocyte slippage and fibrotic interstitial growth and to a degenerating process that may end in heart failure. The heart remodelling will produce in the ventricles a set of anatomical and functional changes, including increased wall stress, slimming of the wall, chamber dilation, increase of the sphericity, alteration in the blood flow particularly in the left ventricle [25] and a significant loss of cardiac function.

The ventricular shape change from elliptical to spherical reduces its ejection fraction, because of a change in the apical loop fibre orientation [26]. Another problem caused by the shape change is that the papillary muscles are separated, what leads to regurgitation, contributing to the overload of the heart [21]. Besides, remodelled hearts are more prone to suffer arrhythmias as the membrane potential is altered and because of the interstitial fibrotic growth that may affect conductivity [17].

The end stage of the degeneration is the heart failure, when the heart is unable to pump enough blood to match the metabolic needs of the tissues. Current treatments aim to avoid reaching this point.

1.1.3.- Conventional therapies

Clinical practices aim to limit the severity and extension of the AMI by rapidly restoring the blood flow (reperfusion), alleviating the oxygen demand [27] and reducing reperfusion injury. This can be done with different treatments or combinations of them.

Pharmacological approaches involve the use of anticoagulant therapies and thrombolytic drugs to remove the clot. Vasodilators like nitrates are also used to favour the dilation of the vessels; aspirin to avoid platelet aggregation, beta blockers to reduce the heart pace, as well as morphine to reduce the pain are employed, aspiring to reduce the work load and to protect the cardiac tissues from the accumulated harmful substances [28].

Another group of therapies are the percutaneous coronary interventions; they physically reopen the vessel via catheterization. There are different techniques: the regular angioplasty uses a catheter with a balloon that is inflated in the place of the thrombus to reopen the lumen [29], or allows the permanent implantation of a stent in the vessel to keep it open. There is a wide variety of these devices depending on

their composition, whether they release drugs or are biodegradable or not, etc. [27, 30].

These therapies restore the blood flow to the infarcted zone, but reperfusion therapy is not exempt of risks: it is a complex process that can induce apoptosis by the micro-environmental changes that the recovery of the blood supply induces (formation of free radicals, calcium release, neutrophils, ...) [31]. So it has to be done carefully and there is always a compromise between limiting the infarction extension due to the time without oxygen and the induced apoptosis due to the reperfusion. Reperfusion done soon after the onset of the ischemia is very advantageous, saving more tissue by restoring the blood flow than the tissue that will be lost because of the toxic substances released in the reperfusion.

More invasive, surgical therapies involve different techniques with different objectives: to restore a proper blood flow in areas that lack it (by-pass surgery), to restore the normal elliptical geometry (Dor and Batista procedures), to restore the wall stress to normal (dynamic cardiomyoplasty) to limit the pathologic dilation [9], or in the most severe cases, to replace the organ. However, this last option is very limited given the lack of available donors [32], the associated risks and the need for immunosuppressive therapy.

All the aforementioned treatments basically limit the damage of the acute episode and the remodelling process, but do not regenerate the damaged tissue and do not avoid the ventricular remodelling following an AMI.

1.2.- Cell therapy and cardiac tissue engineering (extracted from [1])

1.2.1.- New ways to heal the heart

For many years, the heart has been considered a fully differentiated organ, with no myocyte regeneration after birth [33]. Recently it has been proved that myocytes have a limited regenerative capacity, around 1% of the cells per year at the age of 20 and it is reduced to 0.3% at the age of 75 [34]. This restoration is achieved thanks to a small population of cardiac stem cells [35]. Nevertheless, their potential is limited and in any case it is not enough to regenerate the heart if it suffers severe damage, like the one provoked by a myocardial infarction. New therapies under development like cell therapy or tissue engineering, aim to boost this limited regenerative potential of the native tissue by employing cells, drugs, factors or patches.

The objective of cell therapy is to heal the damaged tissue by implanting stem cells into the pathologic myocardium. In the case of tissue engineering approaches, cells are combined with materials and bioactive molecules to again try to recover the injured tissue (see Figure 1.1). The employed materials will support cells, provide them 3D organization, protect them, stimulate and guide its growth, maintain them in the site of interest, etc.; in sum, they will act as an artificial extracellular matrix during the regeneration process. As an advantage, the use of materials either injectable, or *ex vivo* conformed (gels –patches- or scaffolds) has an additional effect: the implantation of a material in the scarred ventricular wall, increases its thickness and by Laplace's law, this increase leads to a reduction in the wall stress. This side-effect could be by itself very positive, even if no regeneration is achieved, to limit ventricular remodelling and improve the quality of life of cardiac patients [28].

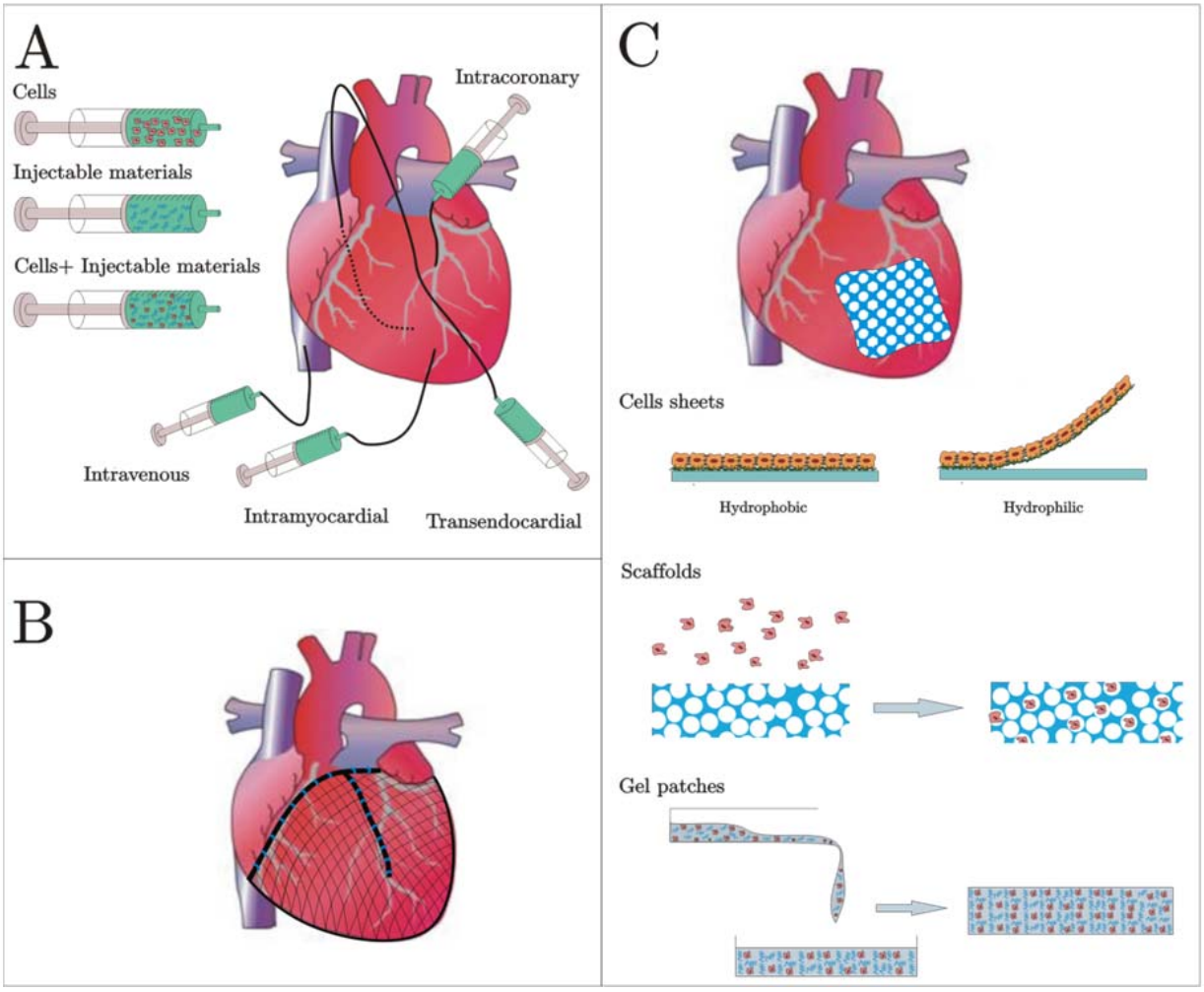

Figure 1.1: (A) Classical cell therapy and injectable materials in the heart, sketch inspired in [36]. (B) Ventricular restrain device. (C) Tissue engineering approaches with cell sheets, scaffolds or gel patches, sketch inspired in [37].

1.2.2.- Cell cardiomyoplasty: how and why?

Cellular cardiomyoplasty appeared as a promising therapeutic approach. This name encloses the therapies that use the injection of cells, from different origins, directly into the heart attempting to obtain an improvement in the reduced heart function after an ischemic insult (Figure 1.1 A). The injected cells are envisaged to induce angiogenesis, inhibit apoptosis, help to recover the hibernating myocardium, activate endogenous repair mechanisms, and create new contractile tissue that will eventually

replace the damaged one. Also they are expected to reverse the remodelling process that led to ventricular dilation [38].

Different ways to deliver cells into the damaged heart have been explored: intracoronary infusion (with the hope that cells will migrate through the vessels and be hosted in the infarcted area) or directly into the infarcted area either by intramyocardial or percutaneous endocardial injection [39]. The advantage of injecting them directly into the infarcted area is that this will ensure that cells are delivered in the site of interest.

An important drawback of this technique is the low engraftment into the heart tissue of the supplied cells. The retention of the cells in the heart seems to be determined by the cell type and delivery route [40]. It has been estimated that in humans 50-75 min after intracoronary injection of bone marrow cells only 1.3-2.6% of the injected cells remain in the myocardium [41]; besides, after 2 hours less than 10% of the injected cells survive [35]. Many causes can be advanced: the heart beats, so cells can easily be pumped out of the heart; the solution in which cells are injected has a low viscosity, so cells can be washed away; the mechanical loss of the cells through the injection hole left by the needle, etc. [42]. A different contributing cause to the low cell engraftment is that the injured heart is not a cell-friendly environment, collagen fibres have changed from type I to type III, which has worse properties in terms of adhesion and promoting angiogenesis, what can induce anoikis [2]. The conditions in the infarcted myocardium are very hostile for the cells: hypoxic conditions (studies show that the survival of injected cells decreases towards the centre of the scar); cytokines, inflammatory factors, etc., are present in the damaged myocardium, and can negatively affect the survival of the injected cells. Immunological rejection can be another cause reducing cell survival [43]. An interesting approach is to train cells prior to their implantation for them to resist the hostile conditions they will find in the implantation site [44].

The fact that most of the cells did not graft into the host myocardium in the studies performed to date, that there is a very limited transdifferentiation of implanted cells into beating cardiomyocytes (the differentiation reported in animals may have been fusion events between native cardiomyocytes and injected cells [43]), and that a wide range of non-myogenic cells also induce an improvement of the ventricular function [39], suggests that the mechanism leading to this enhancement cannot be only myogenesis regenerating the myocardium. The pathways through which cell implantation induces improvements in cardiac function remain to be elucidated, but different events that can take place simultaneously have been proposed. The most remarkable are the induction of angiogenesis (formation of new vessels) and the improvement in the myocardial perfusion, the reduction of the wall stress because of the increase in cell mass [45] and the paracrine effect of the injected cells [35].

Cell sources under study

Many different cells types have been employed in the numerous studies that have been performed. Autologous cell sources are interesting because they do not require immunosuppression treatment of the patient and there is no risk of illness transmission. In this group are included bone marrow cells [44], adipose derived stem cells [46], cardiac stem cells [47], skeletal myoblasts [48] or induced pluripotent stem cells [49]. The problem of the autologous cells is that prior to implantation cells need to be extracted and expanded. This whole process in some cases may take several weeks, limiting its application in the acute state. Besides, autologous cells coming from patients that suffer other conditions like diabetes or are simply aged, may have limited proliferation and attachment [50]. On the contrary, allogeneic cells could be ready to use whenever a patient needs them, but would require immunosuppressive therapy after their implantation, and there is always a remaining risk of illness transmission. Among the allogenic stem cells under study there are the embryonic stem cells [51], umbilical cord cells [52] or amniotic fluid stem cells [53].

As previously said, a great variety of cells have been employed and the initial promising results obtained in animal models made this technique to move very fast to clinical trials, even if the mechanisms involved in the observed improvements were unknown [54]. Unfortunately, the results obtained from the clinical trials were not as good as expected and some were contradictory between them. One possible contributing cause to this discrepancy is that studies are carried out in young healthy animals, while patients susceptible to receive these treatments normally are aged people and in many cases with other co-morbidities [55].

Cell sheets

The use of cell sheets is based on detaching the cells from the culture surface without trypsinizing them; in that way cells maintain the adhesion and membrane proteins as well as the natural pro-survival and maturation environmental cues that the ECM provides [56] (Figure 1.1 C). Besides, the electromechanical connections are preserved [57]. As a consequence, the results obtained with cell sheet fragments are superior to those with dissociated cells. For instance, cardiomyocyte sheets were found to functionally integrate within the host tissue in a rat myocardial infarct model [58].

Cell sheets can be obtained by employing temperature-responsive plates whose behaviour switches from hydrophobic to hydrophilic when the temperature is lowered below 37°C [56]. The muscle mass loss following an infarction is significant, up to 50 g [59], so the amount of cells needed to overcome this loss is obviously not covered with a single sheet of cells. Some groups have tried to obtain thicker grafts by overlapping several monolayer cardiomyocyte sheets, which adhere one to another forming gap junctions and intercellular adhesions within minutes [60].

1.2.3.- Injectable gels

As previously stated, cell cardiomyoplasty presents problems in terms of cell attachment and survival. Cells usually reside in a determinate microenvironment which regulates their fate and function. The surrounding ECM with its chemical and biophysical cues is a key element, so the lack of cell-ECM interaction limits their survival [61].

Aiming to overcome the problems of cells supply, alternative approaches are considered in current studies. The use of natural or synthetic materials in an injectable format, alone or together with cells, has been investigated to limit remodelling and improve both cell attachment and survival upon implantation in the heart (Figure 1.1 A). Ideally, they should be tailored to be amenable to delivery with minimally invasive catheter based procedures [59]. The injectable materials have to cure or self-assemble rapidly (without the need or the release of toxic components) once delivered in the site of interest. As injected, they adopt the shape of the cavity, and may increase the stiffness and thickness of the ventricular wall [62]. Simulations show that the injection of non-contractile materials with proper mechanical properties can contribute to limit the stress the ventricular wall withstands, thus helping to limit the remodelling [63].

These materials can help to keep the cells in the site of interest, provide them a 3D environment and also protect them from the hostile environment represented by cytokines and hypoxic conditions, reactive oxygen species, etc., consequence of the infarcted condition of the site [43]. The injected gels can provide a cell friendly environment that will prevent anoikis [59]; they can also include adhesion motifs and then actively contribute to cell attachment. Moreover, they can be used as a controlled release system providing in a sustained way drugs or growth factors to improve cells survival, integration and proliferation [35]. And in the case of biodegradable materials, their degradation products may provide additional chemicals that stimulate cells.

Among others, the ideal injectable material should be biodegradable, have a low immunogenicity, be non-cytotoxic, non-adhesive and have antithrombogenic properties, adequate mechanical properties, provide stiffness to the scar but at the same time being compliant with the heart beating and transmit properly the mechanical stimuli to the cells, induce angiogenesis or at least not disturb the angiogenic activity after incorporation, be capable of delivering cells and or bioactive molecules [64].

The *in situ* gelling biomaterials employed can be classified into natural or synthetic materials depending on their origin. Synthetic materials are made in the laboratory, so their properties can be tuned to match the desired characteristics: their mechanical properties, degradation, morphology and mesh size (porosity) can be tuned as desired [65]. Besides, they are free from animal origin components and the risks related therewith. However, they may not have as good biological performance as biologically derived materials [2]. In the group of injectable synthetic biomaterials there are, among many others: N-isopropylacrylamide (NiPAAm) alone [66] or copolymerized [67]; poly(ethylene glycol) (PEG) alone [68], copolymerized [69] or combined with vascular endothelial growth factor (VEGF) [70], or the self-assembling peptides (SAPs) [71] that will be discussed in more detail in section 1.5.3.

Natural or biological biomaterials refer to those from animal or vegetal origin. They are very similar to macromolecular substances which the biological environment is prepared to recognize [72]. Among them there are: fibrin [73], chitosan [74], Matrigel® [75], hair keratin [76], hyaluronic acid [77], alginate [78], collagen [79], gelatin [80] and ECM-derived materials [81].

1.2.4.- Pre-formed gels and scaffolds

What is the point?

An alternative approach in the field of cardiac tissue engineering implies the use of biomaterials to produce patches and implant them epicardially onto the infarcted tissue, conveniently adapted to its size and shape. These patches can be pre-loaded with cells (incorporated within their pores in the case of microporous scaffolds, or encapsulated in the case of a gel conformed before implantation) and growth factors or drugs, and act as a cell supply, a mechanical reinforcement [82] to the infarct scar to avoid ventricular dilation and a drug release system simultaneously.

Attending to the type of strategy, three groups can be distinguished, in terms of the nature of the matrices: biodegradable scaffolds, permanent or biostable scaffolds, and decellularized tissue-derived scaffolds. With the use of biodegradable scaffolds, it is expected that the matrix will degrade as the surrounding tissue is regenerated; the degradation products should be non-toxic and metabolized by the body. By using permanent scaffolds, the idea is that they will be infiltrated by the host tissue and contribute to the regeneration, but also act as a permanent mechanical restraint to limit ventricular dilation (Figure 1.1 B and C). The approach of scaffolds derived from decellularized tissue is based on the use of tissues whose cells are removed with a set of washes and the remaining ECM maintains the architecture, the vessels path, and the mechanical properties similar to those of the native tissue and the proteins and adhesion molecules. The more aggressive the washes and treatments are, the lower the risk of allogenic immune reaction is, but undesired washout of adhesion proteins and architecture damage can be associated [56, 83].

Requirements of the scaffolds

In the cardiac patch strategy a key aspect is to find a material that matches the required properties. The material needs also to be cell-friendly, non-cytotoxic and

promote cell attachment and proliferation, and it must also be non-immunogenic [84]. The scaffolds should provide a 3D environment to the cells with a porous structure able to guide cardiomyocytes alignment and promote maturation [85], also induce the development of a contractile phenotype and the electro-mechanical coupling of the implanted cells among them, and also with the host tissue [86, 35] and needs to be easily vascularized [50].

The mechanical properties exhibited by the scaffolds should be adequate to their application in heart tissue engineering. It implies that they should ideally be compliant with contractions and exhibit non-linear elasticity, as well as be capable to adapt to the shape of the heart in all the phases of the heartbeat. Anisotropy to mimic the directionally-dependent electrical and mechanical properties of the native myocardium could be desirable [87]. The stiffness of the material employed affects the phenotype and contractile properties of the neonatal cardiomyocytes [88], and has to be carefully tuned to meet physiological conditions.

Related problematic

As all the approaches described so far, the use of patches also has some advantages, disadvantages and unsolved problematic. An important inconvenience is that the application of a patch in the heart needs a much more invasive technique than a catheter-delivered system, as it requires a surgical procedure to be implanted. As advantage, the fact that the materials are synthesized and conveniently prepared out of the body can be outlined. It implies that there is no limitation in the preparation procedure and in the use of solvents (if they are properly removed at the end of the fabrication process and do not induce cytotoxicity). Therefore, the range of chemistries and techniques available to obtain scaffolds with different architectures broadens. In addition, the mechanical properties of polymer scaffolds may be tuned to match more closely those of the heart muscle than with gelly biomaterials.

Besides, cells can be pre-cultured *in vitro* within them prior to implantation if desired.

Unlike native myocardium, where the greatest distance between capillaries is around 20 microns [59], scaffolds are not vascularized *a priori*. Then, cells seeded in the scaffolds have their oxygen and nutrients supply limited to their molecular diffusion through the thickness of the scaffold. Given the fact that cardiomyocytes have great consumption rates of nutrients and oxygen diffusion results in an insufficient supply for thick constructs. Consequently, to obtain a thick engineered tissue with viable cells throughout its thickness, pre-vascularization or improved diffusion throughout the scaffold until it is vascularized is key for the implant to succeed. Otherwise, cell density will be concentrated in the external parts and cell viability will be compromised in the centre of the scaffold if the distance to the surface is greater than a critical value estimated around 100 microns [89]. For example, the influence of oxygen concentration in cell density and viability in collagen scaffolds was studied, and results showed that the former decreases linearly with the distance to the surface and as a consequence the latter decreases exponentially [90].

Many attempts have been done in this direction, like the incorporation of oxygen carriers to the culture medium to simulate the effect of the haemoglobin in the blood [91], or the addition of the growth factor platelet derived growth factor BB (PDGF-BB) to protect cardiomyocytes from apoptosis [92]. Another strategy is based on the use of scaffolds releasing growth factors to enhance the vascularization process, like basic fibroblast growth factor (FGF) [93], VEGF [94] and Thymosin beta-4 [95]. In a different approach, capillary [96] or channelled [97] structures, or the native vascular network [98, 99] of decellularized tissues are proposed to favour the vascularization of the construct. The culture of endothelial cells prior to implantation of cardiac myocytes has also been explored [100]. Another possibility is to pre-implant the

scaffold to pre-vascularize it prior to its implantation in the final site [101]. Pre-culturing the scaffolds *in vitro* in rotating bioreactors [102], spinner flasks [89], orbital mixed dishes [103] or perfusion bioreactors have also been considered as good options, particularly the last ones. All in all, despite the great efforts put into play and the improvements achieved, obtaining vascularized constructs is still an unsolved problem.

Biomaterials employed as scaffolds

Many different types of materials have been considered for its use as patches in cardiac tissue engineering. According to their origin we can distinguish again: biological-derived materials, decellularized tissues and synthetic materials.

Biological-derived materials employed as scaffolds in cardiac tissue engineering cover: collagen either as a scaffold [104] or as a hydrogel, combined with different cell types [105, 22], modified with RGD [106] or functionalized with interleukin-10 plasmid [107] and even has been studied in the MAGNUM phase I clinical trial [108]; gelatin [109]; fibrin [110]; alginate alone [111] or modified to improve its non-adhesive nature [112]; polysaccharides such as pullulan and dextran [113]; silk fibroin alone [114] or combined with chitosan and hyaluronic acid [115] among others, or chitosan combined with carbon nanofibres to improve its conductivity [116]. Decellularized extracellular matrices have been proposed as scaffolds in many studies [117] and by means of this technique, rat hearts capable to pump blood have been successfully obtained [118].

Synthetic materials include: polylactic acid and polyglycolic acid (PLA and PGA) [56] that are usually blended as poly(lactic–co-glycolic acid) (PLGA), or with other polyesters, to combine their properties as desired. PLGA has been employed as electrospun fibrous membranes [119] or as porous beads [120]. PLGA has been mixed

with laminin [121] or carbon nanofibres [122]. Poly(epsilon-caprolactone) (PCL) [123] has been proposed for myocardial regeneration for example in 3D constructs obtained by overlapping electrospun PCL mats. It is usually combined with PLA, PGA or its copolymer poly-glycolide-co-caprolactone (PGCL) [124]. Polyurethanes can be used to obtain fibrous scaffolds by electrospinning [125] or porous elastic scaffolds [126]. Cell attachment on polyurethane-based porous scaffolds has been improved by pre-treating them with laminin [127]. Poly(glycerol sebacate) (PGS) [128] has been proposed in very different geometries [87], and also coaxially electrospun with gelatin [129] to enhance cell adhesion and proliferation or modified in other ways [130].

In particular, acrylate-based materials have not been widely exploited for cardiac tissue engineering yet, but the interest on them is increasing for their versatility of processing and variety of properties obtained. For example, scaffolds made of poly(2-hydroxyethyl methacrylate-co-methacrylic acid) [131] have been proposed for their use in cardiac tissue engineering.

1.3.- Combinatorial approaches

1.3.1.- Searching for synergy

Elaborated regenerative strategies targeting complex tissues such as the cardiac require the use of advanced biomaterials. As previously discussed in section 1.2.4, the requirements for a scaffold to be successful are multiple. It has to be easily colonized by cells and integrate within the host tissue as well as provide spatial three-dimensional organization. It has also to act as a mechanical support for the non-contractile infarcted tissue and yet being compliant with the heartbeat movement. And, given its thickness, it has to be vascularizable in order to ensure the nutrient and oxygen diffusion into the core of the construct.

Another aspect to take into account is that the produced synthetic scaffolds need porosities high enough to allow cell infiltration and migration, as well as diffusion of oxygen, nutrients, cells wastes,... Given the size of such pores and cells size, the scaffolds provide a 3D environment in a much higher scale than that of cells. Therefore, what is being considered a 3D substrate from our point of view, from a single cell perspective becomes a flat surface with a certain curvature [132]. Consequently, providing an environment that mimics more closely the extracellular matrix with the employed materials will certainly have a positive effect on cell behaviour.

Taken all together, obtaining a single-component scaffold matching all these desired properties is a terribly hard task. Thereby, materials exhibiting different properties and with different structures have been combined in the last years in more sophisticated strategies to obtain hybrid materials that exploit the advantages of all its components. Attending to the obtained structures and their aim they can be classified into different categories.

Firstly, some strategies entail the filling of the pores of a base scaffold. The rationale is to use one material that provides a 3D structure and mechanical properties, which is previously obtained. Next, it is filled with a different material which may have better cell-related properties and that may lodge drugs or growth factors to be released *in situ*. In this group two subcategories can be distinguished. The first one refers to the approaches in which a filler occupies the whole space between the pores and the methods that only provide a coating of the pores' inner surface leaving the pores partially empty. Other interesting systems involve the physical combination of materials with different properties. A wide range of systems proposed are included in this group. The second category encloses those procedures that apply surface treatments to polymers surfaces and, once the surface is activated, other groups or another material can be grafted onto it.

1.3.2.- Filling the pores

In this group of strategies, the intention is to entirely fill, and therefore clog the pores of macroporous scaffolds with a gel-like material to enhance the biological performance of the former.

The use of hydrogels to fill the pores of previously assembled scaffolds has proved to provide some interesting results. For instance, when chitosan scaffolds were filled with fibrin, cardiomyocyte retention within the pores was improved, and the constructs were capable to contract and transmit measurable forces when electrically stimulated [133]. In the absence of the filling, the forces were not transmitted and the construct was unable to contract. In another work, hybrid cardiac constructs were obtained by combining an elastomeric knitted fabric (Hyaff) with fibrin [134]. The presence of fibrin helped to immobilize the seeded cells and therefore the cell density reached increases. Similarly, web-like collagen microsponges were incorporated in the openings of a PLGA knitted mesh [135], increasing cell homogeneity and seeding

efficiency. The mesh provided proper mechanical properties, and made it easy to handle; and with the collagen sponges, cell interaction was enhanced. Type I collagen has been used to hydrophilize the pores of poly(DL-lactide-co-caprolactone)-poly(lactic–co-glycolide acid) (PLACL-PLGA) scaffolds [124]; the use of this composite system improved cellularity, contractility and cardiac markers expression (Tn-I and Cx-43) of neonatal rat heart cells seeded with Matrigel®. Hyaluronic acid (HA) has been employed as a filler for the pores of PLLA [136] and PCL [137] macroporous scaffolds, profiting from the bioactive properties of HA and the adequate mechanical properties of the polyesters. In a distinct combination, PLGA yarns were knitted into a mesh, and then collagen-chitosan solutions were poured on them. After lyophilization, porous collagen chitosan scaffolds reinforced with a PLGA mesh were obtained. They were tested subcutaneously, and proved to promote cell infiltration and blood vessel ingrowth. This system was firstly envisaged for dermal tissue engineering, but could be applied for other tissues as well [138, 139]. A more innovative procedure to obtain scaffolds with a hydrogel filling the pores involves the use of a CAD-CAM multi-head deposition system. As an example, with this device a synthetic polymer could sequentially (PLGA and PLLA in this case) be deposited to form channels, and then those channels were filled with the hydrogel (HA, gelatin and atelocollagen); these steps were repeated over and over until the hybrid scaffold was obtained [140]. The system combining both materials exhibited improved cell adhesion and proliferation.

Despite the examples presented so far, the base scaffold can also be from biological origin. For example, in a very interesting work, a fully biologically derived hybrid scaffold was proposed [141]. As scaffold, providing good handling characteristics, human decellularized myocardium was employed; and it was combined with fibrin loaded with human mesenchymal progenitor cells. It was found that the use of this composite had a remarkable impact on vascularization and myogenesis, showing a

great potential for cardiac repair. In another system, a porcine bladder acellular allograft was filled with a thermosensitive hydrogel containing PLGA nanoparticles loaded with VEGF [142].

Self-assembling peptides have also been used in combination with scaffolds to enhance their biological performance. Among others, silk microfibers obtained by knitting fibres were used as a frame for silk sponges obtained by freeze drying, and next the ionic polypeptide RAD16-I was incorporated in the open spaces among pores [143].

The gel can be used to fill and encapsulate cells at the moment of the seeding. For instance, composite PLLA-PLGA scaffolds loaded with Matrigel® were co-cultured with endothelial cells (ECs), cardiomyocytes and embryonic fibroblasts simultaneously [144], for ECs to provide vasculature and act synergically with cardiomyocytes to improve cell survival and proliferation. In a different work, cells were seeded in PGS scaffolds and entrapped using Matrigel® [145]. Cells were also encapsulated with fibrin and added into a PGA (polyglicolic acid) mesh to increase the system manipulability [146], which gave very good results for cartilage; a way to adapt this system for cardiac tissue engineering was under investigation.

1.3.3.- Coating the pores

Alternative proposals involve either only coating the inner surface of the scaffold pores or the external area of fibrous scaffolds or nanoparticles, providing a better interface between cells and the materials, but without encapsulating them or forming a net surrounding them. Authors targeting these types of structures claim that they will facilitate cell colonization and migration, as well as will leave more space for cell ingrowth and for the exchange of nutrients, oxygen and wastes than approaches that entirely fill the pores [147].

As previously explained, fibrin was proposed as a filler but also as a coating for PLLA fibrous [147] and macroporous scaffolds [148] by applying specific techniques that prevent the solution from clogging the pores. Cell colonization and homogeneity was improved and in the case of macroporous scaffolds the elastic modulus increased. PLLA scaffolds have been also coated with chitosan solutions forming a foam microstructure inside them [149]. The microstructure can be tuned by changing the chitosan solution concentration and simultaneously be used as a controlled release system [150]. In a more sophisticated proposal, fibrous scaffolds with an external coating of gelatin were produced by coaxial electrospinning [151]. In another research, electrospun nanofibres of PCL were coated with an amphiphile self-assembling peptide (SAP) containing an RGDS ligand [152]; authors were capable to coat the PCL fibres without compromising the PCL network. Cell performance improved thanks to the SAP addition.

Cell-adhesion mediating proteins of the ECM (fibronectin, laminin, fibrin, elastin or collagen type I and III) have been used as coatings in synthetic scaffolds to enhance the ECM formation and better control cell behaviour [153]. In [154], a coating consisting in a mixture of fibrin, fibronectin, gelatin, growth factors and proteoglycans proved to be a good substrate for human umbilical vein endothelial cells in PCL scaffolds.

Another concept entails the coating of microparticles employed as scaffolds. For example, chitosan microparticles were 'decorated' with HA by adsorption from an acidic HA solution [155], and silk fibroin aqueous solutions were explored as coatings for drug controlled release [156]. Coatings can have other applications besides improving cellularity, like reducing the inflammatory reaction upon implantation. For instance, PLGA microspheres were coated with MSH (melanocyte stimulating

hormone, an anti-inflammatory hormone) by physical adsorption in [157], to decrease the inflammatory reaction they cause *in vivo.*

1.3.4.- Blending and combining polymers

This strategy seeks the synergy of two or more materials in the composition of the polymeric matrix, by combining them during the process of production. Hereafter, a set of examples is related.

For instance, chitosan was blended with HA at different proportions, and after the freeze-drying procedure, porous scaffolds combining both materials were obtained [158]. In another work, hybrid scaffolds composed at different ratios of gelatin/HA were obtained by freeze-drying followed by crosslinking with 1-ethyl-3-(3-dimethylaminopropyl) carbodiimide hydrochloride (EDC) [80]. It turned out to be an interesting system for soft tissues. The cell adhesion on the scaffolds could be tuned by varying the gelatin fraction.

As regards electrospun membranes, PCL/gelatin or PCL/collagen-elastin were electrospun to obtain fibrous scaffolds with pore size depending on polymer concentration [159]. Combining a synthetic polymer with proteins allows to simultaneously improve both the mechanical properties and the biological performance. Blending the proteins with the PCL avoided the need for crosslinking agents, such as glutaraldehyde. In a different system, a PLLA electrospun membrane was combined with a co-electrospun HA membrane by consecutive electrospinning, in order to obtain a bilayered membrane with an adhesive side and a non-adhesive one [160]. The use of PLLA provided a handling film easily colonized by cells whereas HA exhibited a non-adherent behaviour. In line with the above, hybrid biomaterials were obtained by simultaneous co-electrodepositing a PCL/collagen mixture solution, and a gelatin/HA (loaded or not with VEGF and PDGF-BB) [161]. With this mixture of

materials authors claimed that they obtained a potentially truly vascularizable scaffold. In a more sophisticated proposal, highly aligned nanofibres of PCL/collagen/gelatin nanofibres were obtained with a greater protein content on the surface by means of the rotary jet spinning technique [162]. Because of the alignment, anisotropic mechanical properties and a Young's modulus in the range of cardiac muscle were obtained. Moreover, the addition of proteins improved the sarcomere formation as compared with pure PCL.

Microspheres of combinations of materials can also be obtained either to be used as scaffolds, to encapsulate cells or as systems for controlled delivery of molecules. For example, PLLA was combined with gelatin through a water/oil emulsion in order to increase its hydrophilicity targeting to improve cells affinity for this material [163]. In a different approach, alginate and collagen were combined to produce microspheres that encapsulated cardiomyocytes with a drop by drop system in a gelling bath [164]. This system allowed cells proliferation and the production of multilayer interconnected tissues. Moreover, the cells had features of a well-organized cardiac-like tissue and contracted spontaneously in a synchronous way. PLGA was combined with PEG-g-CHT (poly(ethylene glycol)-grafted-chitosan), to obtain microspheres with a modified-in-emulsion-solvent-evaporation method for controlled release of proteins. The release kinetics could be controlled by changing the PEG-g-CHT fraction [165].

With the aim of improving the mechanical properties of a base soft material, a variety of alternatives have been proposed so far, some of which are commented hereafter. Scaffolds of chitosan combined with gelatin and having a PCL core were produced [166], where the PCL core provided surgical handling, suturability and a higher tensile strength. The combined use of gelatin and chitosan targeted a good cell adhesion while providing a porous structure and mechanical properties allowing

cardiomyocytes migration and function. In another work, PGA fibres were employed to reinforce mechanically fibrin scaffolds with good biological performance [167]. Alternatively, in [168], poly(lactide-co-epsilon-caprolactone) knitted meshes embedded in between two layers of collagen obtained by compression allowed a uniform cell distribution, and better manipulability. Analogously, multilayer hybrid scaffolds were obtained by compression, having as a core an electrospun silk fibroin mat and both faces covered with a dense collagen layer [169]. This system was tested with mesenchymal stem cells, which exhibited a uniform distribution.

Another type of combination refers to the addition of conductive nanoparticles to the polymeric matrix, in order to improve the electric properties of the scaffolds that are usually very poor. For instance, HEMA (hydroxyethyl methacrylate)-based scaffolds were combined with gold nanoparticles [170]. As an effect of the good mechanical and electrical properties, the expression of connexin-43 of neonatal rat cardiomyocytes was enhanced. Polyvinyl alcohol combined with bovine serum albumin (BSA) was also loaded with gold nanoparticles; charged fibrous scaffolds were obtained by electrospinning, and again the cardiomyogenic differentiation was enhanced because of the better conductivity [171].

A problem associated with biodegradable scaffolds is that their degradation products might alter the microenvironment; for instance, the PLLA degradation products acidify the pH. Combining them with other materials can alleviate or solve this inconvenience. For example, in [172] PLLA was combined with chitin fibres, which degradation products were mend to neutralize those of PLLA.

1.3.6.- Treat and graft

This category encloses those procedures involved in the application of surface treatments to polymers in order to chemically modify their nature at the surface

level, and next grafting molecules onto them. Grafting biomolecules on the polymer surface can help, for instance, to have better control over cell adhesion and survival.

In general, the treatments proposed aim to create functional groups in the polymer surface, like carbonyl, carboxyl or amine groups. There are different surface modifications applicable to a polymer to improve cell adhesion onto it: ultraviolet radiation, beam ions (oxygen, nitrogen, noble gases or halogens), plasma treatments, etc. For instance, polyethylene was plasma-activated and bioactive molecules such as glycine, PEG, BSA or colloidal carbon particles were grafted onto the surface [173]. As a consequence of the introduced modifications, cells adhered and grew better. Scaffolds combining chitosan and gelatin were surface modified to incorporate HA chains [174], and the biological and mechanical behaviour as well as their biostability were improved. Polyhydroxyalkanoate-based materials were also coated with HA after a lipase treatment to increase the hydrophilicity of the substrate [175], and the importance of obtaining substrates with appropriate hydrophobic/hydrophilic proportions. Hydrophobic polymers were coated in [176] with highly hydrophilic ultra-thin layers, obtained by covalent immobilization of polysaccharides using a reductive amination reaction after a previous plasma activation of the polymer surface. In another study, polymethylmethacrylate fibres surfaces were functionalized with collagen I through different methods. It was observed that not the largest amount of adsorbed proteins but the type of linking determined the best cell attachment and proliferation *in vitro* [177].

In this section, the technique of layer by layer (LbL) deposition can also be commented. It consists in alternatively adsorbing two or more oppositively charged water soluble polymers onto a substrate. Many different combinations have been proposed, like chitosan/alginate [178], chitosan/HA [179] or chitosan/silk [180], among others. LbL can be further combined with treat and graft techniques: in [181],

hyaluronic acid and chitosan were layer by layer deposited onto PLGA surfaces previously rendered positively charged by aminolysis. The resulting material exhibited non-adherent properties but the multilayers covalently functionalized with collagen improved cell adhesion.

1.4.- Purpose of the study

The goal of this work was to obtain multifunctional materials (constructs), serving as cell carriers and drug-releasing platforms, by combining pre-formed elastomeric scaffolds with *in situ* assembling/crosslinking gels in the scaffold's pores, for application as ventricular patches in cardiac tissue engineering. These constructs are expected to show an enhanced biological performance as compared to bare scaffolds arising from the synergy of both components,

Non-biodegradable polymeric scaffolds based on poly(ethyl acrylate), PEA, were used because of its good mechanical properties and biocompatibility. The scaffolds are obtained with two different architectures: either with interconnected spherical pores or cylindrical orthogonal pores. The PEA scaffolds' pores are coated or filled with two different bioactive hydrogels: hyaluronan, HA, and the self-assembling peptide, SAP, RAD16-I. HA was chosen for its biocompatibility and angiogenic potential of its degradation products. As regards the SAP, it was selected because it self-assembles into 3D networks mimicking the ECM and has shown a good biological performance as well.

As a result of such combination a material is obtained with adequate mechanical properties, easy to handle, stable and cell friendly, with enhanced oxygen and nutrients diffusion, prompt for cell colonization.

The specific objectives of this Thesis were:

1.- To set up the procedures to obtain hybrid constructs combining PEA porous matrices with two bioactive gels in their pores, HA and RAD16-I, in different coating typologies, and characterize them from the morphological, physico-chemical and mechanical point of view.

2.- To determine the mechanical properties of these scaffolds as well as their resistance to fatigue loading to ascertain their feasibility for the proposed application.

3.- To assess the suitability of these scaffold-gel constructs to be used as controlled release systems, by employing a model protein.

4.- To evaluate the biological performance of the scaffolds filled with the bioactive gels.

In order to fulfil the presented objectives, firstly the employed materials are presented. The influence of the preparation processes on the properties of all employed materials was studied by means of a morphological and physico-chemical characterization. Bearing in mind the application for which these constructs were intended, the mechanical performance under fatigue cycles was especially considered. Procedures for incorporating the gels into the scaffolds were studied, paying a special attention to the different morphologies of the coated layer. The interaction between RAD16-I and PEA surfaces was a specific subject of enquiry. The use of the scaffold/gel constructs as a platform for drug and protein delivery was considered and characterized through experiments with a model protein.

In vitro studies were performed to ensure that the resulting materials were not cytotoxic. Cell seeding efficiency and cell viability experiments permitted a comparison of the scaffold-gel constructs and the bare scaffolds as to their biological performance. Finally, the endothelization potential of the scaffold-gels constructs was evaluated *in vitro* with HUVECs (human umbilical vein endothelial cells) cultures.

The work leading to this Thesis took place in the framework of the FP-7 project RECATABI [182] (REgeneration of CArdiac Tissue Asissted by Bioactive Implants),

financed by the European Commission in the 7th Framework Programme. Some of the materials developed in the present study were among those implanted in a sheep model of chronic infarct by Dr. J.C. Chachques in the Hôpital Européen Georges Pompidou (Paris), in the framework of the collaboration of the above-mentioned project. The results derived from these collaborations are not shown as are out of the scope of this Thesis.

1.5.- Candidate materials

As previously discussed, combining materials creates synergies that can boost the advantages that presents each component separately. Hence, in this work hybrid scaffolds have been obtained by combining materials with very different properties and nature, in order to benefit from the advantages that each constituent introduces and to overcome the limitations that each component might present.

The materials chosen for this Thesis are composed on the one hand of a hydrophobic porous scaffold, made of poly(ethyl acrylate) (PEA) exhibiting different morphologies. It will be responsible for the mechanical integrity, manipulability and structural organization of the construct. This scaffold will be combined with hyaluronan or the self-assembling peptide RAD16-I. Basically, the types of combinations that will be dealt with in this work will cover from thin pore coatings to complete fillings. The incorporation of these materials to PEA scaffolds, both highly hydrophilic and with a gel-like aspect, aims to improve the biological performance of the base material as well as to facilitate a controlled release of active molecules.

Right after the main features of each component are presented, and their uses and applications are shortly reviewed to provide a general idea of the interest of bringing them to a combined system.

1.5.1.- Acrylates

Ethyl acrylate, EA, (Figure 1.2) belongs to the family of alkyl acrylate polymers, which is a family of monomers that are flammable, volatile, mildly toxic and colourless [183]. Acrylates can be polymerized by different processes but the use of one or another polymerization method has no great impact on main properties of the resulting polymer such as glass-transition temperature [184]. Despite its toxicity as a monomer, once EA is polymerized, post-polymerized and carefully washed to remove any trace or residual monomer, poly(ethyl acrylate), PEA, is non-cytotoxic.

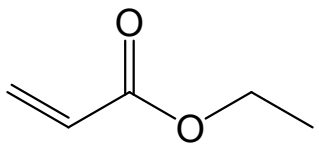

Figure 1.2: Chemical structure of ethyl acrylate (EA).

PEA is hydrophobic and behaves as an elastomer both at room temperature and at body temperature, thus it is capable to recover its shape after applied stresses. This rubber-like behaviour occurs because the main chain motions are not hindered, hence its glass transition temperature is quite low [184]. Moreover, its elastic modulus is in the range of those of biological tissues, and it is easily handled and suturable.

Cells do not attach directly to the materials surface but to the serum or ECM proteins previously adsorbed into the material surface [185]. PEA has been shown to favour the adhesion of proteins such as laminin [186] or fibronectin [185, 187] and to facilitate the formation of a protein network that contributes to increase cell adhesion despite the hydrophobicity of the material. The fact that these mediating proteins are capable of spontaneously forming this network on its surface is an indicator of the potential biocompatibility of this material.

Several different cell types have been tested with PEA and its copolymers with other acrylates, with very promising results. Fibroblasts and human umbilical vein endothelial cells (HUVECs) were cultured on a series of acrylate copolymers, and a trend was observed: the more hydrophobous the material, the better cell behaviour in terms of adhesion and spread was attained [188]. A similar trend was found when chondrocytes were seeded on acrylates with uniformly distributed hydrophobic groups; however, when the materials were produced with hydrophobic and hydrophilic nanodomains, the results improved [189]; similarly occurred with keratocytes [190]. Acrylates were also seeded with dental pulp stem cells, which uniformly covered the material surfaces. An acrylate-based substrate for neural cells was obtained, where stromal cells act as neurotrophic pumps [191]. PEA was found to support the culture and survival of neurons derived from neural stem cells as well; however, the outcome was better if a small hydrophilic fraction was added [192]. In the case of neural explants, a greater fraction of hydrophilic material improved cell attachment and differentiation [193]. Acrylates are additionally a suitable substrate for Schwann cells adhesion and proliferation [194]. Osteoblasts have also been cultured on acrylates, and cell behaviour was directly correlated with the fibronectin fibrillogenesis on the surface [187]. Finally, acrylate rich materials have also been studied as feeder-free substrates for both human embryonic stem cells and induced pluripotent stem cells, being found to promote colony formation [195].

In the scope of tissue engineering, acrylates have been employed to produce three-dimensional scaffolds with different architectures. Among other possibilities, ordered cylindrical orthogonal pores [196], spherical sponge-like interconnected pores [197], cylindrical elongated pores [198], or combinations of them have been obtained. The use of different pores typologies aims to biomimic tissues with different structures. For instance, the last ones were intended for axonal guidance [199] or dentin regeneration [200], and the scaffolds with cylindrical orthogonal pores have been

tested for brain tissue regeneration in rats [199]. Scaffolds combining a channelled porosity with spherical interconnected pores have been proposed for cardiac tissue engineering [131], for the channels to guide cardiomyocyte alignment and organization and the pores to allow nutrients and oxygen diffusion. Moreover, when implanted, they were found to be vascularizable without inducing great inflammatory response.

In particular, in this work PEA has been polymerized from EA via radical and crosslinked with ethylene glycol dimethyl acrylate (EGDMA) (Figure 1.3). The monomer and crosslinker radicals, transferred from a thermal or photo-initiator that attacks the double bound, react to generate a polymer network. Specifically, PEA scaffolds with spherical interconnected pores and grid-like interconnected channels are envisaged in this Thesis to be used for myocardial regeneration. As previously said, these scaffolds will be combined with hyaluronan and a self-assembling peptide to improve molecules diffusion throughout the scaffolds, enhance their biological performance, as well as to have a means to deliver molecules of interest.

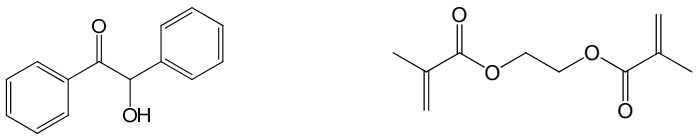

Figure 1.3: Chemical structure of the initiator benzoin (left), and the crosslinker EGDMA (right).

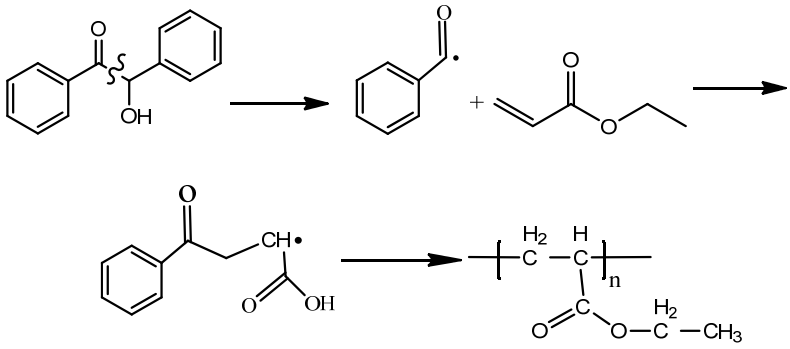

Figure 1.4: Scheme of the polymerization reaction of ethyl acrylate into poly(ethylacrylate): formation of radicals, transfer to monomers, chain growing and termination.

1.5.2.- Hyaluronan

Hyaluronic acid (HA) (Figure 1.5) was isolated for the first time in 1934 by Karl Meyer and John W. Palmer [201]. Initially it was named hyaluronic acid because it was obtained from the vitreous humour of the eye and contained uronic acid: hyaloid (vitreous) and uronic acid. But in 1986 Balazs *et al.* proposed to rename it as hyaluronan, to underline that it is a polyanion [202]. Many other different names have been proposed, among them, as a curiosity "highly ironic acid" was proposed [203] to emphasize the subtleties and intrinsic difficulties associated to the handling of this material.

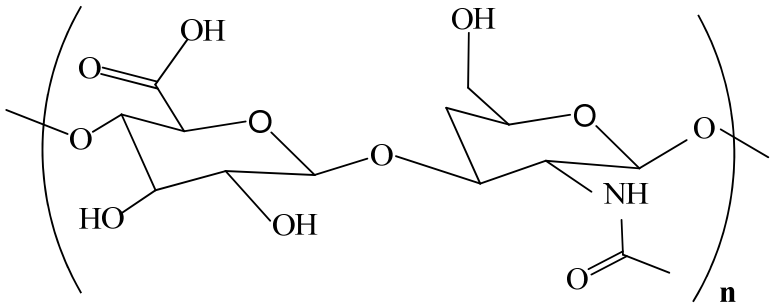

Figure 1.5: Chemical structure of hyaluronic acid.

HA is a linear non-sulfactated glycosaminoglycan. The repeating units of this linear polysaccharide are formed by (β,1-4)-D glucuronic acid and (β,1-3)-N-acetyl-D-glucosamine [204]. It can be found in the native state as a high molecular-weight polymer reaching a molecular weight up to several millions of Daltons [203]. Hyaluronan is ubiquitously present in the human body in a great variety of tissues at different concentrations. It can also be obtained from different sources: bacterial, rooster comb, shark skin and bovine eye ball [205].

Given its unique physico-chemical properties and biological characteristics, it plays a multitask role. HA has a high capacity for water retention and therefore regulates

water homeostasis: transports ions and nutrients and also preserves hydration [206]. This capability of retaining water enables it to bear compression loads in joints [207]. HA is a viscoelastic polymer, and because of its rheological properties it acts also as a natural lubricant in the joints. HA exhibits a high viscosity in aqueous solution even at low concentrations because of its high hydrodynamic radius in water. However, the hydrodynamic radius can be reduced by varying the pH of the starting solution [208], which allows the preparation of HA solutions at higher concentrations with lower viscosities. This might be of interest during the preparation of HA-based materials.

Regarding its biological role HA was found to influence cells behaviour. Hyaluronan interacts with other constituents of the ECM, to create cell-protective environments [209]. HA also interacts with cells through specific binding sites named hyaladherins [206], and regulates their behaviour; it can activate cell receptors like CD44 that can trigger intracellular signalling cascades that determine cytoskeleton activation and affect cell migration [210]. HA also mediates biological events, such as cell proliferation and differentiation during development [211]. Albeit, the hydrophilic and polyanionic nature of the HA does not particularly favour attachment to the anionic cell surfaces, and better cell adhesion is observed for HA with low than for HA with high molecular weight [212].

Another interesting feature of this molecule, is that its degradation products, 4-25 sugar units long, are capable to promote angiogenesis [213], by inducing endothelial cells proliferation and migration through the activation of a signal transduction pathway [214]. It has been reported that the use of HA oligosaccharides *in vivo* increased the mean number of blood vessels per mm. However, longer units of HA are not angiogenic; even worst in the case of high molecular weight HA, which can become anti-angiogenic [215].

Given its good biocompatibility, biodegradability and non-immunogenicity [216], HA has turned a frequently used polymer in the biomedical field for many different applications, [217] as wound dressing [218], to inhibit cell adhesion in the prevention of surgical adhesions [219], to avoid protein absorption [220], for knee viscosupplementation [221], as a component of implants [222], in cosmetics [223], as a scaffold for tissue regeneration [209], as a drug carrier for controlled release [224] or for cell encapsulation [225].

Nonetheless, the use of HA as a biomaterial is restrained by several issues, namely: short time of residence in the site of interest, water solubility, low mechanical properties and lack of manipulability. To overcome these limitations, modifications of the HA structure or crosslinkings have been proposed. The variety of crosslinkers and modifications introduced are very wide [226], but can be classified according to the HA functional group attacked: the carboxyl group, the hydroxyl group or other groups previously introduced in the sugars of the HA structural unit [209]. When the reaction occurs through the carboxyl group, a crosslink via ester linkage is obtained. On the other hand, when the hydroxyl group is involved, the crosslink takes place via ether linkage. In the case of previously modified hyaluronan, the outcome depends on the type of modification previously introduced [226]. Depending on the crosslinker agent of choice, different degrees of crosslinking can be achieved. Therefore, materials produced with different crosslinkers exhibit different physico-chemical characteristics [209]. For instance, materials with anisotropic swelling can be obtained by crosslinking up to different extents in different areas by the consecutive use of a chemical crosslinking followed by a patterned photo-crosslink [227].

Hyaluronan, either alone or combined with other biomaterials, has been proposed in cardiac tissue engineering approaches *in vitro* and *in vivo*. It has been used as a knitted HYAFF (hyaluronan benzyl ester) mesh *in vitro* to culture neonatal rat

myocytes inducing cell organization into sarcomeric structures and spontaneous contraction [228]. A glass substrate was provided with HA microchannels for the cardiomyocytes to preferentially attach and form beating cardiac organoids in the fibronectin-coated glass lane [229]. Different HA hydrogels [64] implanted *in vivo* demonstrated to be suitable for new artery formation in ischemic myocardium. Two weeks after implantation in the hind limb of rats, the hydrogels were degraded with low immune response and induced strong angiogenesis. HA can also be used as a scaffold to lodge mesenchymal stem cells (MSCs) in a localized and controlled manner into the infarcted heart area [230], allowing the migration of the seeded cells from the scaffold to the border zone of the infarct. When HA alone (without cells, drugs or growth factor), was directly injected in an infarcted heart, it was capable of increasing the thickness of the heart wall and inducing functional recovery [231].

To overcome its limitations, hyaluronan has been combined with other materials. For instance, HA mechanical properties can be tuned by combining it with alginate by the use of an hydrazone-based crosslinking [232]. Moreover, this material allowed the generation of a contractile tissue when it was used to encapsulate neonatal rat cardiomyocytes. The degradation of the HA-based biomaterials can also be tuned by using a crosslinker with MMP degradable peptides [233]. The addition of these peptides improved cell spreading. A hydrophilic pH-sensitive nanofibrous hydrogel was co-assembled with HA, and was capable of supporting both neonatal rat cardiomyocytes and human embryonic stem cells derived cardiomyocytes [234]. Cardiosphere-derived cells were delivered in mice using a thiolated hyaluronan-based hydrogel covalently linked or not with thiolated denatured collagen. It was observed that the retention rate achieved with the hydrogel without collagen was similar to that of cells delivered in phosphate buffer saline, either by a low physical retention or poor cell survival and adhesion of HA [77]. HA combined with collagen was also used to fill the pores of a decellularized urinary bladder to allow cell delivery into the

scaffold [235]. In the *in vivo* study in a mouse model of myocardial infarction, the functional benefits observed were attributed to a paracrine effect.

The promising results obtained in cardiac applications combined with the angiogenic potential of the degradation oligosaccharides, makes HA a good candidate for its use in easily vascularizable scaffolds for cardiac tissue engineering.

In this Thesis, HA is used to coat or completely clog the pores of acrylic scaffolds. Divinylsulfone (DVS) is used as crosslinker of HA chains (Figure 1.6). This crosslinking reaction occurs very fast in alkaline solutions at room temperature; DVS crosslinks HA chains by forming ether bonds between the hydroxyl group of two HA molecules. After the crosslinking process, very stable, easily handled hydrogels are obtained.

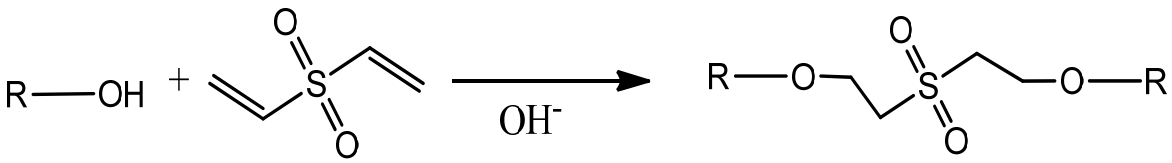

Figure 1.6: Scheme of the HA hydroxyl group reaction with divinylsulfone in basic media forming ether bonds. Modified from [209].

1.5.3.- Self-assembling peptides

Self-assembling peptides (SAPs) are a relatively new family of synthetic materials. This group of materials has in common the peculiarity that are formed from short peptides, which under a change in their environment, like a pH modification or the addition of salts [71], are capable to undergo a self-assembling process. Molecular self-assembly is defined as "the spontaneous organization of molecules under thermodynamic equilibrium conditions into structurally well-defined arrangements due to non-covalent interactions" [236]. These interactions include hydrogen bonds, Van der Waals forces, hydrophobic-hydrophilic interactions and water mediated hydrogen bonds [237].

There are different types of self-assembling peptides, attending to the structure they adopt after their self-assembly process. Type I SAPs form beta sheet structures in aqueous solution. Type II SAPs form beta-sheet structures at room temperature but can adopt alpha–helix structures at high temperatures and can maintain them after cooling to room temperature for several weeks. For its part, type III SAPs form monolayers on surfaces that can pattern cell growth [236].

When a pH change is induced or a salt is added to a type I SAP, the charges are partially neutralized and the alternating hydrophilic and hydrophobic amino acid residues of the peptide can adopt beta-sheet structures. When the peptides are in the beta-sheet configuration, have two surfaces, one polar with ionic side chains and other non-polar rich in alanines. Both surfaces are complementary to one another [238] and can form ionic pairs (dimers). If the concentration is high enough, and the conditions are adequate, the oligopeptides can assemble to form a 3D network that mimics the ECM, with fibres in the range of 10-20 nm diameter and mesh sizes (pores) about 50-100 nm in diameter [236]. The size of the mesh can be tuned by changing the peptide concentration [239].

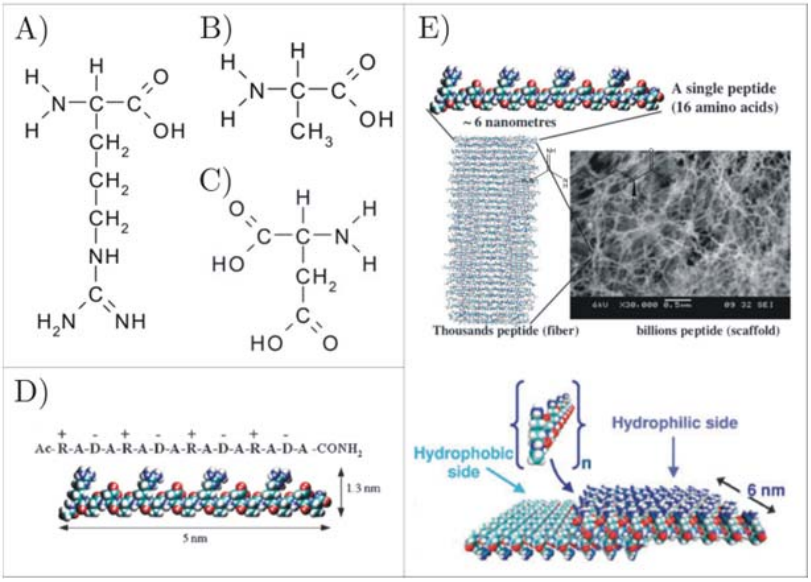

Figure 1.7: Chemical structures of arginine (A), alanine (B) and aspartic acid (C). Molecular drawing of RAD16-I in beta–strand conformation (D) and schematic representation of the self-assembling process (E), adapted from [240] with permission of the Royal Society of Chemistry.

The adopted beta-sheet configurations are stable through pH or temperature variations up to pH 11 and 90°C [241]. This great stability entails the need of a deep characterization to minimize the risks associated with its use *in vivo*, because these SAPs are structurally similar to amyloids [242], which regulate biological functions and also have been related with several pathologies and neurodegenerative disorders such as Alzheimer. Nevertheless, results obtained both *in vitro* and *in vivo* so far have been very positive as will be exposed next.

Since SAPs are synthetic, present several advantages over animal-derived ECM materials like Matrigel® or collagen membranes. There is no risk of illness transmission and all the batches are homogeneous, *i.e.*, there is no variation in the amount of impurities, residual proteins or growth factors among lots [243]. Moreover, RAD16-I (Ac-RADARADARADARADA-CONH2) and RAD16-II (Ac-RARADADA RARADADA-CONH2) SAPs were proved to be non-immunogenic and to produce no inflammatory reactions in animals [243, 244].

SAPs have arisen a lot of interest because of their great potential in regenerative medicine. As previously said, they can mimic the extracellular matrix and even more can be used to encapsulate cells. But providing a fibrous ECM-like environment does not guarantee success; the constituent sequence of the peptide is also important. When HUVECs were cultured into four different SAPs, it was observed that cells were only capable to form elongated structures and connected capillary-like structures in RAD16-I and RAD16-II, precisely the peptides exhibiting better cell adhesion [245]. Combining several cell types with peptides might also be of interest. Indeed, when endothelial cells were cultured in a SAP and subsequently cardiomyocytes were added, the cardiomyocytes acquired spatial organization and endothelial cells exerted a protective effect on them [100].

The intended applications of these peptides are very vast, and have been tested with many different cell types. The SAPs suitability for cell attachment has been verified with a wide variety of cells (see [238]), with positive results. Despite the good biological performance achieved, the mechanism by which cells attach to the peptide chains is still unclear; so far it has been established that cells do not attach to SAP via RGD-dependent integrin receptors [246]. Interestingly, SAP lack of known cell adhesion sites, therefore they could act instead as templates on which cells can deposit its own matrix [245].

In the works listed next, not only the adhesive properties but the SAPs bioactivity was evaluated. Among others, SAP have been employed with mouse embryonic fibroblasts; the obtained 3D structures can help to recreate *in vitro* certain morphogenetic processes [247]. In a different work, mouse embryonic stem cells and mouse embryonic fibroblasts were cultured in RAD16-I to study its influence on osteogenic differentiation [248]. Hepatocyte-like spheroid clusters were also obtained [249] thanks to the use of RAD16-I that provided a truly 3D environment. In the

field of neuro-regeneration SAPs have also been intensely studied. RAD16-I biocompatibility was tested with human neural stem cells, exhibiting good cell survival and allowing cell migration and neural differentiation [250]. RAD16-II was reported to support functional synapse formation [251]. For its part, another class of peptides, the amphiphiles, was reported to promote axon elongation and inhibit glial scar formation after spinal cord injury in mouse models [252].

Interestingly, self-assembling peptides can be used as injectable cell carriers. For instance, RAD16-I was proved to be capable of maintaining cells in the site of interest when used as a delivery system of different types of cells into the heart. For example, when injected in combination with cardiac progenitors in mice, angiogenesis and differentiation into cardiomyocytes and vascular smooth muscle cells was reported [253]. RAD16-II likewise has been shown to create microenvironments in the infarcted myocardium that are infiltrated with endothelial and smooth muscle cells, suggesting its potential for vascularization [71]. Indeed, it was also observed that combining RAD16-II with neonatal cardiomyocytes increased the density of endogenous α-sarcomeric actin positive cells.

These peptides can be 'decorated' if needed by attaching sequences either to the N-terminus or the C-terminus to enhance their biological performance. For example, the laminin-derived YIGSR and RYVVLPR sequences and the type IV collagen TAGSCLRKFSTM sequence have been attached to RAD16-I and the formation of cell confluent monolayers was enhanced [254]. In other works, RAD16-I was modified to incorporate cell adhesion, differentiation, bone marrow homing motifs and osteogenic growth peptide, showing the ease of incorporating different motifs into the peptide and the biological potential of such modification [255, 256]. RAD16-I modified with the RGDSP motif was injected in combination with marrow derived cardiac stem cells into a myocardial infarction model in rat, enhancing the efficiency of

transplantation and improving the cardiac function [257]. Another SAP, the Q11 (Ac-QQKFQFQFEQQ-Am), has also been chemically modified to stiffen the obtained matrix, and improve its manipulability, simultaneously with the addition of adhesion motifs that enhanced HUVECs proliferation [258]. The use of a 3D system enhanced neural progenitor survival and differentiation, but functionalizing RAD16-I with laminin-I was found to be essential for the growth of human neural progenitor cells in 3D patterns [239]. Hepatocytes functionality can be maintained [259] by using a functionalized peptide with the GRGDSP motive.

Interestingly, SAPs gels can be used as a controlled release system by incorporating growth factors, drugs or peptides to induce cell fate. The self-assembling peptide RAD16-II can be used as a drug vehicle as it is capable to bind to PDGF-BB; in combination, it can be used as a controlled release system in the heart able to protect cardiomyocytes, reduce infarct size and maintain cardiac function [260]. RAD16-II has been used to deliver PDGF and FGF [261]. The first is arteriogenic and the second is angiogenic; their combination targets endothelial cells and vascular smooth muscle cells. Infarct size and cardiomyocyte apoptosis were considerably reduced in rats with the combined use of these factors and the SAP. The capillary and arterial density was recovered, and cardiac function was improved. RAD16-II combined with insulin-like growth factor 1 (IGF-1), a cytokine that protects and promotes cardiomyocytes growth, has also been used as a delivery system for cardiomyocytes. The addition of IGF-1 acted reducing cell apoptosis and improving systolic function [262]. When cardiac progenitor cells (CPC) were delivered with a self-assembling peptide tethered to IGF-1, not only the injected but also the resident CPC were activated and contributed to the observed regeneration [263].

Even after the self-assembly, SAPs are very week materials, difficult to manipulate, move or implant if is not through injection. Therefore, it might be of interest to combine them with other materials to provide the structural integrity and manipulability that these peptides lack. For instance, SAPs have been used in combination with Schwann cells, to fill the lumen of cellulose tubular membranes, to enhance nerve regeneration in rats [264]. In a quite different work given its application, a porous titanium foam was filled with an amphiphile peptide that was capable of encapsulating cells and nucleate hydroxyapatite [265] for bone regeneration.

In the present work, the RAD16-I peptide is used as pores' filler in the acrylic scaffolds, to improve its integrity and manipulability. RAD16-I is composed of arginine (R), alanine (A) and aspartic acid (D) distributed as Figure 1.7 shows. The fibres obtained after the self-assembling of the gel are 5-10 nm thick.

Chapter 2:

Materials and methods

2.- Materials and methods

2.1.- Materials

2.1.1.- Bulk materials

Acrylates

Films of the homopolymers poly(ethyl acrylate) (PEA, Figure 1.2) and poly(acrylic acid) (PAAc) (Figure 2.1) as well as a 90% wt. EA, 10% wt. AAc copolymer (P(EAcoAAc)) were obtained by UV polymerization. Briefly, ethyl acrylate (EA; 99%, Sigma-Aldrich) and acrylic acid (AAc; 99%, Sigma-Aldrich) were stirred at the given proportions with 2% wt. of ethylene glycol dimethyl acrylate (EGDMA; 98% Sigma-Aldrich, Figure 1.3) as crosslinker and 1% wt. of benzoin (Scharlab, Figure 1.3) as initiator for 15 min at room temperature (RT). Then, the solutions were injected between two glass plates separated by a wire of 0.8 or 1.2 mm diameter, and placed in an UV oven for 8 h for the polymerization to occur. Subsequent post-polymerization was carried out at 90°C for 24 hours.

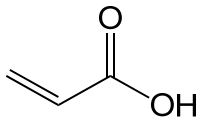

Figure 2.1: Chemical structure of acrylic acid.

At that moment films were washed for 24 h in boiling ethanol (EtOH), which was changed every 8 h. Finally, films were dried at room conditions for 24 h, under vacuum 24 h more and under vacuum at 60°C for 24 extra hours before any ensuing experiment.

Hyaluronan

In order to obtain hyaluronan (HA, Figure 1.5) discs, hyaluronic acid sodium salt, (99%, Sigma, 1.63 MDa, obtained by fermentation of streptococcus equi bacteria) was dissolved in a 0.2 M aqueous sodium hydroxide (NaOH; extrapure, Scharlau) solution to a final concentration of 5% wt. by gently shaking for 24 h and stirring at 200 rpm for 2 extra hours. Once HA was perfectly dissolved, divinyl sulfone (DVS; 97%, Aldrich, 118.15 Da, Figure 1.6) was added in a 90% DVS/HA monomeric unit molar ratio to the HA solution and stirred at 300 rpm for 1 minute. Then, the DVS/HA solution was poured into a 8.5 cm diameter Petri dish and the crosslinking reaction was let to occur for 24 h. The obtained gel was punched into 5 mm-diameter discs. The discs were washed 5 times for 24 h in a 50/50 vol. acetone/distilled water mixture. At that point, the discs were dried in an oven at 40°C for 5 h followed by 24 h of vacuum at RT. Samples were kept under vacuum and darkness until used.

2.1.2.- Spin coated materials

PEA and P(EAcoAAc) films to be used for spin coating were obtained as previously described in section 2.1.1, but without adding the crosslinker in order to allow their subsequent dissolution.

After the post-polymerization, the obtained films were intensely dried under vacuum and temperature (60°C) in order to remove any residual monomer trace remaining in the samples. Next, PEA films were dissolved in toluene (synthesis grade, Scharlab) to a final concentration of 2% wt. by stirring overnight. Analogously P(EAcoAAc) films were dissolved in an 80/20 vol. toluene/dioxane (extra pure, Scharlab) mixture to a final concentration of 2% wt.

Finally, ultra-thin polymer films were obtained on 12 mm diameter glass coverslips by spin casting 100 µL of the polymer solutions at 3000 rpm with an acceleration of

3000 rpm/s for 30 s in a spin coater (Brewer Science). Once obtained, samples were dried under vacuum and 60°C overnight to remove any trace of solvents.

2.1.3.- Scaffolds with orthogonal pores

PEA scaffolds with orthogonal pores (PEA-o hereafter) were obtained with a nylon template previously prepared, following the procedure presented in [196]. Concisely, eight or sixteen layers of nylon fabrics (SAATI S.A., Barcelona, Spain) with nominal thread diameter equal to 150 μm and mesh opening of 300 μm were sintered under pressure and temperature. The porogen template was placed between glass plates and a mixture of EA monomer with 0.1 wt.% of azo-bis-isobutyronitrile (99%, Fluka), AZBN, (Figure 2.2) as thermal initiator, and 2 wt.% of EGDMA as crosslinker was injected in it and polymerized for 24 h at 60°C. Next a 24 h post-polymerization step at 90°C was carried out. Finally, the materials were washed in 30% nitric acid aqueous solution (HNO_3; 60%, Scharlab), repeatedly changed, during 4 days to dissolve the nylon template. Then, scaffolds were washed in boiling water for 16 h (the water was changed every 8 hours) to remove nitric acid traces. Finally, scaffolds were dried following the same steps as for films. The resulting thickness was around 1 mm for the scaffolds prepared with 8 layers templates, and near 1.6 mm for those prepared with templates having 16 layers.

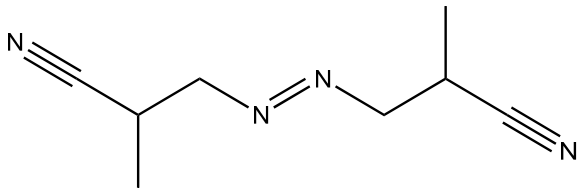

Figure 2.2: Chemical structure of azo-bis-isobutyronitrile.

2.1.4.- Scaffolds with spherical pores

PEA scaffolds with spherical pores (PEA-s hereafter) were obtained by using a PMMA template obtained by sintering microspheres (PMMA; Colacryl dp 300) with pressure and temperature, following the procedure described in [197]. These templates were also placed between glass plates and then, the EA monomeric solution with 2% wt. EGDMA and 1% wt. benzoin was injected and polymerized with UV light for 24 h and finally post-polymerized for 24 h extra hours at 90°C. The PMMA template was leached by acetone in a soxhlet. Once PMMA was completely removed, acetone was progressively exchanged with water and then the scaffolds were dried following the same steps as for films.

2.1.5.- Nitric acid treatment

PEA films were cut either in (0.5x2.5 cm^2) bars or punched in discs of 5, 7 or 10 mm diameter depending on their intended use. Samples were immersed in a HNO_3/water 1/1 vol. solution and placed in a shaker for 4 days and 16 hours (PEA-4d), 8 days and 16 hours (PEA-9d) or 16 days and 16 hours (PEA-17d). These nitric acid treatments simulated the washes applied to remove the nylon template employed to produce the scaffolds with cylindrical, orthogonally interconnected pores. At the given times, samples were removed, dried with a filter paper and washed for 16 h in boiling water (the water was changed every 8 hours). Next, they were left overnight in fresh water and afterwards dried for 24 h at room conditions, followed by 24 h under vacuum at RT and finally dried for 24h at 40°C in vacuum.

2.1.6.- Hyaluronan coating

Scaffolds coating procedure

Hyaluronan solutions to coat the pores of scaffolds were prepared as follows: HA was dissolved in 0.2 M NaOH(aq) solution at concentrations of 0.5%, 1% 2% and 5% (wt/wt %) as previously described in the 2.1.1. section.

Given the hydrophobicity of the employed scaffolds, the HA solution was forced into their pores by applying vacuum with a syringe. Briefly, 1x1 cm^2 or 1 cm diameter scaffold, was introduced into a syringe, next the HA aqueous solution was loaded and all the air was removed. Then the syringe tip was sealed and 5 strokes of 4 mL each were applied, so that the HA solution penetrated the scaffold's pores.

Once the sample was uniformly soaked with the HA solution, in order to achieve a uniform drying and to avoid the contact of the soaked material with any surface, a thin thread was passed transversally to the samples and they were hanged from it. Samples were dried at room conditions for 24 h, and then under vacuum for another 48 h, and finally 24 h extra under vacuum and with temperature (40°C). Samples were subjected from 1 to 5 filling-drying cycles.

Crosslinking of the hyaluronan coating

The HA coating on scaffolds obtained as described above was crosslinked with divinyl sulfone (DVS, 97%, Aldrich, 118.15 Da). First of all, samples were immersed during 20 min in 5 mL of a 80/20 vol. mixture of acetone (synthesis grade, Scharlau) and 0.2 M NaOH aqueous solution with a pH of 11-12 adjusted with HCl (≥99.8%. Sigma-Aldrich). DVS was next added in a 90% DVS/HA monomeric unit molar ratio, dissolved in 1 mL of the 80/20 acetone/NaOH solution. Samples were left in the solution for 24 h to ensure that the crosslinking reaction was completed. Then, samples were rinsed with a 20/80 vol. acetone/distilled water mixture for 30 min. Afterwards samples were washed with distilled water for 30 min, and finally were dried as previously described, hanging from a thread at room conditions, then under vacuum and finally under vacuum with temperature. A group of coated samples, were swollen for four days immersed in PBS, were frozen by immersion in liquid nitrogen for 10 minutes, and then lyophilized at -80°C in a LyoQuest-85 (Telstar).

2.1.7.- SAP combination with polymeric materials

Preparation of the self-assembling peptide solution

The self-assembling peptide employed was RAD16-I (Puramatrix, BD Biosciences). The SAP starting solution was sonicated for 30 minutes, and then diluted with ultradeionized water to a final concentration that varied depending on the experiment. The stock solution was sonicated again prior to each use in order to disrupt the aggregates that could be formed during storage.

SAP adsorption on films

Spin coated samples of 12 mm diameter of PEA and P(EAcoAAc) were incubated in 100 μL of SAP solution each for 1 hour at 37°C, for the SAP to adsorb on the material surface. Different concentrations were used depending on the experiments ranging from 0.1% down to 0.025%. To self-assemble the peptides, samples were transferred into a chamber with a NaOH(aq) 12 M ambient, and left in this atmosphere for 4 hours, analogously to the procedure employed in [266].

Scaffolds and SAP combination

An analogous procedure to that followed to obtain the HA coatings was followed. Briefly, polymeric scaffolds were placed in a syringe and then the SAP solution was loaded; the luer tape of the syringe was sealed and several strokes of 4 mL were applied to ensure the penetration of the solution inside the scaffold's pores. In some cases, the scaffolds were pre-conditioned by filling the pores with distilled water applying pressure with a syringe prior to the filling with the peptide, to facilitate the entrance and distribution of the peptide through the scaffold pores.

2.2.- Experimental techniques

2.2.1.- Scanning electron microscopy (SEM)

A JSM-5410 scanning electron microscope, (JEOL Ltd., Tokyo, Japan), was employed to morphologically characterize the obtained materials (either bare scaffolds or coated with HA). Both samples' surfaces and inner sections were observed. Samples were immersed in liquid nitrogen and fractured when frozen to expose the inner cross section without damaging the porous structure. Prior to observation, samples were sputter-coated with gold. The working distance was fixed at 15 mm and the acceleration voltage at 10 and 15 kV.

2.2.2.- CryoSEM

Swollen samples were mounted in a specimen holder and immersed in nitrogen slush. Once frozen, the samples were transferred into a JSM 6300 microscope (JEOL Ltd., Tokyo, Japan) in the cryoSEM mode. An inner section was then exposed by fracturing the sample, and the ice sublimation was started at -80°C. After 40 minutes of sublimation, samples were sputter-coated with gold and examined at 20 kV of acceleration voltage.

2.2.3.- Energy Dispersive X-ray Spectroscopy (EDS)

Salts deposition on the surface and cross sections of bulk PEA fatigued or measured in PBS immersion was assessed by microanalysis in an Energy Dispersive Spectrometer from Oxford Instruments, attached to the Scanning Electron Microscope JSM 6300 (JEOL Ltd., Tokyo, Japan). Samples were previously sputter-coated with carbon under vacuum. Spectra were taken at 10 kV

2.2.4.- Atomic force microscopy (AFM)

AFM images were obtained in a Multimode AFM device equipped with NanoScope IIIa controller (Digital Instruments-Veeco) operating in tapping mode in air, to characterize the interaction between the SAP and the studied polymers. Silicon-cantilevers (Veeco, Manchester, UK) were used with force constant of 2.8 N/m and resonance frequency of 75 kHz. The phase signal was set to zero at a frequency of 5-10% lower than the resonance frequency of the tip, as suggested by the manufacturer. Drive amplitude was 600 mV and the amplitude set point was 1.8 V. The ratio Asp/A0 was kept equal to 0.8.

The observed samples were polymeric spin coated films with a SAP gel coating adsorbed on the surface as previously described in 2.1.7. Once the films were retrieved from the NaOH atmosphere, the excess of SAP solution was carefully removed with a paper, and then samples were gently rinsed with ultradeionized water. They were subsequently dried for 30 min under a lamp, mounted and observed under the AFM.

2.2.5.- Density measurements

The densities of the films with different chemistries or after acid rinses of different length, as well as those of scaffolds with coating treatments were evaluated with a Mettler Toledo AE-240 balance with a sensitivity of 0.01 mg combined with a density accessory kit (Mettler ME 33360) through Archimedes' principle. Perfectly dry samples were weighed in air and immersed in N-octane (95%, Fluka), at RT, and [Equation 2.1] was applied:

$$\rho = \frac{\rho_{N-oct} \cdot W_{air}}{W_{air} - W_{N-oct}} \qquad \textbf{[Equation 2.1]}$$

where ρ_{N-oct} is the density of N-octane (0.703 g/cm^3), W_{air} is the measured weight of the discs in air and W_{N-oct} is the weight of the discs immersed in N-octane, and ρ is the measured density of the sample. Density was determined in triplicate for each composition and treatment.

2.2.6.- Porosity

The porosity, π, of the bare and filled scaffolds was calculated by applying:

$$\pi = \frac{V^{pores}}{V^{app}} = 1 - \frac{mv}{V^{app}} \qquad \text{[Equation 2.2]}$$

m being the sample's weight, v the specific volume of the bulk material ($v = 1/\rho_{bulk\ material}$) and V^{app} the apparent volume (obtained by measuring its height and diameter, and assuming that the sample is cylindrical).

2.2.7.- Contact angle measurements

In order to study the surface wettability of different materials (or the same material after different treatments), the contact angle of 3 μL drops of water (extra pure, Scharlau), formamide (99.5%, Aldrich) and diethylenglycol (99%, Aldrich) were measured on the surface of the materials. A Dataphysics OCA instrument (DataPhysics Instruments GmbH, Filderstadt, Germany) was used for this purpose. Samples treated with nitric acid or containing acrylic acid units (Chapter 3), were measured either in their dry state or after swelling by immersion in water for 48 h to increase the polymeric chains mobility.

Spin coated samples either bare or with RAD16-I adsorbed on their surface (Chapter 6) were measured in their dry state, or after swelling in a 100% relative humidity (RH) atmosphere for 3 days, to elucidate the influence of maintaining the samples in RH (as occurs during the preparation of AFM samples with RAD16-I adsorbed) on their wettability.

In order to further characterize the interaction of the SAP with the different bulk materials, the contact angle of 3 μL drops of the SAP solution at 0.1% and 0.025% concentrations was also determined. Measurements were carried out at least 10 times for each liquid, material composition and treatment.

2.2.8.- Swelling kinetics experiment

Samples in Chapter 3 were swollen by immersion in different media to study the influence of chemistries or acid rinsing treatments in terms of swelling degrees. These media were: water, 0.2 M NaOH(aq) phosphate buffer solution (PBS) or aqueous solutions with constant ionic strength but different pH. In particular, solutions with an ionic strength of 1.0 M and with pH of 2, 4.6 and 8, respectively were prepared according to [267] with Na_2HPO_4 (extra pure, Scharlab), citric acid anhydrous (Sigma-Aldrich) and KCl (Sigma-Aldrich). These swelling experiments were performed at RT until no weight change was further detected.

For PEA-o scaffolds having their pores coated with hyaluronan (samples referred in Chapter 5), the water sorption capacity was evaluated by immersion in PBS, and in a vapour ambient at 37°C and 66% RH (water activity equal to 0.66). Samples were placed in a tightly sealed test tube each over a supersaturated potassium iodide (extra pure, Scharlau) aqueous solution [268], avoiding any contact of the samples with the solutions.

Bulk PEA before and after being fatigued under cyclic loading (Chapter 4) were swollen in EtOH and 50/50 EtOH/water mixtures at RT until no weight change was further observed.

In all experiments samples were weighed vacuum-dried before the immersion and swollen at selected time points. After withdrawal at such points, the liquid remaining

on the surface was carefully removed with a filter paper prior to weighing. The water uptake was determined with [Equation 2.3], where W_t is the weight of the sample swollen at time t and W_0 is the weight of the dry one. Water content (WC) was determined in triplicate for each time point and composition or treatment, as:

$$WC = \frac{W_t - W_0}{W_0} \qquad \text{[Equation 2.3]}$$

The equilibrium water content (EWC) was considered as the final water content obtained, when no further weight variation was observed.

2.2.9.- Differential scanning calorimetry (DSC)

Differential scanning calorimetry measurements were undergone in a Metter Toledo DSC 823e (Mettler-Toledo Inc., Columbus, OH, USA) calorimeter to determine the thermal properties of the samples. Specimens were scanned in 30 μL pierced pans from -100ºC to 200ºC at 10ºC/min, under nitrogen atmosphere with a flux of 60 mL/min. Calibration was previously made with indium and zinc standard. Glass transition temperature (T_g) was determined as the midpoint with the software of the device (MettlerSTARe Software), and the heat capacity increase (ΔC_p) was determined for that T_g.

2.2.10.- Thermogravimetric analysis (TGA)

Thermogravimetric analyses were made in a TA SDT Q600 thermobalance (TA Instruments, New Castle, DE, USA) in order to estimate the composition and thermal degradation of the samples. Briefly, thoroughly dry specimens (dried under vacuum and 60ºC for at least 24 h before measurement) weighing around 11 mg were scanned from 25ºC to 1000ºC at 10ºC/min under a nitrogen flux of 50 mL/min.

2.2.11.- Fourier Transformed infrared spectroscopy (FTIR)

A Thermo Nicolet Nexus FTIR (Thermo Fischer Scientific Inc., Waltham, MA, USA) spectrometer was employed to determine the surface composition of bulk samples before and after different treatments. The spectra were obtained in the ATR mode (Attenuated Total Reflection), with a resolution of 8 cm^{-1}, between 500 and 4000 cm^{-1} as the average of 68 scans.

2.2.12.- Toluidine blue staining

Discs of different materials (PEA, PAAc and its 90/10 copolymer) and nitric acid treatments (Chapter 3 samples) were immersed in a 0.1% toluidine blue (Sigma-Aldrich) aqueous solution for 30 s, followed by a gently rinse with distilled water to remove the excess of staining. This dye revealed the presence of acidic groups either introduced by adding acrylic acid units in the composition or by the nitric acid treatment.

2.2.13.- Alcian blue staining

Hyaluronan presence in coated PEA-o samples was assessed by alcian blue staining (Chapter 5). Samples were immersed in an alcian blue solution (at 1% wt./vol. in distilled water at pH 1–2, 8GX certified, Sigma-Aldrich) for 10 min and then rinsed with distilled water for 2 min prior to their visual observation.

2.2.14.- Congo red staining

A 0.1% wt./vol. congo red (Fisher) aqueous solution was employed to coarsely quantify the substrate-SAP interaction, as well as the effectiveness of the filling of the scaffolds' pores with it. Congo red is a specific dye for beta sheet structures, which is the secondary structure adopted by the SAP once the self-assembly occurs.

Once the protocol was tuned up, it was decided to immerse the samples in the congo red aqueous solution for 20 min, and wash with distilled water for 30 min prior to their examination.

2.2.15.- Protein loading and controlled release study

BSA was used as a protein model to evaluate the potential of the considered materials as a controlled release system. PEA scaffolds with cylindrical pores, coated with HA or filled with RAD16-I were studied as controlled release systems.

In order to do that, samples were loaded overnight at 37°C in 1.2 mL of a 1 mg/mL BSA (2 mg/mL in 0.9 % aqueous solution, Thermo scientific) solution in PBS. After the absorption, samples were transferred into 1.2 mL of fresh PBS each to follow the protein release. The supernatant was collected at selected time points (1, 2, 3, 4, 5, 6, 7, 8, 24, 48, 72, 96, 120, 144, 168, 192, 216 and 240 hours) and replaced with fresh PBS tempered at 37°C.

The BSA concentration in the supernatant was determined with a Micro BCA Protein assay kit (Thermo Scientific) following the manufacturer's instructions. Briefly, 100 μL of supernatant were mixed with 100 μL of the BCA mixture of reagents, incubated for 2 h at 37°C and read with a Victor Multilabel Counter 1420 spectrophotometer (Perkin Elmer, Waltham, MA; USA) at 570 nm. A standard curve ranging from 0 up to 100 μg/mL was employed to translate the absorbance values into concentrations.

2.2.16.- Dynamic mechanic thermal analysis (DMTA)

Dynamic mechanic thermal analysis measurements were carried out in a Seiko DMS210 instrument (Seiko Instruments Inc., Chiba, Japan) to determine the influence of the nitric acid on the mechanical properties of the PEA samples

(Chapter 3). Samples were scanned from -60ºC to 200ºC at 2ºC/min, at a frequency of 1 Hz and tension mode. Specimens were rectangular, 1 mm thick and approximately 5 mm wide.

2.2.17.- Compression tests

Mechanical compression tests were performed in an EXSTAR TMA/ss6000 equipment (Seiko Instruments Inc., Chiba, Japan). Bulk samples, bare scaffolds and filled scaffolds cylindrically shaped, with a diameter of 6 or 8 mm depending on the experiment, were measured. Experiments were carried out at RT and the load was increased from 0 to 150 g at 10 $g \cdot min^{-1}$ for the scaffolds combined with the SAP series. In the case of the HA discs and scaffolds coated with HA, samples were immersed in PBS during measurements; the load was uniformly distributed over the surface, a preload of 1 g was applied and the loading rate was 20 $g \cdot min^{-1}$ up to 450 g. The compressive moduli were obtained as the initial slope of the stress-strain curves in the linear deformation region.

2.2.18.- Mechanical tensile tests

Films and bare scaffolds were cut into test rods of 0.5x3 cm^2 approximately. Stretching tests were performed in a stress-strain Microtest SCM3000 95 (Microtest SA, Madrid, Spain) machine at a stress rate of 1% the initial length per minute until fracture. The elastic moduli were determined as the slope of the initial linear region of the strain-stress curves. All measurements were carried out at least in triplicate. All the moduli measured on porous materials are apparent, yet to facilitate the reading will be simply referred as elastic modulus.

2.2.19.- Torsional fatigue experiments

Square samples of bulk PEA and PEA-s measuring approximately 3x3 cm^2 were fatigued under torsional stress in a Microtest TEM/15/MA V1047 series device.

Samples were clamped from the ends and submitted to a rotating alternating movement of one of the clamps at a frequency of 1 Hz and a velocity of 90º/s for 7 days. After this testing period, samples were unclamped, and two discs of 8 mm diameter were punched from each. These circular samples were measured in a Perkin Elmer DMA8000 device in the dry state and after a 3 days swelling in PBS, under room conditions or immersed in PBS, respectively. The measurements performed were frequency scans from 0.01 Hz up to 100 Hz at 37ºC with a shear displacement of 0.05 mm.

2.2.20.- Tensional fatigue experiments

Bulk PEA and PEA-s test rods measuring 3x0.5 cm^2 were fatigued under tension stress in a Microtest SCM 4000 98 device. Samples were clamped from the ends and submitted to an alternating movement of one of the clamps producing a sinusoidal strain with amplitude of 30% the initial length of the sample and a frequency of 1 Hz. This fatigue program was performed either in the air at 37ºC or immersed in PBS at 37ºC for 7 days. Samples treated in immersion were previously swollen for 3 days. Once fatigued, samples were measured in a Perkin Elmer DMA8000 device following a frequency scan from 0.01 up to 100 Hz and a tension displacement of 0.05 mm. Measurements were performed with the samples fatigued in the air and immersed, either immersed in PBS after a previous swelling or dry in the air.

After testing, samples were rinsed with distilled water to remove any PBS salts that might have deposited on their surface. Once dried, samples were measured as explained in the Mechanical tensile tests section, until fracture.

2.3.- *In vitro* experiments

2.3.1.- Materials sterilization and conditioning

All the materials were sterilized prior to their use in cell culture experiments. Briefly, films were sterilized by exposing each side of the material to UV light for 2h. Bare scaffolds were sterilized by gamma radiation at 25 kGy from a 60Co source (Aragogamma, Barcelona, Spain). Scaffolds coated with HA were sanitized with EtOH/water 70/30 vol. solutions.

Preceding any cell culture, both films and scaffolds were conditioned by washing them three times with Dulbecco's Phosphate Buffer Saline (DPBS, Sigma-Aldrich) cell culture medium with 10% foetal bovine serum (FBS; Invitrogen) or ultradeionized water, depending on the experiment.

2.3.2.- Cell cultures

L929 fibroblasts

The L929 cell line of mouse fibroblasts (C34/An connective tissue, Sigma Aldrich) in its 9 to 18 passage was employed for a set of experiments. Cells were cultured until confluence in 75 cm^3 culture flasks, with 4.5 g/l glucose Dulbecco's Modified Eagle Medium (DMEM, Gibco) containing glutamine (Invitrogen), 10% of FBS, and 1% of penicillin/streptomycin (P/S, Life Technology). After reaching confluence, cells were trypsinized as explained in [160], collected and centrifuged at 1000 rpm for 5 min. Next they were resuspended, counted and diluted to the desired cell density.

For experiments contained in Chapter 3.2.3, fibroblasts were seeded on DPBS conditioned films, at a density of 5000 cells per sample sized for 96-well plates (ϕ= 5 mm) and 9800 cells on samples in 48-well plates (ϕ= 7 mm), in 20 and 40 μL

medium drops, respectively. Cells were cultured for 30 minutes to optimize adhesion and next the culture medium was completed up to 200 and 500 μL, respectively.

For Chapter 5 experiments, fibroblasts were seeded at a density of $2 \cdot 10^5$ cells in 20 μL drops in 10 mm diameter PEA-o scaffolds coated with HA, previously conditioned overnight in PBS and 1 h in DMEM containing FBS. Seeded scaffolds were firstly incubated for 30 min in a Titramax 101 shaker (Heidolph instruments, Germany) inside the incubator and after that time the medium was completed.

In the case of Chapter 6 experiments, fibroblasts were seeded into bare and SAP-filled scaffolds. Prior to their seeding, scaffolds were washed twice with either DPBS (for the bare scaffolds) or water (for the scaffolds to be filled right after with RAD16-I). The seeding on 8 mm diameter samples was performed by means of two different procedures:

(a) Static seeding: 10^5 cells were seeded on the upper surface of each piece of scaffold suspended in 20 μL of 10% sucrose (Sigma–Aldrich) aqueous solution. The samples were kept for 30 min in the incubator at 37°C, and then the culture medium was completed.

(b) Dynamic seeding: the cells were seeded on the scaffolds in the same number and way as above, but then the culture plate was smoothly shaken in a Titramax 101 shaker for 30 min; next the culture medium was completed.

In all experiments the employed culture medium was DMEM (4.5 g/L glucose) supplemented with 10% FBS, 1% P/S and was renewed every day or every two days.

Human Umbilical Vein Endothelial Cells (HUVECs)

HUVECs (Human Umbilical Vein Endothelial Cells; Gibco) in its 4th to 5 th passage, were cultured in F75 with Medium 200 (Invitrogen) supplemented with LSGS (Low serum growth supplement, Invitrogen) and 0.1% gentamicin (Gibco) and 1% P/S until 80% confluence was reached. Then, cells were trypsinized, collected and centrifuged at 180 g for 7 minutes. Cells were resuspended, counted and diluted up to the desired density.

In the case of Chapter 3.2.3 experiments, films were pre-conditioned by overnight immersion in DMEM with FBS. The employed cell density was 20 μL drops with 7700 cells for the 5 mm diameter samples and 15000 cells in 40 μL drops for the 7 mm diameter discs. 30 minutes after the seeding, the medium was completed and renewed every day.

Regarding the Chapter 6 experiments, prior to their seeding, scaffolds were washed twice with either DPBS (for the bare scaffolds) or water (for the scaffolds to be filled right after with RAD16-I). Cells were counted and seeded at a density of $4{\cdot}10^5$ cells per 8 mm diameter scaffold, and $4{\cdot}10^4$ cells per film in a drop of 40 μL and 10 μL, respectively. Scaffolds were firstly incubated for 30 min in the shaker named above, inside the incubator and after that time the medium was completed. The culture medium was renewed every day.

Co-culture of HUVECs and mesenchymal stem cells (MSCs)

In the co-culture experiment presented in Chapter 6 a commercial cell line of human mesenchymal stem cells derived from adipose tissue (gently provided by Dr. Ulises Gómez-Pinedo from the "Laboratorio de Medicina Regenerativa/Neurología y Neurocirugía", Instituto de Neurociencias, Hospital Clínico San Carlos, Madrid) in its 6th passage were cultured until confluence in F175 cm^3 culture flasks with Ham's F-12

nutrients mixture with 1% L-glutamine (Life technologies), 10% FBS and 1% P/S. Once confluence was reached, cells were trypsinized, collected and centrifuged at 1000 rpm for 5 min. Next, they were resuspended, counted and combined in a 1 to 3 proportion with HUVECs cultured and trypsinized as described in the previous sections.

Bare and SAP-filled scaffolds (both PEA-o and PEA-s), 5 mm diameter, were seeded with $4{\cdot}10^5$ cells in 20 μL drops, kept 30 min in the shaker inside the incubator and after that time the medium was completed. Bulk materials employed as references were analogously seeded but with $12{\cdot}10^4$ cells, because films present less surface available for the cells to attach. The employed medium for the co-culture experiment was a 1 to 3 mixture of MSCs and HUVECs media.

2.3.3.- Cell density assessment

Cell seeding efficiency, viability and proliferation rate was studied with the colorimetric assay MTS ((4,5-dimethylthiazol-2-yl)-5-(3-carboxymethoxyphenyl)-2-(4-sulfophenyl)-2H-tetrazolium, Cell titer 96 Aqueous One Solution cell proliferation assay Promega, USA). Concisely, after the selected times of culture, samples were gently rinsed with DPBS and moved into a new 96-well plate. A mixture of the MTS-reagent with phenol red free medium was prepared in a 1 to 5 proportion, and 200 μL of this solution were added into each well. After three hours of incubation in the dark inside the incubator (37°C and 5% CO_2), 100 μL aliquots were placed into new wells and their absorbance was measured with a Victor Multilabel Counter 1420 spectrophotometer (Perkin Elmer, Waltham, MA; USA) at 490 nm. Three replicates per time, material and treatment were measured in duplicate. Polystyrene wells were employed as positive control (C+) and the MTS reactant solution incubated in a well without cells as a negative control (C-).

Cell density was also estimated by means of a Quant-iT™ PicoGreen® dsDNA Assay Kit (Invitrogen). Briefly, at the selected times samples were washed with PBS and frozen in a -80°C freezer. Once thawed, samples were digested with Proteinase K (Roche) diluted 1 to 20 in DPBS at pH 8.1 for 16 h under gently shaking; next, the enzyme was inactivated for 10 min at 90°C. As soon as they were tempered, the samples were vortexed for 1 min and centrifuged for 1 min at 650 g. Next, 28.7 µL of the samples and standards were mixed with 28.52 µL of the Picogreen reagent at 1:200 concentration in Tris-EDTA (TE) buffer, and 100 µL more of TE buffer were added into each well in a 96-well plate. After 5 min of incubation, samples' fluorescence was measured in the above named spectrophotometer at an emission wavelength of 535 nm.

2.3.4.- Immunocytochemistry

At the selected time points, samples were gently rinsed with DPBS twice and fixed with a 4% paraformaldehyde (PFA; Panreac) solution at RT. After 10 min the solution was removed and the samples were rinsed with DPBS three times.

Subsequently, samples were incubated at RT with blocking and permeabilizing buffer (BPB) for 1 hour. BPB was composed of DPBS (Sigma-Aldrich), 10% FBS and 1% triton x-100 (Sigma-Aldrich). Finally, two 5 min DPBS rinses were done.

Once samples were blocked and permeabilized, different protocols were applied for a set of experiments:

DAPI staining

Samples were incubated with 1:5000 4′,6-diamidino-2-phenylindole dihydrochloride (DAPI; Sigma)/H_2O solution for 10 min, followed by two DPBS rinses.

DAPI and phallacidin staining

Samples were incubated with Biodipy-FL phallacidin (Invitrogen) at a concentration of 1:200 in DPBS with 10% BSA (Bovine Serum Albumin Fraction V; Roche), for 1 h at room temperature in the dark. Afterwards, samples were rinsed again twice with DPBS and incubated with 1:5000 DAPI/H_2O solution for 5 min; two final DPBS rinses were done.

DAPI, phallacidin and vimentin immunostaining

Samples were incubated with phallacidin 1:200 and Vimentin (Sigma 1:100) in a 1% BSA/DPBS solution for 1 h at RT. After two DPBS rinses, samples were incubated for 5 minutes with a 1:5000 DAPI/H_2O solution. As a final step, samples were rinsed twice with DPBS.

HUVECs immunostaining against CD31 and VE-cadherin

Samples were incubated overnight, in the dark, at 4°C, in a solution of BPB containing mouse monoclonal antibody against PECAM-1 (CD31; Chemicon) in a 1:100 concentration and rabbit polyclonal anti-human VE-cadherin (CD144; Abcam) in a 1:100 proportion. Then, the samples were rinsed with DPBS three times for 5 minutes. Subsequently, the secondary antibodies goat anti-mouse Alexa 488 and goat anti-rabbit Alexa 647 (Invitrogen, 1:200) were added and samples were incubated for 1 h at RT followed by a wash for 5 minutes with DPBS. Finally, samples were stained with DAPI as previously described.

MSC and HUVECs co-culture immunostaining against CD31 and DAPI

Samples were incubated overnight, in the dark, at 4°C, in a solution of BPB containing mouse monoclonal antibody against CD31 as described above. Then, samples were rinsed with DPBS for 5 minutes three times. Subsequently, the secondary antibody, goat anti-mouse Alexa 647 (Invitrogen, 1:200) was added

and incubated for 1 h at RT; next, samples were washed for 5 minutes with DPBS. Finally, samples were stained with DAPI as previously described.

After the staining protocols, samples were mounted with Fluorsave reagent (Merck Milipore), coverslipped and examined with either a fluorescence microscope (Leica DM6000B), a Nikon eclipse 80i fluorescence microscope, or a confocal laser scanning microscope (CLSM; Zeiss 780 Axio observer z1).

In order to observe the inner sections of the cultured scaffolds, they were rinsed twice with PBS after the staining protocols and before being mounted, next cryopreserved in 30% sucrose, embedded in frozen section compound (Leica) and finally cut into 100 μm slices with a cryostat HM 520 (Microm).

2.3.5.- Haematoxylin-eosin staining

Given the autofluorescence of some of the materials employed, it was impossible to follow the morphology of cells cultured therein. Haematoxylin-eosin stainings were performed instead. Analogously to immunocytochemistry samples, at the given time points, samples were fixed with formaldehyde as previously described. The staining protocol consisted in a first rinsing of the samples with distilled water for 3 minutes, followed by other 3 minutes rinse with tap water. At that point samples were covered with a filtered haematoxylin solution according to Mayer (Sigma-Aldrich) and incubated for 10 minutes at RT. Next, a bluing solution (composed by tap water, $NaHCO_3$ 1% wt./vol. (Fluka) and $MgSO_4$ 0.0667% wt./vol. (Scharlab)) was added for 1 minute and 30 seconds. Once removed, type B eosin (Sigma) was added and incubated for 10 minutes at RT. Finally, samples were rinsed with tap water, mounted with a glycerol (Sigma)/water 85/15 vol. mixture, coverslipped and observed with a petrographic microscope (Nikon).

2.3.6.- Morphological characterization of biological samples by SEM

Cells morphology after culture in different materials was observed by scanning electron micrographies. First of all, at the selected times, cultured samples were fixed by immersion in 2.5% glutaraldehyde (Electron Microscopy Science) in 0.1 M Phosphate buffer (PB) for 1 hour at 37°C at the selected time points. Afterwards, samples were post-fixed with osmium tetroxide (OsO_4; Electron Microscopy Science) for 1 hour, followed by three rinses with distilled water. Next, samples were dehydrated by immersing them in aqueous solutions with increasing fraction of ethanol (30%, 50%, 70%, 96%, and 100% of ethanol). Once dehydrated, the samples were critical point dried with an Autosambri 814 instruments (Rockville, MD, USA). As a last step, samples were sputter coated with gold before observation under a SEM (Hitachi S-4800) at 10 kV.

2.3.7.- Flow cytometry

Analysis of HUVECs cultured in bare or RAD16-I filled PEA-s scaffolds

Flow cytometry measurements were performed to evaluate the expression of the endothelial marker CD31 and the VE-cadherin. Therefore, at the selected time points (1 and 7 days), cultured samples were trypsinized and right after were blocked for 30 min with BSA 1%/DPBS. Next, samples were incubated for 30 min at 4°C with mouse monoclonal anti-human CD31 (1:100) and rabbit anti-human VE-cadherin (1:100). After being rinsed with DPBS, cells were incubated another 30 minutes in the dark at 4°C with Alexa 488 and Alexa 647 (Jackson Immunoresearch, 1:200) diluted with PBSA. Finally, the cells were rinsed twice with DPBS and acquired with a flow cytometer (FC500) (n=10.000 per group). Each group formed by a cell pool from 5 samples was analyzed with the RXP software.

The cytometry study of the experiment performed with HUVECs was completed by analysing the cells individually with an ImageStream device (Amnis Corporation

USA) at day 7. Hence, after their incubation with primary and secondary antibodies (CD31, VE-Cadherin), cultured scaffolds were trypsinized, and the cells for imaging flow cytometry were diluted to $5{\cdot}10^5$ in 70 μL of FACS Buffer (buffered saline solution containing BSA 1%). Images (n=10.000 per group), were acquired using the ImageStream imaging flow cytometer with a blue 488 nm laser, and a bright field lamp at 60x magnification. Classifiers were set to eliminate cell debris and clusters prior to data acquisition based on low and high bright field areas, respectively. After acquisition, a compensation matrix was applied to all data aiming to correct spectral overlap. All analyses were completed on a population of spectrally compensated, single cells and by using IDEAS (Image data exploration and Analysis Software, Amnis Corporation).

Analysis of MSCs and HUVECs co-cultured in bare or RAD16-I filled PEA-o or PEA-s scaffolds

Flow cytometry measurements were performed to evaluate the evolution of each cell subpopulation with time. Therefore, at the selected time points (2 and 7 days), 5 samples per group were trypsinized, pooled, and right after were blocked for 30 min with BSA 1%/DPBS. Next, samples were incubated for 30 min at 4°C with FITC mouse Anti-Human CD31 (1:5) and APC mouse anti-human CD90 (1:20, BD Bioscience) diluted with PBSA. Finally, cells were rinsed twice and resuspended with DPBS and acquired with a flow cytometer High Speed Cell Sorter MoFlo (Beckman-Coulter, CA, USA). 1:300 propidium iodide (1 mg/mL in water, Sigma-Aldrich) was added to the cell suspension to discard the dead cells from the flow cytometry analysis.

2.3.8.- VEGF release quantification

The VEGF (vascular endothelial growth factor) release to the culture medium during the co-culture experiment was quantified by means of a human VEGF Enzyme-

Linked ImmunoSorbent Assay (ELISA, R&D systems, DY293B). The medium supernatant was collected every two days, and then the kit was used following manufacturer's instructions.

2.4.- Statistics

Results are expressed as mean ± standard deviation from at least three replicates. Data were analysed pair wise with an ANOVA test with Statgraphics Centurion XVI.I. Statistically significant results are noted on the plots. Significance was assigned at p-values< 0.05.

Chapter 3:

Scaffolds' initial characterization

3.- Scaffolds' initial characterization

3.1.- Abstract

The aim of this chapter is to present the main features of the poly(ethyl acrylate) (PEA) scaffolds that have been be employed over the following chapters. Two structures have been handled: PEA scaffolds with spherical interconnected pores (PEA-s) and PEA scaffolds with cylindrical orthogonally interconnected pores (PEA-o).

In order to obtain these different architectures, different procedures are followed. In the case of PEA-s, templates of poly(methyl methacrylate) (PMMA) microspheres that are removed by particle leaching with acetone are employed to obtain porous sponge-like structures, whereas in the case of PEA-o, templates of nylon fabrics that are removed with nitric acid were used to obtain the grid-like porosity.

First of all, the morphological characteristics of the scaffolds will be described with the help of scanning electron micrographies. Then the results of the physico-chemical characterization of the scaffolds (and bulk PEA as control samples) will be discussed. This section includes differential scanning calorimetry plots and thermogravimetric analyses. In the light of these experiments, it was found that both preparation procedures had certain effect on PEA matrices, derived from a slight dissolution of PMMA in the monomeric mixture or a chemical attack of nitric acid on PEA side chains. Therefore a subsequent characterization was undertaken to assess such modifications and the consequences thereof.

For PEA-o, it was possible to employ a simplified model to investigate the nitric acid effect on PEA, isolated from other factors. Bulk (2D) PEA discs were treated with nitric acid during 4 (PEA-4d), 9 (PEA-9d) and 17 days (PEA-17d) in order to

simulate the washes conducted to remove the nylon templates. These samples were object of a complete physico-chemical characterization.

Finally, a biological evaluation was performed in which the behaviour of fibroblasts and human umbilical vein endothelial cells (HUVECs) was evaluated when each cell type was cultured on PEA, acid-treated PEA or a 90/10 EA/AAc copolymer.

3.2.- Results

3.2.1.- Preliminary characterization

As previously explained, the scaffolds employed in this Thesis, present two different morphologies, corresponding to the so-called PEA-s and PEA-o scaffolds.

The PEA-s scaffolds have a porosity of 80.8 ± 3.5%, which is obtained by employing a template made of sintered microspheres of PMMA with diameters ranging from 80 to 180 microns. When these spheres are removed, after the polymerization of the polymer in between the remaining voids, structures like those shown in Figure 3.1 A-B are obtained. Wide pores are produced by the spaces left by the leached PMMA spheres, leaving struts of around 5 microns corresponding to the voids between any two spheres, and throats with varying sizes up to 40 microns in diameter are obtained in the areas where the inter-connections between two PMMA microspheres used to be.

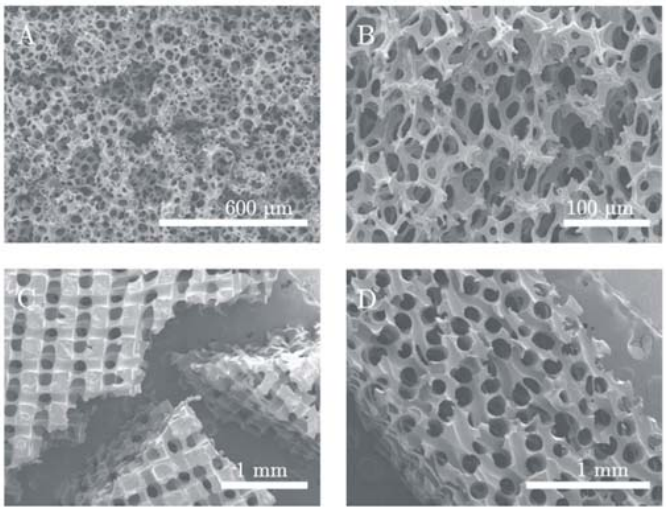

Figure 3.1: Scanning electron micrographies of PEA-s (A and B) and PEA-o (C and D).

On the other hand, PEA-o scaffolds have lower porosity, 76.4 ± 6.1%. This type of scaffolds were obtained by sintering nylon fabrics with pressure and temperature,

filling the spaces with monomeric solution, and once everything was perfectly polymerized, removing the nylon fabrics by several washes with nitric acid. The obtained cylindrical pores have diameters of 149.08 ± 17.02 μm, which coincides with the nominal diameter of the thread. As can be seen in Figure 3.1 C-D, it is a much more closed structure, with thicker struts when compared with PEA-s. However, it is a much more organized structure with parallel cylindrical channels in each plane and perpendicular to the channels in the other two main directions of the space, which might be interesting for the intended application. In both cases smooth surfaces with no microporosity were obtained.

The thermogravimetric plots for both types of scaffolds and the bulk PEA are shown in Figure 3.2 A. The results obtained for the three materials revealed several differences among the studied materials. The PEA-2D main thermal degradation has its onset at 380°C and continues up to 422°C, leaving a solid residue of 3%. In the case of PEA-o, the thermal degradation is shifted towards lower temperatures as compared with the bulk PEA, starting at 360°C, but leaves a similar percentage of solid residue. In the case of the PEA-s, the beginning of the thermal degradation is displaced towards still lower temperatures, with the onset near 340°C; besides, it exhibits a different slope. Once the main degradation is passed (PEA-s offset is at 425°C), again both PEA-s and PEA 2D exhibit a similar behaviour leaving approximately the same value of solid residue (3%).

When the weight derivative *vs.* temperature is considered (Figure 3.2 B), in the case of PEA-o, the peak is as wide as that of the bulk PEA, but the maximum value reached is a bit lower; as commented before, it is in addition slightly displaced towards lower temperatures. Regarding the PEA-s profile, it looks like the superposition of two curves, showing more clearly the change in the slope observed in the previous graph of residual weight. When this secondary band of the PEA-s is

compared with that of PMMA employed as porogen in its fabrication, it can be observed that the main peak for the latter appears in this same range.

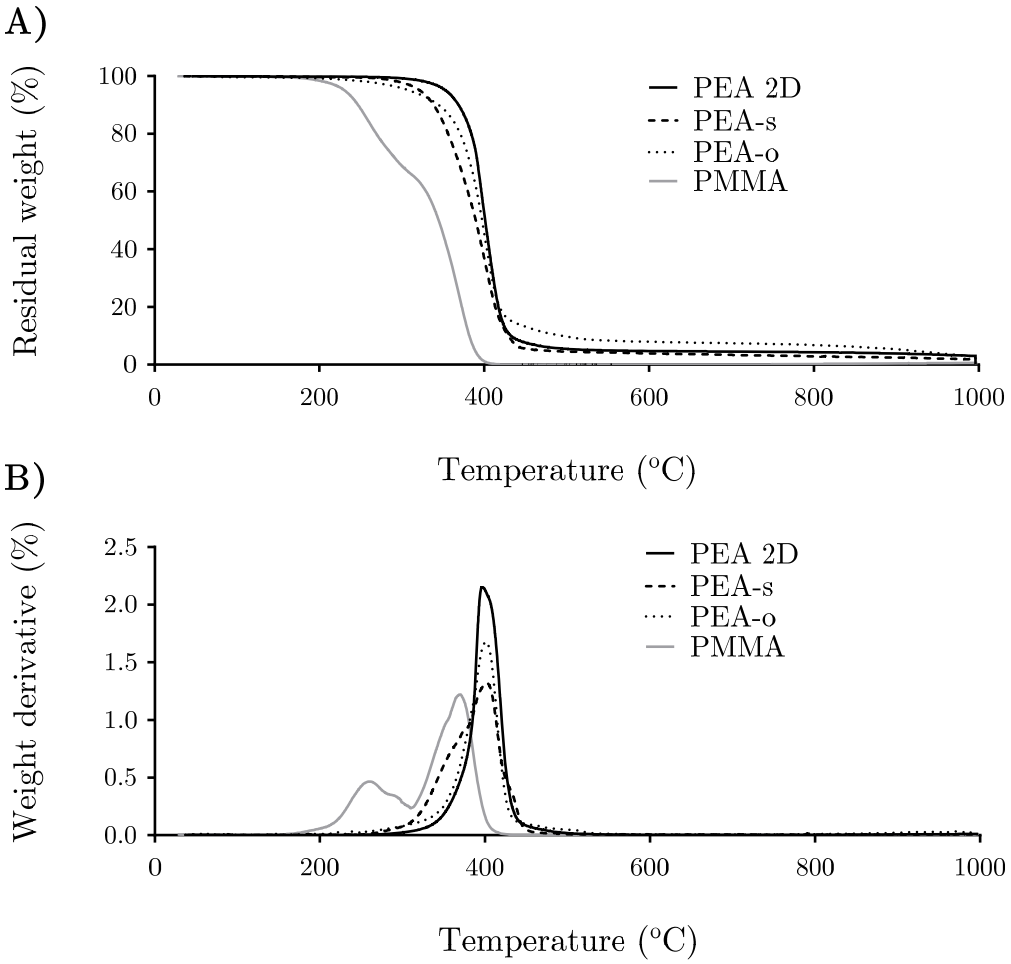

Figure 3.2: Thermogravimetric analysis of bulk PEA (PEA-2D), and PEA scaffolds with spherical pores (PEA-s) or cylindrical orthogonal pores (PEA-o), as well as PMMA microspheres.

The normalized heat flow is plotted versus temperature in Figure 3.3 A. With these curves the glass transition temperature was determined, *Tg*, and at this precise temperature, the specific heat capacity increment, *ΔCp*, was estimated.

In the case of PEA-o, a shift towards higher temperatures is observed for the glass transition (Figure 3.3 B), the *Tg* changing from -16.30°C for PEA-2D up to -0.4°C for PEA-o. But it is not the only change observed; when the *ΔCp* are compared

(Figure 3.3 C), an increase of the value from 0.390 J/gK for PEA bulk to 0.470 J/gK for the scaffolds with cylindrical orthogonal pores can be seen. In the case of scaffolds with spherical pores, a more moderate displacement of the glass transition temperature towards higher values (-5.14°C) is observed, while the ΔCp experiences a reduction, reaching a value of 0.321 J/gK. PEA-s also exhibits a peak around 140°C and a subtle change in the slope. When compared, it is observed that these alterations in the liquid line, match with the beginning of the glass transition and ageing peak observed for the PMMA template.

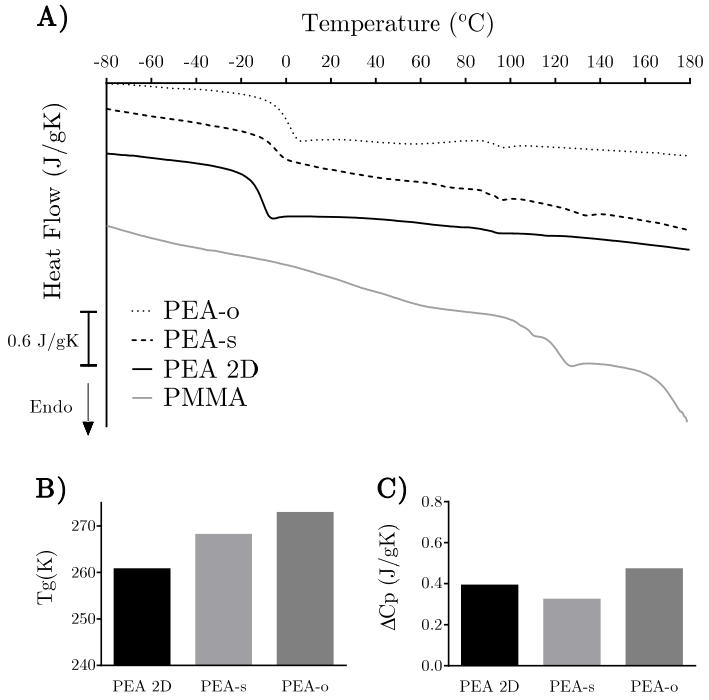

Figure 3.3: Thermograms plotting the heat flux per unit mass as a function of temperature (A) for PEA films, PEA scaffolds with spherical interconnected pores (PEA-s), and with cylindrical orthogonal pores (PEA-o), and PMMA microspheres. Glass transition temperature (B) and heat capacity increase (C) for the different materials.

3.2.2.- Nitric acid effect on PEA

The results obtained in the previous section suggest that the nitric acid rinses followed to remove the nylon template have an effect on the PEA structure and consequently on its properties. To have a complete understanding of the changes taking place, a further characterization was required.

Considering the results obtained from a preliminary study, in which an anomalous swelling in basic media was observed (data not shown), it was hypothesized that the effect the nitric acid has on PEA is the hydrolysis of a number of its side chains, transforming several ethyl acrylate units into acrylic acid (AAc), and giving place to a random copolymer containing EA and AAc units. In order to prove this hypothesis, a simplified 2D model was employed. PEA bulk films were treated with nitric acid during different times (4, 9 and 17 days) simulating the washes followed to remove the nylon template. These acid-treated PEA films were compared with untreated PEA, PAAc and a 90/10 %wt. P(EAcoAAc) copolymer.

Physico-chemical and mechanical characterization

By means of the obtained FTIR spectra (Figure 3.4), the changes introduced in the chemical structure of PEA by the HNO_3 rinses were revealed. The bands at 3500 and 3200 cm^{-1}, characteristic for hydroxyl groups are not present in the untreated PEA spectra. Nonetheless, the 3200 cm^{-1} band appears for all acid-treated acrylates, whilst the 3500 cm^{-1} band is only present in the PEA-17d spectra. Similarly, the PAAc spectrum exhibits both bands at 3500 and 3200 cm^{-1}, while only the 3200 cm^{-1} band is observed for P(EAcoAAc).

The CH_x (CH_2, CH_3) symmetric and asymmetric stresses appear for all materials in the 2962 and 2888 cm^{-1} region. In the case of PAAc, as for PEA-17d (but not for the

copolymer nor for the less treated PEA), also a wide band attributable to the carboxylic acid group is observed in the 2800 to 2500 cm^{-1} region.

All the studied materials present a well-defined peak at 1715 cm^{-1}, which is characteristic for carbonyl bonds in the carboxyl group. A slight shift of this peak towards lower wavenumbers, together with the appearance at 1600 cm^{-1} of a new one, are observed for the PEA-9d, PEA-17d and PAAc, being both this shift and the width of the peak more pronounced for PAAc.

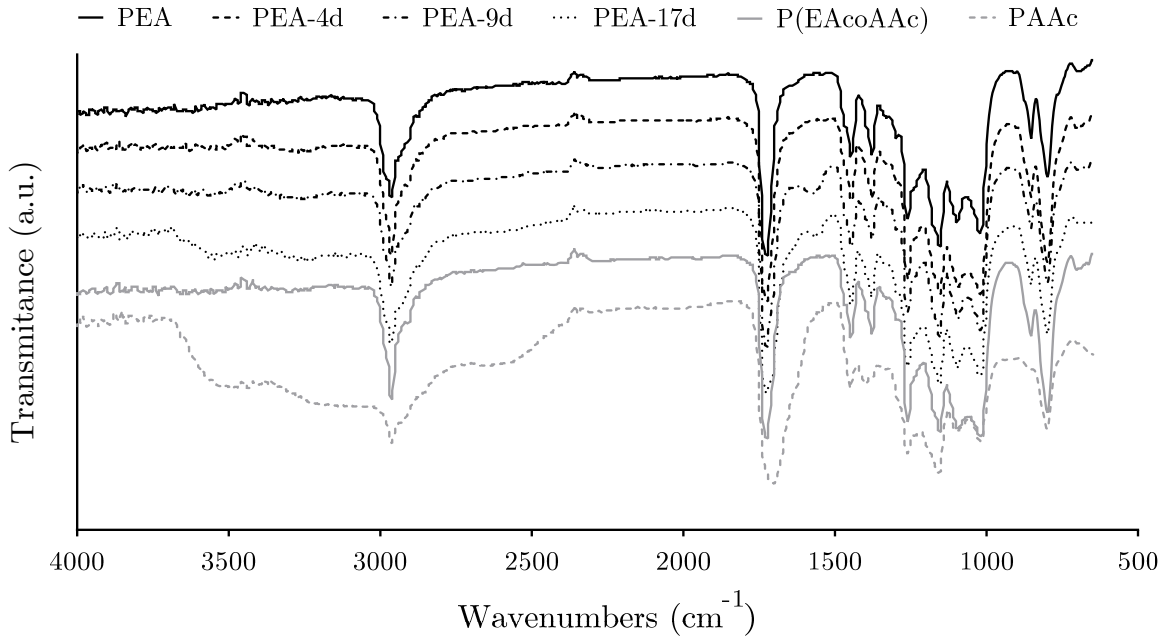

Figure 3.4: FTIR spectra of PEA, PEA treated for 4, 9 and 17 days in nitric acid, PAAc and the copolymer P(EAcoAAc), in the 500 to 4000 cm^{-1} region.

Swelling untreated PEA or 4 days-treated PEA (PEA-4d) in media with different pHs, such as water and a NaOH(aq) solution, revealed that nitric acid transforms PEA into a pH-sensitive material (Figure 3.5). When PEA and PEA-4d samples swollen in water are compared, they only show a slightly different behaviour.

However, when they are swollen in a basic solution, dramatic differences were detected.

When untreated PEA is swollen in water or in NaOH(aq), no significant differences are observed in the water content reached, 1.14% and 2% respectively. Even more, PEA swelling in NaOH(aq) is stabilized after 1 h of immersion. Unlikely, PEA-4d swollen in NaOH(aq) reached a water content near 16% after 1 h, and up to 130% after 24 h. When the treated samples were swollen in water, much lower values were attained: after 24h PEA-4d only exhibited a slightly higher water content than the untreated ones, 2.78% *vs.* 1.14%.

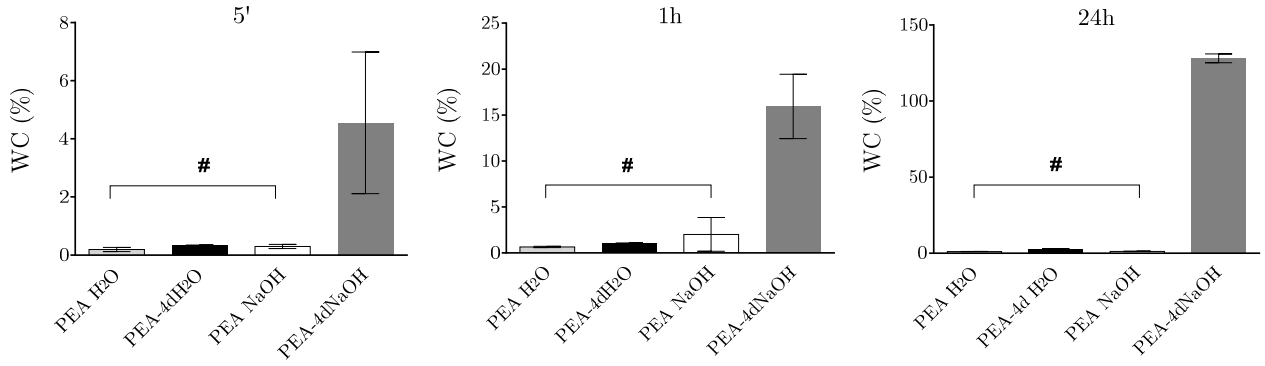

Figure 3.5: Water content of the untreated and 4 days acid-treated PEA samples as a function of time of immersion in water or in a NaOH 0.2M aqueous solution.
(#) No significant differences.

Media with different pH values but constant ionic strength were employed to further characterize the effect the nitric acid treatment and its duration had on PEA by means of water content (Figure 3.6).

When samples were swollen at pH 2 (Figure 3.6 A-B), the equilibrium water content (*EWC*) slightly increased with the time of the acid treatment, changing from 1% for untreated PEA up to around 5% for PEA rinsed with acid for 17 days (PEA-17d).

The copolymer and PEA-9d had a quasi-identical profile. No significant differences were observed between the *EWC* of P(EAcoAAc) and PEA-9d. The P(EAcoAAc) (2.5%) appeared to be more hydrophilic than PEA, but was far from the values reached by PAAc (50%). Similar results and values were obtained for pH 4.6 (Figure 3.6 C-D).

Much different results were obtained when the materials were swollen in a media with pH 8 (Figure 3.6 E-F), *i.e.*, basic media, except for the untreated PEA that maintained an *EWC* near 1%. Samples treated for 4 days in acid, nearly triple the *EWC* reached at lower pH, attaining a value close to 6%. The *EWC* for PEA treated for 9 days was nearly 60%, and for those treated 17 days reached a value of 240%. When these values were compared with the references, much higher values were obtained for PAAc (650%) while P(EAcoAAc) reached a value of 60%, very close to the *EWC* of PEA treated for 9 days.

Generally speaking, PEA exhibited a hydrophobic behaviour independently of the pH of the medium. For the 'scarcely' acid-treated materials (4 and 9 days) and the copolymer, small differences were observed in the reached *EWC* when swollen at pH 2 and 4.6. However, at pH 8 the materials exhibited a hydrophilic behaviour proportional to the immersion time for the treated series or to the fraction of carboxyl lateral groups for the reference materials. Independently of the pH, PEA treated for 9 days followed the same trends and reached *EWCs* very close to those of the copolymer.

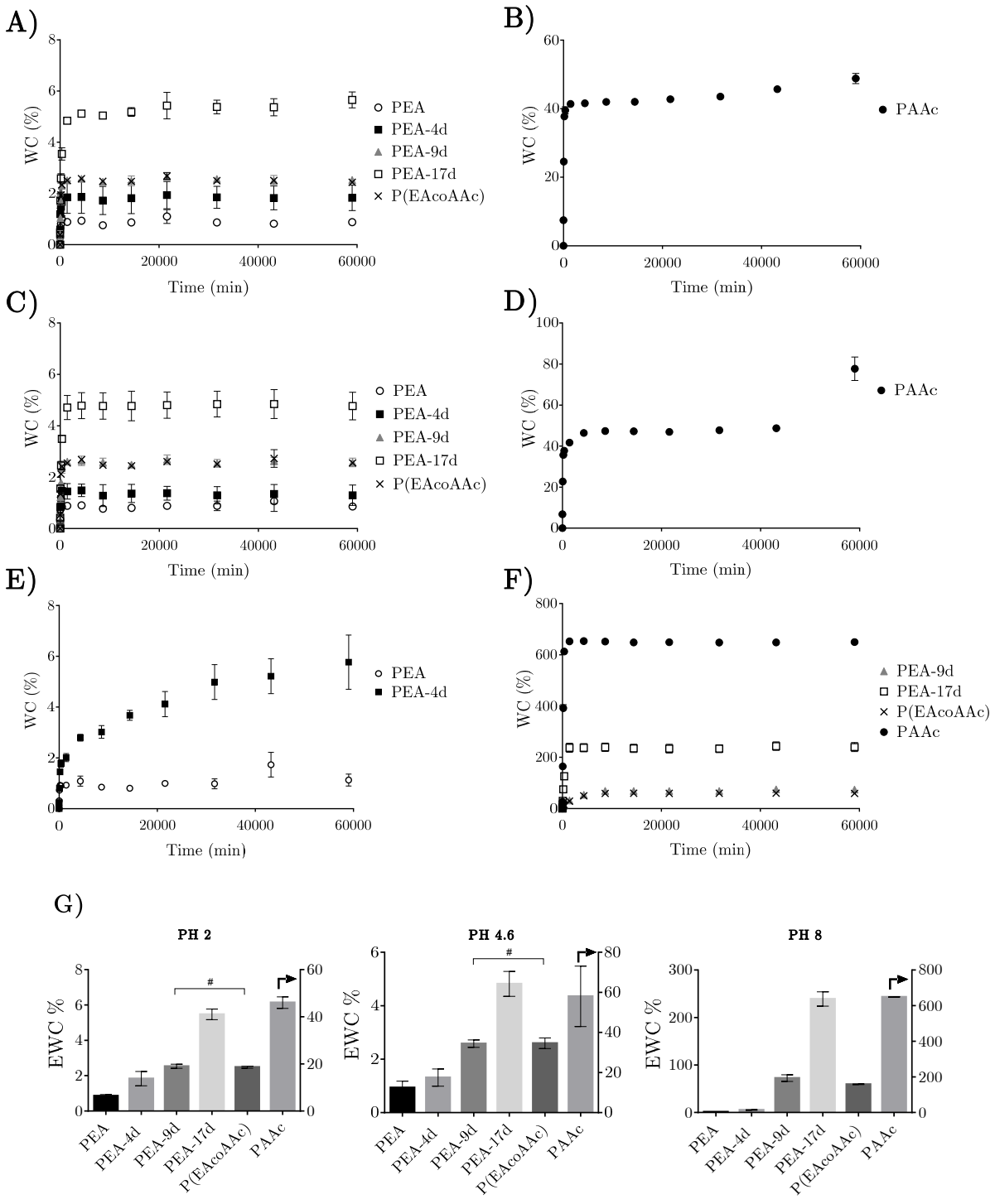

Figure 3.6: Water content of acid-treated PEA samples and P(EAcoAAc) and PAAc references as a function of time of immersion in solutions with pH equal to 2 (A-B), 4.6 (C-D) and 8 (E-F). G) *EWCs* at different pH. Differences are statistically significant unless noted otherwise. For PEA, no significant differences were observed for the *EWCs* through pH. For the PEA-9d and P(EAcoAAc) samples no significant differences were observed between pH 2 and 4.6. (#) No significant differences.

The density was also found to be a parameter sensitive to the nitric acid treatment as follows: the longer the treatment, the greater the density of the resulting material (Figure 3.7). Density changed gradually from 1.134 g/mL for the untreated PEA up to 1.18 g/mL for PEA-17d. The densities of PEA treated for shorter times, PEA-4d (1.147 g/mL) and PEA-9d (1.159 g/mL) were similar to that of the copolymer (1.158 g/mL). Indeed, no statistically significant differences were observed between PEA-9d and the copolymer in these assays. PAAc exhibited, as expected, the highest density, 1.289 g/mL.

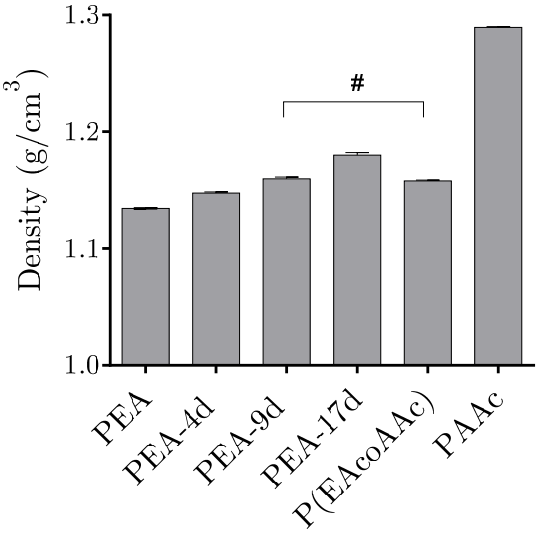

Figure 3.7: Densities of acid-treated PEA samples and P(EAcoAAc) and PAAc references. (#) No significant differences were observed.

PEA glass transition temperature was clearly affected by the nitric acid treatment as well (Figure 3.8 A-B). A displacement towards higher temperatures proportional to the immersion time in acid was observed. The glass transition temperature moves from -12.51°C for untreated PEA up to 22.25°C for PEA-17d. The copolymer thermogram is framed between those of PEA-4d and PEA-9d, and its glass transition temperature (-1.94°C) is an intermediate value between the respective values of these samples (-6.5°C and 1.63°C). In the case of PEA-17d, its thermogram is similar to that of PAAc, however this last's measured *Tg* is a bit lower, 20.99°C.

The heat capacity variation at the glass transition (ΔCp) slightly increased with the duration of the nitric acid treatment as well (Figure 3.8 C). ΔCp changed from 0.39 J/gK for untreated PEA up to 0.453 J/gK after 17 days of treatment. The copolymer exhibited a value in the range of the treated acrylates (0.423 J/gK). And once more, the PAAc value was the highest (0.769 J/gK).

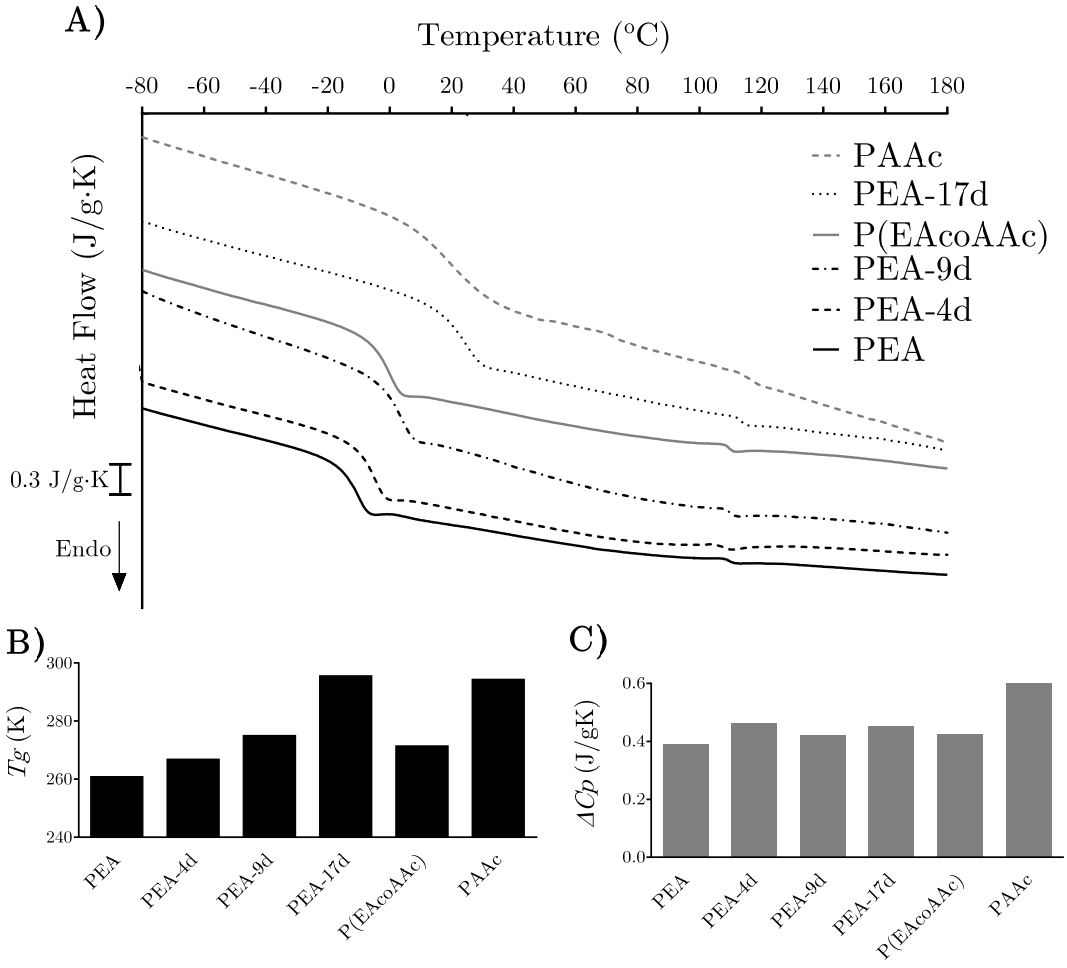

Figure 3.8: Thermograms plotting the heat flux per unit mass as a function of temperature (A) of acid-treated PEA samples and P(EAcoAAc) and PAAc references. Glass transition temperature (B) and heat capacity increase (C) for the different materials.

The acrylates viscoelastic performance was affected by the nitric acid treatment as well (Figure 3.9). At temperatures below 0°C, all the materials displayed a high elastic modulus (10^9-10^{10} Pa), typical of rigid polymers in their vitreous state. The

main relaxation of PEA was observed in the 10°C to 30°C interval. The addition of carboxyl lateral groups shifted the main mechanical relaxation towards higher temperatures, in the -5 to 40°C interval for the P(EAcoAAc). In the case of the acid-treated polymers, the relaxation shift was proportional to the time in acid medium: PEA-4d reached temperature values between those for PEA and P(EAcoAAc), PEA-9d exhibited its drop after the copolymer, and PEA-17d at even higher temperatures. In all cases, the elastic modulus reached after this relaxation was in the order of MPa, which are typical values for elastomers. Similarly, the increase in the temperature at which *tanδ* achieves its maximal value (T_α) is proportional to the duration of the acid attack (Figure 3.9 B and inset). The maximum for P(EAcoAAc) is located between those for PEA-4d and PEA-9d; and again that for PEA-17d even more is shifted to the right. PAAc measurements are missing because the DMTA broke down before performing this experiment.

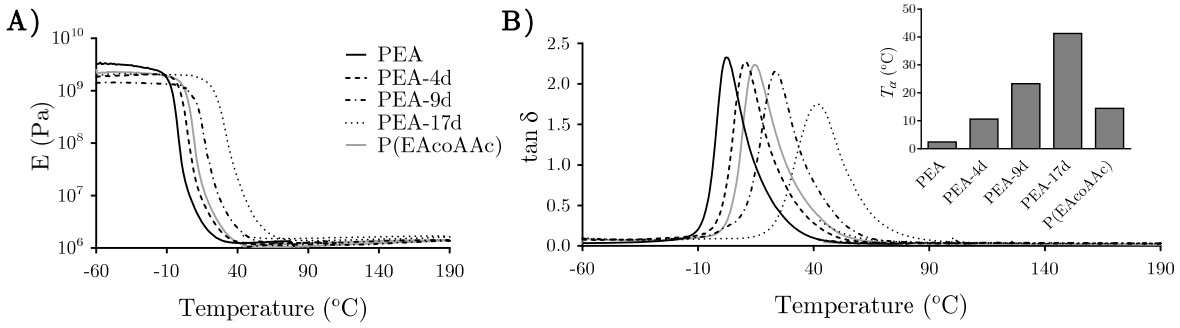

Figure 3.9: Elastic modulus dependence on temperature (A) for acid-treated PEA samples and P(EAcoAAc); *tanδ* as a function of temperature (B), and T_α (inset) for the set of samples.

The chemical modifications occurring in the PEA matrix because of the acid were found to affect the water contact angle on the surface; however, it was only observable when the samples were in their swollen state (Figure 3.10 A-B).

Dry discs of acid-treated PEA were more wettable than untreated PEA, as their contact angle lowered (Figure 3.10 A), but no differences with the duration of the treatment were observed. Both P(EAcoAAc) and PAAc exhibited lower contact angles than the treated samples, because their composition includes lateral acid groups. Surprisingly, despite only 10% of the monomeric units in P(EAcoAAc) contain an acid group, this polymer appeared to be more wettable than PAAc whose units, all of them, contain such group.

Completely different results were obtained when the contact angle measurements were repeated after a previous swelling in water (Figure 3.10 B). The contact angle on swollen PEA was a bit smaller than on its dry state, but yet it was a high value. The contact angle of the treated samples, decreased with the immersion time in acid up to 9 days. PEA-17d behaved anomalously with a contact angle even higher than that of untreated PEA. After swelling, the contact angle of PAAc was lower than that of P(EAcoAAc), as expected given their composition. PEA-4d's contact angle was similar to that of P(EAcoAAc), and PEA-9d had a contact angle close to that of PAAc (although there were no statistically significant differences between them).

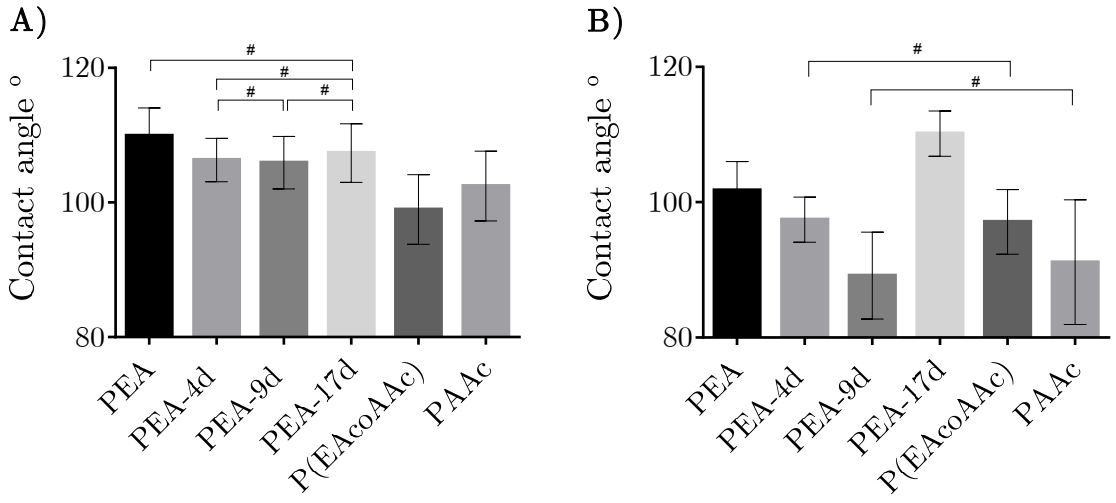

Figure 3.10: Water contact angle measurements on dry (A) and swollen (B) acid-treated PEA, P(EAcoAAc) and PAAc samples. (#) No statistically significant differences.

As the thermogravimetric plots show (Figure 3.11), the nitric acid treatment has an effect on the PEA thermal degradation in terms of lowering the onset temperatures and broadening the main degradation step. Untreated PEA has its main degradation between 380°C and 422°C, and these values gradually change with the duration of the acid treatment, up to 347°C-414°C for PEA-17d. Once more PEA-4d and PEA-9d are framed by the PEA and P(EAcoAAc) profiles, undergoing their main degradation in the 370°C-425°C interval. The nitric acid treatment has also an effect on the solid residue percentage, which increases from 3% for PEA up to 5.4% for PEA-17d. The P(EAcoAAc) decomposition thermogram is not dissimilar to that of PEA-17d, though this last's solid residue coincides with that of PAAc.

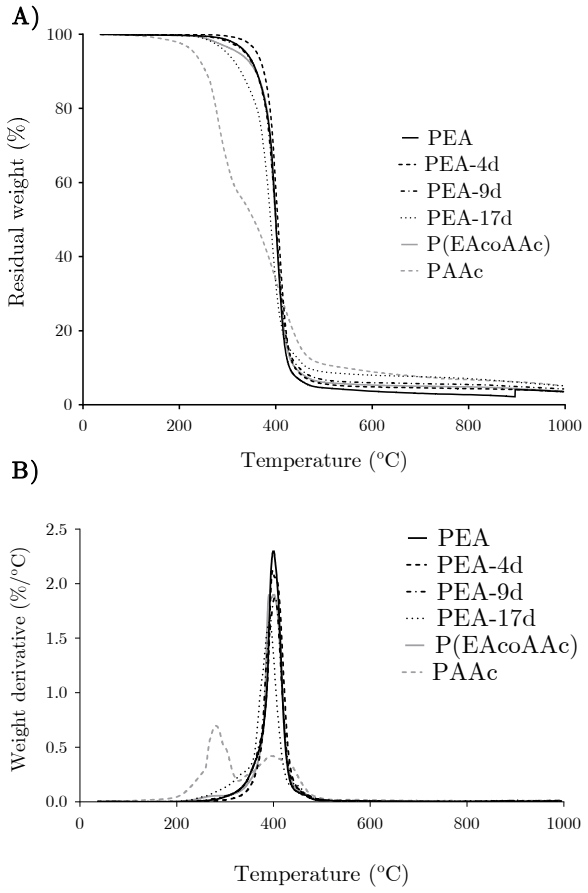

Figure 3.11: Thermograms for acid-treated PEA, P(EAcoAAc) and PAAc samples, plotting the residual mass fraction as a function of temperature (A), and the first derivative of the residual mass fraction as a function of temperature (B).

After staining with toluidine blue, samples were gradually bluer with either the fraction of acrylic acid groups (Figure 3.12 E-F) or the time of treatment in nitric acid (Figure 3.12 A-D). Untreated PEA acquired a light shade, but very subtle and purplish. The colouring of PEA-4d and PEA-9d was very similar to that of P(EAcoAAc) and already in the blue tonality. PEA-17d had a more bluish tone, PAAc being the most stained sample.

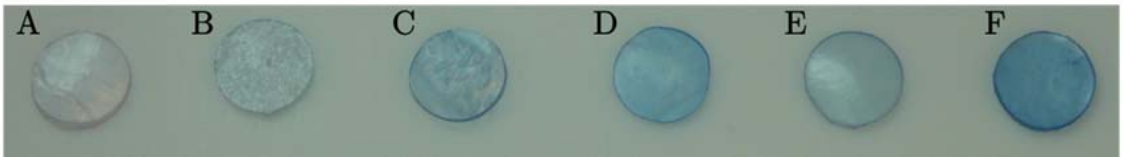

Figure 3.12: Toluidine staining for PEA (A), PEA-4d (B), PEA-9d (C) PEA-17d (D), P(EAcoAAc) (E), and PAAc (F).

3.2.3.- Biological characterization

In the previous sections a complete physico-chemical characterization of PEA and PEA treated with nitric acid was undertaken. The properties exhibited by all the considered materials are compatible with their use in a biological environment. However, to guarantee their suitability for their use in tissue engineering applications requires from *in vitro* experimentation to verify that the produced materials are not cytotoxic and are capable to favour cell attachment and proliferation. In order to proof that, experiments were performed with fibroblasts and HUVECs with the different materials under study.

The MTS results revealed that there were no statistically significant differences for the initial adhesion of fibroblasts among the different materials and control (Figure 3.13 A). Cell-seeded samples did exhibit significant differences (except P(EAcoAAc) at day 1) when compared with the acellular controls, thus indicating that cells effectively attached and proliferated with time. Untreated PEA exhibited the closest

behaviour to the control, and attained greater absorbance values than the other polymeric materials; PEA-4d and P(EAcoAAc) exhibited a more moderate absorbance increase. Given the fact that PEA reached absorbance values close to those of the positive control in fibroblasts culture, in the HUVECs culture those samples were employed as positive controls instead.

Similar results were obtained for the HUVECs MTS assay (Figure 3.13 B). At short times, absorbance levels did not increase significantly for any sample. For the longer time points, HUVECs proliferated remarkably on PEA surfaces, and less on PEA-4d, whereas no statistically significant absorbance increase was observed for P(EAcoAAc).

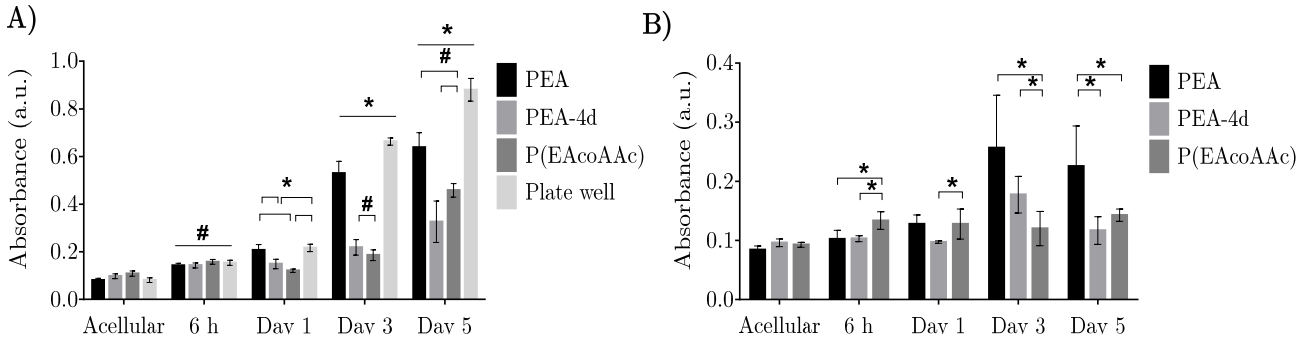

Figure 3.13: MTS results after 6 h, 1, 3 and 5 days culture of L929 fibroblasts (A) and HUVECs (B) on untreated PEA, PEA-4d, P(EAcoAAc) and plate wells.
(*) Differences are statistically significant. (#) Differences are not statistically significant.

In general terms, for all the samples and time points, the MTS outcome with fibroblasts was better than with endothelial cells. On the contrary, the haematoxylin-eosin results showed only slight differences among samples. Fibroblasts proliferated adequately up to the point that after 5 days of culture, cells reached confluence and started to arrange in layers on specific areas of the surfaces (Figure 3.14 D-E, I-J, N-O, S-T). For the P(EAcoAAc), despite the low MTS values, a very good initial adhesion was observed (Figure 3.14 P-T). Although greater values of absorbance

were obtained with the MTS assay for the control wells, the stained samples suggest that the materials under consideration induce an initial adhesion even better than the glass cover (Figure 3.14 A-E). Regarding cell proliferation, both treated PEA and the copolymer exhibited a behaviour comparable to that of the untreated PEA and the control.

Images of haematoxylin–eosin stainings of HUVECs (Figure 3.15) show a better initial attachment on P(EAcoAAc) as compared to the other polymers (Figure 3.15 G). After 5 days of culture, cells had properly proliferated on all studied substrates, and exhibited an elongated morphology. From the first time point (6 h after seeding), it can be observed that cells attach scattered on the surface and form circular structures (Figure 3.15 A, D, G). With time, cells grow into more complex structures maintaining this circular disposition as well as establishing contacts with the surrounding cells.

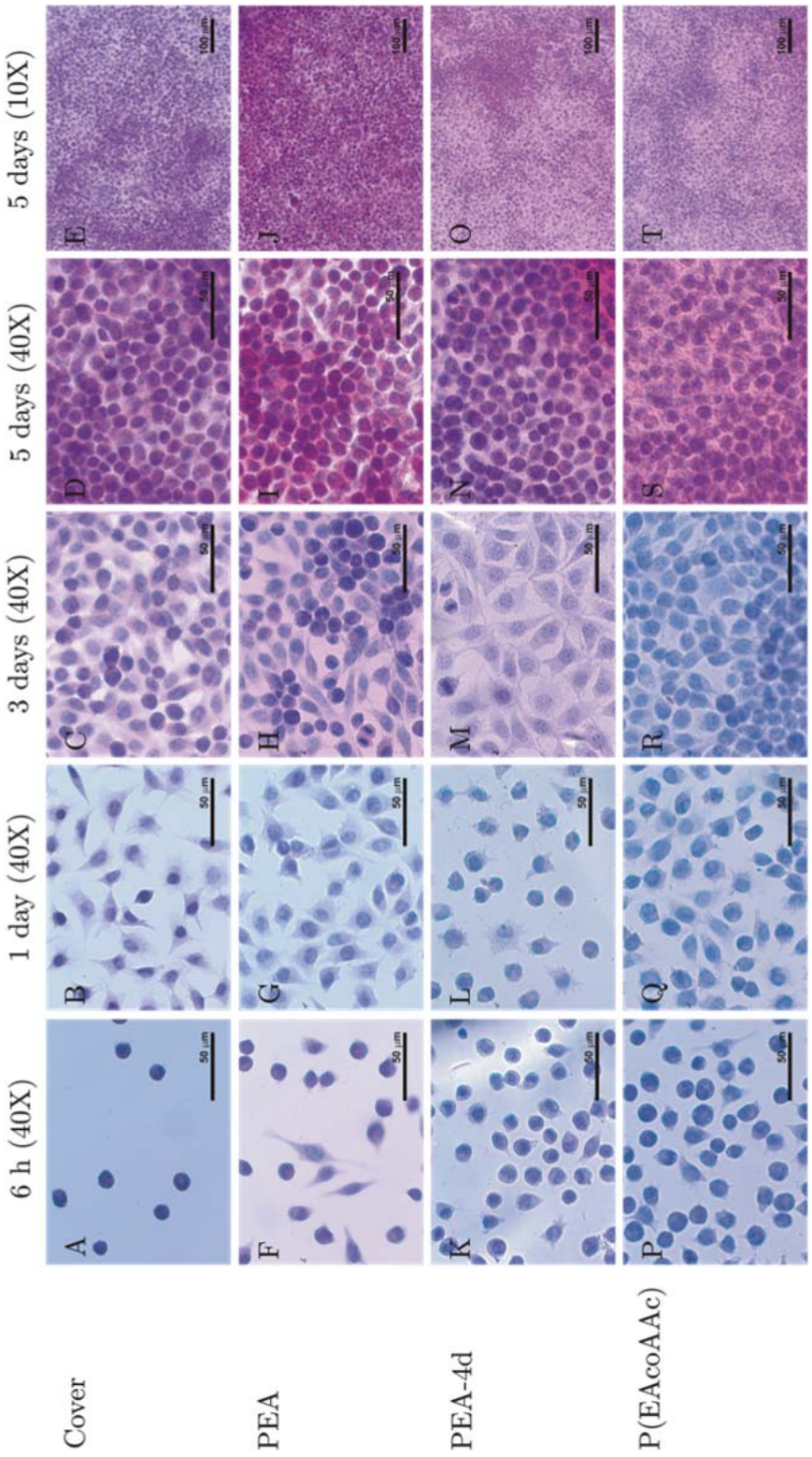

Figure 3.14: Bright field images of samples stained with haematoxylin-eosin after (from left to right) 6 h, 1, 3 and 5 days, and 5 days, after culture of L929 fibroblasts on covers (A-E), PEA (F-J), PEA-4d (K-O) and P(EAcoAAc) (P-T).

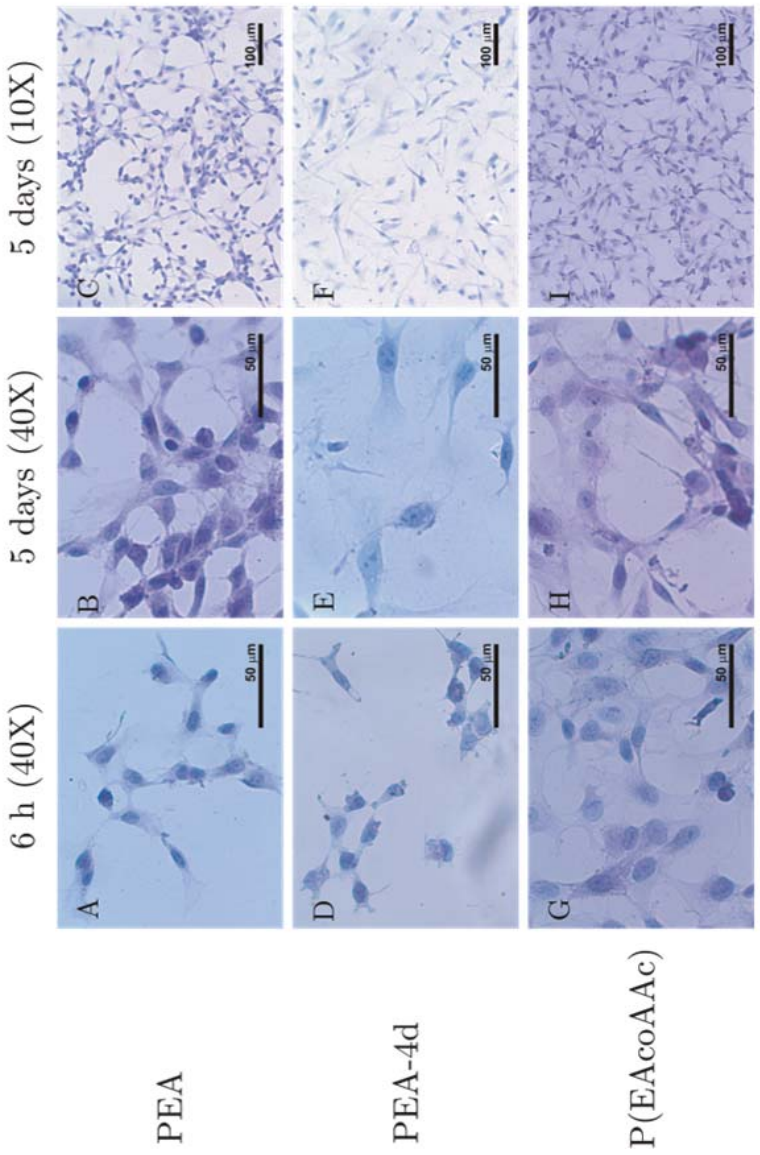

Figure 3.15: Bright field images of samples stained with haematoxylin-eosin after (from left to right) 6 h, and after 5 days at different magnifications of HUVECs culture on PEA (A-C), PEA-4d (D-F) and P(EAcoAAc) (G-I).

3.3.- Discussion

PEA scaffolds exhibiting different morphologies were produced by the use of different porogen templates (Figure 3.1). In both cases, interconnected pores were obtained, albeit the degree of porosity and interconnection were much higher for the scaffolds with spherical pores (PEA-s) than for the grid-like ones (PEA-o). In the case of PEA-o, a more organized structure with parallel and orthogonal micro-channels is obtained, which can be interesting to guide cell growth or to help to obtain organized tissues, as previously reported [131, 269]. In PEA-s, the resulting structure exhibits smaller pores but a greater interconnectivity, which might facilitate cell-cell interaction and diffusion.

If desired, modifications in the resulting structures could be obtained by altering the templates. For instance, in the case of PEA-s, the diameter of the microspheres forming the template could be modified, directly affecting to the size of the resulting pores. Another possibility could be varying the compression rate during the template preparation, to modulate the connectivity between pores. Regarding PEA-o, its morphology could be altered for instance by changing the diameters of the threads or the distance between them.

On the effects of the preparation of PEA-s scaffolds on PEA

After the TGA results (Figure 3.2), the presence of some residual PMMA in PEA-s is suspected, because of the broadening in its weight derivative graph. This anomalous region, precisely matches with the main peak obtained for PMMA. Taken this together with the observed change for PEA-s in the ΔCp, simultaneously with the apparition of a small peak nearby the PMMA melting zone and the slope change (Figure 3.3), it can be stated that a small fraction of PMMA coming from the template, might indeed remain in PEA-s.

After the thorough washes to which the scaffolds were submitted, an extra wash in a shaker with tetrahydrofuran was applied. These lasts washes supernatants were scanned by gel permeation chromatography (data not shown), and no evident PMMA traces were observed. This result confirms that any significant residual PMMA in the scaffolds is neither a cause of incomplete washing of the spheres that could leave residues on the surface of the struts, nor of the PEA network where some PMMA chains could have been entrapped during the polymerization of PEA, because a peak would have been revealed with the GPC scans. Residual MMA units in the PMMA spheres could, nevertheless, copolymerize with EA units of the PEA network, and thus become part of the final polymeric matrix, without leaving any trace in the chromatographic scans.

During its polymerization, the EA monomer is capable of partially swelling the PMMA spheres. If some residual MMA monomer remains entrapped within the particles, it could react with the EA monomer and therefore become part of the PEA network, thus causing the appearance of those peaks. All in all, PMMA belongs to the acrylates family, as PEA, and has a good biocompatibility, which justifies its clinical use in many biomedical applications and bioprostheses for the last decades [270]. Therefore, the presence of a residual fraction of PMMA combined with PEA was not considered a major concern in terms of the biological success of the scaffolds.

On the effects of the preparation of PEA-o scaffolds on PEA

In the case of PEA-o, given the changes in the TGA profiles, in the DSC scans as well as in the subsequent characterization with nitric acid, it can be stated that the acid treatment does have an effect on PEA. The extents of such changes were studied with a simplified model. When the PEA-o scaffolds' features are compared with those of 2D treated materials, it can be singled out that the PEA-o onset of thermal degradation occurs at a temperature very close to that of PEA-9d (360°C *vs.* 368°C).

Regarding the glass transition temperatures, the scaffolds exhibit an intermediate behaviour between PEA-4d and PEA 9d: 1.63ºC, -0.40ºC and -6.5ºC respectively; finally, the ΔCp of the scaffolds is very close to that of PEA-4d (0.470 J/gK *vs.* 0.464 J/gK). These parameters are very characteristic and sensitive to the composition of the material. The fact that the scaffolds' values are very similar to those of the 2D model, validates it as a proper study model and indicates that it is accurate and representative of the system under question.

The scaffolds obtained by means of the removal of polyamide-based porogens with nitric acid experienced increased swelling. This fact arose the hint that this treatment could be inducing a structural modification in PEA: the hydrolysis of the carboxylate group in acid medium leading to an acid group, and thus ethyl acrylate units are replaced by acrylic acid ones.

The appearance of new bands on the FTIR spectra (Figure 3.4) in the 3500 and 3200 cm^{-1} are in good agreement with the proposed modification. The differences observed between the untreated PEA and those treated when swollen in water or in a basic aqueous medium (NaOH 0.2 M) (Figure 3.5), indicate that upon nitric acid treatment, the material becomes more hydrophilic and, more importantly, pH-sensitive.

The increase of the *WC* was proportional to the immersion time for the acid-treated acrylates and to the fraction of acrylic groups for the controls (PAAc and P(EAcoAAc)); interestingly, this increase only was dramatic at basic pH (Figure 3.6). This sensitivity for the basic media confirms the presence of acid groups, which are dissociated in basic media turning polymers into superabsorbents [271]. This gradual modification was visually supported by toluidine staining (specific for acid groups) (Figure 3.12). Those samples containing carboxylic groups introduced either

by a co-polymerization with AAc (P(EAcoAAc)) or by the structural modification induced by the nitric acid treatment, were the more bluish and darker ones.

In the light of the results obtained with different techniques, it can be stated that PEA acid-treated for 4 and 9 days behave similarly to the copolymer: P(EAcoAAc) exhibits a behaviour half way between PEA-4d and PEA-9d through several techniques. For all pHs under consideration, PEA-9d and P(EAcoAAc) attained the same equilibrium values and followed the same trend in the swelling study (Figure 3.6). Analogously, both P(EAcoAAc) and PEA-9d had very similar degradation profiles (Figure 3.11). Regarding the DMTA results, the copolymer main relaxation profile was very close to that of the PEA-4d this time (Figure 3.9). Even visually, with the toluidine blue staining, the colouring of P(EAcoAAc) lies between those of PEA treated for 4 and 9 days (Figure 3.12).

PEA surface properties as well as wettability when in contact with physiological medium are affected by the nitric acid treatment. Regarding the water contact angle measurements performed in the dry state of the materials, few differences with the duration of the acid treatment were observed (Figure 3.10 A). Surprisingly, the copolymer with only a small fraction of AAc groups (10%) showed a lower contact angle than PAAc. These results can be attributed to the different physical state of the studied materials at the temperature of the assay. The presence of acid side groups reduces chain mobility, leading to a vitrification of the materials at room temperature, which leads to a poorer exposure of hydroxyl groups at the surface. Conversely, the presence of water has a plastifying effect that improves chain mobility leading to the expected water contact angle values when measured on samples previously swollen in water (Figure 3.10 B). A proportional reduction of the contact angle, either with the duration of the immersion time in nitric acid or the increase in AAc fraction, was reported, except for PEA-17d.

Considering that the nitric acid affects PEA by only transforming ethyl acrylate units into acrylic acid units, mathematical models can be used to estimate the fraction of each component (EA and AAc) in the treated materials in combination with the density and DSC results.

Assuming additivity, and with the measured densities (Figure 3.7), the fraction of each component in the treated PEA was estimated by means of:

$$\frac{1}{\rho} = \frac{1}{\rho_1} \cdot \omega_1 + \frac{1}{\rho_2} \cdot \omega_2 \qquad \textbf{[Equation 3.1]}$$

where ρ is the density of the mixture, ω_1 and ω_2 are the mass fractions of components 1 and 2, and ρ_1 and ρ_2 are their densities. As a preliminary step, it was verified that the ideal mixture was a good model for this system. In order to do that, the copolymer density, whose composition and individual components' densities were known, was estimated. When the calculated density (1.148 g/mL) was compared with the measured one (1.158 g/mL), the values were considered close enough to apply the ideal mixture equation for the rest of materials whose composition was unknown. For PEA-4d, a fraction of acrylic acid units, ω_2, of 0.09 was obtained, 0.18 for PEA-9d and 0.32 for PEA-17d.

The fraction of each component in the mixture could be determined as well by means of the glass transition temperatures (Figure 3.8 B), assuming miscibility and Fox's equation [272]:

$$\frac{1}{T_g} = \frac{\omega_1}{T_{g1}} + \frac{\omega_2}{T_{g2}} \qquad \textbf{[Equation 3.2]}$$

where T_g is the glass transition of the mixture; T_{g1}, T_{g2} are those of the pure homopolymers PEA and PAAc, ω_1 and ω_2 are the mass fractions of components 1 and 2.

For the PAAc a lower value of glass transition was obtained from the DSC measurements (294 K) than the values reported in the literature, 379 K[273]. Thus, to try to estimate the proportion of AAc units in the treated samples was employed the glass transition temperature of PAAc reported in the literature, 379 K. In this case for the copolymer it was obtained a fraction of AAc of 0.115 (similar to the fraction introduced during its preparation), for PEA-4d, the estimated acrylic acid fraction was 0.093, for PEA-9d it was 0.154, and for PEA-17d 0.31; one more time, laying the copolymer between PEA treated for 4 and 9 days. Being these values in good agreement with the results previously obtained with the density values.

A plausible reason for such a low PAAc's *Tg* value could be found in the EtOH washes to which PEA (before any nitric acid treatment), PAAc and P(EAcoAAc) were subjected. The EtOH employed in these washes could induce the esterification of the AAc units of PAAc and P(EAcoAAc) samples [274]. Therefore these rinses could lead to the formation of ethyl acrylate units in the acrylic acid side chain. However this hypothesis remains unverified so far.

The PEA treated for 17 days exhibited an erratic behaviour over the set of different experiments, either showing values greater than expected given the trend of the other materials, or outside. For instance, independently of the pH media, in the swelling study it reached the highest values, with the exception of PAAc (Figure 3.6). Again its density was greater than those of all the other materials but below that of PAAc. Despite the fact that the thermal degradation profiles of PEA-17d and PAAc are very different (Figure 3.8), the percentages of solid residue left were very similar. In the contact angle measurements, the exception was, once more, PEA 17-d, which notwithstanding a previous swelling it continued to hide its hydroxyl groups, or maybe a further modification decreased its number (Figure 3.10 B). This anomalous performance suggests that such a long treatment in nitric acid induces other chemical

modifications besides the random hydrolysis of side chains, which would require a further characterization.

Effect of the nitric acid treatment on PEA biological performance

Concerning the biological experiments, the MTS assay revealed positive results (Figure 3.13), which turned to be better according to haematoxylin-eosin stainings (Figure 3.14 and Figure 3.15). On all studied substrates (PEA, PEA-4d and P(EAcoAAc)) fibroblasts showed extended morphology and a great density, even surpassing sometimes the positive control. The better outcome achieved by PEA over the copolymer and treated PEA in the MTS test, could be attributed to an initial variation of the pH medium induced by the presence of side carboxyl groups that might affect cells metabolism reducing absorbance levels. The divergences between the MTS results and the stained samples could be explained by the amount of medium on which they were cultured: 200 μL for the samples employed for MTS assays, whereas 400 μL for the stained samples. It is plausible that this increase on the amount of medium was enough to buffer the pH variation induced by the acid groups of the materials.

Another side-effect of the –COOH groups was its interference in the eosin staining. For the cells cultured on P(EAcoAAc) and more moderately for those cultured on PEA-4d, at short times, the eosin staining was not properly fulfilled but replaced by the blue coming from the acidophilic haematoxylin staining due to the material own acid groups. This inconvenience could be avoided when enough cells come to shield this effect of the material surface. For longer time points, the staining was perfectly accomplished with cells cytoplasm coloured in pink.

HUVECs are very sensitive cells, but this did not prevent them from proliferating and assembling into circular structures on all the 2D materials employed. These results broaden the possibility of obtaining vascular-like structures when HUVECs will be seeded into 3D PEA scaffolds.

3.4.- Concluding remarks

The use of porogen templates in combination with particle leaching methods allows the production of PEA scaffolds with different morphologies. In the case of PEA-o, scaffolds exhibiting a grid-like structure with a porosity around 76% were obtained. PEA-o scaffolds are intended to guide and organize cell growth through the orthogonally interconnected channelled pores with diameters in the range of 150 microns. As for the PEA-s scaffolds, a higher porosity was obtained (80%); in this case the spherical interconnected pores in a sponge-like architecture are envisaged to provide a better molecular diffusion. The preparation processes employed leave though a fingerprint on the PEA matrix of the scaffolds when compared with bulk PEA, which has to be taken into consideration.

Regarding PEA-s, the fabrication process leaves a small fraction of MMA units that are incorporated into the polymeric network. Given the contrasted biocompatibility of PMMA, this can be considered as an innocuous incorporation in terms of the biological development of the scaffolds and no more studies have been undergone.

The fabrication of PEA-o with polyamide porogen templates implies the use of nitric acid as solvent. PEA immersed in acid solutions experiences the hydrolysis of its side chains in some units. As a consequence, the acrylate is transformed into an EA-AAc random copolymer. The amount of modified units is proportional to the duration of the acid treatment: a rate of conversion around 10% was estimated for treatments lasting between 4 and 9 days. For longer treatments, such as 17 days studied herein, other changes that would require a further characterization take place.

The chemical changes occurred in the structure translated into variations in the physico-chemical properties of the material, turning PEA into a more hydrophilic, pH-sensitive polymer, able of vitrifying at physiological temperature in the dry state. In the scope of the *in vitro* biological studies, PEA proved to be biocompatible even exhibiting a performance comparable to the positive control. In spite of the changes induced by nitric acid rinses, the polymers were also perfectly suitable for its use in cell culture-related applications.

Chapter 4:

Mechanical performance of PEA scaffolds

4.-Mechanical performance of PEA scaffolds

4.1.- Abstract

The intended application of the materials employed through this Thesis: cardiac tissue engineering, makes of capital importance to undertake an exhaustive characterization of their mechanical performance.

In the first section herein, the elastic moduli under dynamic loading in tension for bulk PEA and both PEA-s and PEA-o scaffolds are compared. The influence of the scaffolds' porosity, the nitric acid rinses to dissolve the nylon fabrics templates and the use of templates based on PMMA spheres on the elastic modulus have been discussed.

In the second section, the PEA-s scaffolds performance under fatigue conditions are studied and compared to that of the analogous bulk material. Two different types of solicitations were applied to the materials: torsion and tension. Both types of solicitations were considered because if the developed materials are to be implanted in the heart, they will be subjected to both of them.

The effect of the fatigue loading on the shear and tension moduli has been evaluated by comparing with non-fatigued materials. Moreover, such influence has been assessed on dry samples measured in air but also on swollen samples and measured in immersion.

In general, the fatigue loading to which the employed materials were submitted had a subtle effect on the mechanical properties, even for the porous materials. The results obtained thereby guarantee their suitability for their use in cardiac tissue engineering.

4.2.- Results

4.2.1.- Elastic moduli of bulk PEA, PEA-o and PEA-s

The elastic modulus of bulk PEA was determined from the initial slope of the strain-stress plots obtained by stretching the sample at a constant rate (Figure 4.1); a value of 0.75 ± 0.09 MPa was obtained. When the same procedure was repeated with the two types of scaffolds under consideration, it was found that the PEA-o modulus suffered a great reduction because of the porosity, reaching a value of 0.04 ± 0.02 MPa; unexpectedly, for the PEA-s (despite its great porosity-higher than in PEA-o-), no relevant reduction on the modulus was observed, yielding a value of 0.78 ± 0.21 MPa.

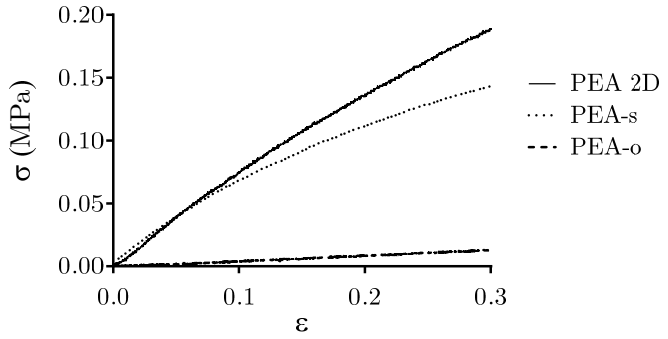

Figure 4.1: Initial section of the strain-stress curves for bulk PEA, PEA-s and PEA-o scaffolds.

4.2.2.- PEA mechanical performance under fatigue conditions

The following fatigue experiments were performed on bulk materials to purely assess the effect of fatigue on the employed polymer, and also for the PEA-s, to study the influence of its porosity and production process on the mechanical performance. Even if the PEA-s modulus is higher than that of PEA-o, given its greater porosity and thinner trabeculae it was thought to be more sensitive to the fatigue effects and thus the fatigue experiments were only performed with this type of scaffolds.

Torsion

The moduli of bulk PEA was determined under shear solicitations at 37°C either dry (D), or swollen and immersed in PBS (S), before and after being submitted to a week of torsional fatigue (Figure 4.2). All the considered series are in the same range of values. Nonetheless, when the area is zoomed, it is observed that the fatigued (F) samples (both D and S) exhibit slightly higher moduli values (146 and 161 kPa, respectively) than non-fatigued (NF) ones (104 and 53 kPa). Subtle differences were detected between the NF materials when measured D or S, the moduli of D samples being slightly higher in the range of frequencies scanned. For all the series, an increase of the moduli with the frequency is observed, which shows the beginning of the main relaxation; this beginning seems to be shifted to a small extent toward higher frequencies in the case of the swollen samples.

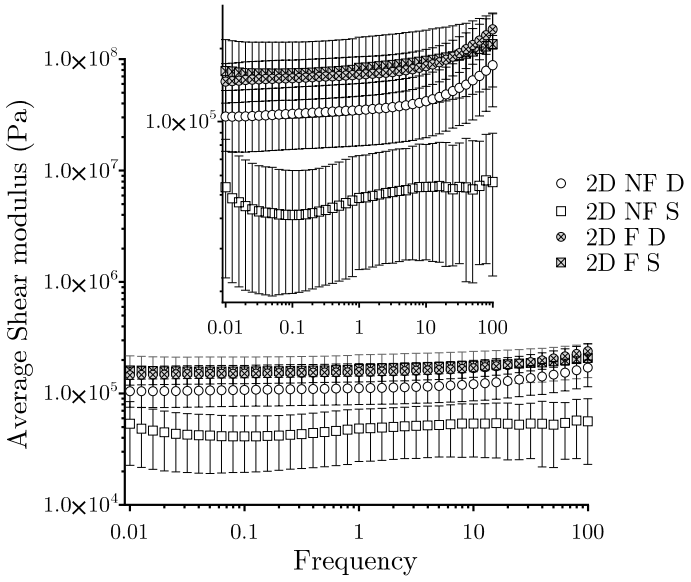

Figure 4.2: Frequency scans of the bulk PEA shear moduli measured at 37°C with samples either dry in air or swollen and immersed in PBS, before and after a week of torsional fatigue.

No differences were detected between the NF and F dry samples in terms of the loss tangent (Figure 4.3), while for the S ones, the fatigue had an effect decreasing the loss tangent in the range of considered frequencies. As previously detected in the

modulus scans, the main relaxation is shifted towards higher frequencies for the S samples.

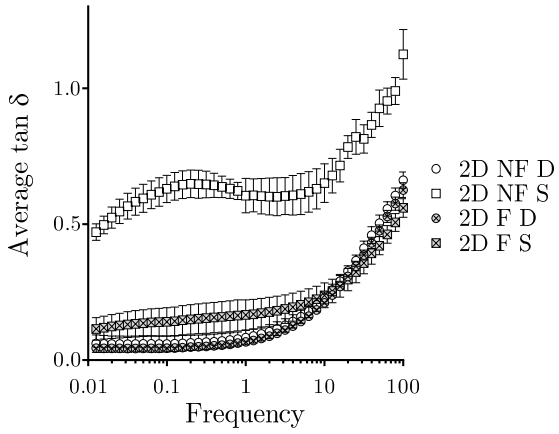

Figure 4.3: Loss tangent for PEA bulk samples fatigued or non-fatigued with torsion solicitations, measured under shear stress dry in air or swollen and immersed in PBS at 37°C.

The effect of torsional fatigue was also assessed for PEA-s scaffolds (Figure 4.4). In this case the moduli values were in the same range as for the bulk materials, and only small differences because of the fatigue or swelling conditions of the samples were detected. Briefly, both NF and F samples, achieved higher modulus values when measured in the dry state (118 and 177 kPa) than S (37 and 80 kPa), F and NF being alternated depending on if samples were S or D. In this case, subtle shifts towards higher frequencies were detected for any series of samples, as the measurements were performed in a narrower range of frequencies: only up to 1 Hz, because of an instrumental limitation (for higher frequencies the equipment entered into resonance and could not properly measure the samples' moduli).

When the loss tangent is analyzed (Figure 4.5), the fatigue is found to reduce it slightly, but combined with swelling it increases it.

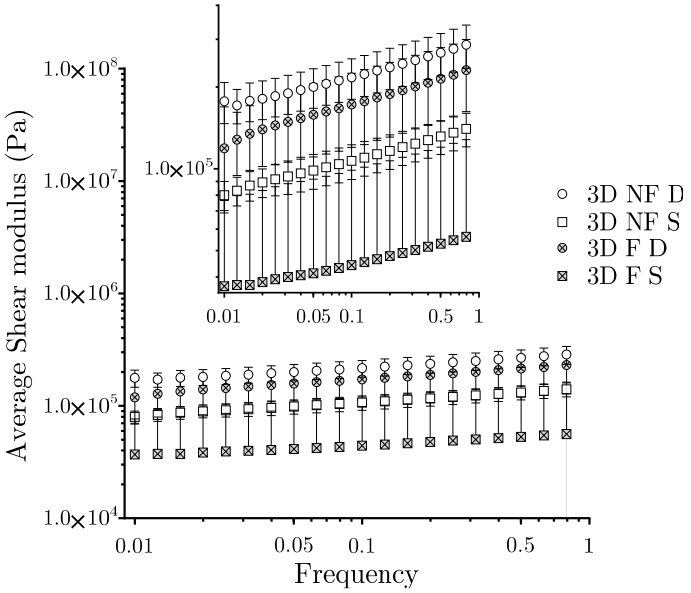

Figure 4.4: Frequency scans of the PEA-s shear moduli measured at 37°C with samples either dry in air or swollen and immersed in PBS, before and after a week of torsional fatigue.

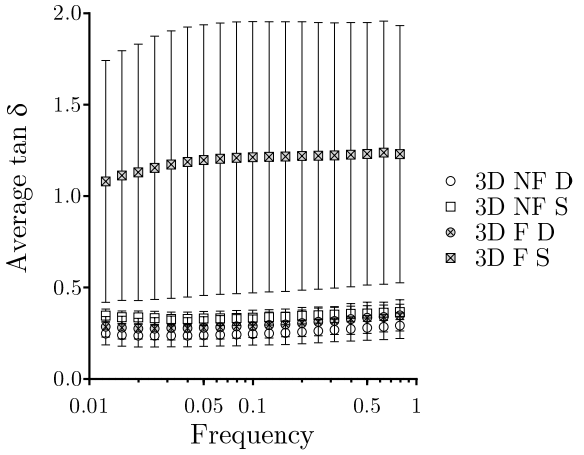

Figure 4.5: Loss tangent for PEA-s samples fatigued or non-fatigued, measured dry in air or swollen and immersed in PBS at 37°C.

Tension

a) Frequency scans

The effect of cyclic unidirectional tension (Figure 4.6) was also assessed through a scan of frequencies under a tension solicitation. In all cases the moduli (which are in the range of 0.77 to 1 MPa), increased with frequency, although this changes are only detected when the area is enlarged. For samples fatigued in air (FA), an increase on the moduli was observed, though the increase was more evident when samples were fatigued immersed in PBS (FI). Meanwhile, swelling the samples induced as well a small increase on the moduli and displaced the resulting curves towards higher frequencies.

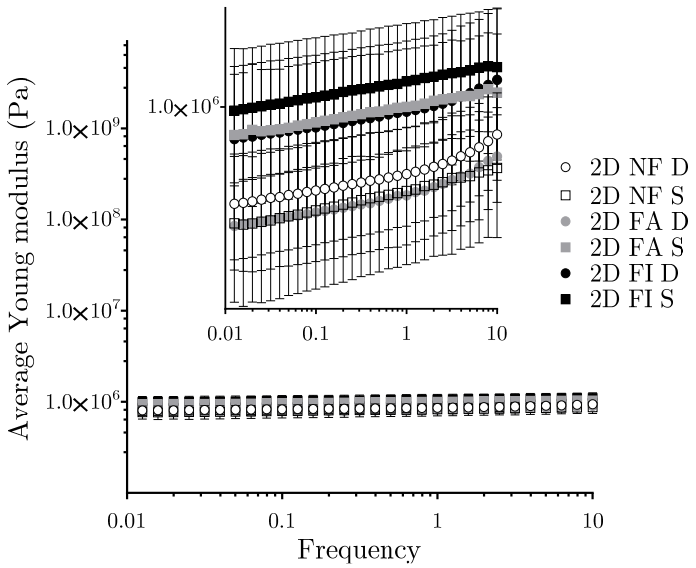

Figure 4.6: Frequency scans of the tension elastic modulus of bulk PEA at 37°C measured either dry or swollen and immersed in PBS, before and after a week of tensional fatigue. Inset: zoom of the area of interest.

No significant differences were observed in the loss tangent plots (Figure 4.7). No effects of the fatigue are observed in this parameter; however, the S samples exhibit slightly lower values, indicating thus that the main relaxation is, as observed in the moduli plots, is displaced towards higher frequencies.

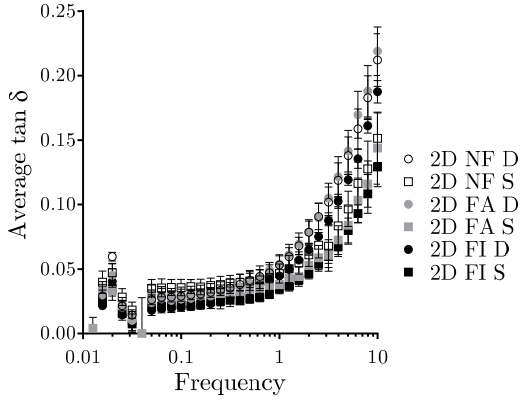

Figure 4.7: Loss tangent values for bulk PEA samples fatigued or non-fatigued under tension, measured dry or swollen and immersed in PBS at 37°C.

Concerning the PEA-s scaffolds, similar results were obtained (Figure 4.8). The measured moduli were in the range of 0.4 to 1.2 MPa, and an increase with the frequency was also observed when the area was broadened. Fatigued samples reached higher moduli values and especially those fatigued in immersion (FI) and measured swollen. However, for the NF PEA-s scaffolds, S samples exhibited lower moduli values. As previously explained, measurements were only performed up to 1 Hz because of equipment limitations.

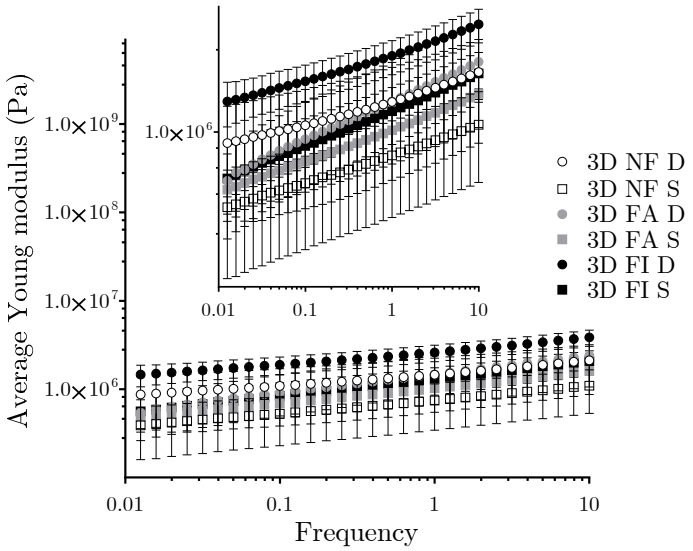

Figure 4.8: Frequency scans of the PEA-s tension elastic modulus at 37°C with samples either dry or swollen and immersed in PBS, before and after a week of tensional fatigue.

Practically no differences among the series were observed in the loss tangent plots (Figure 4.9) as they are almost overlapped.

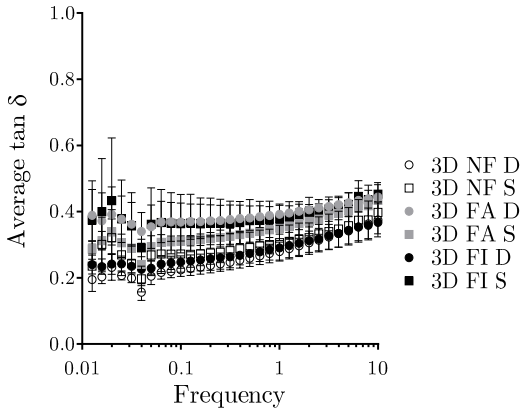

Figure 4.9: Loss tangent for PEA-s samples non-fatigued or fatigued in air or PBS immersion under tension, measured dry or swollen and immersed in PBS at 37°C.

b) Tensile measurements to failure

Analogous experiments to those presented in section 4.2.1 were performed with PEA bulk samples before and after fatigue at 37°C either in air or immersed in PBS (Figure 4.10). For the non-fatigued samples a modulus of 0.67 ± 0.06 MPa was obtained; for the samples fatigued in air a similar value was obtained, 0.59 ± 0.07 MPa, whereas an unexpected increase was observed for the samples fatigued immersed in PBS: 1.79 ± 0.38 MPa.

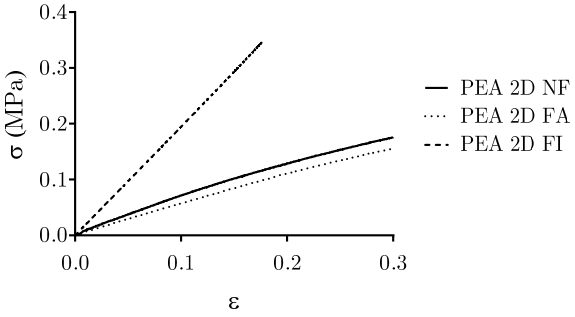

Figure 4.10: Initial section of the strain-stress curves for bulk PEA non-fatigued, fatigued under tension solicitations in air at 37°C, and fatigued under tension immersed in PBS at 37°C.

4.2.3.- Additional results

In order to elucidate if the fatigue was inducing changes in the polymer network of the materials under study, a set of supplementary experiments were performed. FTIR spectra and swelling data were employed to follow any changes in the chemical structure of PEA because of the fatigue. EDS spectra were obtained to evaluate if the amount of deposited salts from PBS in the polymeric matrices was significant enough to induce variations on the measured moduli.

FTIR

As can be observed in the FTIR spectra (Figure 4.11), the characteristic peaks of PEA (like the 1715 cm^{-1} and the wide peak around 2900 cm^{-1}, previously discussed in Chapter 3) are present for all the samples. However, no significant differences can be observed between fatigued and non-fatigued samples with respect to the detected peaks or their height.

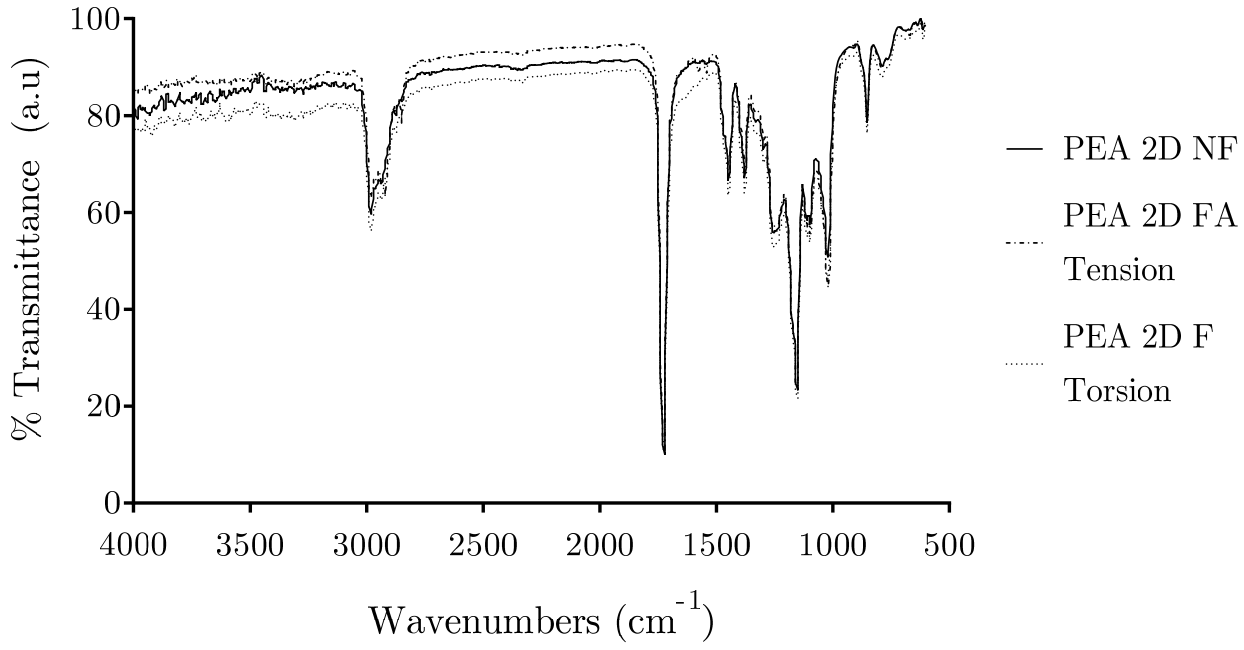

Figure 4.11: FTIR spectra of 2D PEA samples non-fatigued (NF), fatigued under torsion (F), and under traction dry at 37°C (FA), obtained between 500 and 4000 cm^{-1}.

Swelling experiments

No significant differences in the swelling kinetics were detected among the non-fatigued and fatigued samples, either under tension or torsion conditions, when swollen in EtOH/water mixtures or in pure EtOH (Figure 4.12). Nonetheless, differences because of the swelling medium were detected: samples swollen in EtOH reached the equilibrium faster than in EtOH/water mixtures, 1 day *vs.* 3 days.

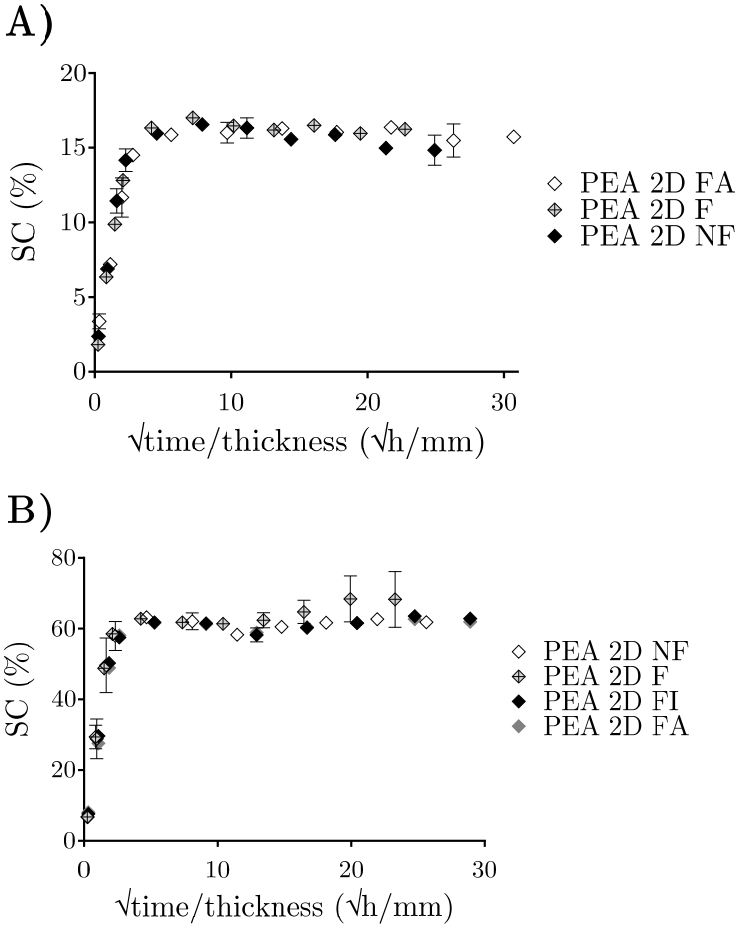

Figure 4.12: Swelling kinetics of samples non-fatigued and fatigued under traction and torsion in a) 50/50 EtOH /water mixtures and b) EtOH.

Analogously, the solvent content in the equilibrium for the samples swollen in EtOH was almost 4 times higher than that of samples swollen in EtOH/water mixtures (61% *vs.* 16%) (Figure 4.13). The values of equilibrium solvent content in EtOH/water mixtures, exhibit significant differences because of applying fatigue to

the samples, while when swollen in EtOH differences are observed only for samples fatigued under torsion.

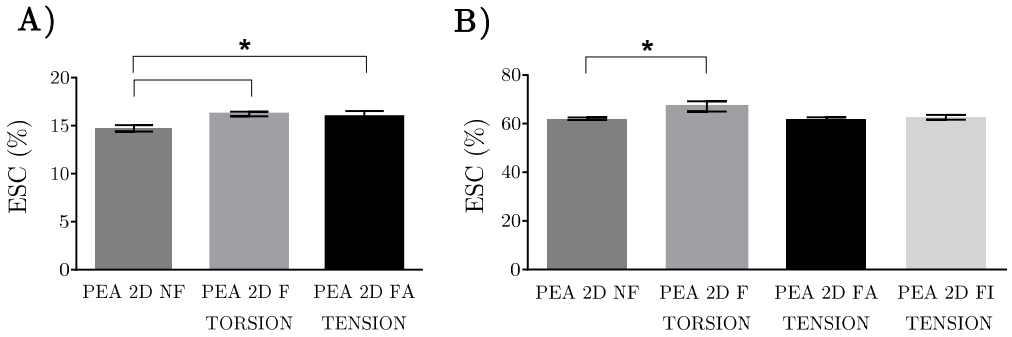

Figure 4.13: Equilibrium solvent content for non-fatigued samples and samples fatigued under tension and torsion in a) EtOH/water and b) EtOH.
(*) Differences are statistically significant.

Energy dispersive X-ray spectroscopy (EDS)

Energy dispersive X-ray spectroscopy was employed to determine if a significant amount of the PBS salts were incorporated into the scaffold structure during the fatigue experiments and could have an influence on the mechanical results obtained. As Figure 4.14 shows, there are no differences in terms of fraction of chemical species incorporated between non-fatigued and fatigued samples, or because of performing it immersed in PBS.

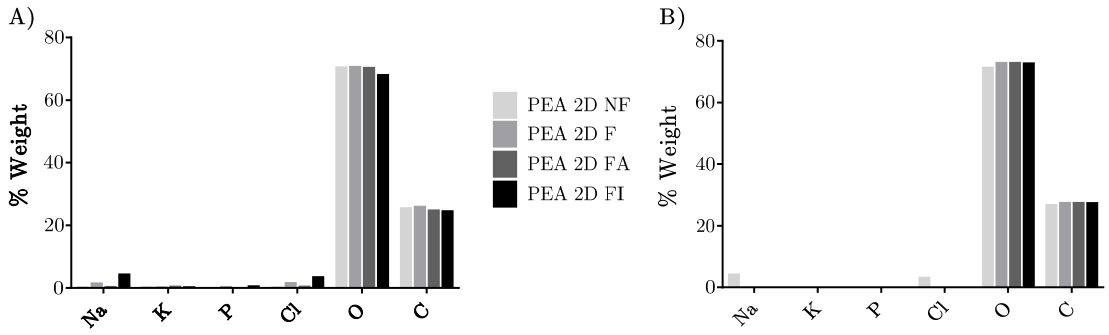

Figure 4.14: Weight percentage of the elements composing the materials' surface (a) and section (b), determined by EDS before and after fatigue under torsion, tension in air or immersed at 37°C.

4.3.- Discussion

On the mechanical properties of the scaffolds employed in this Thesis

The determination of the tensile moduli, as the average of the initial slope of the lineal region of the strain-stress plots of the different replicas (Figure 4.1), revealed a great reduction from the value obtained for the bulk material to that of PEA-o (from 0.75 ± 0.09 MPa down to 0.04 ± 0.02 MPa). The so-called reduced tensile modulus of a scaffold, E_R, normalized taking into account its measured porosity, is to follow $E_R = E(1-\pi)^2$ according to [275], where E is the modulus obtained for the bulk polymer, for PEA films in this case, and π the porosity of the scaffold (76.1 ± 6.1% for the PEA-o scaffolds). When the reduced modulus is compared to the measured PEA-o modulus, the equation fits well the tensile behaviour of the scaffolds (0.04 ± 0.02 *vs.* 0.042 ± 0.02 MPa).

When the reduced modulus is calculated for the PEA-s scaffolds, whose porosity is 80.8 ± 3.5%, a value of 0.028 ± 0.01 MPa is obtained, while the elastic modulus given by the curves is 0.78 ± 0.21 MPa. This discrepancy is not a problem of the model but of the measured samples. As already discussed in Chapter 3, the PEA-s scaffolds production process seemed to leave PMMA traces on the scaffold, thus changing the PEA properties, which is corroborated by these results. As already discussed, given the good biocompatibility and non-cytotoxicity of this polymer, these PMMA traces are not of major concern. Moreover it could be of interest as provides a mechanical reinforcement to the scaffold.

Given the presented range of moduli values for the materials (in the same order as other elastomers [275]), and that the reported range of pressure that the heart withstands at the systolic peak (117 mmHg, *i.e.* 0.015 MPa) and diastole (10 mmHg,

i.e. 1.33 kPa) are in the range of these materials elastic behaviour [276]; the developed materials are perfectly suitable to resist the loads present in the heart.

As briefly presented in the introduction (Figure 1.1 B), therapies involving the application of a mechanical restraint to the heart (to limit the ventricular remodelling that follows a myocardial infarction) are also considered. These approaches include the use of meshes made of different materials such as polypropylene [277], polyesters [278] and even a nitinol metallic alloy [279]. The major drawback of these approaches is that they do not contribute to the regeneration of the damaged tissue. Therefore, in a recent work, the Acorn Corcap (a polyester mesh) was employed in combination with a collagen scaffold to also contribute to the tissue recovery [280]. The materials presented in this Thesis, since have a high enough elastic modulus, and are porous and cell-friendly, could also be useful as a combined system supplying cells and factors besides providing a certain mechanical reinforcement. Evenmore, bulk PEA and PEA-s scaffolds have an elastic moduli above that of the human myocardium (which is in the range of 0.2-0.5 MPa) [28], therefore they are useful as ventricular restraints.

Fatigue parameters

Choosing the parameters employed for the torsional fatigue experiment was not straight forward given the limited and disperse bibliography concerning biomaterials torsional fatigue and the heart mechanical characterization (torsion, withstood pressure, twisting/untwisting rate and dimensional changing, among others).

It was decided to apply the torsional fatigue at the most adverse conditions of the heartbeat. Therefore, as reported by [281], the maximal untwisting rate for human hearts is 90º/s, which is maintained with diastolic dysfunction, and reduced for systolic dysfunction. Thus, 90º/s was selected as the most restrictive twisting rate.

Assuming a heart pace of 60 beats per minute, this leads us to a torsion of 90°/cycle, then 45° of twisting and 45° of untwisting to complete 90° in a cycle in 1 second.
The parameters for the tensional fatigue were more easily determined as there are more references where biomaterials intended for cardiac tissue engineering are submitted to tensional cyclic loading [87, 282, 283]. In these previous works, samples were submitted to cyclic deformations applying a strain of 10 to 20% of the initial length because the physiological value of strain is around 15% [284]. In our case, to be on the safe side, it was decided to reach up to 30% strain: first applying a pre-stress of 15% plus an extra 15% following a sinusoidal, thus oscillating between 0 and 30% of strain.

Effect of fatigue on bulk PEA

The moduli values for all the 2D series measured in shear or tension, before and after fatigue were in the same range: around 0.1 MPa under shear and near 0.8 MPa under tension.

As expected, a subtle increase (only detected when the area is zoomed) is observed on the modulus with the frequency of excitation (for both types of solicitations). Performing a dynamic mechanic test scanning increasing frequencies has a reverse equivalency to scanning reducing the temperature, by the time temperature superposition principle [285]. Herein, the increase in frequency leads towards the transition from the elastic region to the vitreous one. Such a change translates into a reduction of polymer chains mobility which gives place to a modulus increase, whose beginning is observed for the dry samples (the swollen samples are shifted towards higher frequencies, probably because of the water plastifying effect).

Regarding the loss tangent under shear (Figure 4.3 and Figure 4.5), the higher losses are those of the swollen samples. This augmentation implies an increase on the losses

[286], which could be attributable to a dissipative effect of the water entrapped in between the polymer chains [287]. Meanwhile for samples measured under tension, the loss tangent for the swollen samples reaches lower values although it seems to be because of a shift of the main relaxation towards higher frequencies; thus, a broader range of frequencies should be scanned to verify if the swollen samples also exhibited higher values at higher frequencies.

After a week of fatigue the samples exhibit a slight increase on their shear modulus, both measured swollen and dry. Under tension, the greatest values are obtained for the samples fatigued in immersion, and even higher when measured swollen.

Concerning the strain-stress curves presented in Figure 4.10, fatigue under tensional fatigue in air does not induce remarkable changes on the mechanical profiles, nor in the resulting elastic moduli. Different results are obtained for the samples fatigued immersed in PBS, in terms of the profile of the curves and increase in their moduli.

These subtle differences outlined, given the order of magnitude of the results and the error bars, are not of major concern. Moreover, the finding of a slight increase of the mean value is not detrimental for its intended application. Nonetheless, it was attempted to unveil the underlying mechanism (if any) inducing such a change.

The fact that samples fatigued in PBS or measured immersed, exhibited higher moduli values, led to the hypothesis that applying the cyclic stress in PBS immersion (or measuring the moduli in immersion in PBS), allowed salts diffusion and deposition within the polymeric matrix, thus inducing a hardening of the samples by reducing chain mobility because of salt precipitates. Nonetheless, the elemental analysis (Figure 4.14) performed on section and surface areas, detected only small traces of salts while the main composition remained constant. Such a small amount

of salts seems not to be significant enough to explain the differences detected in the moduli values.
The collected FTIR spectra of the samples show (Figure 4.11) that the fatigue does not induce the appearance of new peaks or alters the dimensions of the peaks of the profile, either. Thus, there do not seem to be new functional groups on the studied materials as consequence of their treatment.

Finally, swelling experiments in different media were also undertaken (Figure 4.12 and Figure 4.13). These results (where fatigue increases the equilibrium solvent content), are indicative of the absence of additional crosslinks in the polymeric network because of the fatigue.

In sum, the small variations because of the fatigue are not attributable to the formation of new groups in the chemical structure, neither to variations on the composition of the sample, nor to increases in the degree of crosslinking of the polymeric network. Thus, other explanations were explored.

It was hypothesized that a side effect of applying fatigue loads to the samples could be the induction of polymer chain rearrangements, favouring the diffusion of defects and the untanglement of the chains, resulting in a more regular network with fewer defects and entanglements, which would translate into a reduction of the free volume. This reduction on the free volume would have a direct effect on the elastic moduli of the samples in the sense of slightly increasing it. The fact that fatigued samples reach slightly higher equilibrium solvent contents (Figure 4.13) would be in good agreement with this assumption. Nonetheless, this hypothesis would need to be checked with further experiments, out of the scope of the present work. Density variations or other experiments to elucidate variations on the network disposition could be of interest. Supporting this hypothesis, it has been previously reported that for amorphous

polymers in the glassy state a hardening under strain can take place [288]. Maybe the increase observed in the presented results could be explained by an analogous effect for the materials in the rubber state, which takes into account the distinct behaviour and time constants for these two different states of amorphous polymers.

Effect of fatigue on PEA-s scaffolds

The moduli reached by the scaffolds under shear and tension are of the order of those of bulk PEA despite of the scaffolds porosities (Figure 4.4, Figure 4.8 and Figure 4.10). These results suggest once more that there are traces of PMMA remaining on the PEA-s scaffolds. Although for the fatigued and swollen samples slightly lower values are obtained, the modulus variation observed is not of major concern as again it remains at a high enough level to guarantee the potential success of this material upon implantation. Once more, the slight differences detected in the loss tangent (Figure 4.5), the values being higher for the swollen and fatigued samples, could be attributable to the presence of water dispersing the energy as previously discussed for the bulk material.

The fatigue seems to increase the moduli of the samples, especially when it is performed with the samples swollen in PBS as already discussed for the bulk materials. When compared with the scans of the bulk materials, a greater slope increase is observed for the higher frequencies. The fact that the fatigue induces a greater effect on PEA-s scaffolds than in bulk materials, having the former a much lower fraction of mass than the films, suggests that the previously described hardening phenomenon could be mass-related. The presence of PMMA traces on the scaffolds could also have a certain effect in that sense.

Tensional and torsional modulus comparison

The rubber theory was applied to the obtained results to verify if the inter-relation of both elastic parameters thereby predicted is valid for the performed experiments. A mathematical relation between the elastic modulus in tension (E) and the shear modulus (G) is known [285]:

$$G = \frac{E}{1 + 2\nu} \qquad \text{[Equation 4.1]}$$

where ν is the Poisson ratio, which varies from 0 for incompressible rigid solids up to 0.5 for liquids. As PEA is a rubber in the range of temperatures employed, the Poisson ratio was fixed to $\nu = 0.5$. Solving the equation it was found that the tension elastic modulus should be 3 times the shear modulus. However, the obtained measurements do not fit into this model, with the exception of an isolated case as shown in Table 4.1.

SAMPLES			E/G
2D	NF	D	7.64
		S	14.34
	FA	D	5.26
		S	5.80
	FI	D	6.33
		S	6.13
3D	NF	D	4.70
		S	**2.71**
	FA	D	3.94
		S	12.09
	FI	D	11,45
		S	13.26

Table 4.1: Elastic modulus under tension to shear modulus ratio for the fatigued, non-fatigued, dry or swollen 2D and scaffolds samples.

In general, the shear moduli were lower than expected, especially for the swollen samples. These discrepancies perhaps could be attributable to the conditions employed in these shear measurements.

Although throughout this chapter any small difference was pointed out and intended to explain, in general terms and given the error bars, the discrepancies on the elastic moduli are not significant. Moreover, applying cyclic loads does not produce a dramatic decrease on the materials mechanical performance despite of their porosity, but a certain increase. Thus, these materials are suitable for their intended use.

4.4.- Concluding remarks

The materials employed exhibit an elastic behaviour for the stresses withstood by the heart. Moreover PEA and PEA-s scaffolds exhibit elastic moduli greater than that of the human myocardium; therefore they are capable to provide a mechanical reinforcement to limit the ventricular remodelling.

Preparing PEA in the shape of scaffolds has effects on its mechanical properties. In the case of PEA-o, because of its porosity the elastic modulus under tension is reduced, while it is increased for PEA-s despite their porosity, because of the PMMA traces present.

Bulk PEA and PEA-s scaffolds resist (without significant variations on their mechanical performance) cyclic loading in tension or torsion, for at least one week.

A slight increase on the modulus is observed for the fatigued samples. The supplementary experiments performed revealed that the differences detected between fatigued and non-fatigued samples are not due to the formation of new functional groups, neither to the formation of new crosslinkings nor because of salts deposition within the polymer chains. The variation of the modulus could be a hardening phenomenon taking place; however further systematic studies will be needed to determine the cause of this increase.

Chapter 5:

PEA scaffolds' pores coating with hyaluronan

5.- PEA scaffolds' pores coating with hyaluronan

5.1.- Abstract

The aim of this chapter is to present the hybrid system consisting of PEA porous scaffolds combined with hyaluronan (HA) gel as coating in their pores. PEA scaffolds with different architectures and obtained through the two processes previously explained in Chapter 3, were coated with HA solutions and subsequently, *in situ* crosslinked. In the case of PEA-s, a preliminary study showed the unfeasibility of obtaining a homogeneous and stable HA coating throughout the thickness of the scaffold by means of the procedure set up. This problematic was not found for the PEA-o scaffolds; the PEA-s series was therefore ruled out from the experiments and the subsequent coatings and characterization were undertaken with the PEA-o series.

The influence of several parameters on the amount/thickness of HA gel incorporated within the scaffold pores were studied, including: the concentration of the HA starting solutions, the PEA-o thickness, or the number of filling-drying cycles. By changing these factors a wide variety of coating typologies were obtained. The mass fraction of HA and the porosity were employed as indicators of the degree of clogging of the material pores.

The morphology of the obtained coatings was characterized by conventional scanning electron microscopy (SEM), but also with cryoSEM as it allowed the observation of the coatings in their swollen state, which is very interesting given the hydrogel nature of HA and the intended application of the material (biological environments which are mainly aqueous). Compression tests were performed to assess the influence of the coating on the mechanical performance of the scaffolds.

Experiments were also performed to evaluate the feasibility of using this combined system as construct for controlled release of molecules of interest; bovine serum albumin (BSA) was employed as model protein.

Finally, a preliminary cellular experiment was performed with fibroblasts, to assess the improvement, if any, on the seeding efficiency on account of the HA coating within the scaffold's pores.

The undertaken characterization revealed that PEA-o scaffolds (but not PEA-s) could be successfully combined with HA to obtain a combined system. The scaffold was found to exert a confinement effect on the degree of swelling of HA coating, meanwhile the latter had a reinforcing effect in the scaffold behaviour when compressed. The hybrid material was found to be useful for controlled release applications and suitable for cell culture experiments.

The nomenclature employed from now on to refer to the coatings performed to the scaffolds is: first a number (05, 1, 2 or 5) that indicates the concentration (in %) of the hyaluronan solution utilised, then "HA" followed by a second number indicating the number of filling-drying cycles applied (1, 2, 3, 4, 5). Additionally, those samples that are crosslinked exhibit an "x" following the number of applied cycles. To refer to an entire series of a given concentration in which different number of cycles were applied, an "#" is used; as an example, 5HA# refers to the series of samples coated with 5% HA solutions. Finally, when scaffolds with different thickness are compared, "8L" or "16L" is added at the end, depending on the number of porogen layers, L, employed in the PEA-o scaffold. For example, a 16 layers PEA-o scaffold coated with a 1 wt.% HA solution for 5 cycles and crosslinked will be represented by 1HA5x 16L.

5.2.- Results

5.2.1.- Production of perdurable HA coatings

As starting point, the feasibility of a system consisting of PEA elastomeric scaffolds combined with HA gel was evaluated by three preliminary tests. First of all, the fraction of HA incorporated into the PEA matrix was quantified by weight differences between the bare and the coated scaffold before and after the crosslinking step, ω_{HA}. As Figure 5.1 shows for both PEA-s and PEA-o there is a great influence of the HA solution concentration on the amount of HA incorporated within the pores. The higher the concentration the greater the ω_{HA} achieved. Besides, the PEA-o series achieved greater ω_{HA} when compared with PEA-s scaffolds coated analogously.

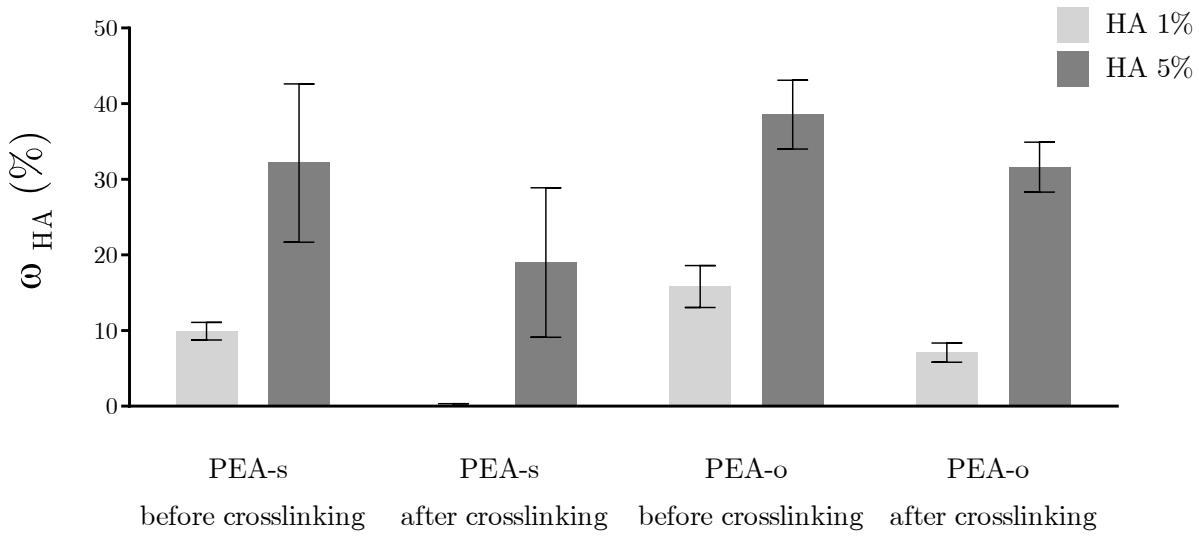

Figure 5.1: Mass fraction of HA (%) retained in the PEA-s and PEA-o scaffolds coated with 1% or 5% HA solutions before and after the crosslinking step.

In the particular case of PEA-s a greater dispersion on the ω_{HA} was observed for the 5 wt.% HA solution, reaching an average value of 32% before crosslinking; nonetheless, after the crosslinking step a ω_{HA} of only near 19% was retained because of the washes carried out and all the manipulation that suffered the samples during

this process. Even worst, in the case of the samples coated with 1 wt.% HA, almost all the HA previously incorporated into the pores (ω_{HA} of nearly 10%), was washed out of the polymeric matrix as will be discussed later.

On the contrary, in the case of PEA-o, less dispersion is observed for the samples with the 5 wt.% HA solution, and a greater HA fraction is preserved within the scaffold after crosslinking, nearly 32%. Moreover, the difference between the ω_{HA} before and after the crosslinking, meaning the amount of HA removed during the process, is significantly reduced (6% for PEA-o *vs.* 13% for PEA-s). In the case of samples coated with 1 wt.% HA solution, better results were also observed for the PEA-o series; despite the fact that the fraction suffers a severe decrease upon crosslinking (almost a 9% reduction), still a ω_{HA} close to 7% remains inside the scaffold's pores.

Next, the non-crosslinked HA coatings and the changes they undergo during the crosslinking step, were morphologically characterized by means of SEM micrographies. As observed in Figure 5.2, when the 1 wt.% HA solution is employed to coat the PEA-s pores, very localized and thin layers reached to cover sporadically some pores. However, after the crosslinking step almost no trace of the thin layers previously obtained are observed; only small scattered remains are detected. When a 5 wt.% HA solution is applied, many throats (especially those with diameters in the range of 10 to 30 μm) are entirely clogged by the HA solution, though the larger pores are not significantly filled. However, after the crosslinking step, only a thin layer of HA coating is detected on the pores surface, even in some regions, as happened with the 1 wt.% PEA-s samples, only scattered remains are observed.

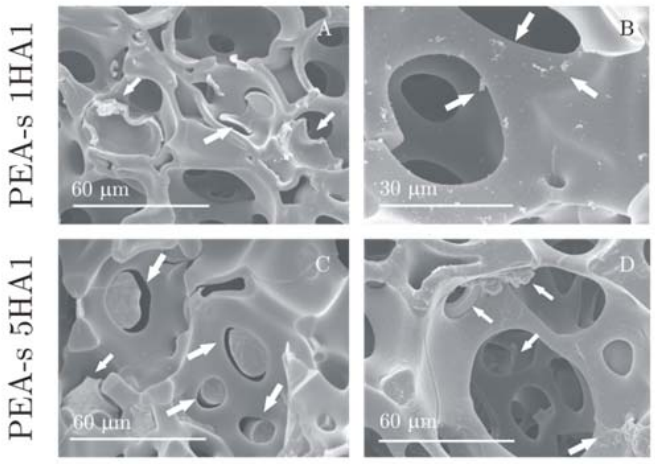

Figure 5.2: SEM images of the PEA-s dry scaffolds 1HA1 (A), 1HA1x (B), 5HA1 (C) and 5HA1x. The arrows point at the adsorbed HA.

In the PEA-o scaffolds coated with 1HA1 (Figure 5.3), before the crosslinking step an uniform coating layers are observed in some pores, and in some cases pores are partially clogged. For those samples coated with 5HA1, many pores present a thick layer that clogs some channels. After the crosslinking, even for the 1 wt.% HA coated samples, in some region continuous thin layers of HA coating were observed. When the HA 5 wt.% solution was employed, some pores were partially clogged after the crosslinking step.

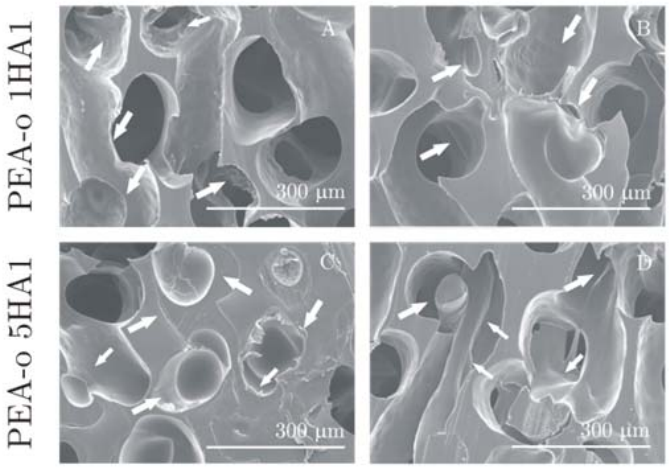

Figure 5.3: SEM images of the PEA-o dry scaffolds 1HA1 (A), 1HA1x (B), 5HA1 (C) and 5HA1x. The arrows point at the adsorbed HA.

Finally, by means of an alcian blue staining, the HA coating evolution in the two types of scaffolds was evaluated. As seen in Figure 5.4, bare PEA-s remains white after the alcian blue staining and rinse. On the contrary, both non-crosslinked samples coated with HA either with a 1 or 5 wt.% solution exhibit a bright blue all over their surface and throughout its cross section. However, the 1 wt.% HA coated and crosslinked sample is hardly bluish, closely resembling the bare PEA-s. As regards the 5HA1x PEA-s, a uniform bright blue colouring remains in the surface; nonetheless, when the cross section is exposed, it can be observed that all the HA has been extruded from the inner pores towards the scaffold external surfaces. As a consequence, all the remaining HA is concentrated in the periphery area of the scaffold.

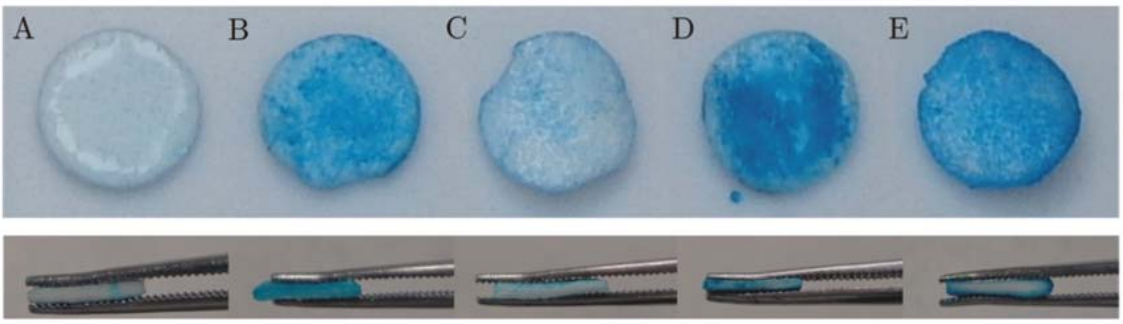

Figure 5.4: PEA-s samples stained with alcian blue after no treatment (A), or after 1HA1 coating (B), 1HA1x coating (C), 5HA1 coating (D) or 5HA1x coating (D).

As for the PEA-o samples, as can be seen in Figure 5.5, the bare scaffold retains a certain light blue shade after the washing step following the alcian blue staining. However, when this colouration is compared with that of the coated scaffolds the differences are evident. Both non- and crosslinked samples coated either with a 1 or 5 wt.% solution exhibit a dark blue colour all over their surface. Regarding the cross sections, all the materials exhibit a uniform blue colouring throughout its section. This uniform staining indicates the presence of HA uniformly distributed through all the pores of the scaffolds.

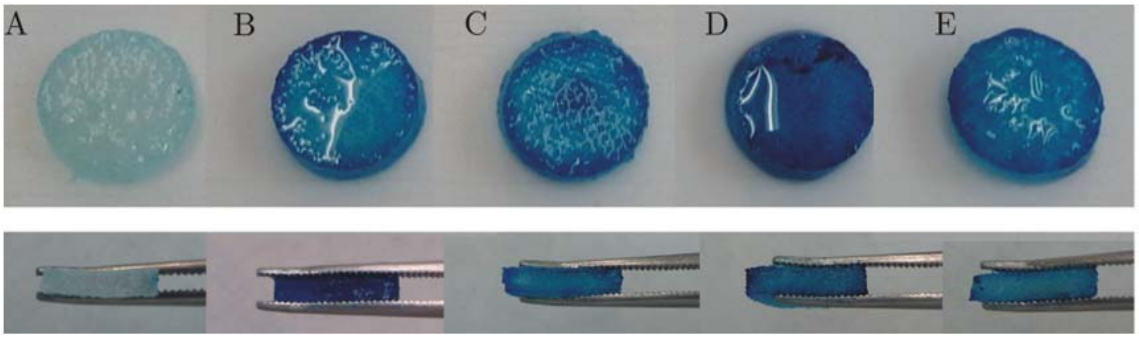

Figure 5.5: PEA-o samples stained with alcian blue after no treatment (A), or after 1HA1 coating (B), 1HA1x coating (C), 5HA1 coating (D) or 5HA1x coating (D).

Taken these results together, as will be discussed later, it was decided to discard the PEA-s series from the study and the following experiments and characterization were only undertaken with bare and coated PEA-o.

5.2.2.- Coating typologies

Different coatings typologies were obtained by coating the scaffolds up to different extents, by means of changing several parameters of the process. The main features of the resulting combined materials were characterized; interestingly, some of the obtained results differed from what was expected.

Coating typologies obtained by changing the solutions concentrations and the number of cycles applied

This first set of materials was obtained by filling scaffolds produced with 8 layers of nylon fabrics as porogen, with HA solutions at two different concentrations (0.5 wt.% and 5 wt.%), and applying different numbers of filling-drying cycles, and in some cases applying a crosslinking step. As a result, a variety of coatings with different behaviour were obtained.

Representative SEM images of the different coatings in their dry state, without applying a crosslinking step are shown in Figure 5.6. The bare PEA scaffolds in a cross section and a frontal view, respectively, are displayed in Figure 5.6 A and B. One coating cycle with the 0.5 wt.% HA solution leaves scattered HA aggregates on the internal surface of the scaffold, as Figure 5.6 C shows. These aggregates become more numerous as the number of cycles increases, but a uniform layer on the surfaces is not obtained even after 5 cycles with this solution concentration (Figure 5.6 D). By contrast, after the first cycle the coating with the 5 wt.% HA solution already leads to a uniform continuous layer.

The effect of further cycles is to increase the thickness of the layer, with the corresponding decrease in the pore diameter as well as the clogging of some pores, as observed in Figure 5.6 E. After the fifth cycle, Figure 5.6 F, the channels are filled with HA to a high degree.

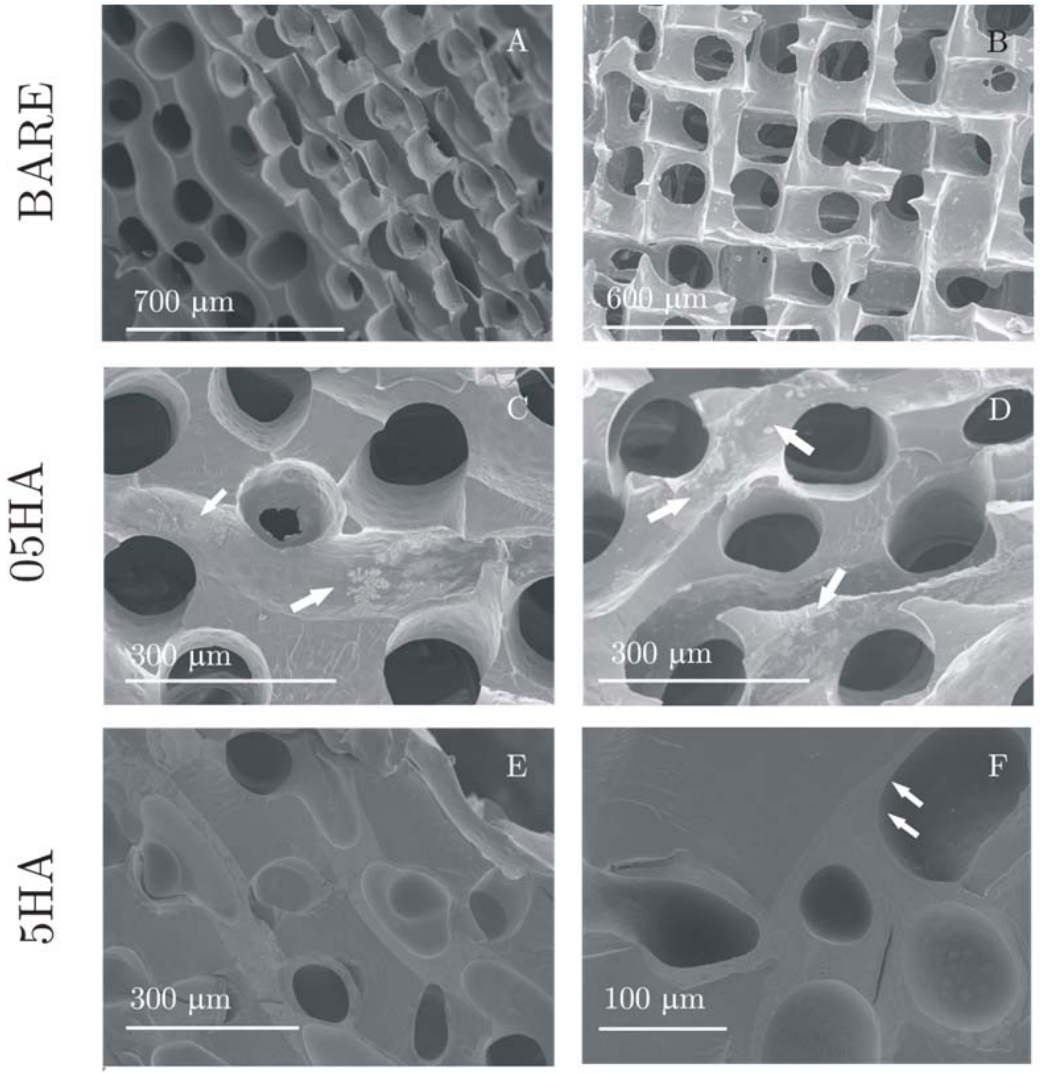

Figure 5.6: SEM images of the dry PEA scaffolds: (A and B) bare scaffold, cross section and frontal view, respectively; (C) 05HA1; (D) 05HA5; (E) 5HA2; (F) 5HA5.
The arrows point at the adsorbed HA.

In order to quantitatively assess the amount of HA incorporated into the PEA-o scaffolds, the HA mass fraction, ω_{HA}, was determined for each concentration and number of cycles after intense drying to only take into account the mass of HA xerogel. As Figure 5.7 A shows, the amount of adsorbed HA increases with the number of filling cycles both for the 0.5 wt.% and the 5 wt.% HA solutions.

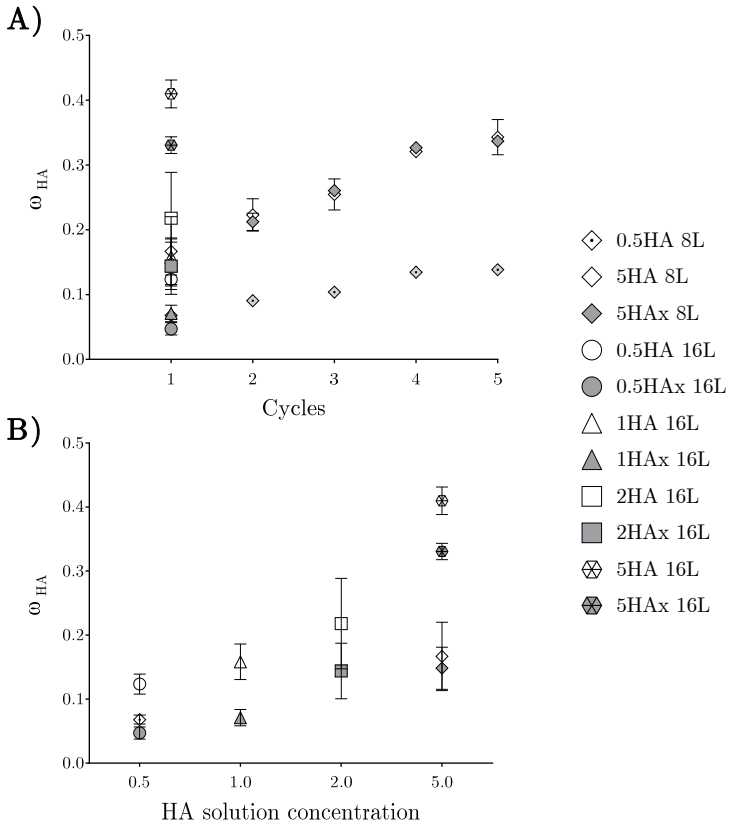

Figure 5.7: Mass fraction of HA, ω_{HA}, as a function of A) the number of cycles and B) the HA solution concentration.

The PEA scaffold adsorbed around 7% of HA in the first cycle with 0.5 wt.% HA solution. Afterwards, the amount of HA absorbed per cycle increases linearly with a gradient of approximately 2% per cycle, except for the last cycle, when it seems to stabilize reaching ω_{HA} a value of 14%. As expected, a 5 wt.% concentration of HA in the solution leads to greater values of adsorbed HA: the amount of HA adsorbed in the first cycle is now about 15% in both the non- and the crosslinked samples, followed by an increase of around 7% in the second cycle and then a linear increase of about 5% per cycle; reaching a value of ω_{HA} near 34%. Thus, the HA mass fraction can be tuned from 7% up to 34%, by changing either the solution concentration or the number of applied cycles.

Figure 5.8 shows the pore volume fraction, π, of the samples as a function of the amount of adsorbed HA. The porosity of the bare scaffolds was around 75% when dry. The figure shows the results in the dry state for the non-crosslinked 05HA# and 5HA# series, and the results for the swollen crosslinked 5HA#x series.

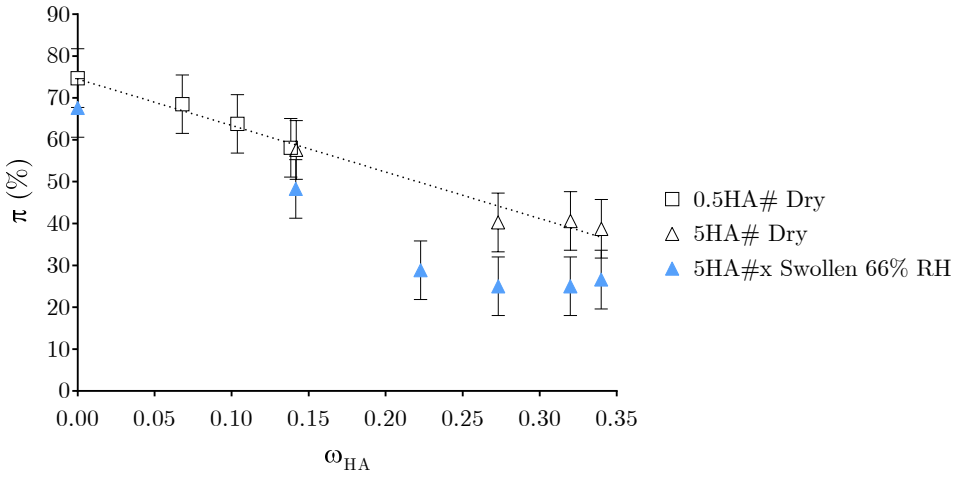

Figure 5.8: Porosity, π, as a function of the mass fraction of HA, ω_{HA}.

As expected, porosity decreases with increasing amounts of coating, up to 40% in the case of the 5HA5 sample. The decrease is monotonous and almost linear in the case of the dry series; in the swollen series the drop stabilizes after a certain mass fraction of HA, around $\omega_{HA} = 0.20$. The porosity of the swollen samples was always markedly lower than that of the dry samples. The measured porosity is visually supported by the SEM micrographies displayed in Figure 5.9, where a decrease of the porosity is observed as HA occupies the empty space of the pores due to both the increasing HA solution concentration and number of filling-drying cycles applied.

The SEM micrographies shown in Figure 5.9 combined with the scheme on the left side, contribute to describe the different coating typologies obtained by applying varying numbers of coating-drying cycles. For the 0.5HA# samples, only HA aggregates are obtained on the internal surfaces of the scaffolds, their density increasing with the number of applied cycles. Regarding the 5HA# samples, after 1

cycle a uniform coating layer is already obtained, which increases again its thickness with the number of cycles.

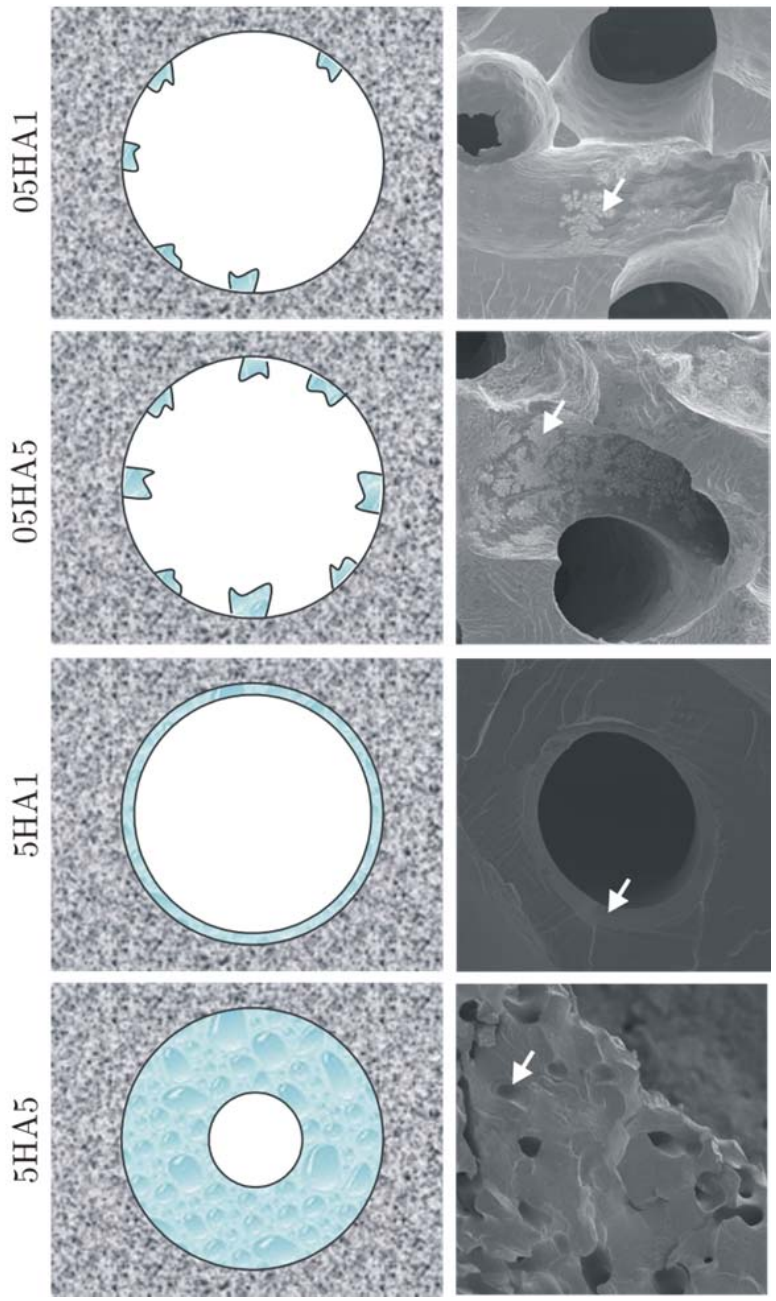

Figure 5.9: SEM micrographies and scheme of the growth of the HA coating in the scaffolds with the concentration of the HA solution and the number of coating cycles, from sporadic aggregates to the complete filling of the pores.

Coating typologies obtained by changing the solutions concentrations and the scaffold thickness

To produce the following set of constructs, thicker PEA-o scaffolds were employed, aiming to optimize the filling with the HA solutions and the uniformity of the coatings. To increase the thickness of the resulting scaffolds, sintered templates of 16 layers of fabric instead of 8 (which is the number of layers of the coated scaffolds presented in the previous section) were employed. The thickness increased from around 1 mm for PEA-o 8L up to near 1.6 mm for PEA-o 16L. In this case, one filling-drying cycle was applied independently of the HA starting concentration, and, in addition to 0.5 and 5 wt.% HA solutions, intermediate concentrations of 1 wt.% and 2 wt.% were also tested.

The mass fraction of HA incorporated into the scaffolds increased linearly with the concentration of the HA employed solutions, ranging from 0.12 for the 0.5 wt.% solution up to 0.41 for the 5 wt.% solution before crosslinking (Figure 5.7 B). The crosslinking step, involving the soaking of the samples in a water/acetone solution, results in the undesired release of a certain amount of HA from the scaffold. The relative loss of HA during the crosslinking process was lower as the HA amount in the scaffold increased. For instance, the scaffolds coated with 0.5 wt.% solution lost nearly 61% of the initially adsorbed HA during the crosslinking, whereas for the scaffolds coated with 5 wt.% HA solution, only 19% of the initial HA mass was lost (Figure 5.7 B).

The SEM micrographies shown in Figure 5.10, in combination with the scheme on the left side, contribute to the understanding of the different coating typologies obtained with the different concentrations of HA solutions after the crosslinking step.

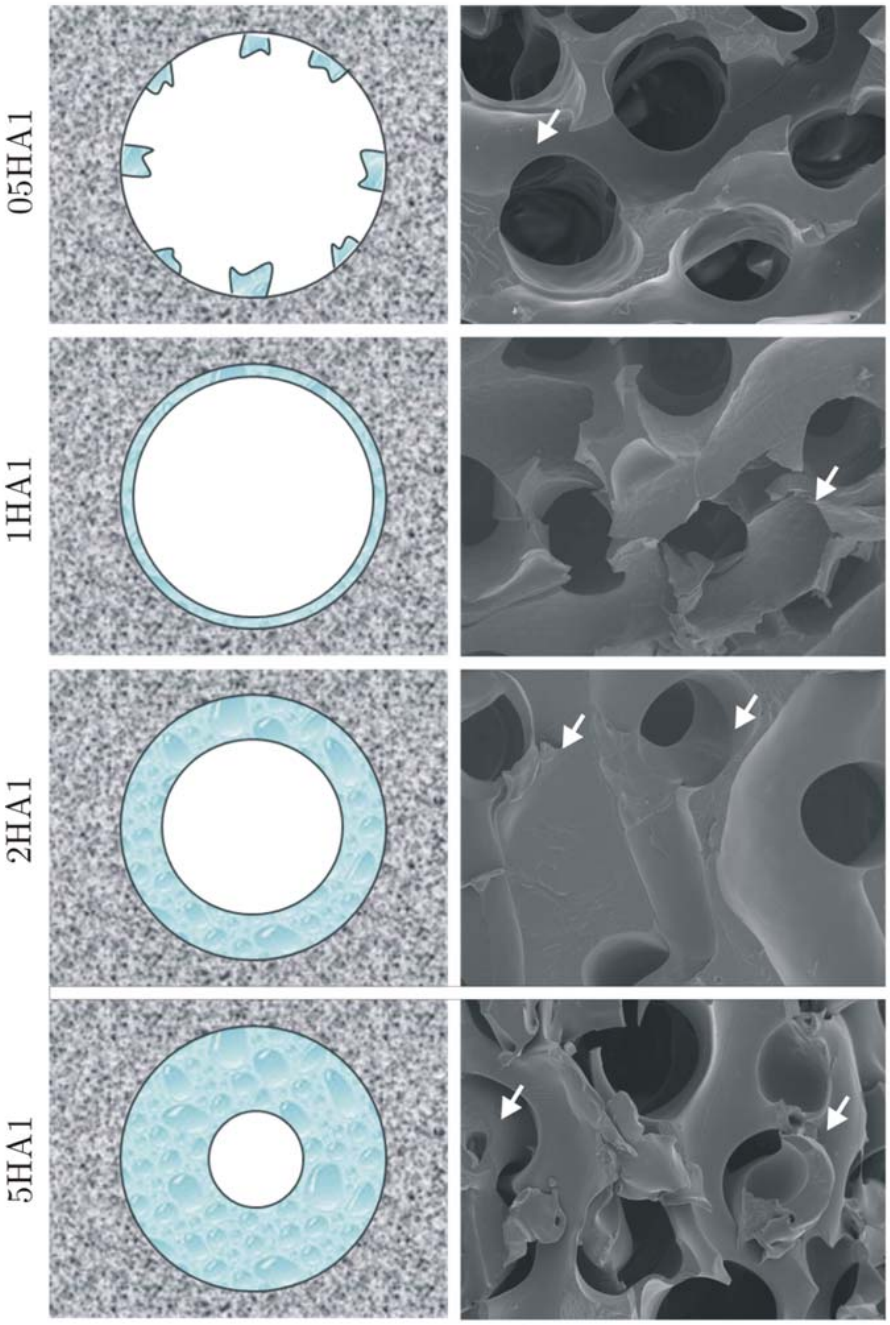

Figure 5.10: SEM micrographies and scheme of the development of the HA coating in the scaffolds as a function of the concentration of the HA starting solution with thick PEA-o scaffolds.

With the lowest concentration (0.5 wt.%), only scattered small aggregates of HA seem to adhere to the scaffolds' pores surfaces. When the samples are coated with the 1 wt.% solution, in some regions the deposition of a thin uniform layer is already

detected. Meanwhile, for the 2 wt.% solution, partially clogged pores are observed. Following the same trend, for the 5 wt.% HA solutions, many pores exhibit an uniform thick layer coating the channels, some of them being completely clogged.

When the results obtained for the 8L scaffolds and applying several filling-drying cycles, are compared to those obtained with 16L scaffolds and changing the HA solutions concentrations, interesting results in terms of the HA fraction are obtained. In both cases the resulting coatings represent the same range of ω_{HA}; however the latter (16L scaffolds and solutions at different concentrations) have the advantage of resulting in a greater HA fraction in only one-step, *i.e.*, the filling process is optimized. Also this procedure has also the drawback of losing more HA during the crosslinking step than does the multi-cycle coating procedure.

The thermogravimetric analysis of a set of samples allowed the study of the thermal degradation profile of the combined system, but also an additional determination of the mass fraction of HA effectively incorporated to the scaffolds.

As the thermogravimetric plots show (Figure 5.11), HA exhibits the lowest onset temperature, and a broad main degradation step between 205°C and 400°C. In the case of the bare scaffold the main degradation occurs between 340°C and 410°C. The coated scaffold thermogram lies between those of its components, and exhibits a very particular degradation profile. The first part of its main degradation follows a similar trend to that of HA although shifted towards higher temperatures (has its onset at 235°C). The second part matches accurately that of PEA-o although leaves a different value of solid residue. Apropos of this, at 700°C HA left 28.8% of its initial mass as solid residue, PEA-o 16L left 8% and the coated scaffold (PEA-o 5HA1x 16L) has a residue of 20.6%.

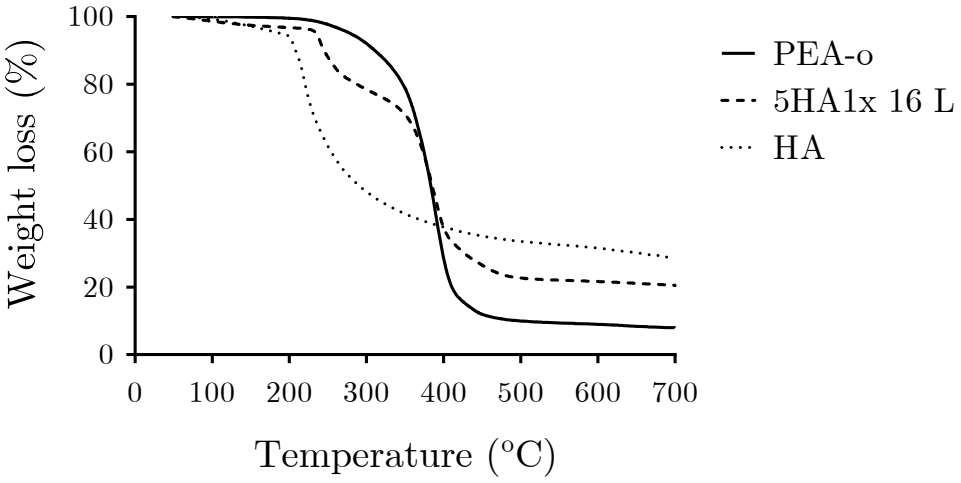

Figure 5.11: Thermogravimetric analysis of bare PEA-o scaffolds, PEA-o 5HA1x 16L scaffolds and HA discs.

5.2.3.- Swelling performance

Swelling performance by immersion in PBS

Coating the scaffolds' surface with HA has a great impact on their swelling behaviour, as observed by immersing them in PBS. This experiment was performed with crosslinked coated scaffolds, otherwise the coating would be dissolved by the PBS thus altering the results. As Figure 5.12 shows, when bare hydrophobic scaffolds are merely placed in PBS, only a small fraction of the liquid is capable to penetrate the scaffolds' pores. A dramatic increase on the equilibrium water content, *EWC*, is observed when the scaffolds are coated with HA solutions; even when the lowest concentration is employed, the water content triples that of the bare scaffold. The *EWC* increases with the ω_{HA} up to a certain value (near 4), but from 0.2 it seems to stabilize and even for high HA mass fractions it seems to decrease.

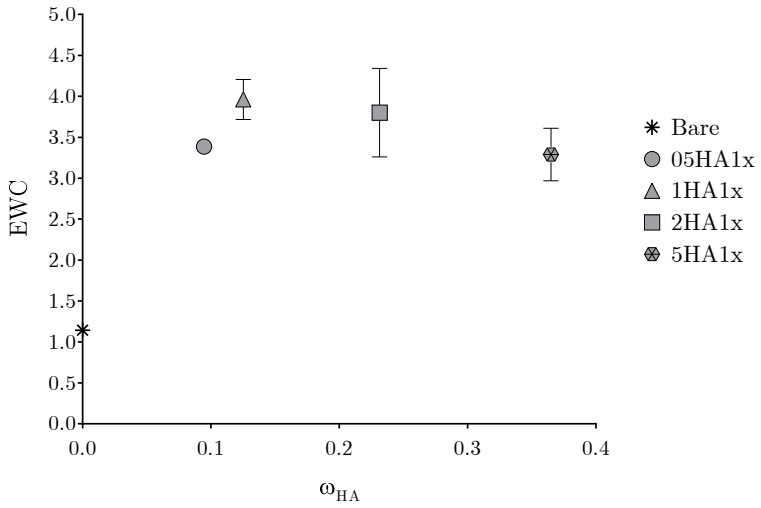

Figure 5.12: Equilibrium water content of coated and bare scaffolds after three days immersed in PBS.

The appearance of coated scaffolds (with HA solutions at different concentrations) either dry or swollen under different conditions, are presented in Figure 5.13. Regarding the cryoSEM images taken for samples swollen by immersion in PBS, it is

observed that as the samples' HA fraction increases, the number of hollow pores decreases. However, the trace left by PBS when sublimated in the CryoSEM device, disguises the HA gel structure that cannot be distinguished from the residue left by water sublimation from the employed buffer.

In order to better observe the HA coating in its swollen state without the PBS artefacts, samples were swollen in a PBS atmosphere, RH(PBS). As these are milder swelling conditions, the induced changes were more moderate. Samples coated with 05HA1x, as when dry, only exhibit few aggregates of HA, whereas in the 1HA1x samples some pores with a uniform coating layer start to be detected. For higher concentrations the effects are more evident: 2HA1x samples present some pores partially clogged, and entirely clogged pores are numerous in the 5HA1x samples. In sum, no great differences with the thoroughly dried samples were detected. Thus, humid atmospheres could be useful to study the EWC of crosslinked samples and establish comparisons with the same non-crosslinked samples without risking the dissolution of the coating; however, they are limited to characterize the morphology of the HA gel in the swollen state.

Therefore, to characterize the coatings swollen by immersion in PBS, avoiding the appearance of the residues left by PBS during the sublimation in the cryoSEM device, yet maintaining the swollen volume, specimens were intensely lyophilized after three days immersed in PBS, and then photographed in conventional SEM. For the lowest concentrations of HA solutions, small unconnected regions are observed (05HA1x) and only thin layers were detected for the 1HA1x. As for the highest concentrations, in the case of 5HA1x many pores are entirely clogged, whereas less for the intermediate concentration, 2HA1x.

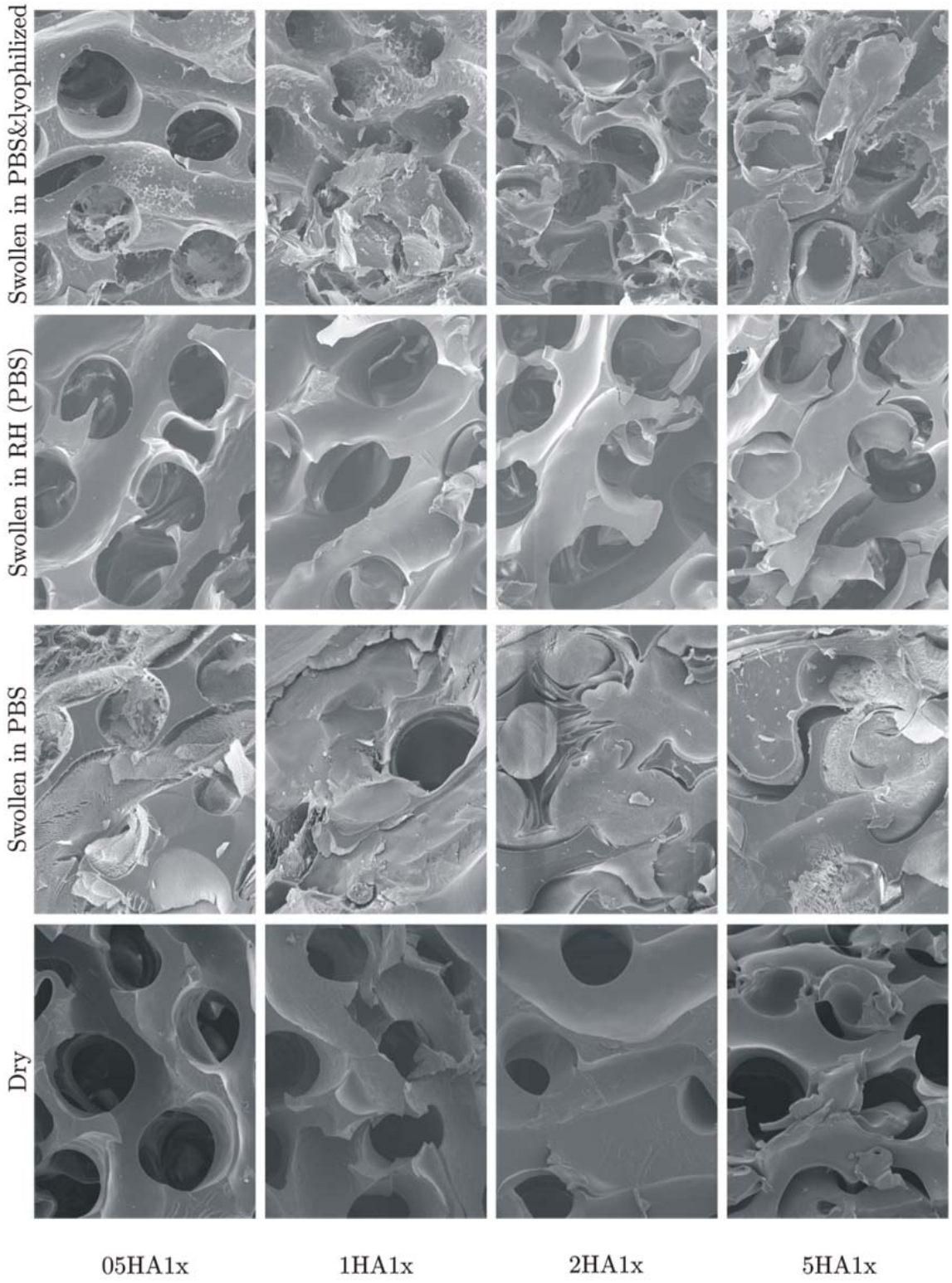

Figure 5.13: SEM and cryoSEM micrographies of PEA-o scaffolds coated with HA solutions of different concentrations in a dry state, swollen by immersion in PBS, swollen under PBS atmosphere and swollen by immersion in PBS followed by a lyophilization step.

Swelling performance in 66% RH atmosphere.

Since non-crosslinked samples cannot be immersed in aqueous solutions without partially dissolving the coating, a humid atmosphere can be employed to assess the swelling performance of the system and compare crosslinked and non-crosslinked samples. Samples were maintained in a 66% relative humidity atmosphere (milder conditions than PBS either as liquid or in a saturated vapour phase), and then weighed at the selected time points. The inset in Figure 5.14 A shows the time course of a representative sorption curve. The samples absorbed water rapidly in the first hours and then slowly reached equilibrium after about 5 days.

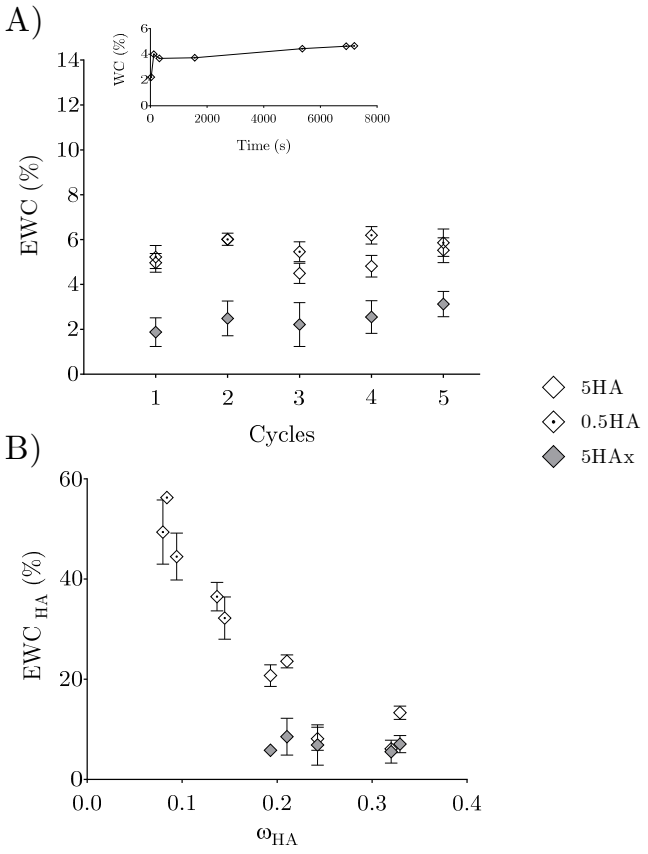

Figure 5.14: A) Equilibrium water content, *EWC*, as a function of the number of coating cycles. Inset: Water sorbed by sample 5HA1, *WC*, as a function of time. B) Equilibrium water content of the HA within the pores, EWC_{HA}, as a function of the mass fraction of HA, ω_{HA}.

Figure 5.14 A also contains the equilibrium values, EWC, of the coated samples. For the bare PEA scaffold, the EWC_{bare} was 1.4%. Non-crosslinked coated scaffolds reached EWC in the range of 4 to 6% independently of the number of cycles and the concentration of the HA solution. The samples with a crosslinked HA coating showed significantly lower absorption values (about 40% of each analogous non-crosslinked coating).

The water sorption data were reworked to refer the amount of water sorbed, which is to be attributed solely to HA, to the mass of HA in the sample (see Figure 5.14 B). Therefore, the EWC_{HA} parameter gives the specific (per HA unit mass) water sorption capacity of HA in the different series of samples. The trend followed by EWC_{HA} with ω_{HA} for the series 05HA#, 5HA# and 5HA#x was: the higher the amount of HA coating the pores (achieved either increasing the concentration or the number of cycles), the lower the amount of water each HA unit mass is able to absorb, covering values from 56% to 5.5%. This tendency is not linear, but slows down after a ω_{HA} of 0.2. The crosslinked samples have specific hydrophilicities EWC_{HA} below the non-crosslinked ones for the same amount of HA, as expected. For instance, given a ω_{HA}= 0.2, the non-crosslinked samples reached and EWC_{HA} around 20% whereas crosslinked samples attained a 6%. Nonetheless, these differences are reduced when the HA fraction increases.

5.2.4.- Influence of coating on the scaffold mechanical performance

The influence of the coating on the mechanical performance of the PEA-o scaffolds was studied by means of compression tests. PEA-o bare scaffolds and HA bulk discs were employed as references, along with the PEA-o scaffolds coated and crosslinked with 0.5, 1, 2 and 5 wt.% HA solutions. Measurements were performed with the materials previously swollen up to equilibrium by immersion in PBS.

All stress-strain curves (Figure 5.15) show a similar convex trend with stiffness increasing progressively as the sample is deformed, and ending with a densification regime. As expected, the HA disc has the lowest compressive stiffness and the greatest deformability.

The scaffolds coated with the less concentrated HA solutions (0.5 wt.% and 1 wt.%), show slightly greater initial compressive modulus than the bare scaffold (18.2 kPa and 20.1 kPa, respectively, *vs.* 17.7 kPa for the latter). However, given the dispersion of the measurements, these differences are not statistically significant. Concerning the scaffolds coated with the more concentrated HA solutions, a greater increase is observed for those coated with 2HA1x and 5HA1x, reaching a modulus that nearly doubles that of the bare scaffold (32.26 and 33.4 kPa, respectively). The increase in the average modulus is proportional to the amount of HA incorporated into the scaffold, even though the HA modulus (11.5 kPa) is lower than that of the bare scaffold. The change in the tendency observed in the curves occurs at a strain of approximately 75% for the bare scaffolds, which is close to its porosity, and at lower strains for the coated ones, up to 50% for those coated with the more concentrated HA solution.

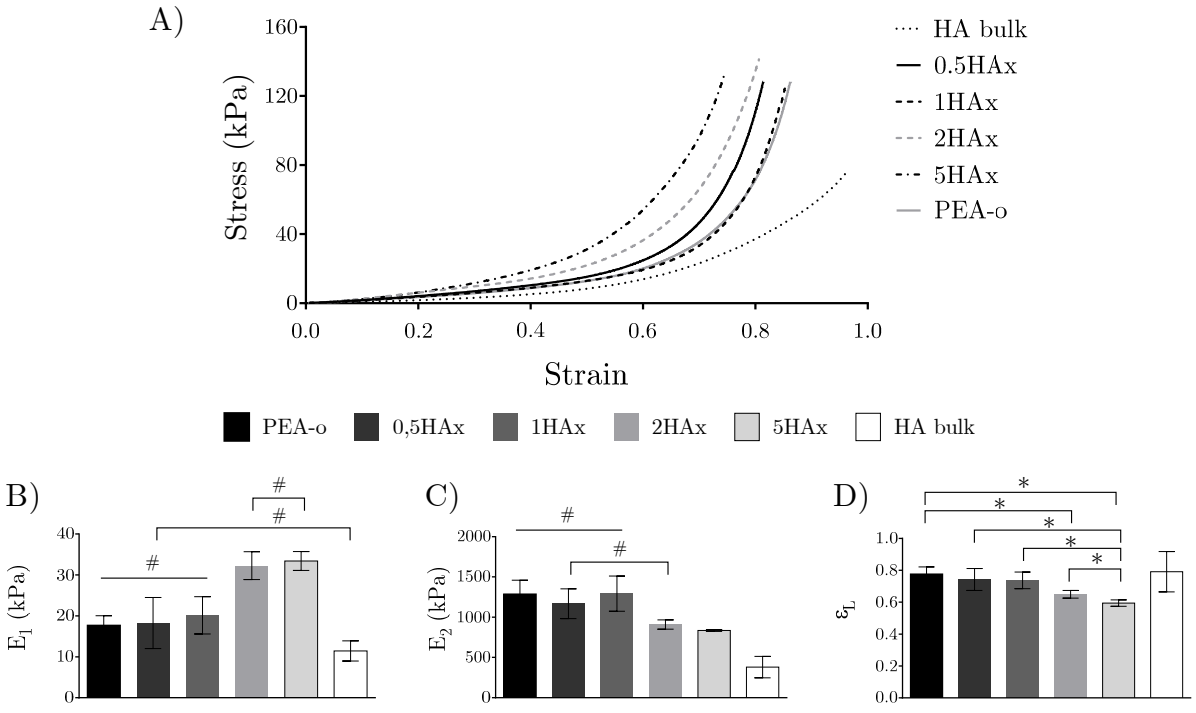

Figure 5.15: (A) Stress-strain curves from the compression tests of PEA-o, bulk HA and scaffolds coated with different HA solutions and crosslinked. (B) Initial compressive modulus E_1, (C) final compressive modulus, E_2, and (D) unitary limit deformation, ε_L, for the different samples. (*) Differences are statistically significant,
(#) differences are not statistically significant

When the final modulus is considered, the scaffolds coated with high HA concentrations (2 and 5 HA wt.% solutions) show a lower modulus than the rest (909.4 and 835.4 kPa), as well as more gradual change of slope. The scaffolds coated with 0.5 and 1 wt.% solutions exhibit moduli close to that of bare PEA-o (1.169 MPa and 1.293 MPa respectively, *vs.* 1.286 MPa for the latter). The HA discs show again the lowest value, 380 kPa.

The greater values of unitary limit deformation are those obtained for the controls, HA discs and bare PEA-o. For the coated scaffolds a clear trend is observed: the higher the HA mass fraction (*i.e.* scaffolds coated with more concentrated HA solutions), the lower the extreme strain value.

5.2.5.- Controlled release study

Firstly, the amount of bovine serum albumin (BSA) loaded in the materials for the controlled release study was determined. Great differences were detected among the bare and coated scaffolds, and the hyaluronic acid discs. The last type of materials was capable to adsorb almost three times more protein per mg of sample than the PEA-o scaffolds or the PEA-o coated ones. As can be seen in Figure 5.16, no significant differences are detected between them in respect of the amount of loaded BSA owing to the HA within the scaffold pores, achieving both bare and coated scaffolds similar values of BSA loaded.

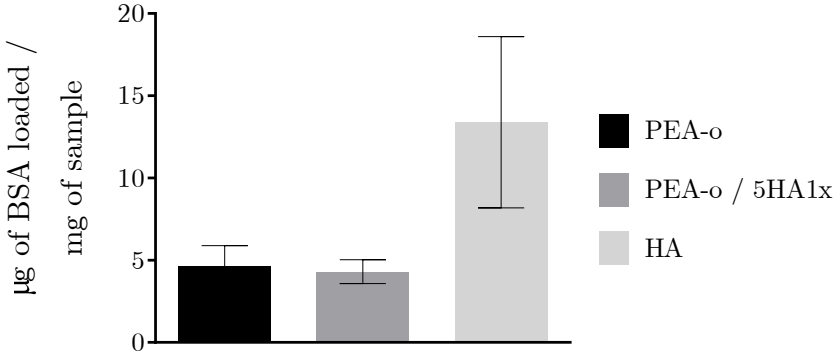

Figure 5.16: Mass of BSA incorporated in the bare scaffolds, HA coated scaffolds, and HA discs, per unit mass of sample.

Figure 5.17 shows the accumulated released fraction of BSA, M_t/M_0, curves in % for the loaded construct and PEA-o and HA controls, where M_0 is the initial (loaded) mass of BSA in each material and M_t is the mass released from it at time t. All materials present a similar trend where two different release regimes can be identified. A burst takes place at the beginning, lasting the first 8 hours, where a significant fraction of protein is released: up to 24% from the HA discs, 52% from the coated scaffolds, and 68% from the bare ones. Then a more sustained release follows up to the end time of the study: 47% from the HA, 85% from PEA-o and 65% from

5HA1x PEA-o after 12 days. In no case the total amount of BSA incorporated was released.

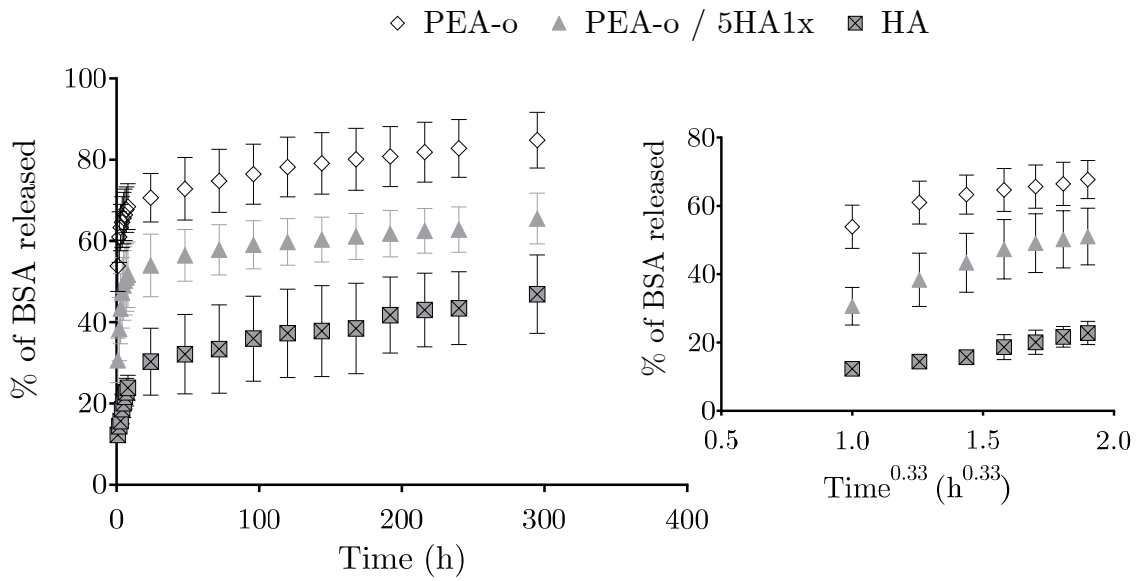

Figure 5.17: BSA release curve in PBS from bare and 5HA1x PEA-o scaffolds, and HA discs: % of accumulated mass of BSA released at time *t vs.* time. Inset: detail of the initial release.

Despite the similarities with respect to the shape of the curves, the different materials exhibit different behaviours indeed. The bare PEA, in sum provides a fast release of the loaded protein; the HA furnish a much more moderate rate of release, although also presents an initial burst, and the coated scaffolds exhibit an intermediate behaviour between its components, reaching much higher values in the initial burst than the HA, but a slower rate in the second regime.

5.2.6.- Effect of coating on seeding efficiency

Coated and non-coated samples were seeded with fibroblasts, cultured for 24h and fixed afterwards. This time was chosen to guarantee a proper adhesion of the cells into the material surface yet avoiding the effect of cell proliferation on the counting.

A constant inconvenience when working with PEA-o scaffolds is their autofluorescence owing to the nitric acid washes of the nylon fabrics employed as porogen, which hydrolyses some ethyl acrylate units into acrylic acid ones. As side effect, the scaffold architecture can be distinguished, apart from the adhered cells (Figure 5.18).

Greater numbers of cells can be found in the cross- and longitudinal section images of the HA-coated scaffolds than in those of the bare ones. The best material in terms of number of retained cells was the PEA-o scaffold with the highest HA fraction (5HA1x).

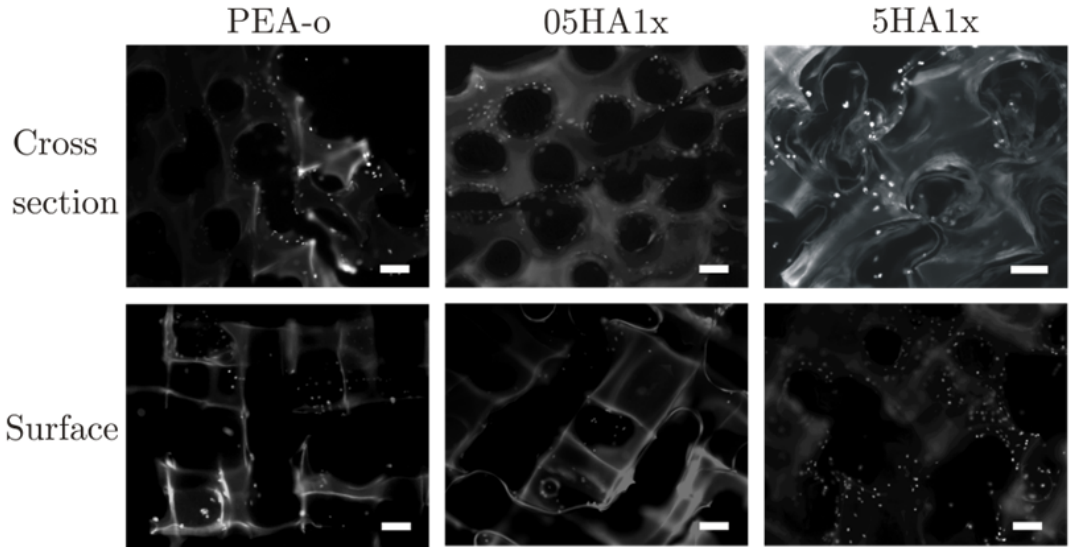

Figure 5.18: Fluorescence microscopy images of the cross-sections and surfaces of PEA-o scaffolds bare or coated with 05HA1x or 5HA1x, seeded with fibroblasts, cultured for 24h (scale bar 100 μm) and stained with DAPI (nuclei).

5.3.- Discussion

The PEA scaffolds studied in this work have either a porous structure constituted by mutually orthogonal cylindrical (grid-like) pores or a spherically interconnected sponge-like structure, resulting from the empty spaces left by the respective porogen templates [196, 197]. As a polymer, PEA is a relatively hydrophobic material; this fact, together with the hydrophilic and highly viscous nature of the HA solutions and the capillarity effect due to the pore diameters represent a set of obstacles in the way of getting a uniform filling of the porous structure. In the present work these difficulties were overcome by employing solutions of the HA polymer in aqueous NaOH in order to achieve lower viscosities [289], and by helping the filling with vacuum, as previously described. In the literature scaffolds made of hydrophobic materials such as PLLA [136] and PCL [137] have also been coated with HA with different typologies with similar procedures.

The HA coatings obtained after the adsorption of HA molecules from more or less concentrated solutions are soluble in water. It was therefore decided to crosslink the HA within the pores once the layer had been adsorbed and dried, by the two-step process with DVS described in the materials and methods section. During the crosslinking step a certain fraction of the HA incorporated during the loading is lost. Two main possible causes were detected: the first step of the crosslinking procedure includes a 30 minutes swelling in an acetone/NaOH(aq) solution. The solubility of HA in the NaOH(aq) solution although is shielded by the presence of acetone (HA is insoluble in this solvent), yet is capable to dissolve a certain fraction of HA. However, because of the very fast crosslinking reaction with DVS [209], no great mass loss should occur because of this step. The second plausible cause involves the step after the crosslinking, which involves two washes in different media. Once the samples are crosslinked, they are washed in an acetone/water mixture. As acetone is a good solvent of PEA, the coated scaffolds get swollen (not dissolved, since PEA is

crosslinked) and their size is much bigger than that of the dry ones. Next, samples are washed with distilled water; as PEA is highly hydrophobic, this abrupt change of solvent leads to a quick and dramatic reduction of the scaffold size, meanwhile the HA does not reduce its size (it might even increase it because of changing from an acetone/water mixture to pure water).

Taking together the results of weighing, alcian blue staining and SEM observations this, with the pores' diameters and interconnections of the PEA-s scaffolds, an extrusion of a non-negligible amount of HA through the pores towards the external areas of the scaffold occurred, resulting in a non-uniform coating of the scaffold. As Figure 5.4 shows, only in the peripheral area an HA coating is observed in this type of scaffolds, leaving their core pores empty. Thus, PEA-s scaffolds could not be satisfactorily coated with HA and crosslinked by using the described method.

For the PEA-o, although the coating procedure was the same and despite the sensitivity of PEA and HA to acetone and water was equivalent, given the greater size and layout of the pores, the scaffolds were capable to accommodate the HA coating throughout their section regardless of the volume changes suffered by both materials. As a consequence, more uniform coatings were obtained within the PEA-o pores (Figure 5.5). Nonetheless, PEA-o coated scaffolds also experience a certain loss of the HA coating during the crosslinking, which can be noted both with the ω_{HA} data (Figure 5.1) and with the alcian blue stained samples that acquire slightly clearer tonalities after the crosslinking step (Figure 5.5). Also a slight contrast is observed between the SEM images (Figure 5.2 and Figure 5.3) and the pictures after alcian blue staining (Figure 5.5), which can be attributed to the different degree of swelling in each technique. SEM samples are perfectly dry, what leads to a reduced volume of the HA whereas the alcian blue stained samples are swollen, therefore HA

occupies a greater fraction of the pores' volume than that observed in the SEM micrographies.

Given the better results obtained with the PEA-o, and the unfeasibility of obtaining a uniform and perdurable coating in the PEA-s scaffolds, the rest of the characterization of the PEA scaffold-HA coating system was only performed with PEA-o ones.

In order to modulate the thickness of the coating layer, several parameters were separately varied: the concentration of the HA solution, the number of consecutive filling-drying cycles to which the sample was subjected, and the thickness of the employed scaffold. By modifying these parameters, it was easy to produce HA coatings with typologies ranging from scattered aggregates, to completely clogged channels, with a uniform coating for the intermediate situations (Figure 5.6, Figure 5.9 and Figure 5.10).

Influence of the number of cycles and of the coating solution concentration on the typology of the adsorbed layer

The weight gain shown in Figure 5.7 proves that HA is effectively adsorbed onto the pore surfaces of the scaffolds, obviously in a greater amount from the 5 wt.% HA solution than from the 0.5 wt.% one, though much less than a tenfold increase. The dependence of the HA mass fraction on the number of cycles is almost linear in both cases. An increase of cycle number with the 5 wt.% solution leads to a steady increase in the layer's thickness (Figure 5.6 E and F). This different way of layer build-up as a function of HA solution concentration explains why samples 05HA5 and 5HA1 can have close HA weight fractions and porosities (Figure 5.9 and Figure 5.8) though having a very dissimilar topology (a disconnected morphology in the first case, versus a continuous one in the second). This also explains the different specific

swelling capacities of the coatings that obtain from each solution concentration (Figure 5.9 and Figure 5.14). Since the last disconnected layer, for the 05HA5 sample, has a HA mass fraction of ω_{HA}=0.145, and the sample 5HA1, already continuously coated, has ω_{HA}=0.167, the transition between both topologies must lie somewhere around ω_{HA}=0.15.

Influence of the coating solution concentration and the scaffold thickness on the typology of the adsorbed layer

As previously discussed, the transition between coatings in the shape of aggregates and continuous layers, lies in an intermediate point near ω_{HA}=0.15; precisely for PEA-o 1HA1 16L, a value of ω_{HA}=0.158 is obtained and these samples already exhibit a uniform thin layer as coating on the pores.

The use of thicker scaffolds intended the fine augment of ω_{HA} without increasing the number of applied cycles, ensuring more uniform coatings throughout the thickness of the scaffolds. Another expected effect of employing thicker scaffolds was the reduction on the amount of HA lost during the crosslinking step, because of a labyrinthine effect of the porosity.

As Figure 5.7 A shows, the scaffolds with 16 layers coated with a 5 wt.% HA solution reached, with a single cycle, an ω_{HA} equivalent to that reached by the 8-layered scaffolds after 5 loading-drying cycles with a 5 wt.% HA solution. However, despite of having similar ω_{HA} values, the resulting coatings are very different (Figure 5.9, Figure 5.10 and Figure 5.6); for the 8L scaffolds such a high ω_{HA} value leads to almost clogging all the pores of the scaffold, whereas the 16L scaffolds seem to still have some empty space to lodge more HA if desired. These differences however might be attributable to the fact that the PEA-o 16L SEM images were taken after the drying

and crosslinking step, which seems to invariably induce changes in the coating morphology.

For HA solutions of 1 wt.% and 2 wt.%, the ω_{HA} reached with 16-layered scaffolds (0.071 and 0.143 respectively), is close to that of the 8 layers scaffolds after 1 cycle with 5% HA solutions (0.148), and the resulting coating typology of the 5HA1 8L seems an intermediate between 1HA1x 16L and 2HA1x 16L.

As HA had to traverse longer paths to be extruded out of the pores, the residence of HA inside the scaffold should be favoured in the 16L PEA-o scaffolds. However, when the 5HA1 16L samples are compared with the 5HA5 8L ones, it turns out that the loss of the formers during the crosslinking step is much higher despite of having a similar final ω_{HA}. This difference can be attributed to the alternate dryings in the filling by steps that compacts HA chains and more effectively avoids the loss on crosslinking, which occurs indeed when the scaffolds are coated in one single step. The immersion time of the scaffolds in acid media to remove the porogen may also have an effect on their swelling during the crosslinking process. The 16L scaffolds have been exposed to longer HNO_3 treatments than the 8L to remove the nylon template; therefore, the fraction of acrylic groups (see Chapter 3) is higher for the former. This translates into a higher degree of swelling that leads to a greater reduction on the scaffold's pores diameters thus favouring the extrusion of HA out of the pores.

The thermogravimetric analysis provided values of solid residue, allowing the calculation of the HA fraction in the coated scaffolds in an alternative way. A ω_{HA} of 36.0 $\pm$ 5% of was obtained for the PEA-o 5HA1x 16L. When this value was compared with the one obtained by weighing the samples before and after the coating (Figure 5.7) being 35.9 $\pm$1 %, both values were found to be in good agreement.

Changes in porosity due to coating of the pores' surfaces

The expected change on the porosity, π, for the coated dry scaffolds with an increasing mass fraction of HA in the scaffold can be deduced to be:

$$\pi = \frac{V^p}{V^{app}} = \frac{V^{app} - V_{bare} - V^{HA}}{V^{app}} = \pi_{bare} - \frac{m \cdot \omega_{HA}/d_{HA}}{V^{app}}$$

$$= \pi_{bare} - \frac{m_{bare}}{(1-\omega_{HA}) \cdot V^{app} \cdot d_{HA}} \cdot \omega_{HA} = \pi_{bare} - \frac{d_{bare}^{app}}{d_{HA}} \cdot \frac{\omega_{HA}}{1-\omega_{HA}}$$

[Equation 5.1]

where π_{bare}^{scff} is the porosity of the bare scaffold, d^{app} is the apparent density of the coated scaffold, and d_{HA} is the density of dry HA. Since $\mathrm{y}/(1-\mathrm{y})$ is a nearly linear function for values of y less than 0.4, according to the above equation, the porosity of the system should fall linearly with ω_{HA}, which is in fact what approximately happens, Figure 5.8; the experimental points for the coated scaffolds, moreover, extrapolate linearly to the experimental value of porosity of the bare scaffold, which is a good indication of the consistency of the results.

In the case of a swollen coated scaffold the relationship between the porosity π_{sw} and ω_{HA} is a bit more involved, but can still be established under mild simplifying assumptions and compared with the experiments. Let the subscript *sw* distinguish the quantities associated with the swollen system, and let λ_{sw}, defined by $V_{SW}^{app} = \lambda_{SW}^3 \cdot V^{app}$, be the-assumedly-isotropic stretch ratio of the swollen scaffold; then

$$\pi_{SW} = \frac{V_{SW}^{pore}}{V_{SW}^{app}} = \frac{V_{SW}^{app} - V_{bare} - V_{HA} - V_{H_2O}}{V_{SW}^{app}}$$

$$= \lambda_{SW}^{-3}\left(\frac{\lambda_{SW}^3 V^{app} - V_{bare}}{V^{app}} - \frac{m}{V^{app}\, d_{HA}} \cdot \omega_{HA} - \frac{m}{V^{app}\, d_{H_2O}} \cdot EWC\right)$$

$$= \lambda_{SW}^{-3}\left(\lambda_{SW}^{3} - 1 + \pi_{bare} - \frac{d_{bare}^{app}}{d_{HA}} \cdot \frac{\omega_{HA}}{1-\omega_{HA}} - \frac{d_{bare}^{app}}{d_{H_2O}} \cdot \frac{EWC}{1-\omega_{HA}}\right)$$

[Equation 5.2]

For stretching ratios of the scaffold close to unity (here the case), one may assume $\lambda_{SW} \approx \lambda_{SW}^{-3} \approx \lambda_{SW}^{3} \approx 1$, and the above expression simplifies to:

$$\pi_{SW} = \pi_{bare} - \frac{d_{bare}^{app}}{d_{HA}} \cdot \frac{\omega_{HA}}{1-\omega_{HA}} - \frac{d_{bare}^{app}}{d_{H_2O}} \cdot \frac{EWC}{1-\omega_{HA}} = \pi - \frac{d_{bare}^{app}}{d_{H_2O}} \cdot \frac{EWC}{1-\omega_{HA}}$$

[Equation 5.3]

If, further, the water gain is referred to the mass of HA in the system by defining

$$EWC_{HA} = \frac{m_{water\ in\ HA}}{m_{HA}} = \frac{m \cdot EWC - m_{bare} \cdot EWC_{bare}}{m_{HA}}$$

$$= \frac{EWC - (1-\omega_{HA}) \cdot EWC_{bare}}{\omega_{HA}}$$

[Equation 5.4]

then we have:

$$\pi_{SW} = \pi - \frac{d_{bare}^{app}}{d_{H_2O}} \cdot \left(\frac{\omega_{HA}}{1-\omega_{HA}} \cdot EWC_{HA} + EWC_{bare}\right)$$

$$= \pi - \frac{d_{bare}^{app}}{d_{H_2O}} \cdot EWC_{bare} - \frac{d_{bare}^{app}}{d_{H_2O}} \cdot EWC_{HA} \cdot \frac{\omega_{HA}}{1-\omega_{HA}}$$

[Equation 5.5]

This equation tells, on the one hand, that the porosity of the swollen system is less than that of the dry system (for the same amount of HA in the scaffold), and, on the other hand, that the fall of porosity with increasing HA content in the scaffold is no longer proportional to ω_{HA}, unless EWC_{HA} itself varies linearly with ω_{HA} (which, as shown later, is not the case). Both predictions are confirmed by the experimental data of the swollen 5HA#x series in Figure 5.8 the porosities of the swollen systems lie always below those of the dry systems of similar HA content, and the linearity of

the drop is lost. An explanation for this non-linearity must take into consideration the changes in the specific hydrophilicity EWC_{HA} of HA due to its typology.

The effect of confinement upon the water sorption capacity of the gel inside the pores of the scaffold

The observed decrease on the EWC for the coated scaffolds swollen in PBS with ω_{HA} (Figure 5.12) arose the hypothesis that a constrained swelling was taking place in the combined system. However, the use of the immersion in a liquid as swelling condition could somehow fake the constrained phenomena as the presence of swollen HA might clog some pores avoiding the media to reach inner parts of the scaffold and reducing the water intake not because of a constrained swelling but because of an inefficient wetting of the hybrid scaffold.

Therefore, analogous experiments were performed in an atmosphere with a RH of 66%, where the pass of liquid wasn't necessary for the HA to swell (Figure 5.14). With the results obtained by using the 66% RH vapour medium, the swelling behaviour of the coated samples can be explained in terms of the interplay between the elasticity of PEA (scaffold constraint) and the increasing hindrance of gel swelling due to surface coverage build-up and the curvature of the confining space (confinement effect), see the situations sketched in Figure 5.19, by means of a thermodynamical analysis of swelling.

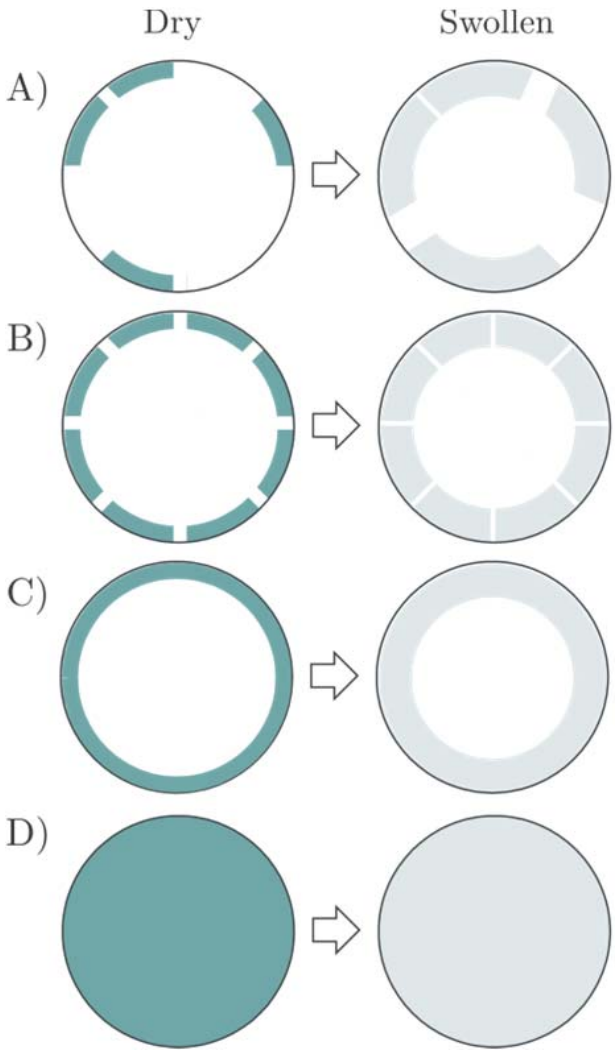

Figure 5.19: The confinement of the HA layer by the scaffold restricts in different ways the swelling capability of HA, depending on its typology.

Let the subscripts 1, 2 and 3 identify in what follows the quantities associated with water, HA and the scaffold, respectively. If ϕ_1 denotes the water volume fraction in the gel, the unconstrained gel in an environment of water activity $a_1^{env} = a^*$ reaches an equilibrium with a value $\phi_1 = \phi_1^*$ determined by the equality of the chemical potential of water in the environment and within the gel: $\mu_1^{env} = \mu_1^{gel}$, or, equivalently, $\mu_1^{env} - \mu_1 = \mu_1^{gel} - \mu_1 \equiv \Delta\mu_1^{gel}$. Here μ_1 is the chemical potential of pure water, $\mu_1^{env} - \mu_1 = RTlna_1^{env}$, and R is the gas constant. If an equation of state for the excess chemical potential of water in the gel $\Delta\mu_1^{gel} = (T, p, \phi_1)$ is known (for

example, the Flory–Rehner equation), then the equilibrium water volume fraction in the system ϕ_1^* is determined (the constants T, p are hereafter omitted for simplicity):

$$RTlna^* = \Delta\mu_1^{gel}(\phi_1^*) \Longrightarrow \phi_1^* = \Phi_1^{gel}(a^*) \quad \text{[Equation 5.6]}$$

where $\Phi_1^{gel}(a)$ denotes the inverse function of $\Delta\mu_1^{gel}(\phi_1)$. In the case of constrained swelling in the same environment of water activity a^* the system to be considered includes the gel (components 1: water, and 2: HA polymer) plus the scaffold (component 3). The equilibrium condition is now $\mu_1^{env} = \mu_1^{sys}$, and $\mu_1^{sys} = \mu_1^{c.gel} + \mu_1^{scff}$ with $\mu_1^{c.gel}$ the chemical potential of water in the constrained gel and μ_1^{scff} the derivative of the elastic free energy of the scaffold with respect to the mol number of water in the system:

$$\mu_1^{scff} = \frac{\partial G_3^{scff}}{\partial n_1} \quad \text{[Equation 5.7]}$$

Thus,

$$RTlna_1^{env} = \mu_1^{env} - \mu_1 = \mu_1^{sys} - \mu_1 = \Delta\mu_1^{gel} - \mu_1^{scff} \quad \text{[Equation 5.8]}$$

Again, this equation determines the equilibrium value ϕ_1^{**} of water in the system once the equation of state of the constrained gel and that of the elastomer scaffold are known. According to the theory of rubber elasticity [290] an elastomer changes its Gibbs free energy when isotropically deformed as $\Delta G^{elas} = \frac{3}{2} n_3 RT(\lambda_3^2 - 1)$ where n_3 is the mol number of chains of the network material of the scaffold (PEA in our case) and λ_3 is the stretch ratio of the scaffold matrix elastomer. Since lodging more molecules of water within the gel implies stretching the scaffold, we have $\partial\lambda_3/\partial n_1 > 0$ and thus the function f_3 defined by:

$$\frac{\partial \Delta G_3^{elas}}{\partial n_1} = \frac{\partial \Delta G_3^{elas}}{\partial \lambda_3}\frac{\partial \lambda_3}{\partial n_1} = RT \cdot f_3(\phi_1) \quad \text{[Equation 5.9]}$$

is always positive.

The Flory–Rehner theory of gel swelling admits for the unconstrained gel's free energy G^{gel} contributions from the mixing of water and polymer (Flory–Huggins term) and from the elastic stretching of the polymer, $G^{gel} = G_{12}^{mix} + G_2^{elas}$, where the change in the elastic free energy of the gel is again given by the theory of rubber elasticity as $\Delta G_2^{elas} = \frac{3}{2} n_2 RT(\lambda_2^2 - 1)$, now with n_2 the mol number of gel chains and λ_2 the gel's stretch ratio due to its swelling, $\lambda_2 = (1 - \phi_1)^{-\frac{1}{3}}$.

As revealed by the SEM pictures and discussed previously, the way in which HA adsorbs on the scaffold pore surfaces ranges from small disconnected clots to a uniform coating depending on the amount of HA adsorbed. The disconnected HA aggregates can swell almost freely not only in the direction normal to the pore's surface, but also laterally, and are constrained solely at their interface with the scaffold surface. As the number of HA aggregates on the pore surface increases the aggregates get closer, and their swelling starts implying lateral interactions. When the pore's surface is completely covered by the HA layer the free lateral expansion of the gel is completely constrained. Once this constraint has developed, the swelling of the layer is additionally influenced by the curvature of the pore surface, see the sketch in Figure 5.19, which sets a further limit to the sorption capacity of HA, since any increase in volume of the gel must result in an increase of the negative curvature of the gel's free (luminal) surface, paying a free energy cost. Thus, it must be assumed that the free energy of the constrained gel $G^{c.gel}$ must have, besides the mixing G_{12}^{mix} and the elastic G_2^{elas} terms considered in the theory of unconstrained swelling, a further contribution G^{topol} depending on a topological-and-form factor φ, such that

$$G^{c.gel} = G_{12}^{mix} + G_2^{elas} + G^{topol} = G^{gel} + G^{topol} \qquad \text{[Equation 5.10]}$$

and

$$\frac{\partial \Delta G^{topol}}{\partial n_1} = RT \cdot lnf(\phi_1, \varphi) > 0, \qquad \text{[Equation 5.11]}$$

holds.

This topological-and-form factor φ is a function of the HA content in the system and of other factors here left unspecified such as connectedness, degree of coverage, and curvature of the interface):

$$\varphi = \varphi(\omega_{HA}, x) \qquad \text{[Equation 5.12]}$$

$x =$ connectedness, surface coverage, curvature, . . . ; it accounts for the influence on the gel's free energy of the topological features of the build-up of the scaffold–gel interface (connectedness, degree of coverage) and of the curvature increase of the swollen gel's free surface as a function of HA content in the scaffold. From (Equation 5.10) and (Equation 5.11) now:

$$\Delta\mu_1^{c.gel} = \Delta\mu_1^{gel} + RT \cdot ln\, f(\phi_1, \varphi) \qquad \text{[Equation 5.13]}$$

and thus, with (Equation 5.8):

$$RT \cdot ln\, a^* = \Delta\mu_1^{gel}(\phi_1^{**}) + RT \cdot ln[f(\phi_1^{**}, \varphi) \cdot f_3(\phi_1^{**})] \qquad \text{[Equation 5.14]}$$

This is the wanted relationship between the constrained equilibrium swelling ϕ_1^{**}, the unconstrained gel equation of state $\Delta\mu_1^{gel}$, the elastomer equation of state f_3, and the constraint function $f(\phi_1, \varphi)$. Two of its consequences deserve consideration.

Firstly, (Equation 5.14) and (Equation 5.6) give:

$$\Delta\mu_1^{gel}(\phi_1^*) = \Delta\mu_1^{gel}(\phi_1^{**}) + RT \cdot \ln[f(\phi_1^{**}, \varphi) \cdot f_3(\phi_1^{**})] \qquad \text{[Equation 5.15]}$$

since thermodynamic stability [291] demands that $\Delta\mu_1^{gel}(\phi_1)$ be a monotonously increasing function of ϕ_1, Equation 5.15 implies that $\phi_1^{**} < \phi_1^*$, or equivalently, $EWC_{HA}^{**} < EWC_{HA}^*$ for any fixed topology φ of the gel coating. This proves that, as intuited, the constraint decreases the equilibrium swelling of the gel in a given environment with respect to the unconstrained swollen gel.

Secondly, the magnitude of the swelling decrement due to constrainment, $\Delta^c\phi_1 \equiv \phi_1^* - \phi_1^{**}$, can be proved to depend, for a fixed a^*, solely on the constraint functions f_3 and φ: if Equation 5.14 is solved for ϕ_1^{**}:

$$\phi_1^{**} = \Psi_1(a^*, \varphi, f_3) \qquad \text{[Equation 5.16]}$$

then,

$$\phi_1 = \Phi_1^{gel}(a^*) - \Psi_1(a^*, \varphi, f_3) \qquad \text{[Equation 5.17]}$$

Moreover, since, from Equation 5.6 and Equation 5.14:

$$\Psi_1(a^*, \varphi, f_3) = \Phi_1^{gel}\left(\frac{a^*}{f(\phi_1^{**}, \varphi) \cdot f_3(\phi_1^{**})}\right) \qquad \text{[Equation 5.18]}$$

The swelling decrement is completely determined by the constitutive properties of the unconstrained gel Φ_1^{gel}, and the values of the constraints f_3 and φ. EWC_{HA} is a monotonously increasing function of ϕ_1, and thus its dependences are the same as those given by Equation 5.16 for a fixed environment activity a^*:

$$EWC_{HA} = \mathrm{F}^{\mathrm{constr}}(\varphi, \mathrm{f}_3) \qquad \text{[Equation 5.19]}$$

These results qualitatively account for the data represented on Figure 5.8 and Figure 5.14. Equation 5.19 explains why, in the same environment of a^*, the specific hydrophilicities EWC_{HA} of the different series of samples differ, Figure 5.14; it also explains the non-linear course of the swollen porosity data on Figure 5.8, since, from Equations 5.5 and 5.19, porosity also depends on the constrainment:

$$\pi_{sw} = \Pi^{constr}(\omega_{HA}, \varphi, f_3) \qquad \text{[Equation 5.20]}$$

Moreover, also because of Equation 5.19, the plot of the quantity EWC_{HA} against ω_{HA} (Figure 5.14 B) is, essentially, a plot of the constraint development as a function of HA increase in the coating. The total constraint on the HA gel develops steeply for approximately $\omega_{HA} < 0.2$, and more smoothly for $\omega_{HA} > 0.2$. This threshold coincides with the transition from an unconnected HA coating (series 05HA#, open squares in

Figure 5.14) to a completely developed continuous HA layer (series 5HA#, open triangles in Figure 5.14). The difference between the EWC_{HA} data of the 5HA# series and the 5HA#x series (blue triangles in Figure 5.14) is due, obviously, to the term G_2^{elas} in Equation 5.10, present in the 5HA#x series but absent in the non-crosslinked 5HA# one: crosslinking always decreases specific swelling relative to the non-crosslinked state.

In Equations 5.18 and 5.19 the function f_3 determines the part of the swelling decrement due to the scaffold elasticity; as read from its definition Equation 5.9, it depends on the amount of scaffold stretch needed to accommodate new water molecules in the gel when swollen. Equations 5.18 and 5.19 cannot discriminate the separate effects of φ and f_3; nevertheless, a consideration of the situations depicted in the sketch of Figure 5.9 leads to the conjecture that scaffold elasticity will start playing a more important role after the complete development of a continuous HA layer, when the increased difficulty for lateral swelling of the gel forces the scaffold to stretch as an alternative competitive way to fit new water molecules, and be the predominant constraint in situations where the pores are completely filled. For a water activity of a^*= 0.66, as was the case here studied, the amounts of water sorbed by the gel are not high, and thus f_3 cannot have a large effect; the nearly constant values of EWC_{HA} for the crosslinked series in Figure 5.14 are a support of this consideration. On the whole, then, one may advance that, at this water activity, the course of EWC_{HA} in Figure 5.14 is basically determined by the topological-and-form constraint on the swelling of HA.

Coating effect on the mechanical performance

The compressive modulus, determined as the slope in the linear region up to a strain of 0.2, increases with the HA fraction (Figure 5.15). This effect can be attributed to the greater difficulty in extrusion of water from HA than from the void scaffold's

pores. Constrained swelling aside, in the scaffolds coated with solutions having the higher concentrations (2HA1x and 5HA1x), a greater fraction of water is entrapped in HA network and lesser water flows freely through the PEA-o pores, *i.e.*, the gelled state of HA impedes such flow. This phenomenon, known as poroelasticity, occurs when porous materials filled with liquids are compressed, because of the incompressibility of the latter [292, 293]. As a result, even if the HA modulus is lower, its presence increases the compressive modulus up to nearly double that of the bare scaffold, thus concluding that the HA induces a reinforcing effect. A similar reinforcing effect has been described in other combined systems [294, 295].

This effect is maintained as the stress increases. The presence of increasing fractions of HA within the pores increases the stresses needed to reach a certain strain. As can be observed in the second linear region in the stress-strain plot (E_2 has been determined as the slope in the stress interval between 100 and 120 kPa, except for the HA, for which it has been determined at lower stress levels), the scaffolds coated with HA solutions with high concentrations are less deformed given the same value of stress. This is an indicator that their filled pores are sooner entirely collapsed. This second compressive modulus, obtained after pores collapse, decreases as PEA is combined with HA. As the HA modulus is lower, the fact of being compressing both types of materials simultaneously leads to the reduction of the resulting average modulus. On the other hand, for the bare scaffolds and the scaffolds coated with 05HA1x and 1HA1x, similar values to those reached by the bare scaffold are obtained, being in accordance with the presented rationale.

Controlled release

The feasibility of employing the combined system composed of a PEA scaffold and hyaluronan filling as a protein (or other molecule) delivery platform was assessed in the controlled release study. The loaded BSA molecules might be in different

locations depending on the considered material. In the case of HA discs, the protein could be either adsorbed on the disc surface or embedded in the swollen HA gel. In the case of the bare scaffolds BSA can be either adsorbed on the surface, or in the liquid filling the pores. The BSA present in the hybrid scaffold would be in a combination of the aforementioned locations.

The BSA release from the materials was carefully analysed, and it was found to exhibit two different regimes (Figure 5.2): the initial burst that occurs within the first 8 hours, and a more sustained release that is maintained up to 12 days.

The initial solute release regime from HA gel and coated PEA scaffolds can be successfully fitted to simple equations according to [296] and [297]; however, in the particular case of PEA bare scaffolds, given the high initial release this model could not be applied.

The simple exponential relation, $M_t/M_0 = k \cdot t^n$ can be employed to fit the HA and PEA-o/5HA1x controlled release results, where M_t/M_0 is the fractional solute release, t is the release time in hours, k is a constant characteristic of the macromolecular network system, and n is the diffusional exponent characteristic of the release mechanism [296]. For HA the equation gives $M_t/M_0 = 0.1194 \cdot t^{0.33}$ (R^2=0.9944) and for PEA-o/5HA1x it is $M_t/M_0 = 0.2269 \cdot t^{0.33}$ (R^2=0.9784). The fact that the best fit is obtained for an n=0.33 in both cases, below the limit of 0.43 that is attributed to pure Fickian diffusion, indicates that the diffusion mechanism taking place is not Fickian, *i.e.,* other factors besides pure diffusion are taking part in this process. These mathematical models are widely employed to describe solvent release from hydrogels. In some cases the parameter k is interpreted as a structural/geometric factor to account for the different tortuosities of the transport path [298]. This could explain why the value obtained for the coated scaffolds is higher than that of HA gel.

In the case of HA, given its highly hydrophilic and swellable nature, changing from a loaded solution to a non-loaded could translate into not only a release of the model protein but also a non-negligible swelling of the polymeric network, thus the model developed by Ritger and Peppas specifically for swellable devices might be applied [297]. In such case, $M_t/M_0 = k_1 \cdot t^n + k \cdot t$ applies, which generalized for alternative geometries implies $k = 1 - (1 - k_2 \cdot t)^n$. The following equation is achieved: $M_t/M_0 = 0.112602 \cdot t^{0.33} + (1 - (1 - 0.003741 \cdot t)^{0.33})$. With this approach the k_1 value is very close to the one obtained with the simple exponential relation; hence the resulting model is like the one obtained for the simple exponential diffusion, plus an extra term associated to the material swelling.

The second release regime exhibits an almost linear profile with time for time points longer than 8 h. Therefore it was decided to fit the results to a linear equation such as: $M_t/M_0 = k \cdot t + a$, where a accounts for the initial release and k for the linear growth with time of the amount released. For HA the fitting is $M_t/M_0 = 0.0006 \cdot t + 0.2935$, for PEA-o/5HA1x it is $M_t/M_0 = 0.0004 \cdot t + 0.5469$ and in this case also the data of bare PEA-o could be fitted, $M_t/M_0 = 0.0005 \cdot t + 0.7101$. The greater a value is obtained for the PEA-o, which is indicative of the greater initial release observed for this material. The fastest second regime release was observed for HA, which precisely had the highest k value in the fitted equation.

Previous works reported that negatively charged proteins are sustainably released from HA hydrogels after an initial burst; meanwhile, the release of positively charged proteins is interrupted after the initial rapid release due to electrostatic interactions with HA [299]. At the pH at which this experiment was performed, 7.4, BSA was above its isoelectric point (4.7) [300], and negatively charged. Therefore, the results obtained for both the HA gel and the PEA+HA construct, exhibiting an initial burst followed by a sustained and continuous slow release are in good agreement. However,

other factors besides interaction of BSA molecules with HA chains need to be taken into account, for instance the porosity; in the case of bare PEA-o and PEA-o/5HA1x, the BSA lodged in the free PBS filling the pores could contribute to the fast release, as it can diffuse to the surrounding media very easily.

Biological development of grid-like PEA scaffolds coated with HA

The presence of HA within the scaffolds' pores (even if it was only a preliminary study), seemed to have a positive effect on the amount of attached cells. In bare scaffolds, cells are detected on the surface as well as in the cross sections showing the feasibility of cell colonization of these materials.

The use of PEA-o 5HA1x appears to surpass the bare scaffold performance, by avoiding the wash out of the seeded cells downwards; this effect would occur by means of the HA coating partially clogging the pores (as it was already shown in the material characterization section), and thus helping to maintain the cells on the upper surface.

Concerning the PEA-o 05HA1x samples, a greater amount of cells are observed in the cross section than on the surfaces. As the coating is less dense, the cells colonization of the scaffold is easier, as the pores are not clogged. Additionally, the HA presence seems to prevent cells from falling from the scaffold into the well yet without hampering the cells spreading and colonization.

5.4.- Concluding remarks

Hyaluronan can be combined with PEA scaffolds as coating in order to obtain hybrid systems composed of two materials of very different nature, on the one hand the hydrophobic acrylic polymer and on the other the highly hydrophilic and water-soluble HA.

Given their different pores shape, interconnectivity degree and tortuosity, with the employed procedure, only for the PEA-o scaffolds, and not with the PEA-s ones, uniform coatings throughout their thickness were obtained. Moreover, it was feasible to finely tune the resulting type of coating.

Pore coatings by hyaluronic acid can be obtained in an ample typology variety by combining solution concentration and adsorption time, or number of filling-drying cycles or scaffold thickness: ranging from scattered aggregates up to totally clogging the scaffolds pores. After the coating, the gel can be further effectively crosslinked to increase its stability and decrease its dimensional change upon swelling.

It was found that the specific swelling capacity of hyaluronic acid and the porosity of the swollen coated scaffolds fall significantly when the amount of HA in the scaffold increases. The drops in both quantities are related to each other, and reflect the increasingly constrained swelling of the HA gel due to its confinement by an elastic, curved and limited space: the pores of the scaffold.

The incorporation of HA within the pores of the PEA-o scaffold enhances the mechanical performance of the material in terms of increasing the initial modulus, and reducing the sample strain under equivalent loadings as compared with the bare ones.

By employing an *in vitro* model, the feasibility of employing PEA-o coated scaffolds as a controlled release system was assessed; it was found that the presence of HA in the pores contributed to obtain a more sustained release of the employed model protein.

The preliminary cellular study performed with fibroblasts suggests that the use of coated scaffolds might enhance the good biological performance of the bare ones, by improving the cell seeding efficiency. Surprisingly, this improvement was not proportional to the HA mass fraction, as a greater cell density was observed for the scaffolds with the thinner HA coating.

Chapter 6:

Combination of PEA scaffolds with RAD16-I gel

6.- Combination of PEA scaffolds with RAD16-I gel

6.1.- Abstract

This chapter deals with the combined system consisting of PEA scaffolds, either PEA-o or PEA-s, and the self-assembling peptide gel RAD16-I. First of all the interaction between PEA or P(EAcoAAc) (to take into account the modification induced by the production process of PEA-o scaffolds explained in Chapter 3) and the self-assembling peptide (SAP) is extensively characterized in a 2D simplified model. By means of the techniques of choice (congo red stainings, atomic force microscopy (AFM), and contact angle measurements), the influence of the polymer hydrophobicity on the interaction has been assessed.

The next step is the combination of the SAP as filling in the scaffolds pores. In order to do that, different procedures and protocols were attempted, and again congo red stainings have been employed to select the optimal one. Both scaffold types (PEA-o and PEA-s), were filled by means of the set up protocol and characterized by cryoSEM, to ensure the effective filling throughout the scaffold thickness.

The effect of incorporating the SAP within the scaffolds pores on their mechanical performance was evaluated with compression tests. The feasibility of employing these hybrid systems as a platform for controlled release was evaluated *in vitro* for the PEA-s scaffolds by using BSA as model protein.

Finally, as these combined systems are intended for their use as cardiac patches, different *in vitro* cultures were assayed targeting the evaluation of the vascularization potential of the construct.

As a preliminary step, cytotoxicity was discarded with fibroblasts cultures, and then several studies with other cell types were performed, with different aims. First the influence of the SAP on the seeding efficiency was studied; fibroblasts were employed for this purpose, and the seeding protocol that optimizes cell uniformity in the pores was established. HUVECs (human umbilical vein endothelial cells) were cultured in the combined system to evaluate the influence of the SAP incorporation on the expression of endothelial markers. Finally co-cultures of HUVECs and mesenchymal stem cells (MSCs) were performed to study their conjoint effect on the biological performance of different scaffold typologies combined with a SAP within the pores.

6.2.- Results

6.2.1.- Study of the substrate-SAP interaction

Congo red staining was employed to characterize the SAP adsorption onto the materials under study. This dye was first applied onto bare spin coated PEA, spin coated P(EAcoAAc) and glass covers to be used as negative controls, to discard their colouration. As can be observed in Figure 6.1 A, D and G, none of the samples acquired any red tonality.

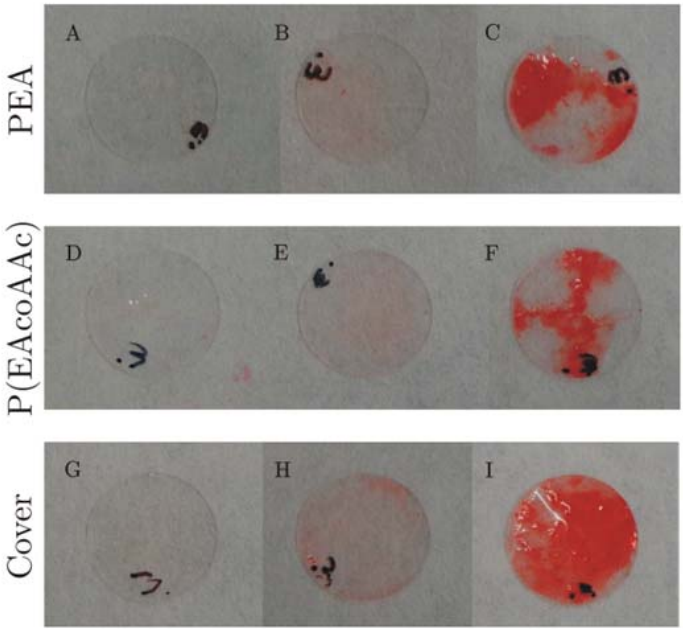

Figure 6.1: PEA and P(EAcoAAc) spin coated samples, and glass covers, with RAD16-I adsorbed on the surface stained with congo red before (2nd column) and after removing the SAP excess (3rd column). Negative control: substrates without SAP (1st column).

When the same procedure was applied onto samples surfaces where RAD16-I had been previously adsorbed, self-assembled and next its excess removed, a very light red shade was detected for all the materials under study (Figure 6.1 B, E and H). This colouring is very subtle, yet when it is compared with the corresponding negative control (where it cannot be perceived at all) the presence of the peptide on

the material surface is revealed. Interestingly, the cover seemed to acquire a stronger colouration. No differences were detected between the studied polymers (PEA and P(EAcoAAc)).

However, congo red staining revealed that when RAD16-I is adsorbed onto the materials, self-assembled but its excess is not removed from the surface, a layer of gel is formed on the surface of all the materials. It is a very weak layer, and during the washes following the staining process some parts might detach from the substrate, as shown in Figure 6.1 F and I. No differences were detected between the two considered polymers despite their different composition and hydrophilicity degree. Nonetheless, covers seem to give rise to a more uniform and stable layer.

By means of AFM images a more exhaustive characterization of the SAP-substrate interaction was performed. As a first step, bare materials were analyzed in order to characterize their surfaces, thus enabling to subsequently identify and distinguish them from the conformation acquired by the adsorbed peptide. As can be observed in Figure 6.2, glass covers present a very characteristic surface roughness that is not detected in the PEA and P(EAcoAAc) spin coated films. This is also an indicator of the success in obtaining a uniform and continuous polymeric layer on the cover. At smaller magnifications such as 5 squared microns windows (images not shown), it was observed that for both materials the density of defects was low.

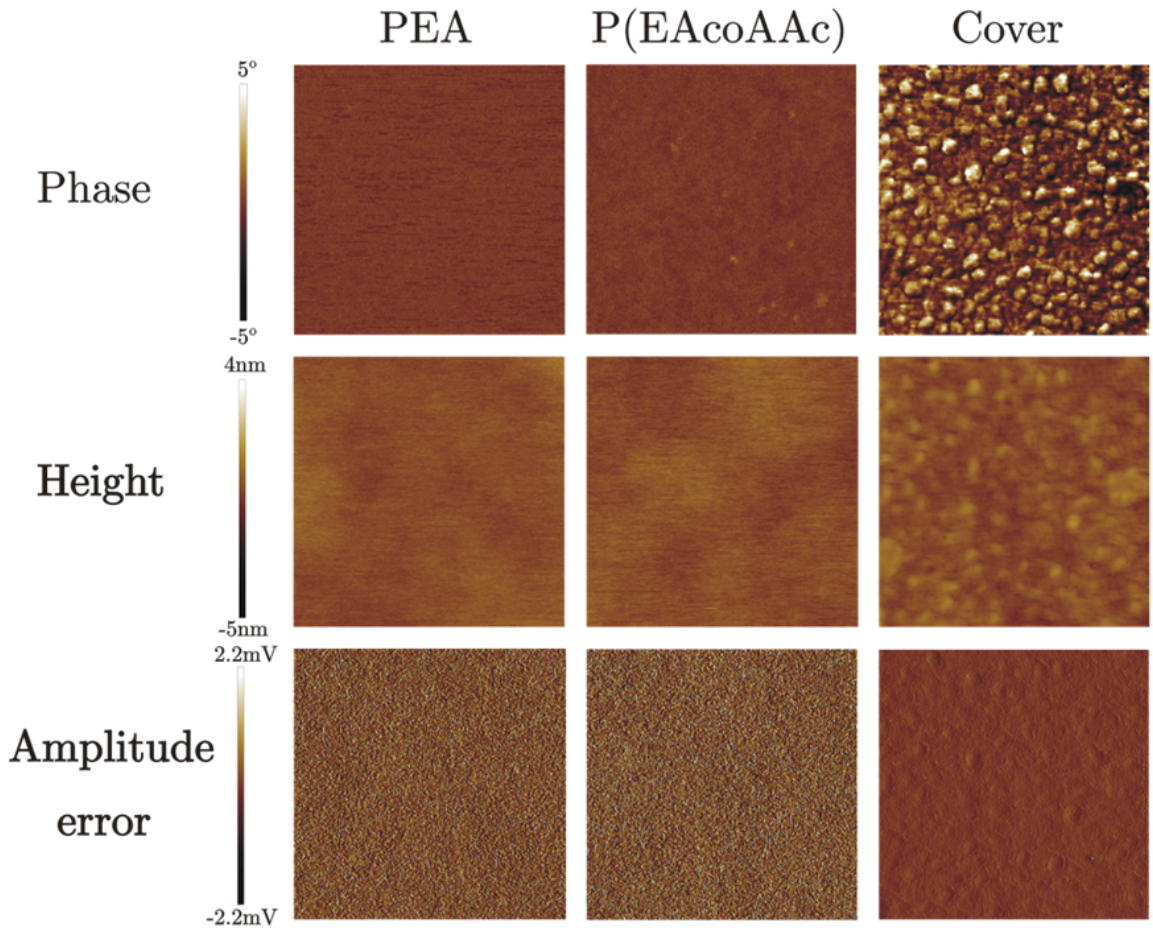

Figure 6.2: AFM images for spin coated PEA and P(EAcoAAc) films and bare covers. Phase (first row), height (second row) and amplitude error (third row) AFM magnitudes.

When RAD16-I was adsorbed on PEA and P(EAcoAAc) at a concentration of 0.1%, a very compact and dense block of peptide adsorbed on the materials surface was observed (Figure 6.3). However, given the high density of nanofibrils, it was impossible to distinguish and establish differences between the conformation or distribution of the peptide because of the different natures of the tested materials. Therefore in the following observations, it was decided to reduce the concentration of the peptide solution.

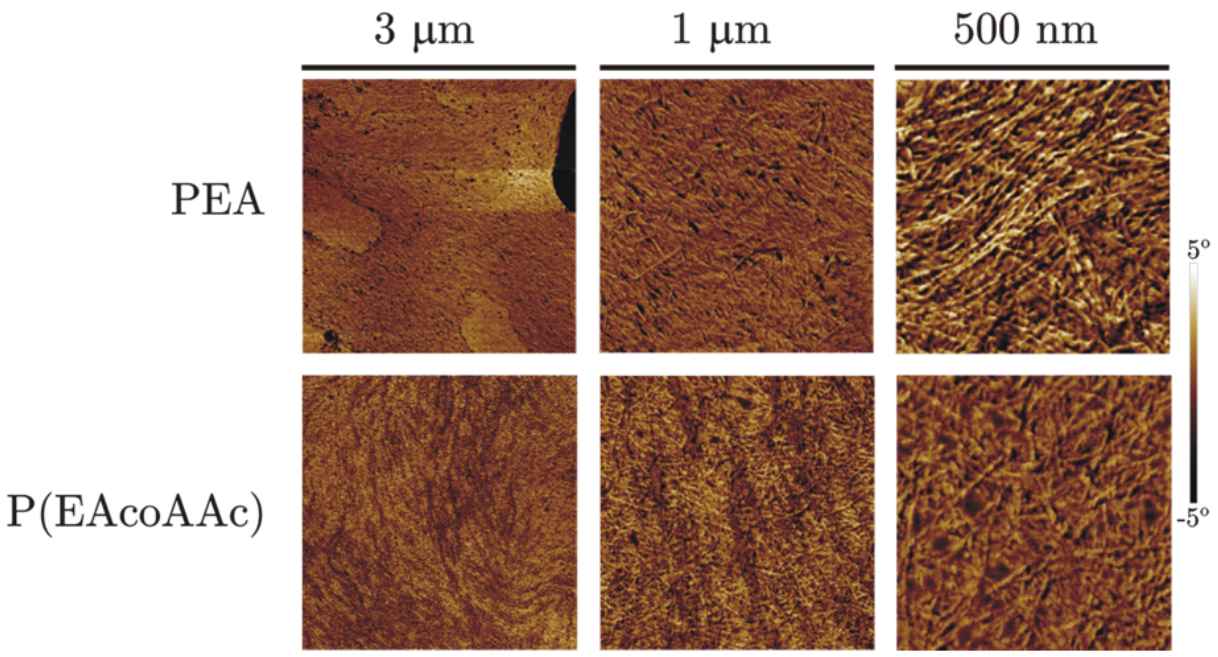

Figure 6.3: Conformation and distribution of the SAP adsorbed at a 0.1% concentration on the surface of PEA (first row) and P(EAcoAAc) (second row), as shown by the phase AFM magnitude.

When the materials were coated with a half diluted solution (*i.e.*, 0.05%) differences between them started to be detected. As can be seen in Figure 6.4, a uniform coating, with a uniform fibre distribution was observed on covers, for all the considered magnifications. In the case of PEA, the formation of gaps and empty spaces in the network formed by the SAP are perceived. As for the P(EAcoAAc), a continuous coating of the surface is also observed; however, in the 3 µm window the resulting structure shows to not be flat, but to present some valleys. Nonetheless, these valleys, unlike the PEA gaps, are uniformly coated with nanofibres as the rest of the film surface. When 500 nm windows are compared, great differences are detected between the distribution of the self-assembled nanofibres on PEA and P(EAcoAAc) substrates. Covers and P(EAcoAAc) display a more similar distribution, though both still exhibit a very dense concentration of nanofibrils that hinders getting information about the substrate influence; for this reason, the concentration of the SAP solution was halved once more, to 0.025%.

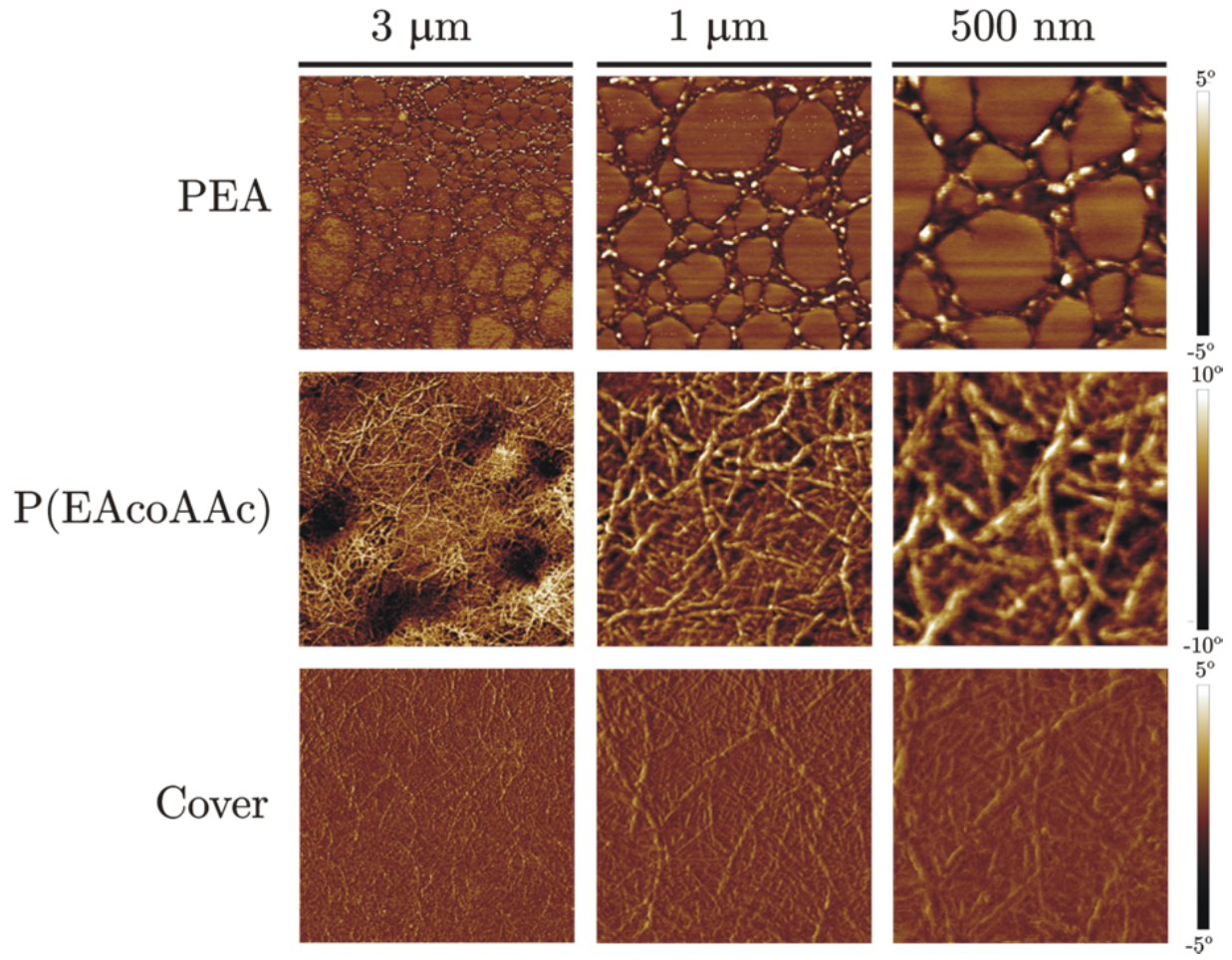

Figure 6.4: Conformation and distribution of the SAP adsorbed at a 0.05% concentration on the surface of PEA (first row) of P(EAcoAAc) (second row) and covers (third row), as observed with the phase AFM magnitude in 3 µm windows (first column), 1 µm window (second column) and 500 nm window (third column).

As can be observed in Figure 6.5 when the RAD16-I is diluted up to 0.025%, the differences among the materials get clearer. As can be observed in the 3 µm images, the SAP does not reach to form uniform layers on PEA, unlike on the cover and P(EAcoAAc), where a uniform layer of peptide is yet obtained. When images at greater magnifications are considered, differences in the resulting net can be clearly detected. For instance on the covers, the RAD16-I self-assembles into straight nanofibres that form a very dense net over the entire surface. In the case of P(EAcoAAc), the peptide self-assembles into a clearer network, formed by circular-like units constituted by straight nanofibres. In the case of PEA a less dense network

is obtained with a more disorganized structure that does not show a patterned distribution.

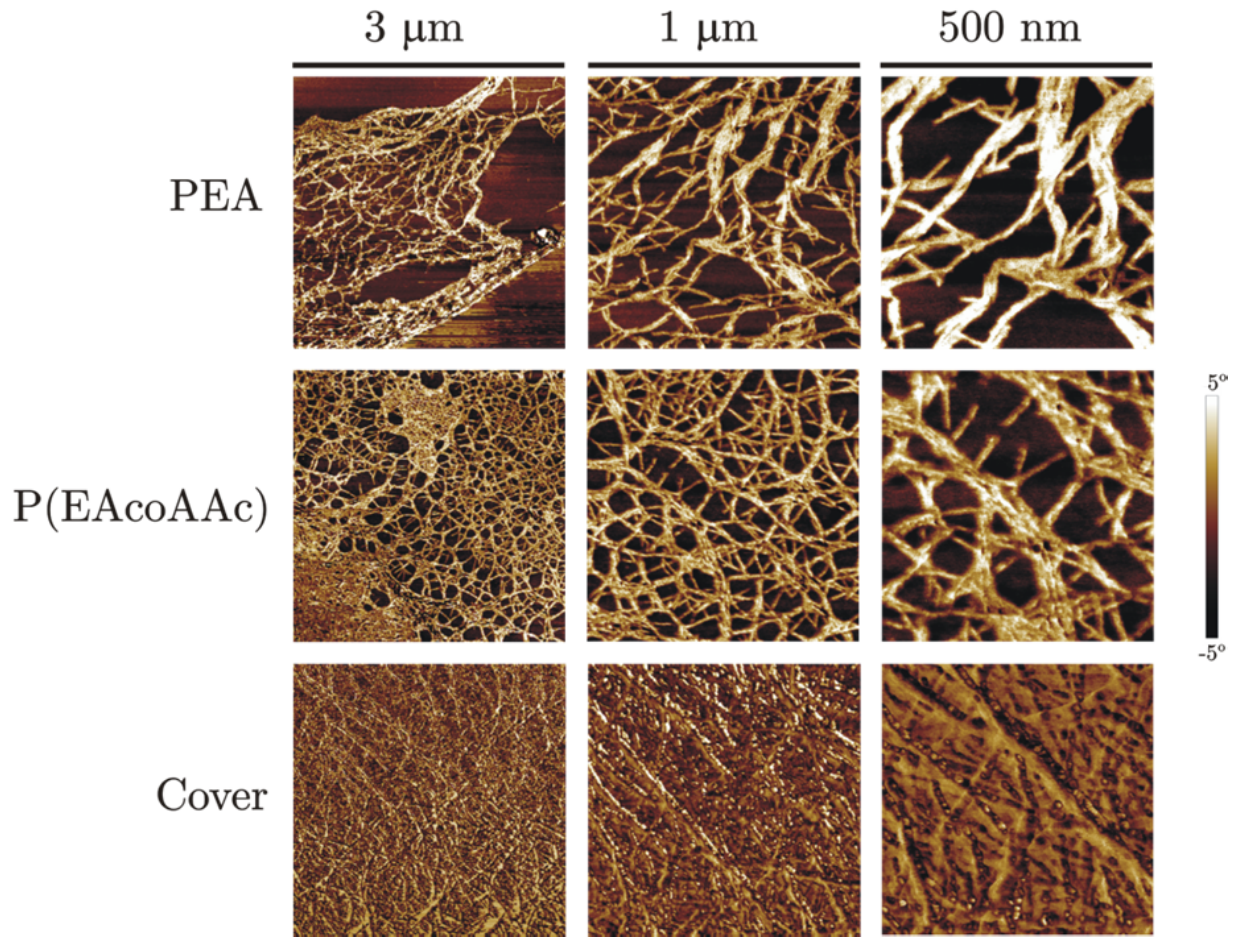

Figure 6.5: Conformation and distribution of the SAP adsorbed at a 0.025% concentration on the surface of PEA (first row) of P(EAcoAAc) (second row) and covers (third row), as observed with the phase AFM magnitude in 3 µm windows (first column), 1 µm window (second column) and 500 nm window (third column).

The differences detected in the AFM images might be attributable to differences in the wettability of the materials' surfaces. Therefore, an intensive study of the contact angles was undertaken.

When the water contact angle was measured (Figure 6.6), the highest was obtained for PEA (90°); the addition of acrylic acid units in the 90/10 copolymer P(EAcoAAc) induced a reduction of it down to 75°. For the bare cover, the lowest contact angle

was measured reaching a value of 46º. For the three studied materials, when the contact angle was measured with diethylenglycol, a dramatic reduction on the mean value was observed: 63º, 56º and 27º respectively. Meanwhile, a more moderate drop was observed for the formamide measurements, PEA reaching a value of 76º, 67º for the copolymer and 42º for the covers.

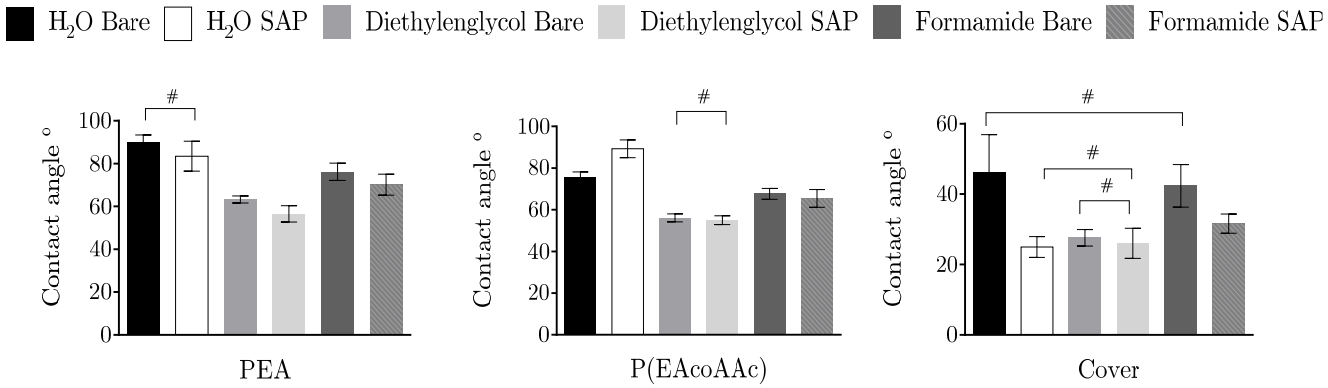

Figure 6.6: Water, diethylenglycol and formamide contact angles on bare or RAD16-I coated PEA, P(EAcoAAc) and covers. (#) Differences are not statistically significant.

The effect of the SAP on the contact angle was evaluated by measuring this parameter on the substrates after formerly adsorbing RAD16-I on their surfaces. For PEA and covers, a trend was observed: the adsorption of RAD16-I on the surface prior to the measurement reduced the obtained contact angle, to a different extent depending on the liquid and the substrate. Differently, for P(EAcoAAc) the water contact angle increased (from 75º up to 89º) when RAD16-I had been previously adsorbed, whereas for the other liquids there was also a reduction of the contact angle values (as occurred with the others substrates).

Additionally, it was decided to measure the RAD16-I contact angle at different concentrations, on dry substrates or on substrates previously swollen to equilibrium in an atmosphere of 100% relative humidity. For PEA and P(EAcoAAc) dry samples, no great differences were detected when the concentration was varied from 0.1 to 0.05% (Figure 6.7); for both solutions and materials the values obtained were

almost the same around 94°. Such high values imply that the contact angle when compared with that of pure water droplets has increased. Differently, for the cover a slight reduction, if any, on the mean value of the contact angle is observed for both RAD16-I concentrations when compared with pure water; nevertheless these differences are very subtle. When swollen, both PEA and P(EAcoAAc) showed a reduction of the contact angle for the three liquids employed. Such behaviour was surprisingly the opposite for the 'swollen' covers, on which increases of the contact angles were found.

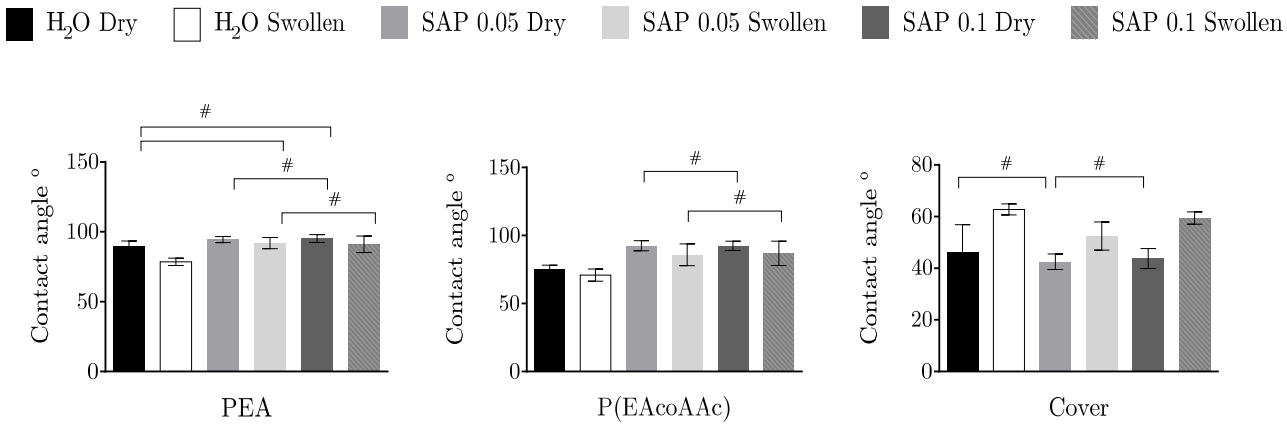

Figure 6.7: Water and RAD16-I at 0.05 and 0.1% concentration contact angles on bare PEA, P(EAcoAAc) and covers, either dried or swollen in a 100% relative humidity atmosphere. # Differences are not statistically significant.

6.2.2.- Scaffolds with spherical interconnected pores combined with RAD16-I gels

Production of homogeneous and stable fillings

Given the different nature of RAD16-I (99% water) and the PEA-s scaffolds (highly hydrophobic), the first milestone was to establish a suitable protocol to properly fill the scaffolds' pores with the SAP. With the help of congo red staining and employing bare scaffolds as negative controls (Figure 6.8 A and B), a procedure was set up. Natural diffusion was found to be insufficient to fill the scaffolds with the peptide solution due to the hydrophobicity of the formers (Figure 6.8 C).

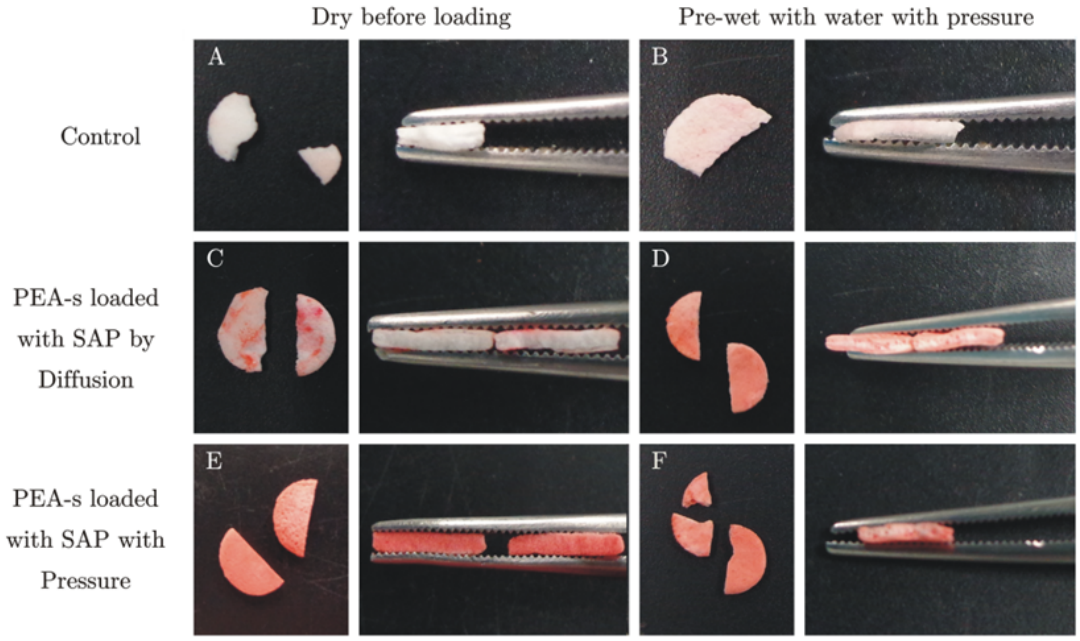

Figure 6.8: Procedure and resulting congo red colouration of PEA-s scaffolds filled with RAD16-I or water (as negative control for the staining) with different staining protocols.

As an alternative it was proposed to pre-wet the scaffold with water to facilitate the peptide diffusion throughout its thickness (Figure 6.8 D); however it seemed yet not enough to obtain a uniform filling. Then pressure was applied to force the solution to penetrate into the pores by the introduction of the scaffold in a syringe with the peptide solution and helping the intrusion of the solution by evacuation (Figure 6.8 E and F). This procedure was applied in combination with pre-wetting the scaffold

with water (Figure 6.8 F) or not (Figure 6.8 E); nonetheless, given the absence of clear differences between them, the pre-wetting step was discarded. The solution could be brought to gelation *in situ* within the pores in 20 min with the same congo red (as it is a salt). No differences were observed with those samples gelled for longer times; thus, 20 min was hereafter the gelation time employed.

CryoSEM images of both PBS (to be used as controls) and SAPs-filled PEA-s scaffolds are shown in Figure 6.9. When water sublimates for cryoSEM observation, the trace of the non-gelled SAP solution appears as parallel walls (Figure 6.9 C).

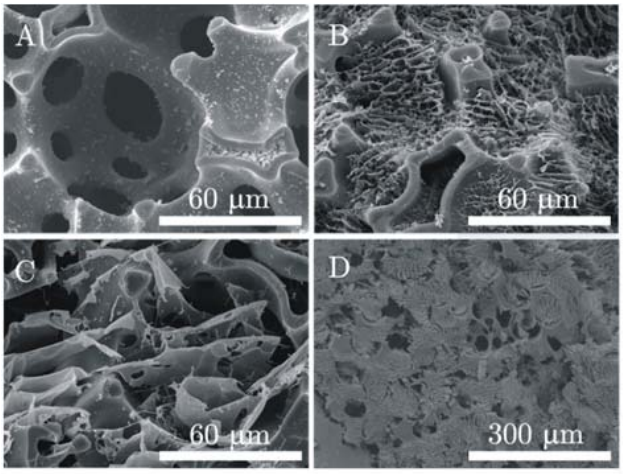

Figure 6.9: CryoSEM cross-section images of: (A) PEA scaffold loaded with PBS, (C) PEA scaffolds loaded with 0.15% SAP solution and (B, D) after gelling with PBS at different magnification.

Once gelled by PBS addition, the SAP nanofibrilar network leaves a honeycomb-like structure in the pores of the scaffolds (Figure 6.9 B and D). These structures cannot be found after water sublimation in the scaffold's pores containing PBS (Figure 6.9 A). As can be observed in Figure 6.9 D the employed procedure guarantees the complete and homogenous filling of all the pores, even in the scaffold core, resulting in the hiding of the scaffolds porous structure by the sublimated peptide filling.

The stability of the SAP filling in the scaffolds when immersed in aqueous media was also morphologically characterized by means of SEM. Figure 6.10 shows that after 1 (A and B) and 7 days (C and D) under culture conditions (*i.e.* 37ºC, immersion in cell culture medium in an incubator) the pores of the scaffold are uniformly filled with the SAP. Figure 6.10 B shows a detail of the self-assembling peptide structure, which forms a dense nanometric net. After 7 days of culture a suitable filling remains, maintaining a proper nanofibrilar structure, although occasionally the filling seems to be slightly less compact.

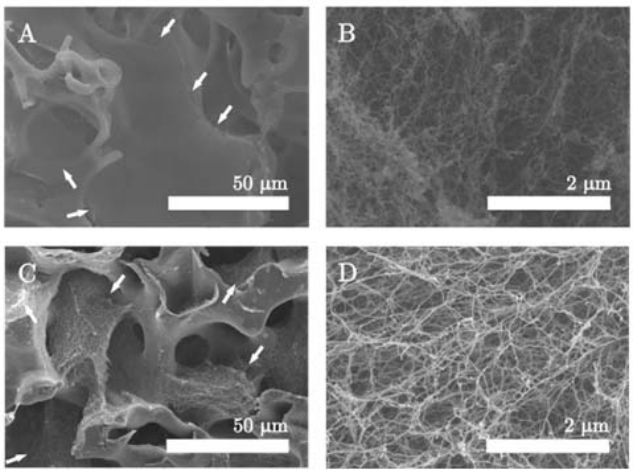

Figure 6.10: SEM images of acellular bare scaffolds filled with RAD16-I after 1 (A and B) and 7 days (C and D) in culture conditions.

Influence of the filling on the scaffold mechanical performance

Compression tests were performed to assess the influence of the filling on the mechanical performance of the PEA-s scaffolds. The compression curves of the scaffolds, either bare or filled with the RAD16-I solution and gelled with PBS, show an overall non-linear dependence of stress upon strain with increasing modulus (Figure 6.11). A first linear deformation region ranges up to 5% strain and 10 kPa stress, followed by a region of increasing slope, which stabilizes in a second linear deformation region for strains greater than 25% at stresses above 100 kPa. The

Young's moduli in both linear deformation regimes are included as insets in Figure 6.11. Those of the scaffolds filled bare were found to be 14.2 ± 1.7 kPa, being the moduli of the scaffolds filled with the gelled peptide slightly greater (25.1 ± 3.8 kPa).

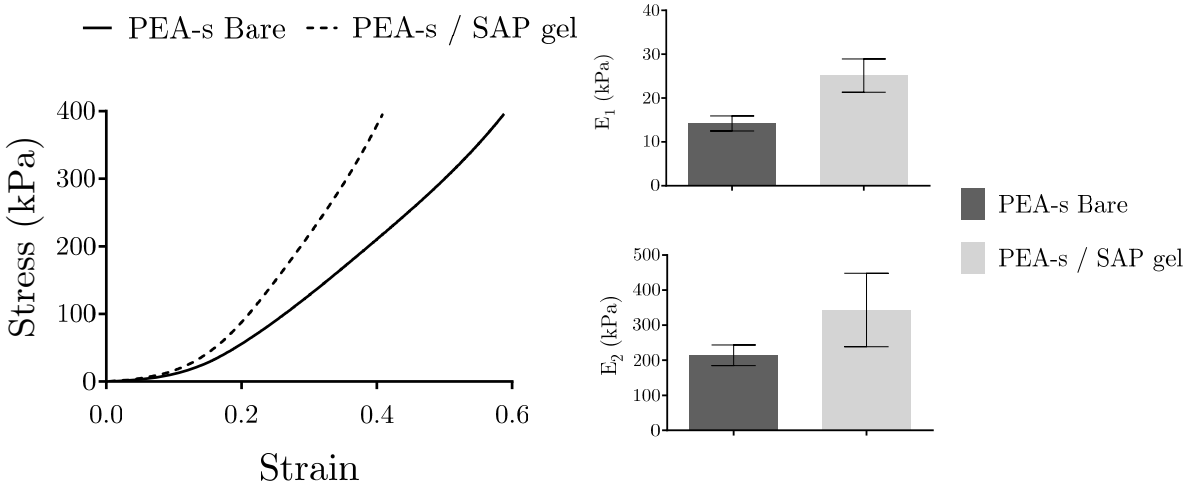

Figure 6.11: Stress–strain curves obtained from compressive experiments performed on PEA-s scaffolds, bare and filled with the SAP gel. Insets: initial Young modulus, E_1, and linear modulus E_2 calculated at strain 0.3.

Controlled release study

The concentration of BSA incorporated to the scaffold's pores, obtained from the mass uptake M_0 and the volume of SAP solution in the pores, resulted in 12.7 mg·ml^{-1}. Unexpectedly, this value is much higher than that of the starting BSA solution, 1 mg·ml^{-1}. Figure 6.12 shows the fractional BSA, M_t/M_0, release curve of the loaded construct, where M_0 is the initial mass of BSA in the scaffold-SAP construct and M_t is the mass released from it at time t. Two different release regimes can be identified: first a fast protein release up to 14.9% of the initial amount of BSA within the first 8 h, and then a slower one from this moment on up to 25% in 10 days.

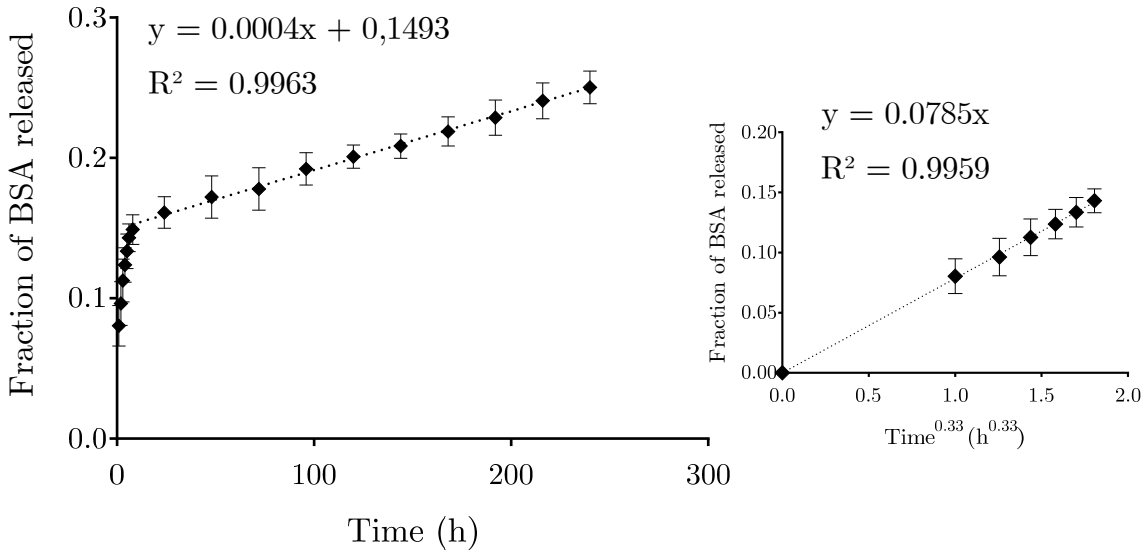

Figure 6.12: BSA release curve from loaded scaffold-gel constructs immersed in PBS: fractional mass M_t/M_0 of BSA released at time t *vs.* time. Inset: fit to a power law function of the data of the initial release regime.

6.2.3.- Scaffolds with orthogonally interconnected pores combined with RAD16-I gel

Production of homogeneous and stable fillings

Congo red staining was employed again as a first evaluation of the success on producing scaffolds with cylindrical interconnected pores (PEA-o) uniformly filled with RAD16-I. As Figure 6.13 shows there is a clear difference between the bare scaffolds and the filled ones. Moreover it can be observed that the gel filling was homogeneously distributed throughout the scaffold thickness.

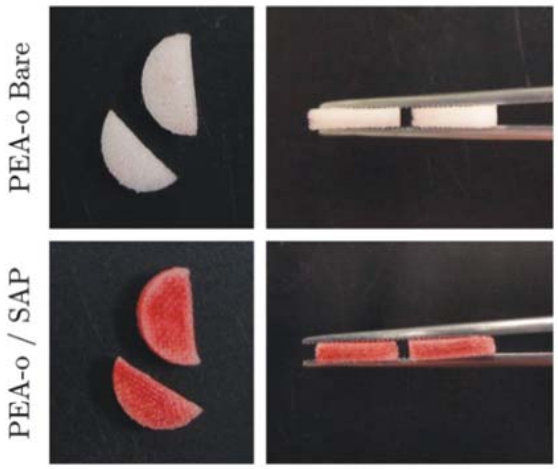

Figure 6.13: Congo red stained samples of bare PEA-o scaffold (first row) and PEA-o filled with RAD16-I gel by applying pressure with a syringe (second row).

The cryoSEM images of both, empty and SAPs-filled PEA scaffolds, in a frontal view and cross section are shown in Figure 6.14. The empty ones (A, B) show the already presented structure consisting of cylindrical interconnected orthogonal pores. The different layers of fabrics can be clearly observed in the cross section image (A). However, when the scaffolds' pores are filled with the peptide, the structure previously shown is totally hidden because of the peptide presence (C, D). Between images C) and D) slight differences in the resulting structures after the water sublimation process in the cryoSEM device are detected.

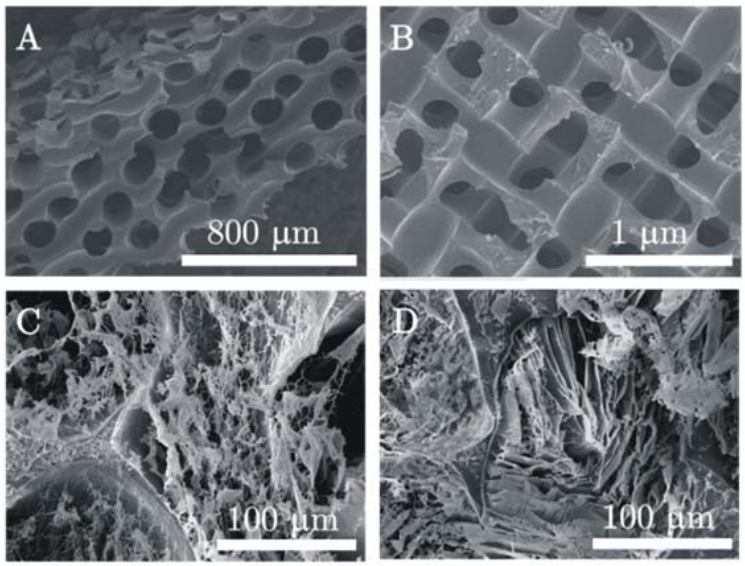

Figure 6.14: SEM images of the PEA-o scaffolds: (A) cross section, (B) surface. CryoSEM cross section images of the PEA scaffolds loaded with 0.25% SAP solution (C) and (D) after gelling with PBS.

Influence of the filling on the scaffold mechanical performance

The PEA-o/SAP combined systems were mechanically characterized by compressive tests, to check any influence of the soft peptide filling on the different stages of the scaffolds compression. The stress-strain profiles of the bare scaffolds and those filled with non-self-assembled SAP, or self-assembled SAP, Figure 6.15, show two different zones: an initial linear behaviour extending up to 30% deformation and 30 kPa stress, the change of slope is abrupt, and the second linear zone occurs for strains greater than 70% at stresses above 200 kPa. From both linear zones, E_1 and E_2, were calculated as the slopes and are shown as insets in Figure 6.15. Only the first compressive modulus increases slightly when the pores are filled with the aqueous peptide solution or gel. The second one does not seem to depend so much on the presence or not of the SAPs or their sol/gel state within the PEA scaffolds, its value remaining quite invariant although a slight reduction is observed for the scaffolds with SAP gelled.

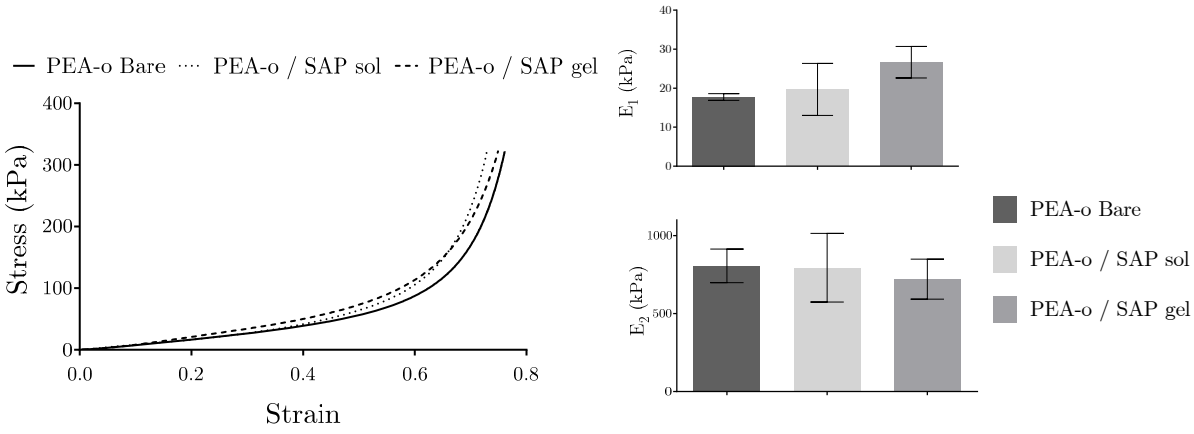

Figure 6.15: Stress-strain curves obtained from compressive experiments performed on bare, filled with SAPs (w/ SAPs sol) and filled with SAPs and gelled (w/ SAPs gel) PEA-o scaffolds. Insets: compressive moduli calculated in the first, E_1, and second, E_2, zone of the profiles.

6.2.4.- Biological performance

In order to assess the biological performance of the hybrid system, first of all, a cytotoxicity test was performed with the PEA-o scaffolds bare and the SAP-filled PEA-o scaffolds.

Once the cytotoxicity of the materials was evaluated and discarded, a seeding protocol to enhance the initial adhesion of cells was established with fibroblasts. The SAP impact alone or in combination with shaking the samples for 30 minutes right after the seeding was evaluated.

The interest of combining these hybrid materials with HUVECs lies in the fact that the first milestone to achieve a vascularizable construct is its colonization by endothelial cells. This combined system thus was also tested with endothelial cells, and the effect of the peptide presence on the expression of specific endothelial markers was exhaustively studied. First the cells spatial distribution and cell-cell contacts were studied through immunocytochemistry dyes. Next, the amount of cells expressing two characteristic endothelial markers, CD31 and VE-cadherin, was quantitatively assessed by means of cytometry, followed by the estimation of the fraction of cells co-expressing both by means of image cytometry.

Subsequently the SAP/PEA scaffolds with either cylindrical orthogonally connected or spherical interconnected pores were co-cultured with HUVECs and MSCs. MSCs addition was expected to exert a paracrine effect on the endothelial cells improving their achievement in terms of migration, scaffold colonization, expression of endothelial cells markers, and the establishment of cell-cell connections. Moreover there are also evidences that the mesenchymal cells are also present in the perivascular niche [301], and are thought to play a key role on the clinical application of regenerative therapy.

The combined system was found to be non-cytotoxic. Moreover, it was found that combining the prior addition of the peptide with 30 min of shaking had a very positive effect on cell density and distribution in the scaffolds pores. The presence of the peptide also improved endothelial cells' markers expression both cultured alone and co-cultured with mesenchymal cells.

Cytotoxicity assay with scaffolds with orthogonal interconnected pores

Figure 6.16 shows the absorbance after the MTS assay on fibroblasts cultured in extracts of bare scaffolds, and filled with SAP and gelled, together with positive (culture medium) and negative (latex) controls, for 1, 3, 7 and 14 days. Neither the scaffolds nor the combined systems are toxic for the cells; conversely, the negative control does show cytotoxic behaviour, as expected. The absorbances given by fibroblasts cultured in the scaffolds' extracts are very similar to those cultured in culture medium: low at short times, increase up to day 7, and decrease afterwards for lack of nutrients (the extracts were not renewed during the experiment).

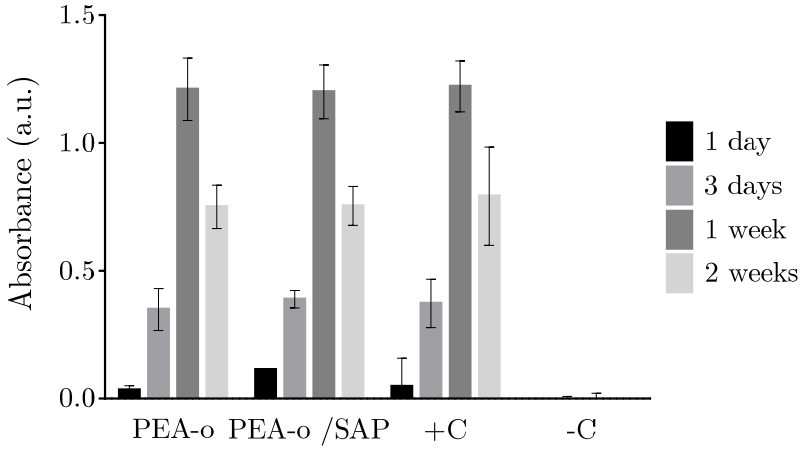

Figure 6.16: Results of cytotoxicity analysis of bare scaffolds and combined systems. MTS test absorbance results for the proliferation of L929 fibroblasts in extracts of bare and SAP-filled PEA scaffolds, positive (culture medium) and negative (extract from latex) controls after 1, 3, 7 and 14 days of culture.

Set up of the cell-seeding protocol with scaffolds with spherical interconnected pores combined with SAP gel

Bare scaffolds filled with PBS and scaffolds filled with the SAP solution were seeded on their upper surface with fibroblasts. After seeding, cells were allowed to diffuse within the scaffold with or without mechanical assistance, and after 30 min, culture medium was added to induce gelation. Figure 6.17 and Figure 6.18 show that more cells colonize the scaffolds when the scaffold's pores are filled with the SAP gel, and consequently after 7 days they have proliferated and occupy all the pores.

Comparison of the images obtained from scaffolds seeded statically and dynamically clearly indicate that the dynamic seeding favors the invasibility of the pores by the cells, which remain encapsulated when the peptide fills the pores, proliferate and are much more numerous after 7 days.

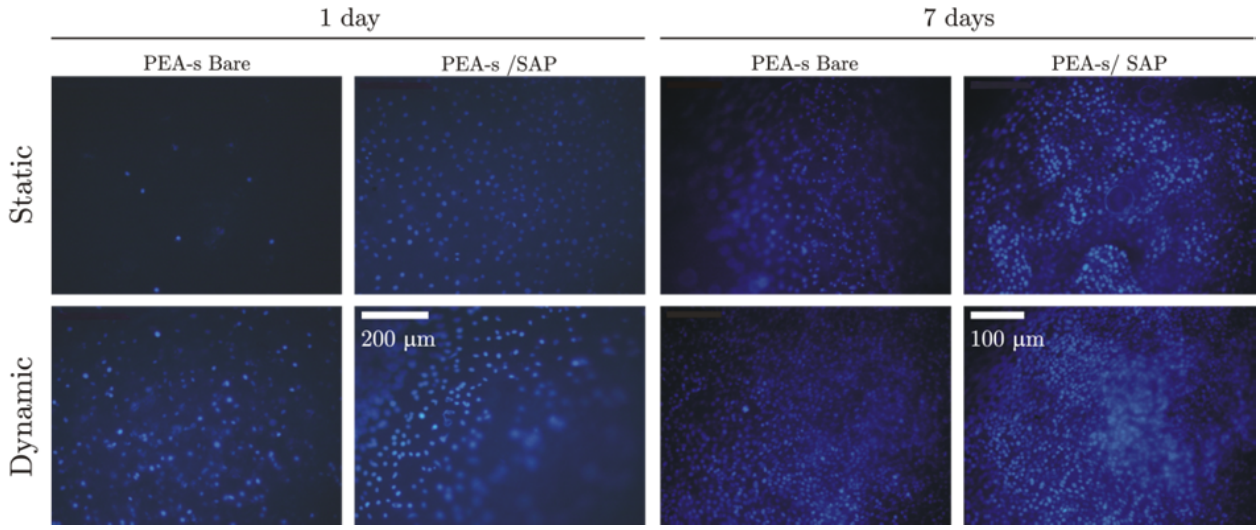

Figure 6.17: Fluorescence microscopy images of the surfaces of PEA-s scaffolds (without and with SAP gel within their pores) seeded with fibroblasts (statically and dynamically) and cultured for 1 day (scale bar 200 µm) and 7 days (scale bar 100 µm); DAPI (nuclei) staining in blue.

Because of the peptide presence within the pores, the cells are more uniformly distributed. However, cells rather adhere to PEA and follow the geometry of the scaffold despite of the SAP filling the pores as can be observed from the actin stain in Figure 6.18.

At this culture time cells display under SEM either an elongated or a more rounded morphology (Figure 6.19 A; see the broken line outlining a pore, and the asterisk, respectively), depending on whether they adhere to the PEA trabeculae or swim within the pores, and they have synthesized a large amount of extracellular matrix. At higher magnification (Figure 6.19 B), such rounded cells seem to be completely embedded in what is probably ECM and SAP gel, filling the pores of the scaffold.

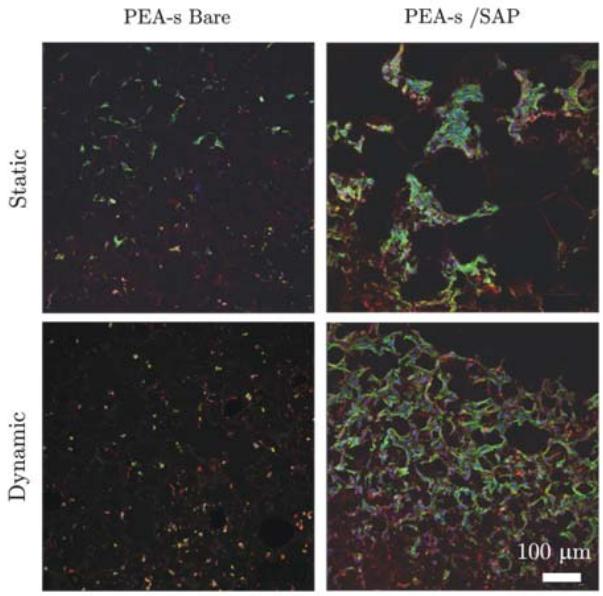

Figure 6.18: Fluorescence microscope images of fibroblasts seeded statically and dynamically in PEA-s scaffolds with and without SAP solution in their pores, cultured for 7 days. DAPI stain for nuclei (blue), phalloidin stain for actin (green) and vimentin stain for cell membrane (red). Images correspond to 100 µm thick internal slices.

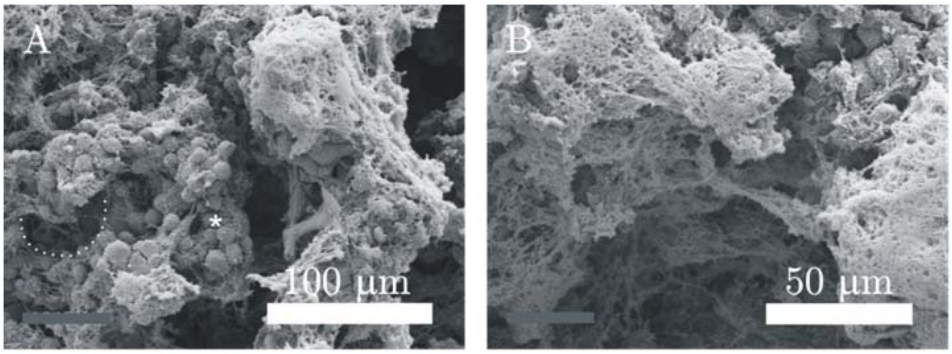

Figure 6.19: SEM images at different magnifications of cross-sections of PEA scaffolds with SAP gel in their pores, seeded dynamically with fibroblasts and cultured for 7 days.

SAP influence on HUVEC cultured on spherical sponge-like scaffolds

First of all, a 2D simplified model was employed to study the influence of the self-assembling peptide on the biological performance of HUVECs. 2D PEA discs bare (PEA(-)) or with SAP previously adsorbed on their surface (PEA(+)) were seeded with HUVECs and cultured; the influence of the peptide on cell adhesion and proliferation was studied.

As can be observed in Figure 6.20, at day 1 (*i*.e., initial adhesion), no differences were detected because of the peptide presence. At day 3, however, the PEA(-) reaches a greater value of absorbance than PEA(+); nonetheless, given the size of the error bar this difference can be due to the occasional detachment of cell plaques because of the formation of SAP clots. Indeed, at day 7 PEA(+) increases considerably while PEA (-) absorbance value is below that reached at day 3.

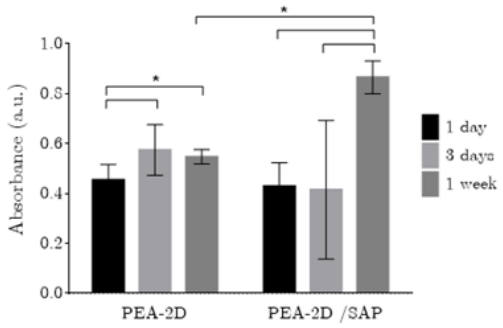

Figure 6.20: MTS results at 1, 3 and 7 days of HUVECs cultured on PEA without (PEA(-)) or with SAP (PEA(+)) previously adsorbed on the surface.
(*) Differences are statistically significant.

The following step was to evaluate the peptide influence on the seeding and proliferation in 3D cultures; thus, bare scaffolds and scaffolds filled with SAP were seeded with HUVECs. The presence of the peptide improved the seeding efficiency (Figure 6.21), and after a week of culture this positive influence was maintained over the time.

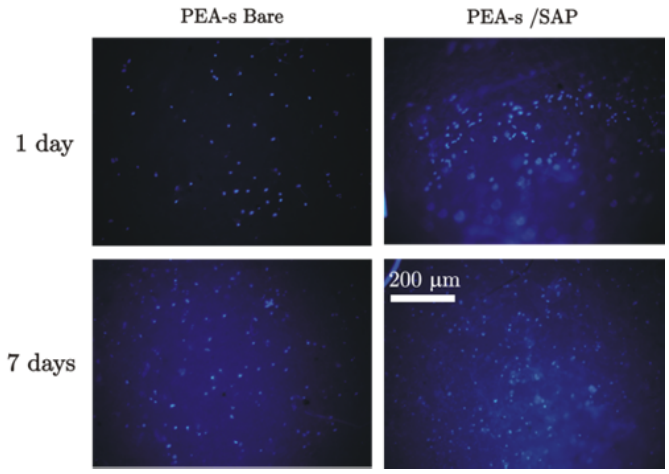

Figure 6.21: Fluorescence microscopy images of the surfaces of PEA scaffolds (without and with SAP gel within their pores) seeded with HUVECs and cultured for 1 day and 7 days; DAPI (nuclei) staining in blue.

In order to characterize the cells distribution and morphology in the scaffold, actin filaments were stained with phalloidin and observed under confocal laser microscope (CLSM). As can be observed in Figure 6.22, cells were properly adhered and were

able to grow in the 3D pores. Moreover, samples cultured in the combined system scaffold/gel, are present at a higher density and exhibiting increased contact areas between them. In the case of bare scaffolds cells were found to follow the topography of the scaffolds, preferably adhering on the edges of the scaffold's pores, adopting circular dispositions and also establishing contacts among them though to a lesser extent than in the hybrid system.

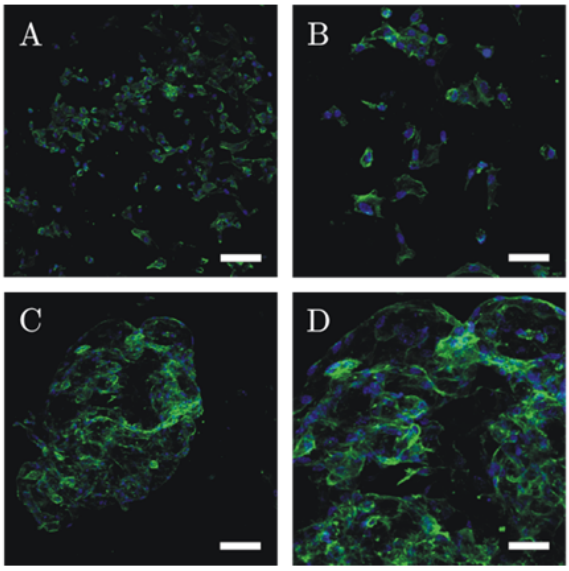

Figure 6.22: CLSM images of HUVECs seeded dynamically in bare PEA scaffolds (A, B) or with the SAP gel filling the scaffolds pores (C, D), and cultured for 14 days. DAPI stain for nuclei (blue) and phalloidin stain for actin (green). Scale bar = 100 μ m (A, C) and 50 μ m (B, D).

The expression of the cell junction clusters CD31 and VE-cadherin was assessed by immunocytochemistry and observed at high magnification under a confocal laser microscope (CLSM) (Figure 6.23). After selected culture times, HUVECs were able to express both markers at cell-cell contact regions in both materials, along the cell border with their neighbours and also with the scaffold surface. More immunopositive cells were observed in the case of PEA-s/SAP (Figure 6.23 C, D) when compared with bare PEA-s (Figure 6.23 A, B).

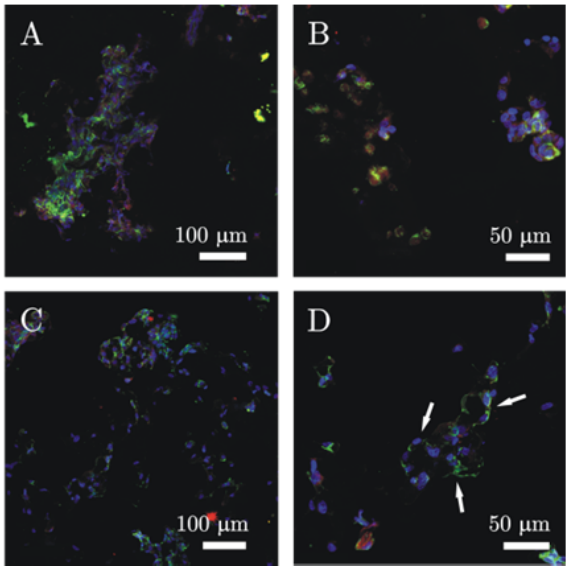

Figure 6.23: CLSM images of HUVECs stained against CD31 and VE-cadherin, cultured for 14 days in bare PEA-s scaffolds (A, B) or PEA-s scaffolds combined with SAP (C, D). Cell-cell contacts are pointed out with white arrows.

In order to monitor the expression of both CD31 and VE-cadherin markers, flow cytometry was employed. After one day of culture the greatest expression of CD31 was obtained for the 2D PEA control (Figure 6.24 A). After 7 days of culture, the expression of this marker was though reduced for both PEA 2D and bare scaffolds, whereas the expression for the cells cultured in the combined system PEA-s/SAP increased reaching the greatest fraction of positive cells for that time point. In the case of the VE-cadherin expression, interestingly different results were obtained (Figure 6.24 B). The greatest fraction of positive cells was obtained for the PEA-s scaffold combined with the SAP for both time points. Nonetheless, for all the considered materials, an increase is observed for the second time point though to a much lesser extent than when PEA-s is combined with the SAP.

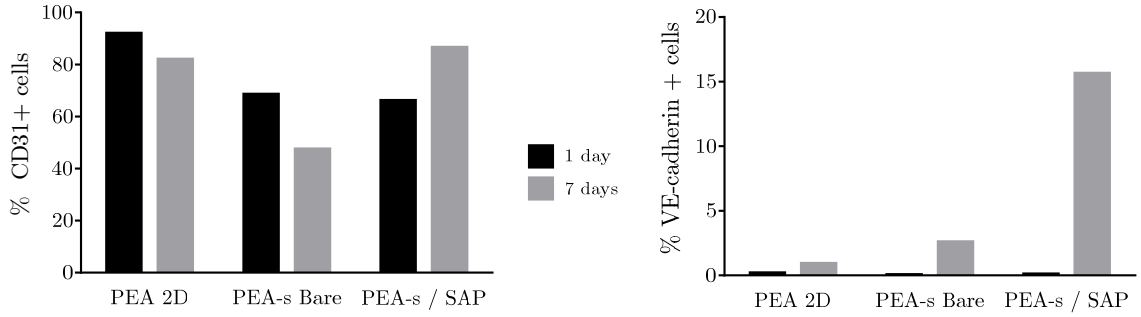

Figure 6.24: Flow cytometry analysis of CD31 (A) and VE-cadherin (B) expression of HUVECs in cultured PEA 2D, PEA-s and PEA-s/SAP.

Next, cell-cell interactions in 3D constructs were further explored by double-labelling and image flow cytometry (AMNIS) in order to analyse the co-expression of VE-Cadherin and CD31 (Figure 6.25). A higher expression of both markers was found in PEA-s/SAP (70.4%) when compared with bare PEA-s (63%). Co-localization of both surface receptors was not detected in any case (data not shown).

Representative images of the obtained fluorescence histograms, which show the frequency of occurrence of different fluorescence intensities, are presented for PEA-s/SAP (Figure 6.25 B), and illustrative images of the cells cultured in PEA-s/SAP are displayed in Figure 6.25 C. These pictures evidence that the CD31 marker is present in a greater fraction of the cells' surfaces than VE-cadherin (endothelial specific cell-cell adhesion molecule) which appears in relatively smaller areas.

SEM images of PEA-s/SAP scaffolds (Figure 6.26) show how HUVECs maintain a rounded morphology after only one day of culture, but how after a week they exhibit a more extended and elongated morphology, and are already coating the surface of the scaffold's pores. These images also reveal that despite the presence of the SAP, cells were also adhered to the PEA surface, and tend to approach and establish contact with others while adopting circular dispositions.

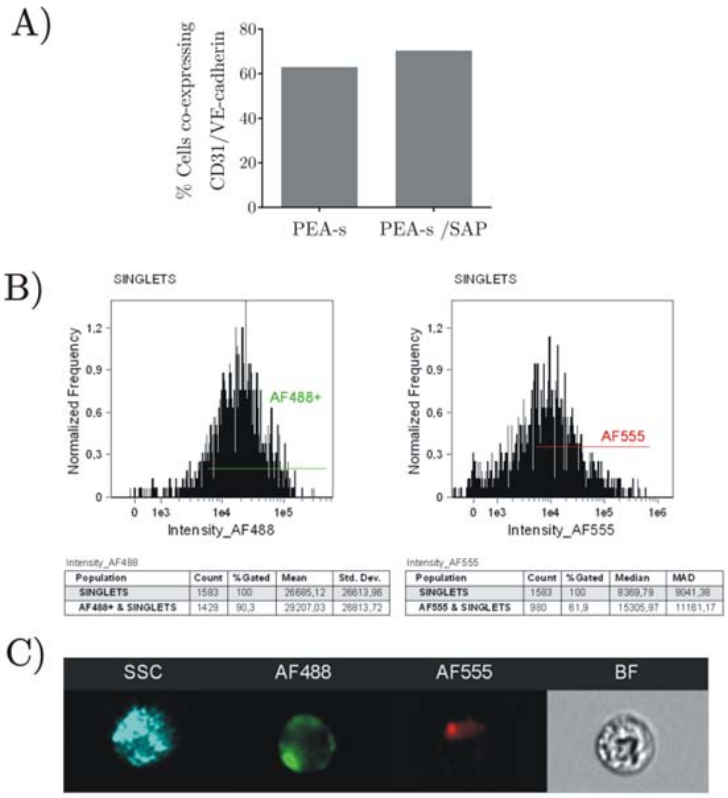

Figure 6.25: Population analysis of CD31 and VE-cadherin co-expression of HUVECs cultured in PEA scaffolds and PEA-SAPs (A). CD31-AF488 and VE-AF555 fluorescence histograms (B). Cells representative images including: SSC (side scatter), CD31-AF488, VE-Cadherin-AF555 and bright field (C).

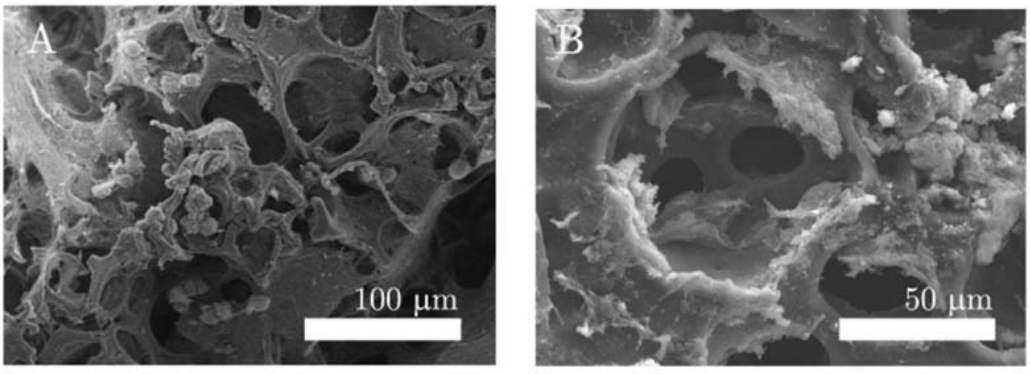

Figure 6.26: SEM images of SAP filled scaffolds seeded with HUVECs and cultured 1 (A) and 7 days (B).

Co-culture experiments performed with grid- and sponge-like scaffolds combined with SAP gel

The biological performance of both types of scaffolds (PEA-s and PEA-o) in combination with self-assembling peptides when seeded simultaneously with HUVECs and MSCs was also assessed. As a first step, flow cytometry was employed to evaluate the fraction of each type of cells present in the co-culture experiments, and the evolution of this proportion with time.

As can be observed in Figure 6.27, for the PEA-o scaffolds, the fraction of endothelial cells (CD31) at shorter times is higher for the bare ones than for those filled with the gel; however, at longer times this fraction is reduced. Oppositely, for the PEA-o scaffolds filled with SAP, the fraction of endothelial cells increased with the culture time. Regarding the mesenchymal cells (CD90), a significant fraction is detected in the PEA-o/SAP system at short culture times. Nonetheless, at longer times the fraction increases for the bare scaffold, while it is maintained for the hybrid scaffold.

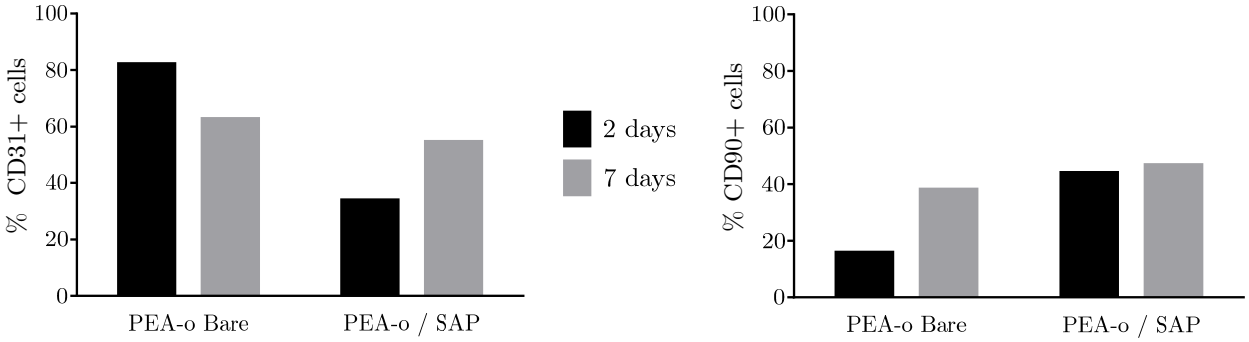

Figure 6.27: Fraction of CD31 and CD90 positive cells in the bare or SAP-filled PEA-o scaffolds after 2 and 7 days of culture.

Different results were obtained for the PEA-s scaffolds (Figure 6.28). Both bare scaffolds and those combined with the SAP showed a drastic reduction on the HUVECs fraction with culture time. Conversely, the fraction of mesenchymal cells greatly increased at longer times.

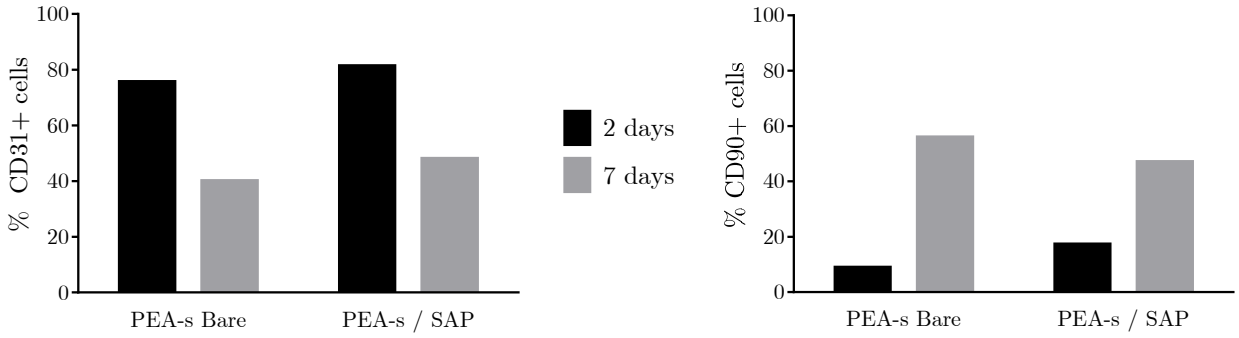

Figure 6.28: Fraction of CD31 and CD90 positive cells in the bare or SAP filled PEA-s scaffolds after 2 and 7 days of culture.

Cell density was assessed for each group of materials by means of quantifying the DNA content with a picogreen assay. As can be observed in Figure 6.29, similar values are attained for the different groups, regardless of the type of porosity and the presence or absence of the SAP, except for the PEA-o/SAP (whose DNA content was unexpectedly low). In all cases the 3D constructs reached higher values than PEA 2D.

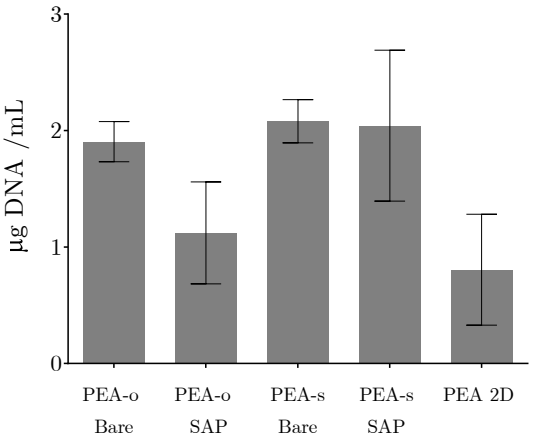

Figure 6.29: DNA content in the different types of scaffolds and 2D control after 7 days of culture.

Cells morphology and distribution throughout the scaffolds were first studied by SEM. As Figure 6.30 shows for the PEA-o samples, both bare and combined with the SAP, a great number of cells are observed. Cells cover the scaffold external surfaces

(both upper and lower). When cross sections are observed, in the case of bare PEA-o cells are uniformly distributed throughout the thickness of the scaffold, and adopt elongated shapes following the cylindrical pores of the scaffold. In the case of PEA-o/SAP, more rounded structures are detected again throughout their thickness. These structures are thought to be a combination of cells, extracellular matrix and peptide; however these elements cannot be distinguished in the SEM images.

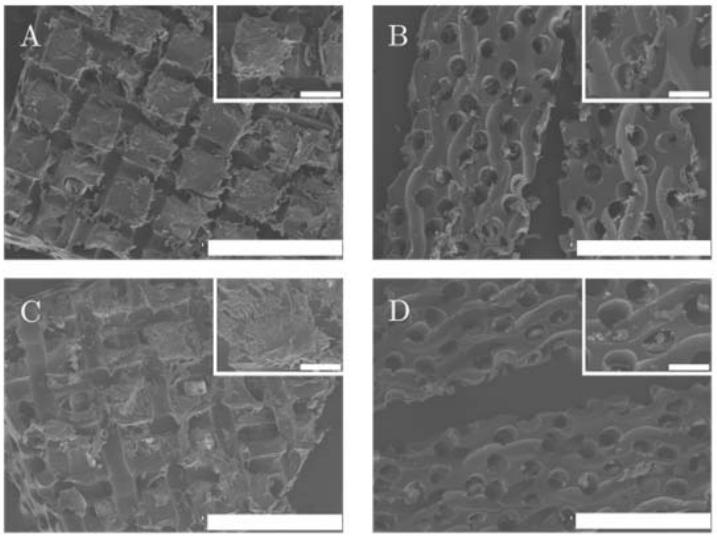

Figure 6.30: SEM images of surfaces and cross-sections of PEA-o scaffolds without (A, B) or with SAP in their pores (C, D), seeded dynamically with HUVECs and MSCs, after 10 days of culture (scale bar: 1 mm). Insets show details of regions of interest at greater magnifications (scale bar: 200 μm).

For the PEA-s scaffolds (Figure 6.31) a layer of cells was also observed on the surface, being it denser in the case of the scaffolds combined with the SAP than in the bare ones. When cross sections were exposed, for the bare scaffolds a high density of cells was detected.

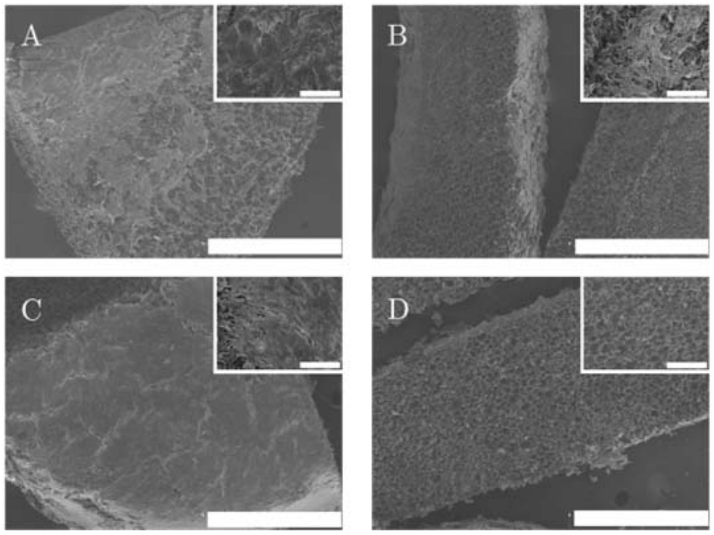

Figure 6.31: SEM images of surface and cross-sections of PEA-s scaffolds without (A, B) or with SAP gel in their pores (C, D), seeded dynamically with HUVECs and MSCs, after 10 days of culture (scale bar: 1 mm). Insets show details of regions of interest at greater magnification (scale bar: 200 μm).

As for the amount of VEGF released into the supernatant by cells cultured in the set of materials (Figure 6.32), it was found that for the PEA-s scaffolds there were no differences between the bare ones and those combined with the SAP. For the PEA-o scaffolds, however, certain differences were detected: a slightly greater release of the growth factor was measured for the bare ones. When both scaffold typologies were compared, it was confirmed that cells cultured in PEA-s scaffolds released greater amounts of VEGF (up to 10 times more) than those in the PEA-o scaffolds do (either bare or combined with SAP). In both types of scaffolds cells released more VEGF than when cultured on a flat substrate (cover).

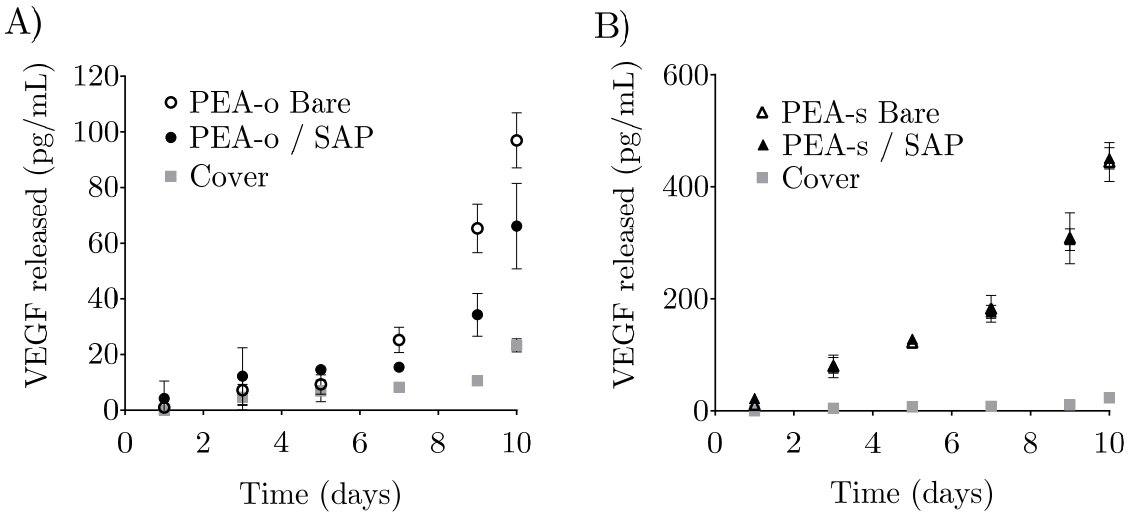

Figure 6.32: Cumulative curves of the VEGF released to the culture medium by cells cultured in PEA-o (A) and PEA-s scaffolds, measured by ELISA.

CLSM images revealed that cells cultured in bare PEA-o (Figure 6.33) spread along the channels and adhered to the scaffold surfaces and edges. Meanwhile, cells cultured in the combined system SAP/PEA-o tend to form clusters of cells and establish connections among them, diving in the gel in the pores.

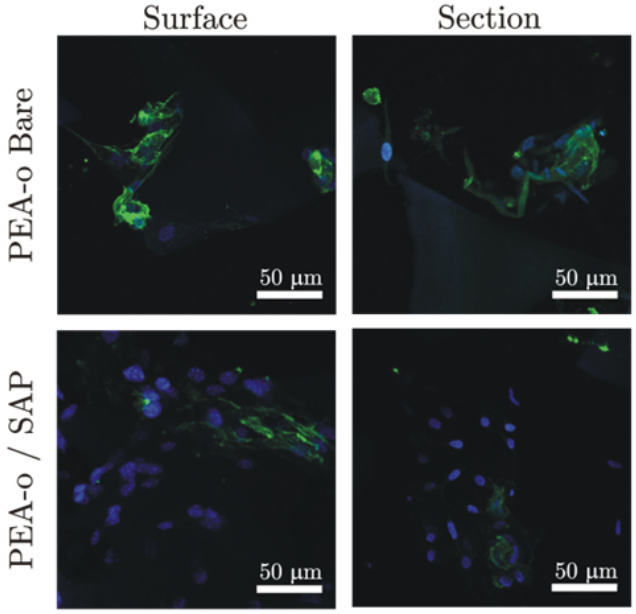

Figure 6.33: CLSM images of HUVECs/MSCs co-cultures after 10 days, stained against CD31 and DAPI, in bare PEA-o scaffolds or PEA-o combined with SAPs.

In the case of PEA-s (Figure 6.34), the surface images show a great cell density in both bare and filled scaffolds. It is very hard to establish differences between them; nonetheless, in the hybrid systems cells seem to follow a more organized distribution on the surface where circular-like cells dispositions are observed, while in the bare ones the distribution seems more chaotic.

When the scaffolds' inner sections were observed, in the case of the PEA-s/SAP (Figure 6.34 D) more complex assemblies of cells were observed, forming circular 3D structures that seem to be the sprout of a tubular-like structure.

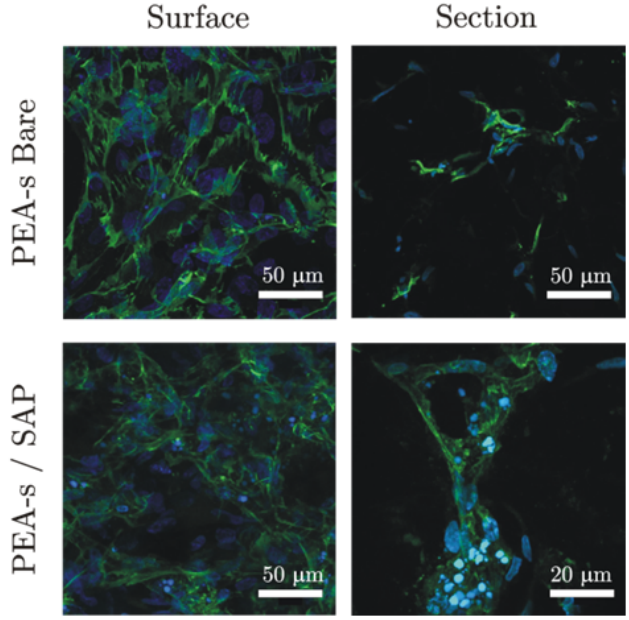

Figure 6.34: CLSM images of HUVECs/MSCs co-cultures after 10 days, stained against CD31 and DAPI, in bare PEA-o scaffolds or PEA-s combined with SAPs.

When greater areas of the inner sections are observed, as in Figure 6.35, again in the PEA-o combined with SAP the cells form spherical clusters, and in the rest of the areas almost no cells are observed, while in the bare PEA-o scaffolds cells are observed on the surface more uniformly spread. Concerning the PEA-s both bare and filled with RAD16-I, cells are observed along the section evenly distributed,

establishing cell-cell contacts among them, and a great fraction adopting circular dispositions. By means of the CD31 specific staining (green) HUVECs can be distinguished from MSCs. As can be observed in Figure 6.35, HUVECs are evenly distributed in the scaffolds inner sections.

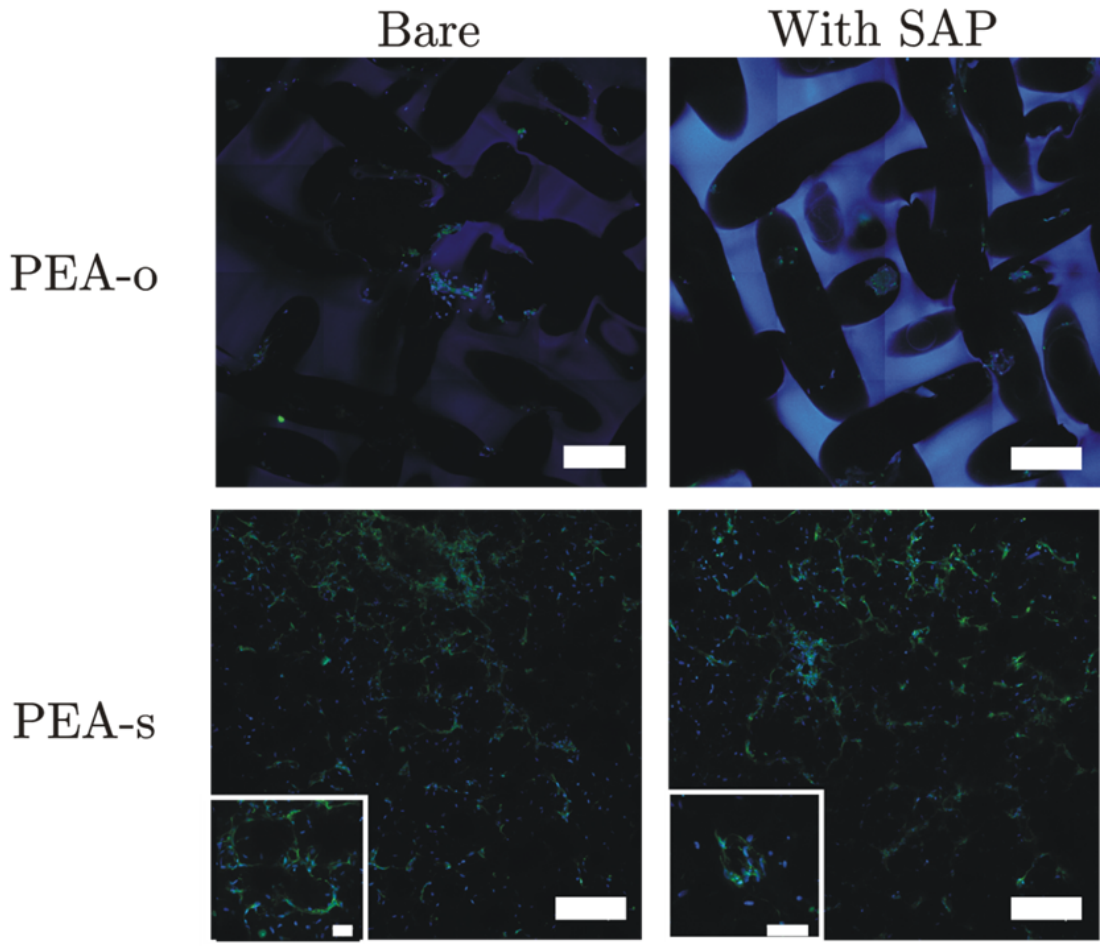

Figure 6.35: CLSM overview images of inner sections of bare (left) and SAP filled (right) PEA-o (first row), and PEA-s (second row) HUVECs/MSCs co-cultures after 10 days. Scale bars: 200 µm, and insets' scale bars: 50 µm.

6.3.- Discussion

On the acrylates interaction with RAD16-I

Congo red dye is commonly used for the characterization of beta-sheet structures in general (like diagnosis of diseases related with this type of structures), but also for the characterization of self-assembling peptides like Q11 [302] or RAD16-I [303], which adopt this specific structure as well. The initial characterization of the peptide interaction with the studied polymers was therefore performed with this dye. This technique allowed to verify that the employed process successfully permitted the adsorption of the peptide on both polymers surfaces and covers (Figure 6.1).

The problematic associated to employing this technique is that after the excess of the SAP gel is removed, samples only acquire a very clear red shade. Covers seem to exhibit the strongest colouration, which is still too clear to allow the establishment of supported differences with the spin coated materials (whose colouration is even clearer).

On the other hand, if the excess of peptide solution is not removed, a different problematic was detected. The SAPs form a dense network that is only attached to the surface of the polymer film or cover by the interaction of the first layer of the peptide in contact with the substrate; therefore, a great mass is attached to the surface by only electrostatic interactions of few molecules. As a consequence regions can be easily removed and washed out during the staining process. In fact this is what happened to the samples C and F in Figure 6.1.

Taken all this together, the congo red staining was found to be a coarse technique for the level of detail and accuracy required to settle the differences among the materials in their interactions with the SAP. Thus, the next characterization was undertaken

with AFM, which has already proved to be very useful in the determination of proteins conformation and interaction with polymeric substrates [304, 305].

When the concentration of the RAD16-I was low enough, it was possible to observe differences in the conformation adopted by the peptide onto the different substrates. A correlation was detected between the better spreading of the peptide on the material and the electronegative atoms present in the substrate. For PEA, in which functional groups the differences in electronegativity are less pronounced than in its copolymer with acrylic acid, the wettability was poorer and as a result the SAP assembled and percolated leaving empty spaces and bare areas. In the case of P(EAcoAAc), the introduction of 10% of units containing the carboxyl group, favoured the formation of a more uniform and regular coating on the surface. However, circular structures leaving empty spaces were yet observed. In the case of covers, as are made of glass the presence of negatively charged oxygen atoms promote a better interaction with the amine groups in the aqueous peptide solution that completely wets the surface; as a result a very dense layer of peptide is obtained and the previously described bare areas are not observed any more. The explained rationale was in good agreement with the water contact angle measurements (Figure 6.6 and Figure 6.7): the highest was obtained for PEA, a bit lower for P(EAcoAAc), and the lowest for covers, which precisely are more uniformly coated by the SAP in the AFM images.

It was also observed that the previous peptide presence in general induced a reduction in the water contact angle for almost all the liquids and substrates considered. Therefore the presence of the peptide alters the contact angle of the material *i.*e., its wettability, which has a direct effect on the way proteins adsorb on the material surface, and this variation could translate into changes in the way cells adhere and interact with the material [306].

It must be noted that a certain discrepancy is detected between the contact angle values presented in Chapter 3 and in this chapter. These differences however, can be attributed to the preparation method of the measured materials, being crosslinked films in the previous chapter, and ultra-thin spin coated films of non-crosslinked polymer in the present chapter. The differences could be a consequence of the latter technique that might promote the production of materials whose polymeric chains are stretched because of the centripetal force employed to obtain them. Having the chains in such a particular disposition might induce certain interactions among the chains' dipoles that when they are in a random coil configuration do not take place. These changes of conformation and availability of hydrophilic domains would translate into different wettability, contact angle and surface free energy values as herein presented.

As already introduced, PEA reached the greatest water contact angle as shown in Figure 6.6, indicating a poorer wettability than the other substrates. Nonetheless, when the RAD16-I solution contact angles were measured at different concentrations, both PEA and P(EAcoAAc) were found to reach very similar values, whereas RAD16-I seemed to have a much better interaction with bare covers as they exhibited a much lower contact angle. The RAD16-I contact angle similarity between PEA and P(EAcoAAc) is somehow in conflict with the AFM images, where differences between PEA and P(EAcoAAc) were detected (Figure 6.2 to Figure 6.5); in said images P(EAcoAAc) seemed to be better wet by the SAP solution than PEA. To elucidate the cause of such despair results, both the RAD16-I (at two concentrations) and water contact angle were measured again but with samples previously swollen under a controlled relative humidity. This experiment allowed taking into account the fact that the adsorption and self-assembly of the peptide prior to the AFM observation is performed under wet conditions. It was observed for the PEA and P(EAcoAAc) a decrease on the water contact angle because of pre-

swelling the samples. Moreover the P(EAcoAAc) reached the lowest values, thus providing a plausible explanation for the better interaction of the copolymer over the homopolymer seen in the AFM images. Surprisingly, for the covers, the contact angles of the swollen samples were higher; a possible cause could be the interaction of water molecules (from the wet atmosphere), with the electronegative groups of the cover surface which therefore are no longer available to interact with the water or peptide solutions. Nonetheless, the reached values are much lower than those measured on the other substrates, which is in good agreement with the AFM images, which show a more uniform coating of the covers than the spin coated substrates.

In order to get a deeper insight, after the contact angle measurements, the surface tension of the materials was calculated. To do this, the Young equation was considered:

$$\sigma_{sl} = \sigma_s - \sigma_l \cdot \cos\ \theta \qquad \textbf{[Equation 6.1].}$$

where σ_{sl} is the interfacial tension between liquid and solid, σ_s is the surface tension of solid, σ_l is the surface tension of the liqud and θ is the contact angle of the liquid on the surface.

When Equation 6.1 is combined with the Owens Wendel Raelble and Kaelble equation, WORK [307]; which is based on Fowkes equation [308] but considers that the surface tension is divided into the components, polar and dispersive:

$$\sigma_{sl} = \sigma_l + \sigma_s - 2 \cdot \left(\sigma_l^d \cdot \sigma_s^d\right)^{\frac{1}{2}} - 2 \cdot \left(\sigma_l^p \cdot \sigma_s^p\right)^{\frac{1}{2}} \qquad \textbf{[Equation 6.2]}$$

the following expression is obtained:

$$\frac{1+\cos\theta}{2} \cdot \frac{\sigma_l}{\left(\sigma_l^d\right)^{1/2}} = \left(\sigma_s^d\right)^{1/2} + \left(\frac{\sigma_l^p}{\sigma_l^d}\right)^{1/2} \cdot \left(\sigma_s^p\right)^{1/2} \qquad \textbf{[Equation 6.3]}$$

Equation 6.3 allows the calculation of the surface free energy of a solid by means of plotting: $\frac{1+\cos\theta}{2}\cdot\frac{\sigma_l}{\left(\sigma_l^d\right)^{1/2}}$ *vs.* $\left(\frac{\sigma_l^p}{\sigma_l^d}\right)^{1/2}$, being the polar and dispersive components of the surface tensions of the samples the y-ordinate and the slope, respectively, and the surface free energy of a solid the addition of both components.

When these equations are applied to the previously acquired contact angle data, the following values were obtained:

Material	σ^d (mN/m)	σ^p (mN/m)	σ (mN/m)	Polarity (σ^p/σ)
Cover bare	5.28	4.44	9.72	0.46
Cover / SAP	5.38	5.14	10.52	0.49
PEA bare	5.48	1.17	6.65	0.18
PEA / SAP	5.53	1.68	7.21	0.23
P(EAcoAAc) bare	5.68	1.97	7.65	0.26
P(EAcoAAc) / SAP	6.07	1.13	7.2	0.16

Table 5.1: Polar and dispersive components of the surface tension, surface free energy and polarity of the studied materials, bare or coated with RAD16-I.

The introduction of carboxyl groups in P(EAcoAAc) translates into a greater polar component than that of bare PEA. Nonetheless, the most polar among the considered materials was the glass cover. When PEA surface free energy is compared with previously published values [194, 285], lower values are obtained here; while regarding the polar component a greater value was obtained. These discrepancies can be a side effect of the materials production method and the measuring conditions procedure.

For both PEA and covers the adsorption of RAD16-I on the surface prior to the measurements induced an increase on the polar component. Simultaneously, in all the

materials, an increase of the dispersive component was induced too because of the peptide. As a consequence, for both PEA and covers, when RAD16-I has been previously adsorbed, the surface free energy and polarity increased. Meanwhile, for P(EAcoAAc) both parameters were reduced when the peptide was previously adsorbed. Nonetheless, during the determination of the polar and dispersive surface tension components of P(EAcoAAc) with RAD16-I, the lowest correlation coefficient was achieved, casting doubt on the reliability of this result.

Combining PEA scaffolds with RAD16-I gel

Combining different materials such as hydrophobic porous PEA and aqueous RAD16-I solutions was not trivial. The presented results show that SAP solutions can be effectively incorporated and gelled within the pores of elastomeric scaffolds, despite the different properties and nature of both components by means of a one-step, easy-to-employ method.

The *in vacuo* SAPs loading and *in situ* gelling procedure allowed to effectively fill both the spherical interconnected PEA-s scaffolds (Figure 6.9) as well as the cylindrical orthogonal pores of the PEA-o scaffolds (Figure 6.13 and Figure 6.14) with the peptide hydrogel. For PEA-o scaffolds, in spite of the relatively little interconnected structure (in comparison to PEA-s sponge-like scaffolds), a uniform filling throughout its volume was also achieved.

For both types of scaffolds, before gelling, the peptide solution leaves under cryoSEM residual stretched-out fibres and more disordered complex structures as its water sublimates in the cryogenic device. After gelation, the SAP continuous network shows a more ordered honeycomb-like structure, which is produced because of a different, more impeded sublimation of its water.

RAD16-I is known to have good stability [241] with time and under culture conditions; it is capable to resist pH variations and temperatures up to 90°C. In fact it has been used in many studies alone as scaffold itself [247, 254, 249, 251]; for instance in one work the SAP stability was maintained up to 33 days [247]. However, it was crucial to verify if when it is self-assembled within scaffolds' pores this stability was maintained or if otherwise it was reduced. It was necessary to elucidate if inducing the self-assembly within the pores produced either an interconnected continuous phase or a discontinuous one of sporadic clots favouring the SAP disaggregation and diffusion to the culture media. As Figure 6.10 shows, the stability of the peptide is not affected by combining it with the scaffold; a continuous phase through the pores is produced. Moreover, these interconnected fillings were maintained with time throughout the scaffold thickness and kept their nanofibrilar structure for at least 7 days.

The differences detected between Figure 6.9 and Figure 6.10 can be attributed to the different techniques employed to obtain the images. In the case of Figure 6.9, the images were obtained by cryoSEM, whereas those depicted in Figure 6.10 were obtained by following standard cell culture fixation, post-fixation, critical point drying and SEM observation.

Filling effect on the mechanical performance

The concentration of SAP in the prepared solutions (0.15% w/v) for injection in the scaffolds' pores is so low that it essentially has the density and viscosity of liquid water; after gelling, the viscosity is somewhat greater, but still the SAP hydrogel has the rheological properties of a mucus (G'=5 Pa [309]), and thus negligible resistance to shearing and tensile stresses, and to manipulation in general as occurs with other SAPs [310]. Nonetheless, in the case of PEA-s, the scaffold-SAP construct presents, in a mechanical respect, an improvement of several orders of magnitude: from moduli

values typical of a mucus (10 to 80 Pa) we pass to values of the order of tens of kPa in the initial region, and up to values close to those of the elastomers near the final region (Figure 6.11); therefore obtaining a manipulable construct, able to withstand tractions, compressions and shears to the extent that a typical elastomer scaffold does. The presence in the scaffold's pores of the filler gel yields a somewhat higher modulus in compression. This effect, poroelasticity, can be attributed mainly to the presence of water in the pores, which is very incompressible, and to its relative difficulty to flow out of the pores upon compression [292, 293]; the gelled state of the SAP results in a somewhat more hindered flow, which translates into somewhat higher linear moduli because of the poroelasticity already discussed in Chapter 5. In these experiments the mechanical effect of the filling gel is evident already at low strains, and persists in the linear deformation region.

In the case of PEA-o scaffolds, the compression behaviour, exhibiting two slopes clearly different, is likely due to the porous orthogonal structure of such scaffolds, which leaves solid PEA pillars that are compressed progressively from the very beginning; here again the resistance of the polypeptide solution and even more that of the gel has an influence increasing the compressive modulus. The abrupt collapse of the pores leads to the second compressive linear behaviour, now independent of the filling for it has been extruded, in any of its physical states (sol or gel), from the pores.

Controlled release

The scaffold-SAP construct is useful also as a platform for drug and molecule delivery, independently of the presence of cells. BSA was employed in this study as a model protein for uptake and release. The SAP hydrogel can be considered as a two-phase system, one phase being a water solution of non-assembled SAP molecules, the other phase constituted by the assembled SAP molecules into a nanofibrilar network.

The BSA molecules sorbed in the scaffold-SAP construct may be thought to reside in three different placements: either solved in the bulk of the watery phase inside the pores, or located in the assembled phase, or, finally, adsorbed onto the surface of the scaffold's pores.

The initial concentration of BSA in the construct was estimated by means of M_0, the mass of gel entrapped in the scaffold, m_{gel}, and assuming that the density of the gel is close to that of water: $[BSA]_{ini}^{construct} = M_0/V^{gel} = M_0 \cdot \rho^{gel}/m^{gel}$. This calculus resulted in a value of 12.7 mg·ml^{-1}, which is much higher than that of the starting solution from which the uptake took place, 1 mg·ml^{-1}. Firstly, this finding confirms that the protein can be easily and efficiently entrapped after the formation of the gel. Secondly, it indicates that the construct is able to concentrate the BSA solution (which might be another useful property for some applications). Since, by thermodynamic equilibrium, the concentration of BSA molecules able to diffuse freely must be similar in the gel phase inside the pores and in the outside watery phase, this difference is indicative of BSA molecules in the construct residing preferentially either adsorbed on the PEA surfaces or trapped within the microphase constituted by the assembled microfibrils. The performed experiments are insufficient to establish the relative importance of both entrapment modes, and further characterization would be needed on this point. The BSA molecule may indeed interact electrostatically with the peptide chains; the amide and acid groups of its molecular structure yield a different net charge of the BSA molecule at different pH values. During the BSA uptake process, which takes place above BSA's isoelectric point, the molecule is negatively charged and thus may interact with residual positively charged groups of the SAP macromolecules. A supporting result is found in reference [311]: with increasing pH, the ionization of the acid groups of the protein and the poly(acrylic acid) in which it was entrapped increased the repulsion forces between

them, and consequently reduced the free space available for the protein molecules in the gel network.

The BSA-loaded constructs are able to release the protein when immersed in PBS. The kinetics of this release has two clearly differentiated time regimes (Figure 6.12). Release is rapid within the first 8 h, during which time ~15% of the total BSA amount is released; thereafter, release is much slower. The residual BSA remaining after 10 days was still 75% of the initial amount, and the plot did not yet show any decrease of the time rate of release.

A good fit of the first stage of the time-release curve to a power law was obtained, $M_t/M_0 = k \cdot t^n$ (inset in Figure 6.12); least-squares fitted values of the k and n parameters turned out to be 0.078 and 0.33, respectively. A value of $n = 0.5$ corresponds to Fickian diffusion from a slab; that is, the case in which the release is controlled by a pure diffusion process, a concentration gradient equalization due to random Brownian motion of the molecules, with no bias in their displacements (Fickian diffusion from a cylinder has $n = 0.45$, and from a sphere $n = 0.43$) [296]. This is here not the case. The fitting of the power law to the second release regime gives $n = 1$ (linear growth with time of the amount released) and $k = 0.0004$ (plus the new parameter $a = 0.1493$ needed to account for the initial release).

Power laws such as the stated one are typically used to describe solvent release from hydrogels [312, 298, 313]; as previously argued in Chapter 5, the parameter k is takes into account the different tortuosity of the transport path. In [312], the authors followed the release of BSA from previously dried poly(N-isopropyl acrylamide) hydrogels, which lasted barely 2 h at 40 °C, and obtained higher values for the k and n parameters of 0.112 and 0.462, respectively. Other BSA-gel systems have also been found to exhibit double kinetics of BSA release, which have been interpreted as an indication of the interference with diffusion-controlled transport of further

mechanisms: swelling or shrinking of the gel matrix (sometimes triggered by pH or temperature changes in the environment) [312, 298, 314], chemical reactions (polymer degradation, drug-polymer interaction, etc.)[315, 298, 311], and processing (heterogeneous crosslinking of the gel, entrapment of the drug on the surface, use of solvents afterwards dried, etc.) or storage conditions (drug saturation at the surface on gel drying, drug migration, etc.) leading to an uneven drug distribution [316]. When hydrogel samples are dried after the protein loading, their swelling usually provokes a burst release [311, 312], due to those molecules near the polymer surface and rapidly transferred to the medium. This is obviously not the case here, as the constructs were not dried after the protein loading. The rapid initial kinetics observed in our system could be related to the electrostatic interactions between the BSA molecules and the oligopeptides forming the gel fibrils. As previously discussed, the excess of BSA within the scaffold/gel construct over the initial concentration of the uptake solution must be attributed to specific interactions of BSA molecules with the PEA polymer chains, or with the assembled SAP molecules, or with both.

Thus, release of the BSA solved in the watery phase of the hydrogel may be expected to be faster than the release of BSA molecules, which are either linked to the peptide nanofibrilar assemblies or adsorbed to the PEA surfaces. A slower release of these BSA molecules must follow, since those specific bonds must be eased.

Cytotoxicity

The cytotoxicity test was performed with PEA-o despite of previous reports on PEA good biocompatibility, in order to discard that the nitric acid treatment or its combination with the SAP might have a deleterious effect on its biological performance. Although with the 2D model shown in Chapter 3, very good biological performance was observed in spite of the nitric acid treatment, it was decided to perform this assay in pursuit of safety. The cytotoxicity assay was performed

according to UNE-EN ISO10993-5 [317] standard. As expected, it confirmed that the scaffolds under study, either bare or combined with the SAP, are not cytotoxic.

Seeding protocol optimization

A seeding protocol was established and optimized with fibroblasts. It was found that the presence of the (non-gelled) SAP solution, within the scaffolds' pores, improved fibroblast colonization in terms of number of cells and uniformity of their distribution. The SAP solution acted as a faster medium for cell invasion of the pores of the scaffolds than mere culture medium. At 7 days of culture cells had proliferated much more when the pores were filled with the SAP gel. The dynamic seeding achieved better results than the conventional one; 30 min of smooth shaking were enough to facilitate cell diffusion throughout the scaffolds and a uniform distribution. The advantage of the SAP-filling for cell colonization may be due to the higher diffusion speed of the cells in this medium than on the scaffold surfaces: PEA is a hydrophobic polymer onto which most cells are willing to adhere and spread, thus delaying their progress through the structure. Swimming through the peptide solution seems a faster way of colonization than creeping on the scaffold's pores surfaces. In these experiments, cells were seeded with the minimum amount of medium, and planted as a droplet onto the SAP-filled scaffold; this procedure avoids their spilling out of the scaffold and optimizes cell seeding. The SAP was gelled later, consequently entrapping the cells inside the pores.

The PEA-s/SAP constructs here developed provide to the cells seeded in them a friendly immediate ECM-like environment through the SAP gel component, while at the same time possess enough mechanical integrity and shape stability thanks to the embracing elastomeric scaffold. The ECM-like SAP gel can surround the cells, improving the survival and migration conditions and can, as previously discussed, at the same time, incorporate and deliver active molecules such as drugs or growth

factors in a controlled manner to regulate cell fate or stimulate an angiogenic response.

HUVECs culture in the PEA-s/RAD16-I combined system

In the experiment performed with HUVECs cultured onto 2D PEA substrates either bare or with RAD16-I adsorbed, no great differences were detected at short times (*i.e.* initial adhesion and proliferation). Nonetheless, at longer time points the presence of the peptide was found to have a positive impact on cell density.

Regarding the 3D structures, because of the porosity, the surface to volume ratio is enhanced, hence much more areas are available for the cells to spread, migrate and colonize. Thus the achieved cell density was higher in the 3D materials, as greater amounts of cells can be lodged within the pores than on a flat substrate. Since the presence of the peptide contributed to maintain the cells within the scaffolds' pores, it was observed that certainly had a positive effect on cell density (as previously discussed from the fibroblasts culture). Even more, infiltration towards the inner regions of the scaffold was observed in both bare and filled scaffolds. Nutrients diffusion into the scaffold is thought to be good enough because of the homogeneous cells distribution.

The presence of a complex 3D environment, such as the scaffold combined with the peptide, proved to be a very interesting culture system: no decrease in the fraction of cells expressing CD31 was detected, and in the case of VE-cadherin a dramatic increase on the fraction of cells expressing this marker was observed. Since VE-cadherin is a protein responsible for the endothelial cells connections [318], the fact that the fraction of positive cells increases is an indicator of the establishment of cell-cell connections, thus pointing at the goodness of this system for culturing and lodging endothelial cells. The potential of HUVECs to form interconnected capillary-

like structures in PEA-s/SAP constructs is supported by the up regulation of these endothelial markers. These results are supported by a previous work that reported the formation of elongated and highly interconnected capillary-like structures when HUVECs were cultured in RAD16-I [245], indicating the adequacy of this peptide for the intended application.

The image flow cytometry (AMNIS) allowed the follow-up of the spatial distribution and localization of the markers: no statistically significant co-localization of the markers expression was found, which is in accordance with previously published works [319]. It served as a verification of the proper stain of the samples: given the impossibility of expressing CD31 and VE-cadherin in the same exact point, a co-localization would have implied an unspecific staining of the markers.

The presence of the peptide increased the fraction of cells co-expressing both factors, suggesting that the number of junctions between endothelial cells might increase when cultured in the peptide 3D context, and thus, indicating that it is a suitable system to promote endothelial cell-cell contacts. Moreover, as both CD31 and VE-cadherin are essential for the formation of endothelial tubes [320], an increase in their expression is a good indicator of the PEA-s/SAP appropriateness for the intended application.

Cells adhesion, spreading and migration are known to be dependent on their cytoskeleton system and morphological organization of their ECM [321, 322]. Therefore, fluorescent phalloidin staining was performed to observe the influence of the self-assembling peptide on the actin filaments disposition. As shown in Figure 6.22, clear differences in actin filaments are observed. Cells growing in PEA scaffolds display extended actin filaments that seem to follow the scaffold topography, whereas

those cultured in the hybrid system (PEA-s/SAP) tend to form more complex structures.

These results confirm that HUVECs adhere, proliferate and spread very well on the PEA hydrophobic surface of the scaffolds; moreover, incorporating a self-assembling peptide within the pores provides a greater degree of interaction among cells. The uncovered better biological performance of the combined materials could be a side effect of the peptide structural features (fibers in the same scale as ECM), and its ability to retain water up to 99.5% w/v [323], which is an environment more alike to the growing conditions that cells have *in vivo*.

MSCs and HUVECs co-culture in PEA-s and PEA-o /RAD16-I combined systems

The evolution of the fraction of endothelial/mesenchymal cells ratio during the experiment seemed to be greatly affected by the SAP presence in the case of PEA-o scaffolds and not as much for the PEA-s scaffolds. HUVECs seemed to adhere better in bare PEA-o than when filled with the peptide. Nonetheless, while there is a reduction of the HUVECs fraction for bare PEA-o after a week, for the SAP-filled PEA-o an increase is observed. It is more remarkable because the fraction of MSCs remained constant in this type of constructs. On the other hand, there is an increase of the MSCs fraction simultaneously with a reduction of endothelial cells for the bare PEA-o with respect of the PEA-s either bare or filled with RAD16-I. Nonetheless, despite this reduction in bare PEA-o scaffolds, a greater fraction of endothelial cells than in PEA-s ones is maintained.

The reduction of the HUVECs fraction in PEA-s scaffolds and the increase in the MSCs fraction (Figure 6.28), taken together with CLSM images (Figure 6.34 and Figure 6.35), might suggest that this decrease of the number of endothelial cells can

be attributed to the formation of cell-cell connections that lead to a lower proliferation via contact inhibition, as discussed in [110].

Concerning the results from the picogreen experiments, the lowest value was achieved for the 2D material, as expected, given the space limitation to lodge cells of a flat non-porous surface (and the consequent lower cell density seeded). In the case of PEA-o scaffolds combined with the SAP, such a low value was not expected given the cells clusters detected in the SEM (Figure 6.30) and CLSM (Figure 6.33) images. Indeed in the SEM images of bare PEA-o (Figure 6.30), a more uniform distribution of the cells throughout the scaffold thickness was observed. These results suggest that bare PEA-o scaffolds provide a better context for these cells co-culture. For PEA-s no differences were detected between the bare scaffold and the scaffold combined with the peptide in terms of the DNA concentration. The CLSM wide areas images of both bare and SAP-filled PEA-s (Figure 6.35) are in good agreement with it, as no meaningful differences concerning cell density and spatial distribution are detected. It is remarkable that for the PEA-s scaffolds a great cell density was observed on the surface in spite of having seeded by injection in the core of the scaffold (Figure 6.31), thus suggesting that the cells were capable to migrate through the scaffold. Concerning the cross section images, the structure tortuosity and irregularities of these scaffolds, hinder the observation of cells; hence, cells can only be clearly distinguished in bare PEA-s in the cross section images.

Since VEGF regulates vascular development and angiogenesis [324], it becomes capital to study its release by cells cultured in the scaffolds under study. Great differences in the concentration of VEGF in the supernatant were observed depending on the material where cells were co-cultured. In the case of 2D materials, the lowest amount was obtained, which is in good agreement with the fact that cells were seeded at a lower cell density and also the picogreen results yield the lowest

quantity of DNA. Nonetheless, in other studies where co-cultures were performed in 2D and 3D materials seeded at equal density and VEGF release was compared, lower values were also reported for the flat substrates [325].

The large difference of VEGF released from PEA-o or PEA-s scaffolds surprises as bare PEA-o showed a similar cell density to PEA-s scaffolds (bare or filled with SAP) according to the picogreen test (Figure 6.29). Nonetheless, cytometry results after 7 days of culture (Figure 6.28) showed that a greater fraction of MSCs was found in PEA-s than in PEA-o scaffolds. VEGF is mainly secreted by MSCs, as reported in [326], and as observed with ELISA results performed on HUVECs culture supernatant (where almost no secretion of VEGF was detected-results not shown-). The increase of the number of CD90 positive cells thus could be a plausible explanation for this increased release of VEGF. The smaller differences detected for the PEA-o can be analogously explained: the bare PEA-o cultured scaffold released greater amounts of the factor, but also displayed a great increase of the MSCs fraction. In sum, PEA-s seemed to have a greater potential to be vascularized than PEA-o scaffolds, as cells cultured in them were capable to release greater amounts of VEGF (which is the growth factor that stimulates endothelial cells to migrate, proliferate and differentiate to form new lumen vessels [327]). Nonetheless experiments at longer time points will be necessary to assess both cell types evolution. The good results obtained with the PEA-s scaffolds are even better when the peptide is incorporated.

Indeed in the PEA-s immunocytochemistry images (especially when combined with the SAP), the cells seem to be forming more complex sprouts and tubular-like structures than in the PEA-o scaffolds. Therefore, the PEA-s scaffolds seem to provide a cell culture system that induces more cell organization into tubular-like structures.

6.4.- Concluding remarks

The substrate/RAD16-I interaction was characterized, and found to be strongly dependent on the substrate hydrophilicity and wettability. The PEA hydrophobic nature provided a poorer interaction with the peptide than P(EAcoAAc), whose AAc hydrophilic groups improved the interplay.

It is feasible to combine SAP-based hydrogels and elastomeric hydrophobic scaffolds (PEA-s and PEA-o). Their pores could be effectively filled with a SAP aqueous solution, despite the low wettability of PEA and the relatively low porosity and close and tortuous structure of these scaffolds, by following an *in vacuo* loading. Once incorporated, the SAPs could be efficiently gelled *in situ* with PBS or culture medium, and formed a stable network within the pores.

The scaffold/SAP platform can also be employed as a protein delivery vehicle with singular features. Furthermore, these constructs do also possess interesting features as active molecules delivery platforms: are capable to provide different releasing kinetics depending on the molecules location.

These hybrid materials are suitable vehicles for cell seeding and cell supply with unique properties: a cell-friendly, ECM-like immediate microenvironment for the cells that facilitates an efficient and uniform cell colonization of the scaffolds, plus shape stability, mechanical consistency and strength. These constructs can then be seeded in a more efficient manner than bare scaffolds, probably because the hydrogel represents a better migration medium for cells. Moreover, they present slightly enhanced mechanical properties and different specific architectures that might conduct cell fate.

In particular, it was found that the incorporation of the peptide within the pores of PEA-s scaffolds improved HUVECs performance in terms of density, cell distribution and endothelial cells markers expression, indicating that the hybrid 3D constructs provide a permissive microenvironment for diffusion of nutrients, gases and growth factors that in combination favour the endothelialisation of the scaffold, which is the first milestone to produce vascularised scaffolds.

When HUVECs were co-cultured with MSCs in either PEA-o or PEA-s scaffolds combined or not with the peptide filling, the PEA-s ones yielded better results in terms of uniform cell distribution, VEGF release and promoted cells organization. Thus, PEA-s have a greater vascularization potential than PEA-o scaffolds, which is enhanced by the peptide presence.

In summary, the resulting constructs combine several of the distinctive advantages of both kinds of materials yielding easy-to-produce and to manipulate systems for cell and factor delivery. Therefore, these combined systems could find application in advanced cardiac tissue engineering therapies.

Chapter 7:

Final discussion

7.- Final discussion

The systems developed in this Thesis exhibit very promising features for their use as cardiac tissue engineering supports: on the one hand their good biological performance points out their usefulness as three-dimensional contexts contributing to the recovery of damaged tissue, and on the other hand their mechanical properties and fatigue resistance make them appropriate as mechanical restraints to limit the evolution of cardiac dilation.

Other groups that developed porous cardiac patches employed other materials such as poly(glycerol sebacate), PGS. It is cell friendly and has a modulus ranging from 57 to 195 kPa (depending on the tension direction) [87], which are of the same order of magnitude as the modulus of the scaffolds employed in this Thesis. On the other hand, cardiac restrain approaches such as the Acorn Corcap [278] cardiac mesh, have suitable mechanical properties to limit the cardiac remodelling but unfortunately induces fibrosis when implanted. For this reason the combination of a restraining device with a more biocompatible material such as collagen patches is under consideration and arising promising results [280]. The Acorn Corcap in particular, has an elastic modulus of 2.57 MPa [328], which is more than three times that of bulk PEA. Nonetheless, given that both types of scaffolds, PEA-s and PEA-o are capable to withstand the stresses present in the heart (0.015 MPa at the systolic peak and 1.33 kPa at diastole [276]), and since it has not been determined which degree of restrain and stretch ratio is optimal, both seem to be to date promising options.

Indeed, as PEA scaffolds are intended to lodge cells, it might be of interest to have a more compliant material for the mechanical solicitations to be transmitted to the cells, since it has been reported that cardiomyocytes stimulation with mechanical

loading improves cells organization [329] and guides cardiomyogenesis from pluripotent stem cells [330].

Recently, the family of acrylic polymers has raised the interest of other groups in the cardiac tissue engineering field [131], which found that they stimulated angiogenesis as well as resulted in a reduced fibrotic response when implanted *in vivo*. PEA is a biostable polymer; therefore, it will not degrade with time as occurs with other cardiac patches such as collagen, that even though provides very good results *in vivo* [331], it is already partially degraded after 12 days [332].

Several combinations of scaffolds with aqueous gels to improve their biological outcome have been explored in previous works. For instance, Matrigel has been employed to encapsulate cells and favour their residence within the scaffolds pores [90]. Analogously, in this work the positive influence of employing the self-assembling peptide RAD16-I was observed through all the experiments undertaken. A common problem to all materials designed for cardiac tissue engineering, to guarantee the survival of cells lodged in their pores, as already discussed, is the need for vascularization [333]; the results issued herein by HUVECs cultures suggest the potential of these constructs to be colonized by endothelial cells, which would be a key step for these systems to be successful upon implantation.

Scaffolds releasing growth factors have been found to yield better results than bare ones, in terms of vascularization [334] and cell survival and tissue formation [94] The constructs here developed, consisting of PEA scaffolds with hyaluronic acid, HA, or peptide gel as pores coating or filling, were capable to provide a sustained release of BSA, which suggests that both of them could also serve as platforms to release growth factors to enhance cells performance.

Thus, it is expected that PEA scaffolds provide mechanical reinforcement and furthermore given their good biocompatibility *in vitro*, improved when combined with ECM-like gels in their pores, have a better integration when implanted than other restraint devices; *in vivo* ongoing studies in infarcted sheep carried out by Dr. J. C. Chachques at the Georges Pompidou European Hospital (Paris) will hopefully confirm this.

Chapter 8:

Conclusions

8.- Conclusions

8.1.- On the scaffolds' features

1. Highly porous poly(ethyl acrylate) (PEA) scaffolds either with spherical interconnected pores (PEA-s) or with cylindrical orthogonal ones (PEA-o) were prepared making use of porogen templates combined with particle leaching, as reported elsewhere. It was found that the procedure followed to obtain PEA-s scaffolds left traces of the poly(methyl methacrylate) (PMMA) porogen in the PEA matrix, inducing slight changes in the properties of the resulting materials.

2. The nitric acid rinses applied to remove the sinterized nylon templates involved in the preparation of the PEA-o scaffolds induced the hydrolization of side chains in a number of EA units. As a consequence, the acrylate is transformed into an EA-AAc random copolymer; the extent of this modification is proportional to the duration of the nitric acid rinses and affects the physico-chemical properties of the polymeric matrix, mainly turning it into a pH-sensitive polymer. Nevertheless, this modification was not detrimental for the biological performance of these PEA-based scaffolds at least for rinsings not exceeding 4 days.

8.2.- On the mechanical performance of PEA scaffolds under fatigue

1. Because of their porosity, PEA-o scaffolds exhibit a reduced elastic modulus (tens of kPa) as compared with that of bulk elastomeric PEA, which is of the order of 1 MPa. The PEA-s scaffolds maintain, despite their greater porosity,

this elastic modulus, because of the MMA incorporated to the polymeric network.

2. The elastic moduli of PEA and PEA-s exceed that of cardiac tissue; and PEA-o although exhibits a lower elastic moduli, can withstand the solicitations present in the heart. They are, consequently, suitable to be used as cardiac restrains to limit ventricular remodelling following an infarction, besides their potential as cell support patches for cardiac tissue regeneration.

3. Bulk PEA and PEA-s scaffolds resist torsion and tension for at least one week without significant variation on their mechanical performance. A slight increase of the elastic modulus was though observed after fatigue, which cause has not been discerned. A plausible explanation might a hardening effect induced by the rearrangement of the polymer chains during the cyclic loading.

8.3.- On the coating of PEA scaffolds' pores with hyaluronan

1. Hybrid scaffolds composed of PEA-o scaffolds and HA uniform aqueous coatings were successfully produced by an *in vacuo* procedure. By changing different parameters of the coating process a wide variety of coating typologies were obtained. These HA coatings could be *in situ* crosslinked to increase their stability.

2. The swelling capacity of the HA coating decreases as its mass fraction in the hybrid increases and the porosity is reduced. A constraining effect of the scaffold's pores and curvature is thought to be inducing such effect. On the other hand, the HA filling increases the mechanical performance of the scaffolds.

3. These PEA-o/HA hybrids could be of interest as cell support constructs, where the HA presence seems to improve cell seeding efficiency; they can be alternatively or simultaneously employed as a controlled release system.

8.4.- On the combination of PEA scaffolds with RAD16-I gel

1. The interaction of self-assembling peptides (SAPs) with PEA-based substrates was highly dependent on their wettability: the presence of a small fraction of hydrophilic groups improves such interaction leading to more uniform lay-outs of the peptide mesh.

2. Both PEA-o and PEA-s scaffolds could be effectively and uniformly combined with the RAD16-I gel as filling in their pores: the peptide solution being loaded by a procedure analogous to that of HA coatings and self-assembled *in situ* with PBS or culture medium.

3. These combined systems are of interest for cell culture applications as the ECM-like gel contributes to improve the seeding efficiency and to promote a uniform cell colonization throughout the scaffold. These constructs can be employed as controlled release systems.

4. Combining PEA-s scaffolds with RAD16-I improves HUVECs performance in terms of cell distribution and endothelial cell markers expression, favouring the endothelization of the construct, which constitutes a critical point upon implantation of a scaffold *in vivo*. The co-culture of HUVECs with MSCs yielded better achievements in terms of cell distribution, VEGF release, and endothelial cells markers expression for PEA-s scaffolds than PEA-o ones. These results were enhanced by the peptide filling of their pores.

Glossary

Glossary

AFM	Atomic force microscopy
AMI:	Acute myocardial infarction
AZBN	Azo-bis-isobutyronitrile
BPB	Blocking and permeabilizing buffer
BSA	Bovine serum albumin
CHD	Coronary heart disease
CPC	Cardiac progenitor cells
CVD	Cardiovascular disease
D	Dry series of samples
DAPI	4',6-diamidino-2-phenylindole
DMEM	Dulbecco's modified eagle medium
DMTA	Dynamic mechanic thermal analysis
DPBS	Dulbecco's phosphate buffer solution
DSC	Differential scanning calorimetry
DVS	Divynilsulfone
E	Elastic modulus
EC	Endothelial cells
ECM	Extracellular matrix
EDS	Energy dispersive X-ray spectroscopy
EGDMA	Ethylene glycol di methyl acrylate
EWC	Equilibrium water content referred to the dry mass of the sample
EWC_{HA}	Equilibrium water content referred to the HA mass in the sample
EtOH	Ethanol
F	Fatigued series in torsion
FA	Samples fatigued in air in tension
FBS	Foetal bovine serum

FGF	Fibroblast growth factor
FI	Samples fatigued immersed in PBS in tension
FTIR	Fourier transform infrared spectroscopy
G	Shear modulus
HA	Hyaluronic acid/ hyaluronan
HCl	Hydrochloric acid
HUVEC	Human umbilical vein endothelial cells
IGF-1	Insulin-like growth factor 1
LbL	Layer by layer deposition
MMPs	Matrix metalloproteases
MSC	Mesenchymal stem cells
MTS	(4,5-dimethylthiazol-2-yl)-5-(3-carboxymethoxyphenyl) -2-(4-sulfophenyl)-2H-tetrazolium
NaOH	Sodium hydroxide
NF	Non-fatigued series
PAAc	Poly-acrylic acid
PBS	Phosphate Buffer Solution
PCL	Polycaprolactone
PDGF	Platelet derived growth factor
PEA	Poly-ethyl-acrylate
PEA-o	PEA scaffolds with cylindrical orthogonally interconnected pores
PEG	Polyethyleneglycol
PEA-s	PEA scaffolds with spherical interconnected pores
P(EAcoAAc)	Poly (ethyl-acrylate-co-acrylic acid)
PFA	Paraformaldehyde
PGA	Poly(glycolic acid)
PGS	Poly(glycerol sebacate)
PLGA	Poly(DL-lactic-co-glycolic acid)

PLLA	Poly(L-lactic acid)
PMMA	Poly(methyl methacrylate)
P/S	Penicillin/streptomycin
RAD16-I	Self-assembling peptide with the repeating units R(Arginine), A(Alanine), D(Aspartic acid)
RH	Relative humidity
RT	Room temperature
S	Swollen series of samples
SAP	Self- assembling peptide
SEM	Scanning electron microscopy
tan δ	Loss tangent
TGA	Thermo gravimetric analysis
Tg	Glass transition temperature
VEGF	Vascular endothelial growth factor
ΔCp	Specific heat capacity increment at the glass transition
ν	Poisson ratio
σ	Surface tension
σ^d, σ^p	Dispersive and polar components of the surface tension
π	Porosity
ρ	Density
ω_{HA}	HA mass fraction in the sample

Publications

Publications

Related to this Thesis

Book chapter:

Arnal-Pastor M, Chachques JC, Monleón Pradas M, Vallés-Lluch A. "Biomaterials for cardiac tissue engineering" In Regenerative medicine and tissue enginering, J.A. Andrades (Editor). Intech, 2013

Published articles:

Vallés-Lluch A, Arnal-Pastor M, Martínez-Ramos C, Vilariño-Feltrer G, Vikingsson L, Castells-Sala C, Semino CE, Monleón Pradas M. Combining self-assembling peptide gels with three-dimensional elastomer scaffolds. Acta Biomaterialia 2013; 9(12): 9451-9460.

Valles-Lluch A, Arnal-Pastor M, Martinez-Ramos C, Vilarino-Feltrer G, Vikingsson L, Monleon Pradas M. Grid polymeric scaffolds with polypeptide gel filling as patches for infarcted tissue regeneration. Conf Proc IEEE Eng Med Biol Soc. 2013; 2013: 6961-6964.

Arnal-Pastor M, Valles-Lluch A, Keicher M, Pradas MM. Coating typologies and constrained swelling of hyaluronic acid gels within scaffolds pores. J. Colloid Interface Sci. 2011; 361(1): 361-369.

Articles under preparation:

Arnal-Pastor M, Comín-Cebrián S, Martínez-Ramos C, Monleón Pradas M, Vallés-Lluch A. A characterization of the physico-chemical alterations of acrylate scaffolds upon removal of porogenic templates with acids. Submitted.

Martínez-Ramos C[#], Arnal-Pastor M[#], Vallés-Lluch A, Monleón Pradas M ([#] Equal contribution). Use of gel fillings in acrylate scaffolds to improve endothelial cells response. To be submitted.

Arnal-Pastor M[#], Martínez-Ramos C[#], Vallés-Lluch A, Monleón Pradas M. ([#] Equal contribution). Influence of the scaffolds morphology on endothelial cells and adipose stem cells co-cultures. Under preparation.

Non-directly related to this Thesis

Published articles:

Arnal-Pastor M, Martínez Ramos C, Pérez Garnés M, Monleón Pradas M, Vallés Lluch A. Electrospun adherent-antiadherent bilayered membranes based on cross-linked hyaluronic acid for advanced tissue engineering applications. Materials Science and Engineering C - Materials for Biological Applications 2013; 33(7):4086-4093.

References

References

[1] Extract from: Arnal-Pastor M, Chachques JC, Monleón Pradas M, Vallés-Lluch A. Biomaterials for Cardiac Tissue Engineering (Chapter 12). Regenerative Medicine and Tissue Engineering Edited by Jose A. Andrades. Ref. DOI: 10.5772/56076, ISBN 978-953-51-1108-5.

[2] Venugopal JR, Prabhakaran MP, Mukherjee S, Ravichandran R, Dan K, Ramakrishna S. Biomaterial Strategies for Alleviation of Myocardial Infarction. Journal of the Royal Society Interface 2011; 9(66): 1-19. DOI:10.1098/rsif.2011.0301.

[3] Walker CA, Spinale FG. The Structure and Function of the Cardiac Myocite: a Review of Fundamental Concepts. The Journal of Thoracic and Cardiovascular Surgery 1999; 118: 375-82.

[4] Di Donato M, Toso A, Dor V, Sabatier M, Barletta G, Menicanti L, Fantini F and the RESTORE Group. Surgical Ventricular Restoration Improves Mechanical Intraventricular Dyssynchrony in Ischemic Cardiomyopathy. Circulation 2004; 109: 2536-43.

[5] Smaill BH, LeGrice IJ, Hooks DA, Pullan AJ, Caldwell BJ, Hunter PJ. Cardiac Structure and Electrical Activation: Models and Measurement. Proceedings of the Australian Physiological Pharmacological Society 2004; 34: 141-9.

[6] Kocica MJ, Corno AF, Carreras-Costa F, Ballester-Rodes M, Moghbel MC, Cueva CNC, Lackovic V, Kanjuh V, Torrent-Guasp F. The Helical Ventricular Myocardial Band: Global, Three-Dimensional, Functional Architecture of the Ventricular Myocardium. European Journal Cardio-Thoracic Surgery 2006; 29: 21-40. DOI: 10.1016/j.ejcts.2006.03.011.

[7] LeGrice IJ, Smaill BH, Chai LZ, Edgar SG, Gavin JB, Hunter PJ. Laminar Structure of the Heart: Ventricular Myocite Arrangement and Connective Tissue Architecture in the Dog. American Journal of Physiology 1995; 269(38): H571-82.

[8] Williams ML, Bhatia SK. Engineering the extracellular matrix for clinical applications: Endoderm, mesoderm, and ectoderm. Biotechnol J. 2014; 9(3): 337-47. DOI 10.1002/biot.201300120.

[9] Chen FY, Cohn LH. The Surgical Treatment of Heart Failure. A New Frontier: Nontransplant Surgical Alternatives in Heart Failure. Cardiol Rev 2002; 10(6): 326-33.

[10] Hoyt RH, Cohen ML, Saffitz JE. Distribution and Three-Dimensional Structure of Intercellular Junctions in Canine Myocardium. Circulation Research 1989; 64: 563-74.

[11] Spach MS, Heidlage JF. The Stochastic Nature of Cardiac Propagation at a Microscopic Level. Electrical Description of Myocardial Architecture and its Application to Conduction. Circ Res 1995; 76: 366-80.

[12] Severs NJ. The Cardiac Muscle Cell. BioEssays 2000; 22: 188-199.

[13] Roger VL *et al.* Heart Disease and Stroke Statistics - 2012 Update A Report From the American Heart Association. Circulation 2012; 125: 2-220.

[14] Vasan SV, Benjamin EJ, Sullivan LM, D'agostino RB. The burden of increasing worldwide cardiovascular disease. In:. Fuster V, Walsh RA, O'Rourke RA, Poole-Wilson P (ed.) Hurst the Heart. 12th edition McGraw-Hill Professional; 2010: 17-46.

[15] World Hearth Organitation. WHO: Programes and projects: Cardiovascular disease: The Atlas of Heart Disease and Stroke; 2004. http://www.who.int/cardiovascular_diseases/resources/atlas/en/

[16] Burke AP, Virmani R. Pathology of myocardial ischemia, infarction, reperfusion and sudden death. In: Fuster V, Walsh RA, O'Rourke RA, Poole-Wilson P (ed.) Hurst the Heart. 12th edition McGraw-Hill Professional; 2010: 1321-1338.

[17] Baig MK, Mahon N, McKenna WJ, Caforio ALP, Bonow RO, Francis GS, Gheorghiade M. The Pathophysilogy of Advanced Heart Failure. Heart & Lung 1999; 28 (2): 87–101.

[18] Nian M, Lee P, Khaper N, Liu P. Inflammatory Cytokines and Postmyocardial Infarction Remodeling. Circulation Research 2004; 94: 1543-1553.

[19] Sun Y, Kiani MF, Postlethwaite AE, Weber KT. Infarct Scar as Living Tissue. Basic Research in Cardiology 2002; 97: 343-347. DOI: 10.1007/s00395-002-0365-8

[20] Christman KL, Lee RJ. Biomaterials For the Treatment of Myocardial Infarction. Journal American College of Cardiology 2006; 48: 907-13.

[21] Mann DL. Mechanisms and Models in Heart Failure: a Combinatorial Approach. Circulation 1999; 100: 999-1008. DOI: 10.1161/01.CIR.100.9.999.

[22] Cortes-Morichetti M, Frati G, Schussler O, Duong Van Huyen JP, Lauret E, Genovese JA, Carpentier AF, Chachques JC. Association Between a Cell-Seeded Collagen Matrix and Cellular Cardiomyoplasty for Myocardial Support and Regeneration. Tissue engineering 2007; 13(11): 2681-2687. DOI: 10.1089/ten.2006.0447.

[23] Jawad H, Ali NN, Lyon AR, Chen QZ, Harding SE, Boccaccini AR. Myocardial Tissue Engineering: a Review. Journal of Tissue Engineering and Regenerative Medicine 2007; 1: 327–342.

[24] Nelson DM, Mab Z, Fujimoto KL, Hashizume R, Wagner WR. Intra-Myocardial Biomaterial Injection Therapy in the Treatment of Heart Failure: Materials, Outcomes and Challenges. Acta Biomaterialia 2011; 7: 1-15.

[25] Mangual JO, Kraigher-Krainer E, De Luca A, Toncelli L, Shah A, Solomon S, Galanti G, Domenichini F, Pedrizzetti G. Comparative numerical study on left ventricular fluid dynamics after dilated cardiomyopathy. J Biomech. 2013; 46(10): 1611-7. DOI: 10.1016/j.jbiomech.2013.04.012.

[26] Chachques JC, Salanson-Lajos C, Lajos P, Shafy A, Alshamry A, Carpentier A. Cellular Cardiomyoplasty for Myocardial Regeneration. Asian Cardiovascular & Thoracic Annals 2005; 13: 287-296.

[27] Ferrero JM Jr, Trénor B., Montilla F., Saiz J., Ferrero Á., Rodriguez B. Wiley. Encyclopedia of Biomedical Engineering. Ischemia (ed.) John Wiley & Sons, Inc; 2006: 1-17. Available from http://onlinelibrary.wiley.com/DOI/10.1002/9780471740360.ebs0661/abstract

[28] Chen QZ, Harding S, Ali NN, Lyon AR, Boccaccini AR. Biomaterials in cardiac tissue engineering: Ten years of research survey. Materials Science and Engineering 2008; 59: 1–37.

[29] Douglas JS Jr, King SB III.Percutaneous coronary intervention. In:. Fuster V, Walsh RA, O'Rourke RA, Poole-Wilson P (ed.) Hurst the Heart. 12th edition McGraw-Hill Professional; 2010: 1427-1457.

[30] Stefanini GG, Kalesan B, Serruys PW *et al.* Long-term clinical outcomes of biodegradable polymer biolimus-eluting stents versus durable polymer sirolimus-eluting stents in patients with coronary artery disease (LEADERS): 4 year follow-up of a randomised non-inferiority trial. Lancet 2011; 378: 1940-8.

[31] Ruwende C, Visovatti S, Pinsky DJ. Molecular and cellular mechanisms of myocardial ischemia-reperfusion injury. In: Fuster V, Walsh RA, O'Rourke RA, Poole-Wilson P (ed.) Hurst the Heart. 12th edition McGraw-Hill Professional; 2010: 1339-1350.

[32] Laks H, Gates RN, Ardehali A, Capouya ER, Moriguchi JD, Kobashigawa JA, Stevenson LW. Orthotopic heart transplantation and concurrent coronary bypass. J Heart Lung Transplant. 1993; 12(5): 810-5.

[33] Anversa P, Leri A, Kajstura J, Nadal-Ginard B. Myocyte Growth and Cardiac Repair. Journal of Molecular and Cellular Cardiology 2002; 34: 91–105.

[34] Bergmann O, Bhardwaj RD, Bernard S, Zdunek S, Barnabe-Heider F, *et al.* Evidence for Cardiomyocyte Renewal in Humans. Science 2009; 324(5923): 98–102.

[35] Wang F, Guan J. Cellular Cardiomyoplasty and Cardiac Tissue Engineering for Myocardial Therapy. Advanced Drug Delivery Reviews 2010; 62: 784–797.

[36] Strauer BE, Kornowski R. Stem cell therapy in perspective. Circulation 2003; 107: 929-934.

[37] Masuda S, Shimizu T, Yamato M, Okano T. Cell sheet engineering for heart tissue repair. Advanced Drug Delivery Reviews 2008; 60(2): 277-85.

[38] Chachques JC. Development of Bioartificial Myocardium Using Stem Cells and Nanobiotechnology Templates. Cardiology Research and Practice 2011. DOI:10.4061/2011/806795.

[39] Pendyala L, Goodchild T, Gadesam RR, Chen J, Robinson K, Chronos N, Hou D. Cellular Cardiomyoplasty and Cardiac Regeneration. Current Cardiology Reviews 2008; 4: 72-80.

[40] Zhou R, Acton PD, Ferrari VA. Imaging Stem Cells Implanted in Infarcted Myocardium. Journal American College of Cardiology 2006; 48(10): 2094–2106. DOI:10.1016/j.jacc.2006.08.026.

[41] Hofmann M, Wollert KC, Meyer GP, Menke A, Arseniev L, Hertenstein B, Ganser A, Knapp WH, Drexler H. Monitoring of Bone Marrow Cell Homing into the Infarcted Human Myocardium. Circulation 2005; 111: 2198-202.

[42] Teng CJ, Luo J, Chiu RC, Shum-Tim D. Massive Mechanical Loss of Microspheres with Direct Intramyocardial Injection in the Beating Heart: Implications for Cellular Cardiomyoplasty. Journal of Thoracic and Cardiovascular Surgery 2006; 132: 628-32. DOI: 10.1016/j.jtcvs.2006.05.034.

[43] Schussler O, Chachques JC, Mesana TG, Suuronen EJ, Lecarpentier Y, Ruel M. 3-Dimensional Structures to Enhance Cell Therapy and Engineer Contractile Tissue. Asian Cardiovascular & Thoracic Annals 2010; 18: 188-198. DOI: 10.1177/0218492310361531

[44] Zenovich AG, Davis BH, Taylor DA. Comparison of Intracardiac Cell Transplantation: Autologous Skeletal Myoblasts *Versus* Bone Marrow Cells. Handbook of Experimental Pharmacology 2007; 180: 117–165.

[45] Forte E, Chimenti I, Barile L, Gaetani R, Angelini F, Ionta V, Messina E, Giacomello A. Cardiac Cell Therapy: The Next (Re)Generation. Stem Cell Reviews and Reports 2011; 7: 1018–1030. DOI: 10.1007/s12015-011-9252-8.

[46] Madonna R, Geng YJ, De Caterina R. Adipose tissue-derived stem cells: characterization and potential for cardiovascular repair. Arterioscler Thromb Vasc Biol. 2009; 29(11): 1723-9.

[47] Makkar RR, Smith RR, Cheng K, Malliaras K, *et al.* Intracoronary cardiosphere-derived cells for heart regeneration after myocardial infarction (CADUCEUS): a prospective, randomised phase 1 trial. The Lancet 2012; 379: 895–904. DOI: 10.1016/S0140- 6736(12)60195-0.

[48] Shafy A, Lavergne T, Latremouille C, Cortes-Morichetti M, Carpentier A, Chachques JC. Association of electrostimulation with cell transplantation in ischemic heart disease. J Thorac Cardiovasc Surg. 2009; 138(4): 994-1001.

[49] Qian H, Yang Y, Huang J, Dou K, Yang G. Cellular Cardiomyoplasty by Catheter-Based Infusion of Stem Cells in Clinical Settings. Transplant Immunology 2006; 16: 135–147. DOI: 10.1016/j.trim.2006.08.005.

[50] Leor J, Amsalem Y, Cohen S. Cells, Scaffolds, and Molecules for Myocardial Tissue Engineering. Pharmacology & Therapeutics 2005; 105: 151-163.

[51] Laflamme MA, Chen KY, Naumova AV, Muskheli V, *et al.* Cardiomyocytes derived from human embryonic stem cells in pro-survival factors enhance function of infarcted rat hearts. Nature Biotechnology 2007; 25(9): 1015-24. DOI: 10.1038/nbt1327.

[52] Hirata Y, Sata M, Motomura N, Takanashi M, Suematsu Y, Ono M, Takamoto S. Human umbilical cord blood cells improve cardiac function after myocardial infarction. Biochemical and Biophysical Research Communications 2005; 327: 609–14. DOI: 10.1016/j.bbrc.2004.12.044.

[53] Yeh YC, Wei HJ, Lee WY, Yu CL, Chang Y, Hsu LW, Chung MF, Tsai MS, Hwang SM, Sung HW. Cellular Cardiomyoplasty with Human Amniotic Fluid Stem Cells: In Vitro and In Vivo Studies. Tissue Engineering 2010; 16(6): 1925-36.

[54] Emmert MY, Hitchcock RW, Hoerstrup SP. Cell therapy, 3D culture systems and tissue engineering for cardiac regeneration. Adv Drug Deliv Rev. 2014; 69-70: 254-69. DOI: 10.1016/j.addr.

[55] Wu J, Zeng F, Weisel RD, Li RK. Stem Cells for Cardiac Regeneration by Cell Therapy and Myocardial Tissue Engineering. Advances in Biochemical Engineering / Biotechnology 2009; 114: 107-128. DOI: 10.1007/10_2008_37.

[56] Alcon A, Cagavi Bozkulak E, Qyang Y. Regenerating functional heart tissue for myocardial repair. Cell Mol Life Sci. 2012; 69(16): 2635-56. DOI: 10.1007/s00018-012-0942.

[57] Shimizu T, Yamato M, Kikuchi A, Okano T. Cell sheet engineering for myocardial tissue reconstruction. Biomaterials 2003; 24(13): 2309-2316.

[58] Furuta A, Miyoshi S, Itabashi Y, Shimizu T, Kira S, *et al.* Pulsatile cardiac tissue grafts using a novel three-dimensional cell sheet manipulation technique functionally integrates with the host heart, in vivo. Circ Res 2006; 98(5): 705–712.

[59] Vunjak-Novakovic G, Lui KO, Tandon N, Chien KR. Bioengineering Heart Muscle: A Paradigm for Regenerative Medicine. Annu. Rev. Biomed. Eng. 2011; 13: 245–67.

[60] Haraguchi Y, Shimizu T, Yamato M, Kikuchi A, Okano T. Electrical coupling of cardiomyocyte sheets occurs rapidly via functional gap junction formation. Biomaterials 2006; 27(27): 4765–4774.

[61] Ye Z, Zhou Y, Cai H, Tan W. Myocardial regeneration: Roles of stem cells and hydrogels Advanced Drug Delivery Reviews 2011; 63(8): 688-97.

[62] Habib M, Shapira-Schweitzer K, Caspi O, Gepstein A, Arbel G, Aronson D, Seliktar D, Gepstein L. A combined cell therapy and in-situ tissue-engineering approach for myocardial repair. Biomaterials 2011; 32(30): 7514-23.

[63] S.T. Wall, J.C. Walker, K.E. Healy, M.B. Ratcliffe, J.M. Guccione, Theoretical impact of the injection of material into the myocardium: a finite element model simulation. Circulation 2006; 114(24): 2627-35.

[64] Shen X, Tanaka K, Takamori A. Coronary Arteries Angiogenesis in Ischemic Myocardium: Biocompatibility and Biodegradability of Various Hydrogels. Artif Organs. 2009; 33(10): 781-7.

[65] Giraud MN, Armbruster C, Carrel T, Tevaearai HT. Current state of the art in myocardial tissue engineering.Tissue Eng. 2007; 13(8): 1825-36.

[66] Jeong B, Kim SW, Bae YH. Thermosensitive sol-gel reversible hydrogels. Adv Drug Deliv Rev. 2002; 54(1): 37-51.

[67] Li Z, Guo X, Matsushita S, Guan J. Differentiation of cardiosphere-derived cells into a mature cardiac lineage using biodegradable poly(N-isopropylacrylamide) hydrogels. Biomaterials 2011; 32(12): 3220-32.

[68] Wang T, Wu DQ, Jiang XJ, Zhang XZ, Li XY, Zhang JF, Zheng ZB, Zhuo R, Jiang H, Huang C. Novel thermosensitive hydrogel injection inhibits post-infarct ventricle remodelling. Eur J Heart Fail. 2009; 11(1): 14-9.

[69] Wang T, Jiang XJ, Lin T, Ren S, Li XY, Zhang XZ, Tang QZ. The inhibition of postinfarct ventricle remodeling without polycythaemia following local sustained intramyocardial delivery of erythropoietin within a supramolecular hydrogel. Biomaterials 2009; 30(25): 4161-7.

[70] Wu J, Zeng F, Huang XP, Chung JC, Konecny F, Weisel RD, Li RK. Infarct stabilization and cardiac repair with a VEGF-conjugated, injectable Hydrogel. Biomaterials 2011; 32(2): 579-86.

[71] Davis ME, Motion JP, Narmoneva DA, Takahashi T, Hakuno D, Kamm RD, Zhang S, Lee RT. Injectable self-assembling peptide nanofibers create intramyocardial microenvironments for endothelial cells. Circulation 2005; 111(4): 442-50.

[72] Biomaterials science An introduction to Materials medicine. Edited by Ratner et al. Part I Chapter I section 2.8 Natural materials IOANNis V. Yannas. 2004 Elsevier Academioc press

[73] Guo HD, Wang HJ, Tan YZ, Wu JH. Transplantation of marrow derived cardiac stem cells carried in fibrin improves cardiac function after myocardial infarction. Tissue Eng Part A. 2011; 17(1-2): 45-58.

[74] Liu Z, Wang H, Wang Y, Lin Q, Yao A, Cao F, Li D, Zhou J, Duan C, Du Z, Wang Y, Wang C. The influence of chitosan hydrogel on stem cell engraftment, survival and homing in the ischemic myocardial microenvironment. Biomaterials 2012; 33(11): 3093-106.

[75] Kofidis T, Lebl DR, Martinez EC, Hoyt G, Tanaka M, Robbins RC. Novel injectable bioartificial tissue facilitates targeted, less invasive, large-scale tissue restoration on the beating heart after myocardial injury. Circulation 2005; 112(9 Suppl): I173-7.

[76] Shen D, Wang X, Zhang L, Zhao X, Li J, Cheng K, Zhang J. The amelioration of cardiac dysfunction after myocardial infarction by the injection of keratin biomaterials derived from human hair. Biomaterials 2011; 32(35): 9290-9.

[77] Cheng K, Blusztajn A, Shen D, Li TS, Sun B, Galang G, Zarembinski TI, Prestwich GD, Marbán E, Smith RR, Marbán L. Functional performance of human cardiosphere-derived cells delivered in an in situ polymerizable hyaluronan-gelatin hydrogel. Biomaterials 2012; 33(21): 5317-24.

[78] Ruvinov E, Leor J, Cohen S. The promotion of myocardial repair by the sequential delivery of IGF-1 and HGF from an injectable alginate biomaterial in a model of acute myocardial infarction. Biomaterials 2011; 32(2): 565-78.

[79] Duan Y, Liu Z, O'Neill J, Wan LQ, Freytes DO, Vunjak-Novakovic G. Hybrid gel composed of native heart matrix and collagen induces cardiac differentiation of human embryonic stem cells without supplemental growth factors. J Cardiovasc Transl Res. 2011; 4(5): 605-15.

[80] Zhang F, He C, Cao L, Feng W, Wang H, Mo X, Wang J. Fabrication of gelatin–hyaluronic acid hybrid scaffolds with tunable porous structures for soft tissue engineering. Int J Biol Macromol. 2011; 48(3): 474-81.

[81] Singelyn JM, DeQuach JA, Seif-Naraghi SB, Littlefield RB, Schup-Magoffin PJ, Christman KL. Naturally derived myocardial matrix as an injectable scaffold for cardiac tissue engineering. Biomaterials 2009; 30(29): 5409-16.

[82] Hashizume R, Hong Y, Takanari K, Fujimoto KL, Tobita K, Wagner WR. The effect of polymer degradation time on functional outcomes of temporary elastic patch support in ischemic cardiomyopathy Biomaterials 2013; 34(30): 7353-63. DOI: 10.1016/j.biomaterials.2013.06.020.

[83] Rajabi-Zeleti S, Jalili-Firoozinezhad S, Azarnia M, Khayyatan F, Vahdat S, Nikeghbalian S, Khademhosseini A, Baharvand H, Aghdami N. The behavior of cardiac progenitor cells on macroporous pericardium-derived scaffolds. Biomaterials 2014; 35(3): 970-82. DOI: 10.1016/j.biomaterials.2013.10.045.

[84] Nerem RM. The challenge of imitating nature. In Lanza R, Langer R, Vacanti J. Principles of tissue engineering. San Diego (Ca) USA: Academic press; 1997 p.9-15.

[85] Zhang D, Shadrin IY, Lam J, Xian HQ, Snodgrass HR, Bursac N. Tissue-engineered cardiac patch for advanced functional maturation of human ESC-derived cardiomyocytes. Biomaterials 2013; 34(23): 5813-20. DOI: 10.1016/j.biomaterials.2013.04.026.

[86] Jawad H, Lyon AR, Harding SE, Ali NN, Boccaccini AR. Myocardial tissue engineering. Br Med Bull. 2008; 87: 31-47.

[87] Engelmayr GC Jr, Cheng M, Bettinger CJ, Borenstein JT, Langer R, Freed LE. Accordion-like honeycombs for tissue engineering of cardiac anisotropy. Nat Mater 2008; 7: 1003–10.

[88] Bhana B, Iyer RK, Chen WL, Zhao R, Sider KL, Likhitpanichkul M, Simmons CA, Radisic M. Influence of substrate stiffness on the phenotype of heart cells. Biotechnol Bioeng. 2010; 105(6): 1148-60.

[89] Carrier RL, Rupnick M, Langer R, Schoen FJ, Freed LE, Vunjak-Novakovic G. Perfusion Improves Tissue Architecture of Engineered Cardiac Muscle. Tissue Eng. 2002; 8(2): 175-88.

[90] Radisic M, Malda J, Epping E, Geng W, Langer R, Vunjak-Novakovic G. Oxygen gradients correlate with cell density and cell viability in engineered cardiac tissue. Biotechnol Bioeng 2006; 93(2): 332-43.

[91] Radisic M, Park H, Chen F, Salazar-Lazzaro JE, Wang Y, Dennis R, Langer R, Freed LE, Vunjak-Novakovic G. Biomimetic approach to cardiac tissue engineering: oxygen carriers and channeled scaffolds. Tissue Eng. 2006; 12(8): 2077-91.

[92] Vantler M, Karikkineth BC, Naito H, Tiburcy M, Didié M, Nose M, Rosenkranz S, Zimmermann WH. PDGF-BB protects cardiomyocytes from apoptosis and improves contractile function of engineered heart tissue. J Mol Cell Cardiol. 2010; 48(6): 1316-23.

[93] Perets, A., Baruch, Y., Weisbuch, F., Shoshany, G., Neufeld, G., & Cohen, S. (2003). Enhancing the vascularization of three-dimensional porous alginate scaffolds by incorporating controlled release basic fibroblast growth factor microspheres. J Biomed Mater Res A. 2003; 65(4): 489-97.

[94] Miyagi Y, Chiu LL, Cimini M, Weisel RD, Radisic M, Li RK. Biodegradable collagen patch with covalently immobilized VEGF for myocardial repair. Biomaterials 2011; 32(5): 1280-90.

[95] Chiu LL, Radisic M. Controlled release of thymosin β4 using collagen–chitosan composite hydrogels promotes epicardial cell migration and angiogenesis. J Control Release 2011; 155(3): 376-85. DOI: 10.1016/j.jconrel.2011.05.026 .

[96] Davis ME, Hsieh PC, Grodzinsky AJ, Lee RT. Custom design of the cardiac microenvironment with biomaterials. Circ Res. 2005; 97(1): 8-15.

[97] Microfabrication of channel arrays promotes vessel-like network formation in cardiac cell construct and vascularization in vivo Liran Zieber, Shira Or, Emil Ruvinov and Smadar Cohen Biofabrication 6 (2014) 024102 (10pp)

[98] Kaully T, Kaufman-Francis K, Lesman A, Levenberg S. Vascularization--the conduit to viable engineered tissues. Tissue Eng Part B Rev. 2009; 15(2): 159-69.

[99] Bar A, Haverich A, Hilfiker A. Cardiac tissue engineering: ‘‘Reconstructing the motor of life’’. Scand J surg 2007; 96 (2): 154-8.

[100] Narmoneva DA, Vukmirovic R, DavisME, Kamm RD, Lee RT. Endothelial cells promote cardiac myocyte survival and spatial reorganization: implications for cardiac regeneration. Circulation 2004; 110(8): 962-8.

[101] Dvir T, Kedem A, Ruvinov E, Levy O, Freeman I, Landa N, Holbova R, Feinberg MS, Dror S, Etzion Y, Leor J, Cohen S. Prevascularization of cardiac patch on the omentum improves its therapeutic outcome. Proc Natl Acad Sci USA 2009; 106 (35): 14990-5.

[102] Bursac N, Papadaki M, White JA, Eisenberg SR, Vunjak-Novakovic G, Freed LE. Cultivation in rotating bioreactors promotes maintenance of cardiac myocyte electrophysiology and molecular properties. Tissue Eng. 2003; 9(6): 1243-53.

[103] Radisic M, Yang L, Boublik J, Cohen RJ, Langer R, Freed LE, Vunjak-Novakovic G. Medium perfusion enables engineering of compact and contractile cardiac tissue. Am J Physiol Heart Circ Physiol. 2004; 286(2): H507-16.

[104] Araña M, Gavira JJ, Peña E, González A, Abizanda G, *et al.* Epicardial delivery of collagen patches with adipose-derived stem cells in rat and minipig models of chronic myocardial infarction. Biomaterials 2014; 35: 143e151.

[105] Simpson DL, Dudley SC Jr. Modulation of human mesenchymal stem cell function in a three-dimensional matrix promotes attenuation of adverse remodelling after myocardial infarction. J Tissue Eng Regen Med. 2013;7(3):192-202. DOI: 10.1002/term.511.

[106] Chimenti I, Rizzitelli G, Gaetani R, Angelini F, Ionta V, *et al.* Human cardiosphere-seeded gelatin and collagen scaffolds as cardiogenic engineered bioconstructs. Biomaterials 2011; 32(35): 9271-81.
[107] Holladay CA, Duffy AM, Chen X, Sefton MV, O'Brien TD, Pandit AS. Recovery of cardiac function mediated by MSC and interleukin-10 plasmid functionalised scaffold. Biomaterials 2012; 33(5): 1303-14.
[108] Chachques JC, Trainini JC, Lago N, Masoli OH, Barisani JL, Cortes-Morichetti M, Schussler O, Carpentier A. Myocardial assistance by grafting a new bioartificial upgraded myocardium (MAGNUM clinical trial): one year follow-up. Cell Transplant. 2007; 16(9): 927-34.
[109] Mihic A, Li J, Miyagi Y, Gagliardi M, Li SH, Zu J, Weisel RD, Keller G, Li RK. The effect of cyclic stretch on maturation and 3D tissue formation of human embryonic stem cell-derived cardiomyocytes. Biomaterials 2014; 35(9): 2798-808. DOI: 10.1016/j.biomaterials.2013.12.052.
[110] Twardowski RL, Black LD III. Cardiac Fibroblasts Support Endothelial Cell Proliferation and Sprout Formation but not the Development of Multicellular Sprouts in a Fibrin Gel Co-Culture Model. Ann Biomed Eng. 2014; 42(5): 1074-84. DOI: 10.1007/s10439-014-0971-2.
[111] Leor J, Aboulafia-Etzion S, Dar A, Shapiro L, Barbash IM, Battler A, Granot Y, Cohen S. Bioengineered cardiac grafts: A new approach to repair the infarcted myocardium? Circulation 2000; 102(19 Suppl 3): III56-61.
[112] Shachar M, Tsur-Gang O, Dvir T, Leor J, Cohen S. The effect of immobilized RGD peptide in alginate scaffolds on cardiac tissue engineering. Acta Biomater. 2011; 7(1): 152-62.
[113] Le Visage C, Gournay O, Benguirat N, Hamidi S, *et al.* Mesenchymal stem cell delivery into rat infarcted myocardium using a porous polysaccharide-based scaffold: a quantitative comparison with endocardial injection. Tissue Eng Part A. 2012; 18(1-2): 35-44.
[114] Patra C, Talukdar S, Novoyatleva T, Velagala SR, Mühlfeld C, Kundu B, Kundu SC, Engel FB. Silk protein fibroin for cardiac tissue engineering. Biomaterials 2012; 33(9): 2673-80.
[115] Yang MC, Wang SS, Chou NK, Chi NH, Huang YY, Chang YL, Shieh MJ, Chung TW. The cardiomyogenic differentiation of rat mesenchymal stem cells on silk fibroin–polysaccharide cardiac patches in vitro. Biomaterials 2009; 30(22): 3757-65.
[116] Martins AM, Eng G, Caridade SG, Mano JF, Reis RL, Vunjak-Novakovic G. Electrically Conductive Chitosan/Carbon Scaffolds for Cardiac Tissue Engineering Biomacromolecules 2014; 15(2): 635-43. DOI: 10.1021/bm401679q.
[117] Robinson KA, Li J, Mathison M, Redkar A, Cui J, Chronos NA, Matheny RG, Badylak SF. Extracellular matrix scaffold for cardiac repair. Circulation 2005; 112(9 Suppl): I135-43.
[118] Ott HC, Matthiesen TS, Goh SK, Black LD, Kren SM, Netoff TI, Taylor DA Perfusion-decellularized matrix: using nature's platform to engineer a bioartificial heart. Nat Med 2008; 14(2): 213–221.
[119] Zong X, Bien H, Chung CY, Yin L, Fang D, Hsiao BS, Chu B, Entcheva E. Electrospun fine-textured scaffolds for heart tissue constructs. Biomaterials 2005; 26(26): 5330-8.
[120] Huang CC, Wei HJ, Yeh YC, Wang JJ, Lin WW, Lee TY, Hwang SM, Choi SW, Xia Y, Chang Y, Sung HW. Injectable PLGA porous beads cellularized by hAFSCs for cellular cardiomyoplasty. Biomaterials 2012; 33(16): 4069-77.

[121] McDevitt TC, Angello JC, Whitney ML, Reinecke H, Hauschka SD, Murry CE, Stayton PS. In vitro generation of differentiated cardiac myofibers on micropatterned laminin surfaces. J Biomed Mater Res 2002; 60(3): 472-9.

[122] Stout DA, Basu B, Webster TJ. Poly(lactic–co-glycolic acid): Carbon nanofiber composites for myocardial tissue engineering applications. Acta Biomater. 2011; 7(8): 3101-12. DOI: 10.1016/j.actbio.2011.04.028 4.

[123] Ishii O, Shin M, Sueda T, Vacanti JP. In vitro tissue engineering of a cardiac graft using a degradable scaffold with an extracellular matrix–like topography. Journal of Thoracic and Cardiovascular Surgery 2005; 130(5): 1358-63.

[124] Park H, Radisic M, Lim JO, Chang BH, Vunjak-Novakovic G. A novel composite scaffold for cardiac tissue engineering. In Vitro Cell Dev Biol Anim. 2005; 41(7): 188-96.

[125] Rockwood DN, Akins RE Jr, Parrag IC, Woodhouse KA, Rabolt JF. Culture on electrospun polyurethane scaffolds decreases atrial natriuretic peptide expression by cardiomyocytes in vitro. Biomaterials 2008; 29(36): 4783-91. DOI: 10.1016/j.biomaterials.2008.08.034.

[126] Guan J, Fujimoto KL, Sacks MS, Wagner WR. Preparation and characterization of highly porous, biodegradable polyurethane scaffolds for soft tissue applications. Biomaterials 2005; 26(18): 3961–3971. DOI: 10.1016/j.biomaterials.2004.10.018.

[127] Siepe M, Giraud MN, Liljensten E, Nydegger U, Menasche P, Carrel T, Tevaearai HT. Construction of skeletal myoblast-based polyurethane scaffolds for myocardial repair. Artif Organs 2007; 31(6): 425-33.

[128] Chen QZ, Bismarck A, Hansen U, Junaid S, Tran MQ, Harding SE, Ali NN, Boccaccini AR. Characterisation of a soft elastomer poly(glycerol sebacate) designed to match the mechanical properties of myocardial tissue. Biomaterials 2008; 29(1): 47-57.

[129] Ravichandran R, Venugopal JR, Sundarrajan S, Mukherjee S, Ramakrishna S. Poly(glycerol sebacate)/gelatin core/shell fibrous structure for regeneration of myocardial infarction. Tissue Eng Part A. 2011; 17(9-10): 1363-73. DOI: 10.1089/ten.tea.2010.0441.

[130] Ifkovits JL, Devlin JJ, Eng G, Martens TP, Vunjak-Novakovic G, Burdick JA. Biodegradable fibrous scaffolds with tunable properties formed from photo-cross-linkable poly(glycerol sebacate). ACS Appl Mater Interfaces. 2009; 1(9): 1878-86.

[131] Madden LR, Mortisen DJ, Sussman EM, Dupras SK, Fugate JA, Cuy JL, Hauch KD, Laflamme MA, Murry CE, Ratner BD. Proangiogenic scaffolds as functional templates for cardiac tissue engineering Proc Natl Acad Sci U S A 2010; 107(34): 15211-6.

[132] Santos E, Hernández RM, Pedraz JL, Orive G. Novel advances in the design of three-dimensional bio-scaffolds to control cell fate: translation from 2D to 3D. Trends Biotechnol. 2012; 30(6): 331-41. DOI: 10.1016/j.tibtech.2012.03.005.

[133] Blan NR, Birla RK. Design and fabrication of heart muscle using scaffold-based tissue engineering. J. Biomed. Mater. Res. 2008: 86(A); 195–208.

[134] Boublik J, Park H, Radisic M, Tognana E, Chen F, Pei M, Vunjak-Novakovic G, Freed LE. Mechanical Properties and Remodeling of Hybrid Cardiac Constructs Made from Heart Cells, Fibrin, and Biodegradable, Elastomeric Knitted Fabric Tissue Eng. 2005; 11 (7-8): 1122-32.

[135] Chen G, Sato T, Ohgushi H, Ushida T, Tateishi T, Tanaka J. Culturing of skin fibroblasts in a thin PLGA–collagen hybrid mesh. Biomaterials 2005; 26(15): 2559-66.

[136] Antune JC, Oliveira JM, Reis RL, Soria JM, Gómez-Ribelles JL, Mano JF. Novel poly(L-lactic acid)/hyaluronic acid macroporous hybrid scaffolds: Characterization and assessment of cytotoxicity. Journal of Biomedical Materials Research 2010; 94 A(3): 856-869. DOI: 10.1002/jbm.a.32753.

[137] Lebourg M, Rochina JR, Sousa T, Mano J, Ribelles JL. Different hyaluronic acid morphology modulates primary articular chondrocyte behavior in hyaluronic acid-coated polycaprolactone scaffolds. J Biomed Mater Res A. 2013; 101(2): 518-27. DOI: 10.1002/jbm.a.34349.

[138] Wang X, Li Q, Hu X, Ma L, You C, Zheng Y, Sun H, Han C, Gao C. Fabrication and characterization of poly(L-lactide-co-glycolide) knitted mesh-reinforced collagen-chitosan hybrid scaffolds for dermal tissue engineering. J Mech Behav Biomed Mater. 2012; 8: 204-15. DOI: 10.1016/j.jmbbm.2012.01.001.

[139] Wang X, You C, Hu X, Zheng Y, Li Q, Feng Z, Sun H, Gao C, Han C. The roles of knitted mesh-reinforced collagen-chitosan hybrid scaffold in the one-step repair of full-thickness skin defects in rats. Acta Biomater. 2013; 9(8): 7822-32. DOI: 10.1016/j.actbio.2013.04.017.

[140] Shim JH, Kim JY, Park M, Park J, Cho DW. Development of a hybrid scaffold with synthetic biomaterials and hydrogel using solid freeform fabrication technology. Biofabrication 2011; 3(3): 034102. DOI: 10.1088/1758-5082/3/3/034102.

[141] Godier-Furnémont AFG, Martens TP, Koeckert MS, *et al.* Composite scaffold provides a cell delivery platform for cardiovascular repair. Proceedings of the National Academy of Science of the United States of America 2011; 108(19): 7974–7979. DOI: 10.1073/pnas.1104619108.

[142] Geng H, Song H, Qi J, Cui D. Sustained release of VEGF from PLGA nanoparticles embedded thermo-sensitive hydrogel in full-thickness porcine bladder acellular matrix. Nanoscale Res Lett. 2011; 6(1): 312. DOI: 10.1186/1556-276X-6-312.

[143] Chen K, Sahoo S, He P, Ng KS, Toh SL, Goh JC. A hybrid silk/RADA-based fibrous scaffold with triple hierarchy for ligament regeneration. Tissue Eng Part A. 2012; 18(13-14): 1399-409. DOI: 10.1089/ten.TEA.2011.0376.

[144] Caspi O, Lesman A, Basevitch Y, Gepstein A, Arbel G, *et al.* Tissue engineering of vascularized cardiac muscle from human embryonic stem cells. Circ Res. 2007; 100(2): 263-72.

[145] Park H, Larson BL, Guillemette MD, Jain SR, Hua C, Engelmayr GC Jr, Freed LE. The significance of pore microarchitecture in a multi-layered elastomeric scaffold for contractile cardiac muscle constructs. Biomaterials 2011; 32(7): 1856-64. DOI: 10.1016/j.biomaterials.2010.11.032.

[146] Ameer GA, Mahmood TA, Langer R. A biodegradable composite scaffold for cell transplantation. J Orthop Res. 2002; 20(1): 16-9.

[147] Filová E, Brynda E, Riedel T, Bacáková L, Chlupác J, Lisá V, Houska M, Dyr JE. Vascular endothelial cells on two- and three-dimensional fibrin assemblies for biomaterial coatings. J Biomed Mater Res A. 2009; 90(1): 55-69. DOI: 10.1002/jbm.a.32065.

[148] Gamboa-Martínez TC, Gómez Ribelles JL, Gallego Ferrer G. Fibrin coating on poly (L-lactide) scaffolds for tissue engineering. Journal of Bioactive and Compatible Polymers 2011; 26(5): 464–477.

[149] Mano JF, Hungerford G, Gómez Ribelles JL. Bioactive poly(L-lactic acid)-chitosan hybrid scaffolds. Materials Science and Engineering C 2008; 28: 1356–1365.

[150] Prabaharan M, Rodriguez-Perez MA, de Saja JA, Mano JF. Preparation and Characterization of Poly(L-lactic acid)-Chitosan Hybrid Scaffolds With Drug Release Capability. J Biomed Mater Res B Appl Biomater. 2007; 81(2): 427-34.

[151] Zhao P, Jiang H, Pan H, Zhu K, Chen W. Biodegradable fibrous scaffolds composed of gelatin coated poly(epsilon-caprolactone) prepared by coaxial electrospinning. J Biomed Mater Res A. 2007; 83(2): 372-82.

[152] Tambralli A, Blakeney B, Anderson J, Kushwaha M, Andukuri A, Dean D, Jun HW. A hybrid biomimetic scaffold composed of electrospun polycaprolactone nanofibers and self-assembled peptide amphiphile nanofibers. Biofabrication 2009; 1(2): 025001. DOI: 10.1088/1758-5082/1/2/025001.

[153] Sales VL, Engelmayr GC Jr, Johnson JA Jr, Gao J, Wang Y, Sacks MS, Mayer JE Jr. Protein precoating of elastomeric tissue-engineering scaffolds increased cellularity, enhanced extracellular matrix protein production, and differentially regulated the phenotypes of circulating endothelial progenitor cells. Circulation 2007; 116(11 Suppl): I55-63.

[154] Pankajakshan D, Philipose LP, Palakkal M, Krishnan K, Krishnan LK. Development of a Fibrin Composite-Coated Poly(ε-Caprolactone) Scaffold for Potential Vascular Tissue Engineering Applications. Journal of Biomedical Materials Research Part B: Applied Biomaterials 2008: 87B (2); 570–579. DOI: 10.1002/jbm.b.31146

[155] Almalik A, Donno R, Cadman CJ, Cellesi F, Day PJ, Tirelli N. Hyaluronic acid-coated chitosan nanoparticles: Molecular weight-dependent effects on morphology and hyaluronic acid presentation. Journal of Controlled Release 2013; 172: 1142–1150.

[156] Bayraktar O, Malay O, Ozgarip Y, Batigün A. Silk fibroin as a novel coating material for controlled release of theophylline. Eur J Pharm Biopharm. 2005; 60(3): 373-81.

[157] Go DP, Palmer JA, Gras SL, O'Connor AJ. Coating and release of an anti-inflammatory hormone from PLGA microspheres for tissue engineering. J Biomed Mater Res A. 2011. DOI: 10.1002/jbm.a.33299

[158] Correia CR, Moreira-Teixeira LS, Moroni L, Reis RL, van Blitterswijk CA, Karperien M, Mano JF. Chitosan scaffolds containing hyaluronic acid for cartilage tissue engineering. Tissue Eng Part C Methods. 2011; 17(7): 717-30. DOI: 10.1089/ten.tec.2010.0467.

[159] Heydarkhan-Hagvall S, Schenke-Layland K, Dhanasopon AP, Rofail F, Smith H, Wu BM, Shemin R, Beygui RE, MacLellan WR. Three-dimensional electrospun ECM-based hybrid scaffolds for cardiovascular tissue engineering. Biomaterials 2008; 29(19): 2907-14. DOI: 10.1016/j.biomaterials.2008.03.034.

[160] Arnal-Pastor M, Martínez Ramos C, Pérez Garnés M, Monleón Pradas M, Vallés Lluch A. Electrospun adherent antiadherent bilayered membranes based on cross-linked hyaluronic acid for advanced tissue engineering applications. Mater Sci Eng C Mater Biol Appl. 2013; 33(7): 4086-93.

[161] Ekaputra AK, Prestwich GD, Cool SM, Hutmacher DW. The three-dimensional vascularization of growth factor-releasing hybrid scaffold of poly (epsilon-caprolactone)/collagen fibers and hyaluronic acid hydrogel. Biomaterials. 2011; 32(32): 8108-17. DOI: 10.1016/j.biomaterials.2011.07.022.

[162] Badrossamay MR, Balachandran K, Capulli AK, Golecki HM, Agarwal A, Goss JA, Kim H, Shin K, Parker KK. Engineering hybrid polymer-protein super-aligned nanofibers via rotary jet spinning. Biomaterials 2014; 35(10): 3188-3197.

[163] Lazzeri L, Cascone MG, Danti S, Serino LP, Moscato S, Bernardini N. Gelatine/PLLA sponge-like scaffolds: morphological and biological characterization. J Mater Sci Mater Med. 2006; 17(12): 1211-7.

[164] Bai XP, Zheng HX, Fang R, Wang TR, Hou XL, Li Y, Chen XB, Tian WM. Fabrication of engineered heart tissue grafts from alginate/collagen barium composite microbeads. Biomed Mater. 2011; 6(4): 045002. DOI: 10.1088/1748-6041/6/4/045002.

[165] Falabella CA, Jiang H, Frame MD, Chen W. In vivo validation of biological responses of bFGF released from microspheres formulated by blending poly-lactide-co-glycolide and poly(ethylene glycol)-grafted-chitosan in hamster cheek pouch microcirculatory models. J Biomater Sci Polym Ed. 2009; 20(7-8): 903-22. DOI: 10.1163/156856209X444330.

[166] Pok S, Myers JD, Madihally SV, Jacot JG. A multilayered scaffold of a chitosan and gelatin hydrogel supported by a PCL core for cardiac tissue engineering. Acta Biomater. 2013; 9(3): 5630-42. DOI: 10.1016/j.actbio.2012.10.032.

[167] Hokugo A, Takamoto T, Tabata Y. Preparation of hybrid scaffold from fibrin and biodegradable polymer fiber. Biomaterials 2006; 27(1): 61-7.

[168] Engelhardt EM, Micol LA, Houis S, Wurm FM, Hilborn J, Hubbell JA, Frey P. A collagen-poly(lactic acid-co-ε-caprolactone) hybrid scaffold for bladder tissue regeneration. Biomaterials 2011; 32(16): 3969-76. DOI: 10.1016/j.biomaterials.2011.02.012.

[169] Ghezzi CE, Marelli B, Muja N, Hirota N, Martin JG, Barralet JE, Alessandrino A, Freddi G, Nazhat SN. Mesenchymal stem cell-seeded multilayered dense collagen-silk fibroin hybrid for tissue engineering applications. Biotechnol J. 2011; 6(10): 1198-207. DOI: 10.1002/biot.201100127.

[170] Jin-Oh You, Marjan Rafat, George J. C. Ye, and Debra T. Auguste Nanoengineering the Heart: Conductive Scaffolds Enhance Connexin 43 Expression Nano Lett. 2011: 11; 3643–3648.

[171] Ravichandran R, Sridhar R, Venugopal JR, Sundarrajan S, Mukherjee S, Ramakrishna S. Gold Nanoparticle Loaded Hybrid Nanofibers for Cardiogenic Differentiation of Stem Cells for Infarcted Myocardium Regeneration. Macromol. Biosci. 2013. DOI: 10.1002/mabi.201300407

[172] Li X, Liu X, Dong W, Feng Q, Cui F, Uo M, Akasaka T, Watari F. In vitro evaluation of porous poly(L-lactic acid) scaffold reinforced by chitin fibers. J Biomed Mater Res B Appl Biomater. 2009; 90(2): 503-9. DOI: 10.1002/jbm.b.31311.

[173] Parizek M, Kasalkova N, Bacakova L, Slepicka P, Lisa V, Blazkova M, Svorcik V. Improved Adhesion, Growth and Maturation of Vascular Smooth Muscle Cells on Polyethylene Grafted with Bioactive Molecules and Carbon Particles. Int. J. Mol. Sci. 2009; 10: 4352-4374.

[174] Mao JS, Liu HF, Yin YJ, Yao KD. The properties of chitosan-gelatin membranes and scaffolds modified with hyaluronic acid by different methods. Biomaterials 2003; 24(9): 1621-9.

[175] Wang YW, Wu Q, Chen GQ. Reduced mouse fibroblast cell growth by increased hydrophilicity of microbial polyhydroxyalkanoates via hyaluronan coating. Biomaterials 2003; 24(25): 4621-9.

[176] Dai L, StJohn HAW, Bi J, Zientek P, Chatelier RC, Griesser HJ. Biomedical coatings by the covalent immobilization of polysaccharides onto gas-plasma-activated polymer surfaces. Surf. Interface Anal. 2000; 29: 46–55.

[177] Polini A, Pagliara S, Stabile R, Netti GS, Roca L, Prattichizzo C. et al. Collagen-functionalised electrospun polymer fibers for bioengineering applications. Soft Matter 2010; 6: 1668–1674.

[178] Yuan W, Dong H, Li CM, Cui X, Yu L, Lu Z, Zhou Q. pH-controlled construction of chitosan/alginate multilayer film: characterization and application for antibody immobilization. Langmuir 2007; 23(26): 13046-52.

[179] Kujawa P, Schmauch G, Viitala T, Badia A, Winnik FM. Construction of viscoelastic biocompatible films via the layer-by-layer assembly of hyaluronan and phosphorylcholine-modified chitosan. Biomacromolecules 2007; 8(10): 3169-76.

[180] Nogueira GM, Swiston AJ, Beppu MM, Rubner MF. Layer-by-Layer Deposited Chitosan/Silk Fibroin Thin Films with Anisotropic Nanofiber Alignment. Langmuir 2010; 26(11): 8953–8958.

[181] Croll TI, O'Connor AJ, Stevens GW, Cooper-White JJ.A Blank Slate? Layer-by-Layer Deposition of Hyaluronic Acid and Chitosan onto Various Surfaces. Biomacromolecules 2006; 7(5): 1610-22.

[182] www.recatabi.com

[183] Ohara T, Sato T, Shimizu N, Prescher G, Schwind H, Weiberg O, Marten K, Greim H. Acrylic Acid and Derivatives. 2006 Wiley-VCH Verlag GmbH & Co. KGaA, Weinheim. DOI: 10.1002/14356007.a01 161.pub2

[184] NG McCrum, BE Read, G. Williams. Anelastic and dielectric effects in polymer solids. Dover publications Inc. New York 1991.

[185] Gugutkov D, Altankov G, Rodríguez Hernández JC, Monleón Pradas M, Salmerón Sánchez M. Fibronectin activity on substrates with controlled -OH density. J Biomed Mater Res A. 2010; 92(1): 322-31. DOI: 10.1002/jbm.a.32374.

[186] Rodríguez Hernández JC, Salmerón Sánchez M, Soria JM, Gómez Ribelles JL, Monleón Pradas M. Substrate chemistry-dependent conformations of single laminin molecules on polymer surfaces are revealed by the phase signal of atomic force microscopy. Biophys J. 2007; 93(1): 202-7.

[187] Rico P, Rodríguez Hernández JC, Moratal D, Altankov G, Monleón Pradas M, Salmerón-Sánchez M. Substrate-induced assembly of fibronectin into networks: influence of surface chemistry and effect on osteoblast adhesion. Tissue Eng Part A. 2009; 15(11): 3271-81. DOI: 10.1089/ten.TEA.2009.0141.

[188] Campillo-Fernández AJ, Unger RE, Peters K, Halstenberg S, Santos M, Salmerón Sánchez M, et al. Analysis of the biological response of endothelial and fibroblast cells cultured on synthetic scaffolds with various hydrophilic/hydrophobic ratios. Influence of fibronectin adsorption and conformation. Tissue Eng 2009; 15: 1331-1341.

[189] Pérez Olmedilla M, García-Giralt N, Monleón Pradas M, Benito Ruiz P, Gómez Ribelles JL, Cáceres Palou E, et al. Response of human chondrocytes to a non-uniform distribution of hydrophilic domains on poly(ethyl acrylate-co-hydroxyethyl methacrylate) copolymers. Biomaterials 2006; 27: 1003-1012.

[190] Campillo-Fernández AJ, Pastor S, Abad-Collado M, *et al.* Future design of a new keratoprosthesis. Physical and biological analysis of polymeric substrates for epithelial cell growth. Biomacromolecules 2007; 8: 2429-2436.

[191] Soria JM, Sancho-Tello M, García Esparza MA, *et al.* Biomaterials coated by dental pulp cells as substrate for neural stem cell differentiation. J Biomed Mater Res Part A 2011; 97: 85-92.

[192] Martínez-Ramos C, Lainez S, Sancho F, García Esparza MA, *et al.* Differentiation of postnatal neural stem cells into glia and functional neurons on laminin-coated polymeric substrates. Tissue Eng Part A. 2008; 14(8): 1365-75. DOI: 10.1089/ten.tea.2007.0295.

[193] Soria JM, Martínez-Ramos C, Benavent V, *et al.* Survival and differentiation of embryonic neural explants onto different biomaterials. J Biomed Mater Res Part A 2006; 79: 495-502.

[194] Soria JM, Martínez Ramos C, Bahamonde O, *et al.*. Influence of the substrate's hydrophilicity on the in vitro Schwann cells viability. J Biomed Mater Res A. 2007; 83(2): 463-70.

[195] Mei Y, Saha K, Bogatyrev SR, Yang J, Hook AL, *et al.* Combinatorial development of biomaterials for clonal growth of human pluripotent stem cells. Nat Mater. 2010; 9(9): 768-78. DOI: 10.1038/nmat2812.

[196] Rodríguez Hernández JC, Serrano Aroca A, Gómez Ribelles JL, Pradas MM. Three-dimensional nanocomposite scaffolds with ordered cylindrical orthogonal pores. J Biomed Mater Res B Appl Biomater 2008; 84(2): 541-9.

[197] Brígido Diego R, Pérez Olmedilla M, Serrano Aroca A, Gómez Ribelles JL, Monleón Pradas M, Gallego Ferrer G, Salmerón Sánchez M. Acrylic scaffolds with interconnected spherical pores and controlled hydrophilicity for tissue engineering. J Mater Sci Mater Med. 2005; 16(8): 693-8.

[198] Vallés Lluch A, Campillo Fernández A, Gallego Ferrer G, Monleón Pradas M. Bioactive scaffolds mimicking natural dentin structure. J Biomed Mater Res B Appl Biomater. 2009; 90(1): 182-94. DOI: 10.1002/jbm.b.31272.

[199] Martínez-Ramos C, Vallés-Lluch A, *et al.* Channeled scaffolds implanted in adult rat brain. J Biomed Mater Res A 2012; 100: 3276-3286.

[200] Vallés-Lluch A, Novella-Maestre E, Sancho-Tello M, Pradas MM, Ferrer GG, Batalla CC. Mimicking natural dentin using bioactive nanohybrid scaffolds for dentinal tissue engineering. Tissue Eng Part A. 2010; 16(9): 2783-93. DOI: 10.1089/ten.TEA.2010.0090.

[201] Meyer K, Palmer JW. The Polysaccharide of the vitreous humor. J. Biol. Chem. 1934; 107: 629-634.

[202] Balazs EA, Laurent TC, Jeanloz RW. Nomenclature of hyaluronic acid Biochem J. 1986; 235(3): 903.

[203] Stern R, Asari AA, Sugahara KN. Hyaluronan fragments: an information-rich system. Eur J Cell Biol. 2006; 85(8): 699-715.

[204] Perng CK, Wang YJ, Tsi CH, Ma H. In Vivo Angiogenesis Effect of Porous Collagen Scaffold with Hyaluronic Acid Oligosaccharides. J Surg Res. 2011; 168(1): 9-15. DOI: 10.1016/j.jss.2009.09.052.

[205] Kogan G, Soltés L, Stern R, Gemeiner P. Hyaluronic acid: a natural biopolymer with a broad range of biomedical and industrial applications. Biotechnol Lett. 2007; 29(1): 17-25.

[206] Fraser JR, Laurent TC, Laurent UB. Hyaluronan: its nature, distribution, functions and turnover. J Intern Med. 1997; 242(1): 27-33.

[207] Allison DD, Grande-Allen KJ. Review. Hyaluronan: a powerful tissue engineering tool. Tissue Eng. 2006; 12(8): 2131-40.

[208] Hardigham T. Chapter 1 Solution Properties of Hyaluronan. In: Chemistry and Biology of Hyaluronan. Garg HG, Hales CA (Editors). Elsevier 2004.

[209] Collins MN, Birkinshaw C. Comparison of the Effectiveness of Four Different Crosslinking Agents with Hyaluronic Acid Hydrogel Films for Tissue-Culture Applications. J. of Applied Polymer Science 2007; 104(5): 3183-3191.

[210] Bourguignon LY, Gilad E, Peyrollier K, Brightman A, Swanson RA. Hyaluronan–CD44 interaction stimulates Rac1 signaling and PKN gamma kinase activation leading to cytoskeleton function and cell migration in astrocytes. J Neurochem 2007; 101(4): 1002–17.

[211] Yang MC, Chi NH, Chou NK, Huang YY, Chung TW, Chang YL, Liu HC, Shieh MJ, Wang SS. The influence of rat mesenchymal stem cell CD44 surface markers on cell growth, fibronectin expression, and cardiomyogenic differentiation on silk fibroin - Hyaluronic acid cardiac patches. Biomaterials 2010; 31(5): 854-62. DOI: 10.1016/j.biomaterials.2009.09.096.

[212] Xu S, Li J, He A, Liu W, Jiang X, Zheng J, Han CC, Hsiao BS, Chu B, Fang D. Chemical crosslinking and biophysical properties of electrospun hyaluronic acid based ultra-thin fibrous membranes. Polymer 2009; 50(15): 3762-3769. DOI:10.1016/j.polymer.2009.06.009.

[213] West DC, Hampson IN, Arnold F, Kumar S. Angiogenesis induced by degradation products of hyaluronic acid. Science 1985; 228(4705): 1324-6.

[214] Gaffney J, Matou-Nasri S, Grau-Olivares M, Slevin M. Therapeutic applications of hyaluronan. Mol Biosyst. 2010; 6(3): 437-43. DOI: 10.1039/b910552m.

[215] Sattar A, Rooney P, Kumar S, Pye D, West DC, Scott I, Ledger P. Application of angiogenic oligosaccharides of hyaluronan increases blood vessel numbers in rat skin. J Invest Dermatol. 1994; 103(4): 576-9.

[216] Richter W. Non-Immunogenicity of Purified Hyaluronic Acid Preparations Tested by Passive Cutaneous Anaphylaxis. Int Arch Allergy 1974; 47: 211–217. DOI: 10.1159/000231214.

[217] Li J, He A, Han CC, Fang D, Hsiao BS, Chu B. Electrospinning of Hyaluronic Acid (HA) and HA/Gelatin Blends. Macromolecular Rapid Communications 2006; 27(2): 114-120.

[218] Matsumoto Y, Kuroyanagi Y. Development of a wound dressing composed of hyaluronic acid sponge containing arginine and epidermal growth factor. J Biomater Sci Polym Ed. 2010; 21(6): 715-26.

[219] Vrijland WW, Tseng LN, Eijkman HJ, Hop WC, Jakimowicz JJ, Leguit P, Stassen LP, Swank DJ, Haverlag R, Bonjer HJ, Jeekel H. Fewer intraperitoneal adhesions with use of hyaluronic acid-carboxymethylcellulose membrane: a randomized clinical trial. Ann Surg. 2002; 235(2): 193-9.

[220] Ombelli M, Costello L, Postle C, Anantharaman V, Meng QC, Composto RJ, Eckmann DM. Competitive protein adsorption on polysaccharide and hyaluronate modified surfaces. Biofouling 2011; 27(5): 505-18. DOI: 10.1080/08927014.2011.585711.

[221] Campoccia D, Doherty P, Radice M, Brun P, Abatangelo G, Williams DF. Semisynthetic resorbable materials from hyaluronan esterification. Biomaterials 1998; 19(23): 2101-27.

[222] Chua PH, Neoh KG, Kang ET, Wang W. Surface functionalization of titanium with hyaluronic acid/chitosan polyelectrolyte multilayers and RGD for promoting osteoblast functions and inhibiting bacterial adhesion. Biomaterials 2008; 29(10): 1412-21. DOI: 10.1016/j.biomaterials.2007.12.019.
[223] Beasley KL, Weiss MA, Weiss RA. Hyaluronic acid fillers: a comprehensive review. Facial Plast Surg. 2009; 25(2): 86-94. DOI: 10.1055/s-0029-1220647.
[224] Luo Y, Kirker KR, Prestwich GD. Cross-linked hyaluronic acid hydrogel films: new biomaterials for drug delivery. J Control Release. 2000; 69(1): 169-84.
[225] Bae KH, Yoon JJ, Park TG. Fabrication of hyaluronic acid hydrogel beads for cell encapsulation. Biotechnol Prog. 2006; 22(1): 297-302.
[226] Burdick JA, Prestwich GD. Hyaluronic Acid Hydrogels for Biomedical Applications. Advanced Materials 2011; 23(12): H41–H56. DOI: 10.1002/adma.201003963.
[227] Zawko SA, Suri S, Truong Q, Schmidt CE. Photopatterned anisotropic swelling of dual-crosslinked hyaluronic acid hydrogels. Acta Biomater 2009; 5(1): 14-22. DOI: 10.1016/j.actbio.2008.09.012.
[228] Gallina C, Dolgetta S, Alloatti G, Levi R, Gallo MP. Development of morphology and function of neonatal mouse ventricular myocytes cultured on a hyaluronan-based polymer scaffold. J Cell Biochem. 2012; 113(3): 800-7. DOI: 10.1002/jcb.23407.
[229] Khademhosseini A, Eng G, Yeh J, Kucharczyk PA, Langer R, Vunjak-Novakovic G, Radisic M. Microfluidic patterning for fabrication of contractile cardiac organoids. Biomed Microdevices. 2007; 9(2): 149-57.
[230] Fiumana E, Pasquinelli G, Foroni L, Carboni M, Bonafé F, Orrico C, Nardo B, Tsivian M, Neri F, Arpesella G, Guarnieri C, Caldarera CM, Muscari C. Localization of mesenchymal stem cells grafted with a hyaluronan-based scaffold in the infarcted heart. J Surg Res. 2013; 179(1): e21-9.
[231] Yoon SJ, Fang YH, Lim CH, Kim BS, Son HS, Park Y, Sun K. Regeneration of ischemic heart using hyaluronic acid-based injectable hydrogel. J Biomed Mater Res B Appl Biomater. 2009; 91(1): 163-71.
[232] Dahlmann J, Krause A, Möller L, Kensah G, Möwes M, Diekmann A, Martin U, Kirschning A, Gruh I, Dräger G. Fully defined in situ cross-linkable alginate and hyaluronic acid hydrogels for myocardial tissue engineering. Biomaterials 2013; 34(4): 940-51. DOI: 10.1016/j.biomaterials.2012.10.008.
[233] Kim J, Park Y, Tae G, Lee KB, Hwang SJ, Kim IS, Noh I, Sun K. Synthesis and characterization of matrix metalloprotease sensitive-low molecular weight hyaluronic acid based hydrogels. J Mater Sci Mater Med. 2008; 19(11): 3311-8. DOI: 10.1007/s10856-008-3469-3.
[234] Ikonen L, Kerkelä E, Metselaar G, Stuart MC, de Jong MR, Aalto-Setälä K. 2D and 3D self-assembling nanofiber hydrogels for cardiomyocyte culture. Biomed Res Int. 2013; 2013: 285678.
[235] Turner WS, Wang X, Johnson S, Medberry C, Mendez J, Badylak SF, McCord MG, McCloskey KE. Cardiac tissue development for delivery of embryonic stem cell-derived endothelial and cardiac cells in natural matrices. J Biomed Mater Res B Appl Biomater 2012; 100(8): 2060-72. DOI: 10.1002/jbm.b.32770.
[236] Zhang S, Altman M. Peptide self-assembly in functional polymer science and engineering. Reactive & Functional Polymers 1999; 41: 91-102.
[237] Zhang S. Fabrication of novel biomaterials through molecular self-assembly. Nat Biotechnol. 2003; 21(10): 1171-8.

[238] Zhang S, Holmes TC, DiPersio CM, Hynes RO, Su X, Rich A. Self-complementary oligopeptide matrices support mammalian cell attachment. Biomaterials 1995; 16(18): 1385-93.

[239] Ortinau S, Schmich J, Block S, Liedmann A, Jonas L, Weiss DG, Helm CA, Rolfs A, Frech MJ. Effect of 3D-scaffold formation on differentiation and survival in human neural progenitor cells. Biomed Eng Online. 2010; 9: 70. DOI: 10.1186/1475-925X-9-70.

[240] Hauser CA, Zhang S. Designer self-assembling peptide nanofiber biological materials. Chem Soc Rev. 2010; 39(8): 2780-90. DOI: 10.1039/b921448h.

[241] Zhang S, Lockshin C, Cook R, Rich A. Unusually stable beta-sheet formation in an ionic self-complementary oligopeptide. Biopolymers 1994; 34: 663-672.

[242] Jung JP, Gasiorowski JZ, Collier JH. Fibrillar peptide gels in biotechnology and biomedicine. Biopolymers 2010; 94(1): 49-59. DOI: 10.1002/bip.21326.

[243] Zhang S, Gelain F, Zhao X. Designer self-assembling peptide nanofiber scaffolds for 3D tissue cell cultures. Semin Cancer Biol. 2005; 15(5): 413-20.

[244] Zhang S, Zhao X, Spirio L. PuraMatrix: Self-assembling peptide nanofiber scaffolds. In: Ma PX, Elisseeff J, editors. Scaffolding in tissue Engineering. Boca Raton, FL: 2005CRC Press. p 217–238.

[245] Sieminski AL, Semino CE, Gong H, Kamm RD. Primary sequence of ionic self-assembling peptide gels affects endothelial cell adhesion and capillary morphogenesis. J Biomed Mater Res A. 2008; 87(2): 494-504. DOI: 10.1002/jbm.a.31785.

[246] Takei J. 3-Dimensional Cell Culture Scaffold For Everyone: Drug Screening.Tissue Engineering and Cancer Biology. AATEX 2006; 11(3): 170-176.

[247] Quintana L, Fernández Muiños T, Genove E, Del Mar Olmos M, Borrós S, Semino CE. Early tissue patterning recreated by mouse embryonic fibroblasts in a three-dimensional environment. Tissue Eng Part A. 2009; 15(1): 45-54. DOI: 10.1089/ten.tea.2007.0296.

[248] Garreta E, Genové E, Borrós S, Semino CE. Osteogenic differentiation of mouse embryonic stem cells and mouse embryonic fibroblasts in a three-dimensional self-assembling peptide scaffold. Tissue Eng. 2006; 12(8): 2215-27.

[249] Semino, C. E., Merok, J. R., Crane, G. G., Panagiotakos, G. & Zhang, S. Functional differentiation of hepatocyte-like spheroid structures from putative liver progenitor cells in three-dimensional peptide scaffolds. Differentiation 2003; 71: 262–70.

[250] Thonhoff JR, Lou DI, Jordan PM, Zhao X, Wu P. Compatibility of human fetal neural stem cells with hydrogel biomaterials in vitro. Brain Res. 2008; 1187: 42-51.

[251] Holmes TC, de Lacalle S, Su X, Liu G, Rich A, Zhang S. Extensive neurite outgrowth and active synapse formation on self-assembling peptide scaffolds. Proc Natl Acad Sci U S A. 2000; 97(12): 6728-33.

[252] Tysseling-Mattiace VM, Sahni V, Niece KL, Birch D, Czeisler C, Fehlings MG, Stupp SI, Kessler JA. Self-assembling nanofibers inhibit glial scar formation and promote axon elongation after spinal cord injury. J Neurosci. 2008; 28(14): 3814-23. DOI: 10.1523/JNEUROSCI.0143-08.2008.

[253] Tokunaga M, Liu ML, Nagai T, Iwanaga K, Matsuura K, Takahashi T, Kanda M, Kondo N, Wang P, Naito AT, Komuro I. Implantation of cardiac progenitor cells using self-assembling peptide improves cardiac function after myocardial infarction. J Mol Cell Cardiol. 2010; 49(6): 972-83.

[254] Genové E, Shen C, Zhang S, Semino CE. The effect of functionalized self-assembling peptide scaffolds on human aortic endothelial cell function. Biomaterials 2005; 26(16): 3341-51.

[255] Gelain F, Bottai D, Vescovi A, Zhang S. Designer self-assembling peptide nanofiber scaffolds for adult mouse neural stem cell 3-dimensional cultures. PLoS One. 2006 Dec 27; 1: e119.

[256] Horii A, Wang X, Gelain F, Zhang S. Biological designer self-assembling peptide nanofiber scaffolds significantly enhance osteoblast proliferation, differentiation and 3-D migration. PLoS One. 2007 Feb 7; 2(2): e190.

[257] Guo HD, Cui GH, Wang HJ, Tan YZ. Transplantation of marrow-derived cardiac stem cells carried in designer self-assembling peptide nanofibers improves cardiac function after myocardial infarction. Biochem Biophys Res Commun. 2010; 399(1): 42-8. DOI: 10.1016/j.bbrc.2010.07.031.

[258] Jung JP, Jones JL, Cronier SA, Collier JH. Modulating the mechanical properties of self-assembled peptide hydrogels via native chemical ligation. Biomaterials 2008; 29(13): 2143-51.

[259] Genové E, Schmitmeier S, Sala A, Borrós S, Bader A , Griffith LG, Semino CE. Functionalized self-assembling peptide hydrogel enhance maintenance of hepatocyte activity in vitro. J. Cell. Mol. Med. 2009; 13(9B): 3387-3397.

[260] Hsieh PC, Davis ME, Gannon J, MacGillivray C, Lee RT. Controlled delivery of PDGF-BB for myocardial protection using injectable self-assembling peptide nanofibers. J Clin Invest. 2006; 116(1): 237-48.

[261] Kim JH, Jung Y, Kim SH, Sun K, Choi J, Kim HC, Park Y, Kim SH. The enhancement of mature vessel formation and cardiac function in infarcted hearts using dual growth factor delivery with self-assembling peptides. Biomaterials 2011; 32(26): 6080-8.

[262] Davis ME, Hsieh PC, Takahashi T, Song Q, Zhang S, Kamm RD, Grodzinsky AJ, Anversa P, Lee RT. Local myocardial insulin-like growth factor 1 (IGF-1) delivery with biotinylated peptide nanofibers improves cell therapy for myocardial infarction. Proc Natl Acad Sci USA 2006; 103(21): 8155-60.

[263] Padin-Iruegas ME, Misao Y, Davis ME, Segers VF, Esposito G, Tokunou T, Urbanek K, Hosoda T, Rota M, Anversa P, Leri A, Lee RT, Kajstura J. Cardiac progenitor cells and biotinylated insulin-like growth factor-1 nanofibers improve endogenous and exogenous myocardial regeneration after infarction. Circulation 2009; 120(10): 876-87. DOI: 10.1161/CIRCULATIONAHA.109.852285.

[264] McGrath AM, Novikova LN, Novikov LN, Wiberg M. BD™ PuraMatrix™ peptide hydrogel seeded with Schwann cells for peripheral nerve regeneration. Brain Res Bull 2010; 83(5): 207-13. DOI: 10.1016/j.brainresbull.2010.07.001

[265] Sargeant TD, Guler MO, Oppenheimer SM, Mata A, Satcher RL, Dunand DC, Stupp SI. Hybrid bone implants: self-assembly of peptide amphiphile nanofibers within porous titanium. Biomaterials 2008; 29(2): 161-71.

[266] Hartgerink JD, Beniash E, Stupp SI. Peptide-amphiphile nanofibers: a versatile scaffold for the preparation of self-assembling materials. Proc Natl Acad Sci USA 2002; 99(8): 5133-8.

[267] P. J. Elving, J. M. Markowitz, I. Rosenthal. Preparation of buffer systems of constant ionic strength. Anal. Chem. 1956; 28 (7): 1179–1180.

[268] L. Greenspan, L Humidity Fixed Points of Binary Saturated Aqueous Solutions. J. Res. Nat. Bur. Stand A Phys. Chem. 1977; 81A: 89–96.

[269] Thomson KS, Korte FS, Giachelli CM, Ratner BD, Regnier M, Scatena M. Prevascularized microtemplated fibrin scaffolds for cardiac tissue engineering applications. Tissue Eng Part A. 2013; 19(7-8): 967-77. DOI: 10.1089/ten.tea.2012.0286.

[270] Frazer RQ, Byron RT, Osborne PB, West KP. PMMA: an essential material in medicine and dentistry. J Long Term Eff Med Implants. 2005; 15(6): 629-39.

[271] Rifi EH, Rastegar F, Brunette JP. Uptake of cesium, strontium and europium by a poly(sodium acrylate-acrylic acid) hydrogel. Talanta, 1995; 42(6): 811–816.

[272] Gedde U. Polymer physics. Chapman & Hall 1995. P70

[273] Brandrup J, EH. Immergut. Polymer handbook,1975 Wiley&Sons. Page III-144

[274] Primo Yúfera E. Química orgánica básica y aplicada. De la molécula a la Industria. Vol. I Chapter 22 p.555.

[275] Gibson L.J., Ashby M.F. Cellular solids: Structure and Properties, Cambridge University Press: Cambridge, 1997.

[276] Grossman W, Jones D, McLaurin LP. Wall Stress and Patterns of Hypertrophy in the Human Left Ventricle. J Clin Invest. 1975; 56(1): 56-64.

[277] Liao SY, Siu CW, Liu Y, Zhang Y, Chan WS, Wu EX, Wu Y, Nicholls JM, Li RA, Benser ME, Rosenberg SP, Park E, Lau CP, Tse HF. Attenuation of left ventricular adverse remodeling with epicardial patching after myocardial infarction. Journal of Cardiac Failure 2010; 16 (7): 590-8.

[278] Pilla JJ, Blom AS, Brockman DJ, Ferrari VA, Yuan Q, Acker MA. Passive ventricular constraint to improve left ventricular function and mechanics in an ovine model of heart failure secondary to acute myocardial infarction. Journal of Thoracic and Cardiovascular Surgery 2003; 126(5): 1467-76.

[279] Klodell CT, Aranda JM, McGiffin DC, Rayburn BK, Sun B, Abraham WT, Pae WE. Boehmer JP, Klein H, Huth C. Worldwide surgical experience with the Paracor HeartNet cardiac restraint device. The Journal of Thoracic and Cardiovascular Surgery 2008; 135(1): 188–195.

[280] Shafy A, Fink T, Zachar V, Lilaa N, Carpentier A, Chachques JC. Development of cardiac support bioprostheses for ventricular restoration and myocardial regeneration. European Journal of Cardio-Thoracic Surgery 2012; 0: 1–9. DOI:10.1093/ejcts/ezs480.

[281] Wang J, Khoury DS, Yue Y, Torre-Amione G, Nagueh SF. Left ventricular untwisting rate by speckle tracking echocardiography. Circulation 2007 27; 116(22): 2580-6.

[282] Akhyari P, Fedak PW, Weisel RD, Lee TY, Verma S, Mickle DA, Li RK.Mechanical stretch regimen enhances the formation of bioengineered autologous cardiac muscle grafts. Circulation 2002; 106(12 Suppl 1): I137-42.

[283] Fink C, Ergün S, Kralisch D, Remmers U, Weil J, Eschenhagen T.Chronic stretch of engineered heart tissue induces hypertrophy and functional improvement. FASEB J. 2000; 14(5): 669-79.

[284] Rappaport D, Adam D, Lysyansky P, Riesner S. Assessment of myocardial regional strain and strain rate by tissue tracking in B-mode echocardiograms. Ultrasound Med Biol. 2006; 32(8): 1181-92.

[285] van Krevelen DW. Properties of polymers. Chapter 13 Mechanical properties of solid polymers. 367-437. Elsevier 1997

[286] Zaimova D, Bayraktar E, Katundi D, Dishovsky N. Elastomeric matrix composites: effect of processing conditions on the physical, mechanical and viscoelastic properties. Journal of Achievements in Materials and Manufacturing Engineering 2012; 50(2): 81-91.

[287] Jo-Yu Wang JY, Ploehn HJ. Dynamic mechanical analysis of the effect of water on glass bead–epoxy composites. Journal of Applied Polymer Science 1996; 59(2): 345-357.

[288] van Melick, H.G.H.; Govaert, L.E.; Meijer, H.E.H. On the origin of strain hardening in glassy polymers. Polymer 2003; 44(8): 2493-2502(10).

[289] A. Maleki, A.L. Kjoniksen, B. Nyström, Macromol. Symp. 2008; 274: 131–140.

[290] B. Erman, J.E. Mark, Structure and Properties of Rubberlike Networks, Oxford University Press, New York, 1997.

[291] J.M. Prausnitz, R.N. Lichtenthaler, E. Gomes de Azevedo, Molecular Thermodynamics of Fluid-Phase Equilibria, Prentice Hall, New York, 1999.

[292] Detournay E, Cheng AH-D, Fundamentals of poroelasticity. In: Fairhurst C, editor. Comprehensive rock engineering: principles, practice and projects, vol.II, Analysis and design method. New York: Pergamon; 1993. p. 113–71.

[293] Fornells P, García-Aznar JM, Doblaré M. A finite element dual porosity approach to model deformation-induced fluid flow in cortical bone. Ann Biomed Eng 2007; 35: 1687–98.

[294] Gong Y, He L, Li J, Zhou Q, Ma Z, Gao C, Shen J. Hydrogel-filled polylactide porous scaffolds for cartilage tissue engineering. J Biomed Mater Res B Appl Biomater. 2007; 82(1): 192-204.

[295] Zhao H, Ma L, Gong Y, Gao C, Shen J. A polylactide/fibrin gel composite scaffold for cartilage tissue engineering: fabrication and an in vitro evaluation. J Mater Sci Mater Med. 2009; 20(1): 135-43.

[296] Ritger PL, Peppas NA. A simple equation for description of solute release. I. Fickian and non-Fickian release from non-swellable devices in the form of slabs, spheres, cylinders or discs. J Controlled Release 1987; 5: 23–36.

[297] Ritger PL, Peppas NA. A simple equation for description of solute release II. Fickian and anomalous release from swellable devices. J Controlled Release 1987; 5: 37–42.

[298] Lin C-C, Metters AT. Hydrogels in controlled release formulations: network design and mathematical modeling. Adv Drug Deliv Rev 2006; 58: 1379–408.

[299] Lee F, Chung JE, Kurisawa M. An injectable hyaluronic acid-tyramine hydrogel system for protein delivery. J Control Release. 2009; 134(3): 186-93. DOI: 10.1016/j.jconrel.2008.11.028.

[300] Ge S, Kojio K, Takahara A, Kajiyama T. Bovine serum albumin adsorption onto immobilized organotrichlorosilane surface: influence of the phase separation on protein adsorption patterns. J Biomater Sci Polym Ed. 1998; 9(2): 131-50.

[301] Saleh FA, Whyte M, Genever PG. Effects of endothelial cells on human mesenchymal stem cell activity in a three-dimensional in vitro model.Eur Cell Mater. 2011; 22: 242-57; discussion 257.

[302] Collier JH, MessersmithPB.Enzymatic Modification of Self-Assembled Peptide Structures with Tissue Transglutaminase.Bioconjug Chem. 2003; 14(4): 748-55.

[303] Kakiuchi Y, Hirohashi N, Murakami-Murofushi K. The macroscopic structure of RADA16 peptide hydrogel stimulates monocyte/macrophage differentiation in HL60 cells via cholesterol synthesis. BiochemBiophys Res Commun. 2013; 433(3): 298-304. DOI: 10.1016/j.bbrc.2013.02.105.

[304] Pérez-Garnes M, González-García C, Moratal D, Rico P, Salmerón-Sánchez M. Fibronectin distribution on demixednanoscale topographies. Int J Artif Organs. 2011; 34(1): 54-63.

[305] Salmerón-Sánchez M, Rico P, Moratal D, Lee TT, Schwarzbauer JE, García AJ. Role of material-driven fibronectin fibrillogenesis in cell differentiation. Biomaterials 2011; 32(8): 2099-105.

[306] Coelho NM, González-García C, Planell JA, Salmerón-Sánchez M, Altankov G. Different assembly of type IV collagen on hydrophilic and hydrophobic substrata alters endothelial cells interaction. Eur Cell Mater. 2010; 19: 262-72.

[307] Owens DK, Wendt RC. Estimation of the Surface Free Energy of Polymers. Journal of Applied Polymer Science 1969; 13(8): 1741–1747.

[308] Frederick M. Fowkes ATTRACTIVE FORCES AT INTERFACES. Ind. Eng. Chem. 1964; 56 (12): 40–52. DOI: 10.1021/ie50660a008.

[309] Allen P, Melero-Martin J, Bischoff J. Type I collagen, fibrin and PuraMatrix matrices provide permissive environments for human endothelial and mesenchymal progenitor cells to form neovascular networks. J Tissue Eng Regen Med. 2011; 5(4): e74-86. DOI: 10.1002/term.389.

[310] Jangwook P. Jung, Julia L. Jones, Samantha A. Cronier, Joel H. Collier.Modulating the mechanical properties of self-assembled peptide hydrogels via native chemical ligation. Biomaterials 2008; 29: 2143e2151.

[311] Khoury C, Adalsteinsson T, Johnson B, Crone WC, Beebe DJ. Tunable microfabricated hydrogels – a study in protein interaction and diffusion. Biomed Microdev 2003; 5: 35-45.

[312] Naddaf AA, Tsibranska I, Bart HJ. Kinetics of BSA release from poly(Nisopropylacrylamide) hydrogels. ChemEngProc 2010; 49: 581–8.

[313] Masaro L, Zhu XX. Physical models of diffusion for polymer solutions, gels and solids. ProgPolymSci 1999; 24: 731-75.

[314] He H. Multifunctional medical devices based on pH-sensitive hydrogels for controlled drug delivery. PhD dissertation, The Ohio State University, 2006.

[315] Jiang W, Schwendeman S. Stabilization and controlled release of bovine serum albumin encapsulated in poly(D, L-lactide) and poly(ethylene glycol) microsphere blends. Pharmaceut Res 2001; 18: 878–85.

[316] Huang X, Brazel CS. On the importance and mechanisms of burst release in matrix controlled drug delivery systems. J Controlled Release 2001; 73: 121–36.

[317] Biological evaluation of medical devices - Part 5: Tests for in vitro cytotoxicity (ISO 10993-5:2009)

[318] Halama T, Staffler G, Hoch S, Stockinger H, Wolff K, Petzelbauer P.Vascular-endothelial cadherin (CD144)- but not PECAM-1 (CD31)-based cell-to-cell contacts convey the maintenance of a quiescent endothelial monolayer. Int Arch Allergy Immunol 1999; 120(3): 237-44.

[319] Hordijk PL, Anthony E, Mul FP, Rientsma R, Oomen LC, Roos D. Vascular-endothelial-cadherin modulates endothelial monolayer permeability. J Cell Sci. 1999; 112 (Pt 12): 1915-23.

[320] Matsumura T, Wolff K, Petzelbauer P. Endothelial cell tube formation depends on cadherin 5 and CD31 interactions with filamentous actin. J Immunol. 1997; 158(7): 3408-16.

[321] Llopis-Hernández V, Rico P, Ballester-Beltrán J, Moratal D, Salmerón-Sánchez M. Role of surface chemistry in protein remodeling at the cell-material interface. PLoS One. 2011; 6(5):e19610. DOI: 10.1371/journal.pone.0019610.

[322] Lamalice L, Le Boeuf F, Huot J. Endothelial cell migration during angiogenesis. Circ Res. 2007; 100(6): 782-94.

[323] Akiyama N, Yamamoto-Fukuda T, Takahashi H, Koji T. In situ tissue engineering with synthetic self-assembling peptide nanofiber scaffolds, PuraMatrix, for mucosal regeneration in the rat middle-ear. Int J Nanomedicine 2013; 8: 2629-2640. DOI: 10.2147/IJN.S47279

[324] Holmes K, Roberts OL, Thomas AM, Cross MJ. Vascular endothelial growth factor receptor-2: structure, function, intracellular signalling and therapeutic inhibition. Cell Signal 2007; 19(10): 2003-12.

[325] Neofytou EA, Chang E, Patlola B, Joubert LM, Rajadas J, Gambhir SS, Cheng Z, Robbins RC, BeyguiRE. Adipose tissue-derived stem cells display a proangiogenic phenotype on 3D scaffolds. J Biomed Mater Res A. 2011; 98(3): 383-93. DOI: 10.1002/jbm.a.33113.

[326] Beckermann BM, Kallifatidis G, Groth A, Frommhold D, Apel A, Mattern J, Salnikov AV, Moldenhauer G, Wagner W, Diehlmann A, Saffrich R, Schubert M, Ho AD, Giese N, Büchler MW, Friess H, Büchler P, Herr I.VEGF expression by mesenchymal stem cells contributes to angiogenesis in pancreatic carcinoma. Br J Cancer 2008; 99(4): 622-31. DOI: 10.1038/sj.bjc.6604508.

[327] Favot L, Keravis T, Holl V, Le Bec A, Lugnier C. VEGF-induced HUVEC migration and proliferation are decreased by PDE2 and PDE4 inhibitors. ThrombHaemost. 2003; 90(2): 334-43.

[328] Chitsaz S, Wenk JF, Ge L, Wisneski A, Mookhoek A, Ratcliffe MB, Guccione JM, Tseng EE. Material properties of CorCap passive cardiac support device.Ann Thorac Surg. 2013; 95(1): 148-54. doi: 10.1016/j.athoracsur.2012.07.036.

[329] Vandenburgh HH, Solerssi R, Shansky J, Adams JW, Henderson SA.Mechanical stimulation of organogenic cardiomyocyte growth in vitro. Am J Physiol. 1996 ; 270(5 Pt 1):C1284-92.

[330] Geuss LR, Suggs LJ. Making cardiomyocytes: how mechanical stimulation can influence differentiation of pluripotent stem cells. Biotechnol Prog. 2013; 29(5): 1089-96.

[331] Serpooshan V, Zhao M, *et al.* The effect of bioengineered acellular collagen patch on cardiac remodeling and ventricular function post myocardial infarction. Biomaterials. 2013; 34(36): 9048-55.

[332] Shen YH, Shoichet MS, Radisic M. Vascular endothelial growth factor immobilized in collagen scaffold promotes penetration and proliferation of endothelial cells. Acta Biomater. 2008; 4(3): 477-89.

[333] Pagliari S, Tirella A, Ahluwalia A, Duim S, Goumans MJ, Aoyagi T, Forte G. A multistep procedure to prepare pre-vascularized cardiac tissue constructs using adult stem cells, dynamic cell cultures, and porous scaffolds. Front Physiol. 2014; 5: 210. DOI: 10.3389/fphys.2014.00210. eCollection 2014.

[334] Perets A, Baruch Y, Weisbuch F, Shoshany G, Neufeld G, Cohen S. Enhancing the vascularization of three-dimensional porous alginate scaffolds by incorporating controlled release basic fibroblast growth factor microspheres. J Biomed Mater Res A. 2003; 65(4): 489-97.